



저작자표시-비영리-변경금지 2.0 대한민국

이용자는 아래의 조건을 따르는 경우에 한하여 자유롭게

- 이 저작물을 복제, 배포, 전송, 전시, 공연 및 방송할 수 있습니다.

다음과 같은 조건을 따라야 합니다:



저작자표시. 귀하는 원저작자를 표시하여야 합니다.



비영리. 귀하는 이 저작물을 영리 목적으로 이용할 수 없습니다.



변경금지. 귀하는 이 저작물을 개작, 변형 또는 가공할 수 없습니다.

- 귀하는, 이 저작물의 재이용이나 배포의 경우, 이 저작물에 적용된 이용허락조건을 명확하게 나타내어야 합니다.
- 저작권자로부터 별도의 허가를 받으면 이러한 조건들은 적용되지 않습니다.

저작권법에 따른 이용자의 권리는 위의 내용에 의하여 영향을 받지 않습니다.

이것은 [이용허락규약\(Legal Code\)](#)을 이해하기 쉽게 요약한 것입니다.

[Disclaimer](#)

농학박사학위논문

바이오차와 유기 및 무기 오염물질 간의
흡착 기작 해석

**Interpreting the Sorption Mechanisms
of Biochar with Organic and
Inorganic Pollutants**

2020년 8월

서울대학교 대학원

농생명공학부 응용생명화학전공

이 서 연

(This page intentionally left blank)

A Dissertation for the Degree of Doctor of Philosophy

**Interpreting the Sorption Mechanisms
of Biochar with Organic and
Inorganic Pollutants**

**바이오차와 유기 및 무기 오염물질 간의
흡착 기작 해석**

August 2020

Seoyeon Lee

Applied Life Chemistry Major

Department of Agricultural Biotechnology

Seoul National University

(This page intentionally left blank)

Interpreting the Sorption Mechanisms of Biochar with Organic and Inorganic Pollutants

바이오차와 유기 및 무기 오염물질 간의
흡착 기작 해석

지도교수 노희명

이 논문을 농학박사학위논문으로 제출함
2020년 7월

서울대학교 대학원
농생명공학부 응용생명화학전공
이서연

이서연의 박사학위논문을 인준함

2020년 7월

위원장 김정환 (인)

부위원장 노희명 (인)

위원 배의영 (인)

위원 이상주 (인)

위원 유영 (인)

(This page intentionally left blank)

**Interpreting the Sorption Mechanisms
of Biochar with Organic and
Inorganic Pollutants**

Advisor: Hee-Myong Ro

**A Dissertation Submitted in Partial Fulfillment
of the Requirement for the Degree of**

DOCTOR OF PHILOSOPHY

**to the Faculty of
Applied Life Chemistry Major,
Department of Agricultural Biotechnology**

**at
SEOUL NATIONAL UNIVERSITY**

**by
Seoyeon Lee**

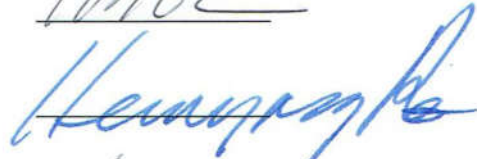
Date Approved

June 25, 2020

JEONG HAN KIM



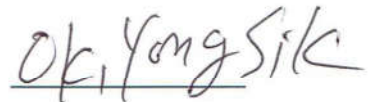
HEE MYONG RO



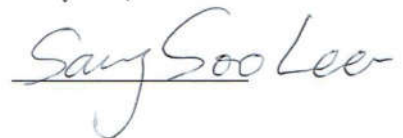
EUIYOUNG BAE



YONG SIK OK



SANG SOO LEE



(This page intentionally left blank)

(This page intentionally left blank)

Abstract

Biochar is a carbonaceous material produced from various feedstocks through pyrolysis, and it has received great attention as an eco-friendly biosorbent because of its considerable sorption capacity for pollutants. Pyrolysis and environmental conditions determine the physicochemical characteristics of biochar and the sorption behavior of pollutants; however, the complex interaction between biochar and pollutants has not yet been comprehensively examined. Therefore, in this study, a literature review regarding the physicochemical characteristics of biochar based on pyrolysis conditions and the sorption of pollutants to biochar were conducted, and laboratory experiments using sorption isotherm with spectroscopy analysis were performed to elucidate and interpret the sorption mechanisms of organic simazine, cationic cadmium and anionic arsenate to *Miscanthus* biochar by changing pyrolysis temperature, pH and background electrolytes. The results indicated that electron donor-acceptor and hydrophobic interactions were the main sorption mechanisms for simazine, and calcium as the background electrolyte showed pore-filling effects by decreasing the sorption capacity compared with sodium. The sorption mechanisms of cadmium and arsenate were identified as partitioning and an outer-sphere complexation. Additionally, an inner-sphere complexation and precipitation were confirmed for cadmium, and an electrostatic cation bridging complexation and hydrophobic interaction were confirmed for arsenate. During sorption with biochar, reduced arsenate species was found. The pH and pyrolysis temperature did not show a general pattern with regard to the sorption of pollutants. The sorption of simazine decreased with increasing pH, while the opposite pattern was observed for cadmium and arsenate. An increased pyrolysis temperature reduced the

sorption of simazine, but the observed trend was inconsistent for cadmium and arsenate. Based on the observations, different pyrolysis temperature and environmental conditions led to distinct sorption patterns between biochar and pollutants because various sorption mechanisms are involved in the sorption process, and the dominant sorption mechanism varies with environmental conditions. Changes in pyrolysis temperature and environmental conditions dominantly affected leachability, bioavailability and toxicity of pollutants; thus, it is essential to comprehensively understand the fundamental interactions among the physicochemical characteristics of biochar, behavior of pollutants and environmental conditions before the utilization of biochar as a biosorbent.

Keyword: Biochar, Pyrolysis temperature, Sorption mechanism, pH-dependent, Electrolyte solution, Simazine, Cadmium, Arsenate

Student Number : 2013-21180

LIST OF CONTENTS

ABSTRACT	i
LIST OF CONTENTS	iii
LIST OF TABLES AND FIGURES	v
LIST OF ABBREVIATIONS	xi
CHAPTER 1. GENERAL INTRODUCTION	1-1
1.1. Definition of biochar	1-1
1.2. Biochar for environmental prospects	1-2
1.3. Ionizable pollutants in the environments	1-5
1.4. Identification of sorption mechanism	1-10
1.5. Aims of dissertation	1-11
Reference	1-15
CHAPTER 2. LITERATURE REVIEW	2-1
List of contents	2-1
Abstract	2-2
2.1. Introcution	2-3
2.2. Physicochemical characteristics of biochar	2-6
2.3. Biochar as universal sorbent	2-20
2.4. Unexpected results in remediation of pollutatns	2-27
2.5. Conclusions	2-31
Reference	2-32
CHPATER 3. INTERPRETING THE pH-DEPENDENT MECHANISM OF SIMAZINE SORPTION TO <i>MISCANTHUS</i> BIOCHAR PRODUCED AT DIFFERENT PYROLYSIS TEMPERATURES FOR ITS APPLICATION TO SOIL	3-1
List of contents	3-1
Abstract	3-2
3.1. Introduction	3-3
3.2. Materials and methods	3-6
3.3. Results and discussion	3-13
3.4. Conclusions	3-37
Reference	3-39

CHAPTER 4. INTERACTIVE EFFECT OF pH AND CATION VALENCE IN BACKGROUND ELECTROLYTE SOLUTIONS ON SIMAZINE SORPTION TO *MISCANTHUS* BIOCHAR PRODUCED AT TWO DIFFERENT PYROLYSIS TEMPERATURES 4-1

List of contents 4-1
Abstract 4-2
4.1. Introduction 4-3
4.2. Materials and methods 4-6
4.3. Results and discussion 4-12
4.4. Conclusions 4-32
Reference 4-35

CHAPTER 5. COMPREHENSIVE INTERPRETATION FOR THE SORPTION MECHANISMS OF Cd²⁺ AND As(V) ON *MISCANTHUS* BIOCHAR USING SCANNING ELECTRON MICROSCOY, X-RAY DIFFRACTION AND PHOTOEMISSION SPECTROSCOPY 5-1

List of contents 5-1
Abstract 5-2
5.1. Introduction 5-3
5.2. Materials and methods 5-6
5.3. Results and discussion 5-10
5.4. Conclusions 5-56
Reference 5-58

CHAPTER 6. SUMMARY AND CONCLUSIONS 6-1

6.1. Summary 6-1
6.2. Conclusions 6-5

ABSTRACT IN KOREAN xii
LIST OF PUBLICATION xiv
ACKNOWLEDGEMENT xv

LIST OF TABLE AND FIGURES

CHAPTER 1. GENERAL INTRODUCTION	1-1
Fig. 1-1 Present study topic of biochar.	1-6
Fig. 1-2 Schematic illustration of environment pollutants behavior in the soil environment.	1-12
CHAPTER 2. LITERATURE REVIEW	2-1
Table 2-1 Ash and elemental contents of the biochar produced various feedstocks and pyrolysis temperatures.	2-15
Table 2-2 Summary of the sorption isotherm parameters and matrix involved in the sorption of organic pollutants produced from various feedstocks at different pyrolysis temperatures.	2-21
Table 2-3 Summary of the sorption isotherm parameters and matrix involved in the sorption of inorganic pollutants produced from various feedstocks at different pyrolysis temperatures.	2-22
Fig. 2-1 Schematic illustration for evolution of porous structures with increasing pyrolysis temperature. This figure is from the previous Dwonie et al. (2012) study, it is included for better understanding the molecular scale transformation of biochar structure.	2-9
Fig. 2-2 Van Krevelen diagram of various biochar derived from various feedstocks under different pyrolysis temperature. The gray symbols indicated the previous study according to Ahmad et al. (2014) and colored symbols represented the updated results in the other previous studies.	2-13
Fig. 2-3 Variation of charged surface of biochar with increasing pH by deprotonated acidic functional groups (e.g., carboxylic, lactonic and phenolic) on biochar surface.	2-17
Fig. 2-4 Schematic illustration of interaction between biochar and ionizable environmental pollutants under changing environmental factors (e.g., pH, ionic valence of cation and anion, and organic matter).	2-25
CHAPTER 3. INTERPRETING THE pH-DEPENDENT MECHANISM OF SIMAZINE SORPTION TO <i>MISCANTHUS</i> BIOCHAR PRODUCED AT DIFFERENT PYROLYSIS TEMPERATURES FOR ITS APPLICATION TO SOIL	3-1
Table 3-1 Physicochemical characteristics of <i>Miscanthus</i> biochar produced at two pyrolysis temperatures at 400 °C (B400) and 700 °C (B700). .	3-15

Table 3-2 X-ray fluorescence (XRF) spectroscopy results of dried <i>Miscanthus</i> and biochar produced at 400 °C (B400) and 700 °C (B700).	3-16
Table 3-3 Isotherm parameters for sorption of simazine on the <i>Miscanthus</i> biochar produced pyrolysis temperature at 400 °C (B400) and 700 °C (B700).	3-33
Fig. 3-1 Stacked ATR FT-IR spectra of dried <i>Miscanthus</i> and biochar produced at 400 °C (B400) and 700 °C (B700). Arrows and numbers indicate the frequency of the vibration mode in the molecular structure.	3-19
Fig. 3-2 Scanning electron micrographs of <i>Miscanthus</i> biochar produced at 400 °C (B400) and 700 °C (B700). All images were recorded with a probe current of 15.5 kV.	3-21
Fig. 3-3 Sorption kinetics of simazine to <i>Miscanthus</i> biochar produced at 400 °C (B400; solid circle) and 700 °C (B700; open circle). The initial pH of simazine solution was 4.5, and the final pH of the mixture was 7.9 for B400 and 9.6 for B700. The initial concentration of simazine was 5 mg L ⁻¹	3-23
Fig. 3-4 Molar fraction of protonated (gray dashed line) and neutral (gray solid line) simazine calculated using the Henderson-Hasselbach equation and of neutral simazine obtained from batch experiments (solid triangle) as a function of solution pH and the first-order degradation kinetics (k_{dg}) of simazine estimated by varying the pH (solid circle with a line).	3-25
Fig. 3-5 Fitting of the Freundlich isotherm to each dataset of simazine sorption obtained at three set pH values [3.0 (circle), 5.5 (rectangle) and 9 (triangle)] for (a) B400 and (b) B700.	3-31
Fig. 3-6 Scatchard plot (y-axis: the ratio of biochar-bound simazine to free simazine, q_{eq}/C_{eq} ; x-axis: q_{eq}) showing two types of sorption mechanism between simazine and biochar obtained at: (a) pH = 3.8 (solid circle) and (b) pH = 7.7 (solid triangle) for B400, and (c) pH = 3.6 (open circle) and (d) pH = 7.9 (open triangle) for B700. Data points represent experimental results. Solid lines represent electrostatic interaction; dashed lines denote hydrophobic interaction.	3-35

CHAPTER 4. INTERACTIVE EFFECT OF pH AND CATION VALENCE IN BACKGROUND ELECTROLYTE SOLUTIONS ON SIMAZINE SORPTION TO *MISCANTHUS* BIOCHAR PRODUCED AT TWO DIFFERENT PYROLYSIS TEMPERATURES

4-1	
Table 4-1 Physicochemical characteristics of <i>Miscanthus</i> biochar pyrolyzed at two temperatures of 400 °C (B400) and 700 °C (B700).	4-13
Table 4-2 XRF results of dried <i>Miscanthus</i> and biochar pyrolyzed at two	

temperatures of 400 °C (B400) and 700 °C (B700).	4-16
Table 4-3 Linear Freundlich and Langmuir sorption isotherm parameters for simazine sorption on <i>Miscanthus</i> biochar produced at two pyrolysis temperatures of 400 °C (B400) and 700 °C (B700) obtained at three pH values in 0.1 M NaCl and 0.05 M CaCl ₂ solutions, with the results of two-way analysis of variance (ANOVA) showing the significance of the effects of two factors and their interaction on each isotherm parameter. The mixture was shaken at 160 rpm for 81h at 25 ± 0.5 °C.	4-25
Table 4-4 FE-SEM/EDS elemental analysis results for two types of biochar produced at 400 and 700 °C (B400 and B700) obtained after simazine sorption at pH 3.5 and 10 in 0.1 M NaCl or 0.05 M CaCl ₂	4-26
Fig. 4-1 Surface charge density (SCD) of <i>Miscanthus</i> biochar produced at two pyrolysis temperatures of 400 °C (B400) and 700 °C (B700) as a function of pH determined by potentiometric titration in 0.05 M CaCl ₂	4-17
Fig. 4-2 Simazine sorption isotherms fitted to the linear Freundlich model in 0.1 M NaCl (rectangles) and 0.05 M CaCl ₂ (triangles) for B400 (a-c, indicated on the left side with solid symbols) and B700 (d-f, indicated on the right side with open symbols) at three pH values of 3.5, 7.5 and 10. The mixture was agitated at 160 rpm for 81 h at room temperature of 25 ± 0.5 °C.	4-23
Fig. 4-3 FE-SEM/EDS images of (a) morphology (black), (b) C (yellow), (c) O (orange), (d) Si (blue), and (e) Na (purple) or Ca (red) for two types of biochar produced at 400 and 700 °C (B400 and B700, respectively), obtained after simazine sorption at pH 3.5 and 10 in 0.1 M NaCl or 0.05 M CaCl ₂	4-27

CHAPTER 5. COMPREHENSIVE INTERPRETATION FOR THE SORPTION MECHANISMS OF Cd²⁺ AND As(v) ON *MISCANTHUS* BIOCHAR USING SCANNING ELECTRON MICROSCOY, X-RAY DIFFRACTION AND PHOTOEMISSION SPECTROSCOPY

Table 5-1 Physicochemical characteristis of <i>Miscanthus</i> biochar pyrolyzed at two temperatures of 400 °C (B400) and 700 °C (B700).	5-11
Table 5-2 Fitting results using the Freundlich isotherms for Cd ²⁺ or As(V) sorption on <i>Miscanthus</i> biochar pyrolyzed at two temperatures of 400 °C (B400) and 700 °C (B700) under three pH conditions (3.5, 7.0 and 10). The mixture was agitated at 160 rpm for 120 h at room temperature (25 °C). The value of K_F is a constant related to sorption capacity (mmol g ⁻¹ (mmol L ⁻¹) ⁻ⁿ), and $1/n$ is the sorption intensity. The R^2 value means the correlation of determination of fitting.	5-21

- Table 5-3** Dissolved ion composition of B400 and B700 by inductively coupled plasma optical emission spectroscopy (ICP-OES) measurements. The bold elements were employed for visual MINTEQ calculation, in which the concentration was above 0.01 mM (concentrations less than 0.01 mM were not included for the calculation). 5-23
- Table 5-4** Possible precipitates calculated using Visual MINTEQ software with dissolved concentrations of six major ions (Ca, K, Mg, Mn, Si and Na) with Cd²⁺ or As(V) ions at pH 3.5, 7.0 and 10. The listed precipitates were categorized because they exceeded saturation (saturation index: $(SI = \log_{10}(I_{AP}/K_{sp}) \gg 0)$). The calculation was conducted at pH intervals of 0.5, but 3 pH points are listed. 5-24
- Fig. 5-1** Surface charge density (SCD) of *Miscanthus* biochar produced at two pyrolysis temperatures of 400 °C (B400) and 700 °C (B700) as a function of pH determined by potentiometric titration in 0.05 M CaCl₂. 5-13
- Fig. 5-2** Kinetic study of the Cd²⁺ and As(V) sorption without controlling the pH conditions for 120 h. Two hundred milligrams of biochar was mixed with 20 mL of 1 mM CdCl₂ or 1 mM Na₂HAsO₄ with 100 mM NaCl as the background electrolyte. The final pH of Cd²⁺ was 6.4 and 6.8 for B400 and B700 and for As(V), and it was 7.1 and 9.9 for B400 and B700, respectively. 5-18
- Fig. 5-3** Sorption isotherm of Cd²⁺ and As(V) at six concentrations (1, 2, 3, 4, 5, 10 mM) and three pH values (3.5, 7.0 and 10) on B400 (a and c) and B700 (b and d). Error bars indicate the standard deviation of triplicate measurements. The dotted line indicated the fitting results of Freundlich model, while the circle, rectangular and triangle indicate pH values of 3.5, 7.0 and 10, respectively. 5-19
- Fig. 5-4** X-ray diffraction patterns of B400 (a) and B700 (b) before the sorption experiment (light gray) and after sorption of Cd²⁺ (dark gray) and As(V) (black) at two different concentrations (1 and 5 mM) at three different pH values (3.5, 7.0 and 10). Seven crystal structures were identified and listed with codes from the American Mineralogist Crystal Structure Database (AMCSD). Capital letters indicate the position of the major peaks of each crystal structure listed above. 5-27
- Fig. 5-5** High-resolution C1s (a and d), O1s (b and e) and Si2p (c and f) XPS spectra of the two biochars (B400 and B700) before the sorption experiment. Spectral components were obtained and subjected to peak

deconvolution using Igor Pro 8 software and X-ray Photoelectron Spectroscopy Tools with the National Institute for Standards and Technology XPS database. White circles and black lines indicate experimental data and the fitting result, respectively. The small spectra in the fitting results indicate the components identified by deconvolution. All spectra were fitted to asymmetric Gaussian-Lorentzian functions (70% Gaussian and 30% Lorentzian). 5-31

Fig. 5-6 High-resolution Na1s XPS spectra of two biochars (B400 and B700) after sorption experiments of Cd²⁺ and As(V) at pH 7.0 and 10. The spectra at pH 3.5 were not illustrated because no significant signals were observed. Spectral components were obtained and addressed by peak deconvolution using Igor Pro 8 software and X-ray Photoelectron Spectroscopy Tools with National Institute for Standards and Technology XPS database. White circles and black lines refer to experimental data and the fitting result, respectively. The small spectra in the fitting result indicate the components by deconvolution. All spectra were fitted to asymmetric Gaussian-Lorentzian functions (70% Gaussian and 30% Lorentzian). 5-33

Fig. 5-7 High-resolution Ca2p XPS spectra of two biochars (B400 and B700) before the As(V) sorption experiment (a and d) and after the sorption experiment at pH 7.0 and 10. The spectra in the Cd²⁺ sorption experiment were not illustrated because no significant signals were observed. Spectral components were obtained and addressed by peak deconvolution using Igor Pro 8 software and X-ray Photoelectron Spectroscopy Tools with National Institute for Standards and Technology XPS database. White circles and black lines refer to experimental data and the fitting result, respectively. The small spectra in the fitting result indicate the components by deconvolution. All spectra were fitted to asymmetric Gaussian Lorentzian functions (70% Gaussian and 30% Lorentzian). 5-35

Fig. 5-8 Field emission scanning electron microscope equipped with an energy dispersive X-ray spectroscopy (FE-SEM/EDS) image of biochar samples under two different pyrolysis temperatures (B400 and B700) at two pH values (3.5 and 10). The colored images represent the elemental distribution of C (yellow), O (orange), Si (blue), Na (light violet), Cl (violet), Ca (red), Al (green) and K (light blue) at the same scale using

SEM-EDS measurements. The FE-SEM/EDS was operated at an accelerating voltage of 10 kV using SE2 mode. This FE-SEM/EDS graph was previously reported, but it was included here as supporting information for the convenience of readers. 5-41

Fig. 5-9 High-resolution Cd3d XPS spectra of two biochars (B400 and B700) at three different pH values (3.5, 7.0 and 10). Spectral components were obtained and identified by peak deconvolution using Igor Pro 8 software and X-ray Photoelectron Spectroscopy Tools with National Institute for Standards and Technology XPS database. White circles and black lines indicate experimental data and the fitting result, respectively. The small spectra in the fitting results indicate the components identified by deconvolution. All spectra were fitted to asymmetric Gaussian Lorentzian functions (70% Gaussian and 30% Lorentzian). 5-43

Fig. 5-10 High-resolution As3d XPS spectra of two biochars (B400 and B700) at three different pH values (3.5, 7.0 and 10). Spectral components were obtained and identified by peak deconvolution using Igor Pro 8 software and X-ray Photoelectron Spectroscopy Tools with National Institute for Standards and Technology XPS database. White circles and black lines indicate experimental data and the fitting results, respectively. The small spectra in the fitting results indicate the components identified by deconvolution. All spectra were fitted to asymmetric Gaussian Lorentzian functions (70% Gaussian and 30% Lorentzian). 5-45

Fig. 5-11 The results of pH adjustment for the sorption isotherm study at pH 3.5. The data indicate the pH before pH adjustments, and the pH was adjusted to pH 3.5. A distinct pattern between Cd²⁺ and As(V) was observed, which was caused by the reduction of As(V) to As(III) and As(0). 5-49

LIST OF ABBREVIATIONS

AFG: Acidic functional group
ANOVA: Analysis of variance
ATR: Attenuated total reflectance
BET: Brunauer-Emmett-Teller
BFG: Basic functional group
CEC: Cation exchange capacity
C_{eq}: Equilibrium concentration of sorbate (mg L^{-1})
CV: Cation valence
C₀: Initial concentration of sorbate (mg L^{-1})
EC: Electrical conductivity
EDA: Electron donor acceptor
EDS: Energy dispersive spectroscopy
FE-SEM: Field-emission scanning electron microscopy
FTIR: Fourier transform infrared spectroscopy
GC: Gas chromatography
ICP-OES: Inductively coupled plasma optical emission spectroscopy
IOP: Ionizable organic pollutant
k_{dg}: Rate of degradation
K_F: Equilibrium constant indicating sorption capacity ($\text{mg kg}^{-1}(\text{mg L}^{-1})^{-n}$)
K_L: Constant related to energy (L mg^{-1})
LSD: Least significance difference
PAH: Polycyclic aromatic hydrocarbons
PT: Pyrolysis temperature
PZNC: Point of zero net charge
q_{cal}: Estimated sorption capacity of sorbate (mg kg^{-1})
Q_{eq}: Concentration of sorbate sorbed on biochar (mg kg^{-1})
q_{exp}: Measured sorption capacity of sorbate (mg kg^{-1})
q_{max}: Maximum sorption capacity (mg kg^{-1})
Δq: Percent normalized standard deviation
SCD: Surface charge density
S_{es}: Electrostatic attraction
S_{hp}: Hydrophobic attraction
SSA: Specific surface area
μECD: Micro electron capture detector
vdW: van der Waals
XRF: X-ray fluorescence
XRD: X-ray diffraction
XPS: X-ray photoelectron spectroscop

CHAPTER 1. GENERAL INTRODUCTION

1.1. Definition of biochar

Biochar is produced from the pyrolysis of various feedstocks such as wood, leaves, or manure under oxygen-limited conditions (Lehmann 2007a; Chen et al. 2008; Zhao et al. 2013). During pyrolysis, feedstocks is transformed to an eco-friendly form of energy as bio-ethanol and a carbon-rich byproduct; this is called biochar, and it possesses a higher recalcitrant carbon content compared with the raw feedstocks (Lehmann et al. 2006). The production of bio-ethanol through the thermal decomposition of feedstocks reduces the emission of methane to the atmosphere compared to its natural decomposition in soil (Woolf et al. 2010; Matovic 2011). Biochar has a porous structure because the specific organic molecular structure in feedstocks decomposes during the pyrolysis process; this structure can function as suitable sorption sites for the remediation of pollutants (Qu et al. 2011; Al-Wabel et al. 2013; Han et al. 2016). Consequently, biochar has received a great attention as a necessary byproduct of producing renewable energy, mitigation of climate change through greenhouse gas emission reduction, recycle of superfluous feedstocks, amendment for improving the soil and water environment, and remediation of environmental pollution (Woolf et al. 2010; Kookana et al. 2011; Mohan et al. 2014b).

The physicochemical characteristics of biochar are mainly determined by the pyrolysis temperature, residence time, heat transfer rate, and type of feedstocks (Kloss et al. 2012; Angin 2013; Qin et al. 2017). Biochar produced from plant such as wood and leaves has distinct physicochemical characteristics produced from animal manure or residue (Zhao et al. 2013; Lu et al. 2016). In general, plant biochar has a higher aromatic carbon content than animal

biomass biochar at the same pyrolysis temperatures of 350, 450, and 750 °C, while alkaline chemical species and cation exchange capacity (CEC) are higher in the animal residues biochar (Domingues et al. 2017). This is because plant biomass has higher contents of cellulose and lignin, whereas animal biomass contains more minerals. Even if an identical feedstocks were employed for the biochar production, the pyrolysis temperature controls the physicochemical characteristics, such as specific surface area and aromatic carbon contents, and both increase at higher pyrolysis temperature. This is a result of the rearrangement of aromatic compounds, featured by a ring of six carbon atoms linked together without oxygen or hydrogen, for stacked and aligned sheets (Chen et al. 2007; Fang et al. 2014). These varieties of biochar have caused adverse effects or unexpected results because of the lack of a fundamental understanding of the physicochemical characteristics of biochar, and the interaction between the various surfaces of biochar and the fate of environmentally fluctuating pollutants were changed (Oleszczuk et al. 2013; Buss et al. 2015).

1.2. Biochar for environmental prospects

The heterogeneity of biochar caused by various types of feedstocks and diverse pyrolysis conditions has caused adverse effects or unexpected results; however, it has also resulted in enormous positive effects as environmental prospects (Mohan et al. 2014b; Inyang and Dickenson 2015; Xiao et al. 2018). This suggests that an extensive understanding of the production, fundamental characteristics, and environmental conditions would enable the design of the byproduct and fundamental characteristics of biochar. As briefly mentioned above, biochar has been reported as a major contributor in five areas: 1) eco-friendly energy production, such as bio-ethanol and bio-diesel (Nanda et al. 2013; Yuan and Macquarrie 2015); 2) climate change

mitigation through the sequestration of carbon in the soils and reduction in the carbon dioxide (Feng et al. 2012; Wang et al. 2012; Mosa et al. 2018) and methane gas (Czimczik and Masiello 2007; Windeatt et al. 2014); 3) recycling of agricultural and environmental waste such as wood, leaves, manure, peat, and sediment (Mukome et al. 2013; Ronsse et al. 2013); 4) stabilization of pollutants and retention of nutrients from leaching (Zhang et al. 2013c; Ahmad et al. 2014; Tan et al. 2015; Xie et al. 2015).

The research fields of biochar can be categorized as production and utilization (Fig. 1-1). The study of production can be characterized as examining the variation of feedstocks, pyrolysis process conditions, comprising pyrolysis temperature, residence time, and heat transfer rate. For the biochar production process, Kloss et al. (2012) reported that biochar produced from straw, spruce, and poplar at pyrolysis temperatures of 400, 460, and 525 °C had different physicochemical characteristics, as different elemental compositions of feedstocks decomposed at different pyrolysis temperatures. Mimmo et al. (2014) found that *Miscanthus* biochar accumulated carbon with increasing pyrolysis temperature, increasing the specific surface area and aromaticity. Chen et al. (2014) also showed that biochar derived from municipal sewage pyrolyzed at 500 to 900 °C had increased contents of ash, pH, and CEC, resulting in different removal capacities of cadmium from the respective biochar. From these studies for biochar production, the variations of feedstocks and pyrolysis temperature are significant key factors that determine the physiochemical characteristics of biochar, and extensive studies have already been conducted to assess the relationship between these key factors and the physiochemical characteristics of biochar (Cantrell et al. 2012; Zhao et al. 2013).

Biochar is utilized for carbon sequestration in the mitigation of climate change, recycling of by-products from agricultural activity, improving soil

fertility, and remediating pollutants (Cha et al. 2016). Many researchers have extensively focused on biochar in the field of climate change mitigation because of its urgent challenge (Barrow 2012; Ahmad et al. 2014; Shaaban et al. 2014). In reducing greenhouse gas emissions, biochar has been recognized as one of the effective ways to alleviate global warming. Woolf et al. (2010) calculated that the production of biochar could reduce the annual net emissions of carbon dioxide, methane, and nitrous oxide by generating eco-friendly energy while reducing the greenhouse gas emission. Vaccari et al. (2011) demonstrated that biochar had remained a long time in the soil with low rates of decomposition; thus, with an increase in it was useful to manage carbon sequestration with increasing the soil organic carbon contents. The application of biochar in the soil environment not only causes carbon sequestration but also yields additional effects, such as energy conservation from recycling of feedstocks and improvement in soil fertility. Sun and Lu (2014) confirmed that clayey soil treated with biochar produced from straw, woodchips, and wastewater sludge developed macroaggregates (5-2 and 0.25–0.5 mm) through resistance to slaking and the incorporation of a particular cohesion. Thus, the available water retention capacity of soils was also increased due to the enhancement of aggregate stability and reorganization of pore space distribution. Rajkovich et al. (2012) showed that the cultivation of corn was more productive in soil amended with biochar pyrolyzed at different temperatures, because of the biochar retention of the nutrient contents. Zhao et al. (2016) also studied the effect of pyrolysis of feedstocks with phosphate fertilizer to improve the biochar capability for nutrient retention, demonstrating a positive effect for cultivation.

Besides carbon sequestration and nutrient retention, the remediation of pollutants using biochar has also received a considerable amount of interest, owing to the eco-friendliness and cost-effectiveness of biochar as a biosorbent

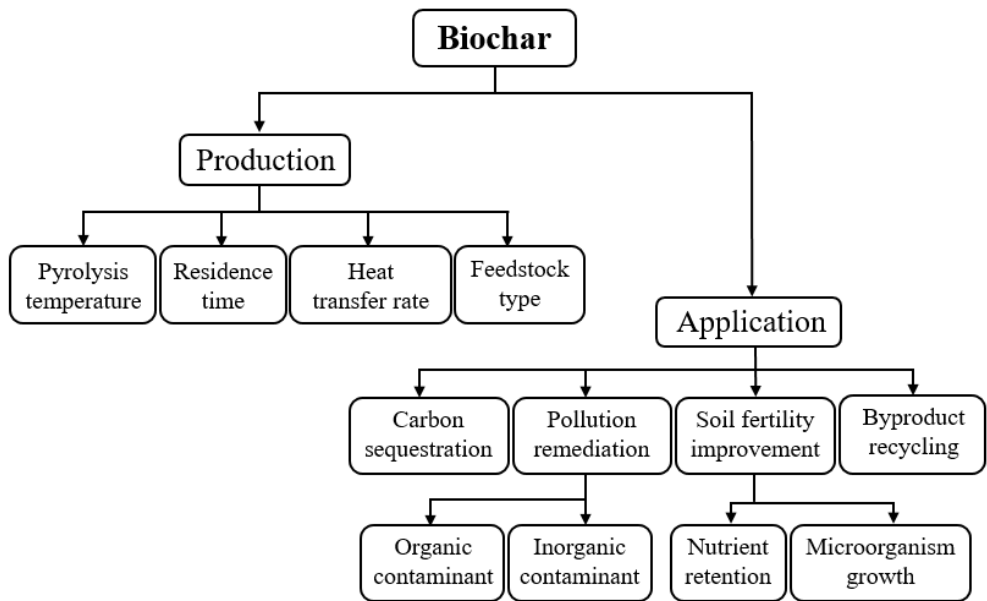
(Tang et al. 2013; Inyang et al. 2016). Zheng et al. (2010) studied the sorption of two triazines to biochar produced green waste; in addition, Zhang et al. (2011) studied the sorption of simazine, belonging to the triazine group; however, their results were different from those of Zheng et al. (2010), owing to the use of different biochar. Chen and Chen (2009) showed that the sorption of naphthalene and 1-naphthol to biochar produced orange peels yielded different results depending on pyrolysis temperature, resulting in a variety of physicochemical characteristics of biochar. The sorption of biochar was shown to be more effective, because they employed different biochar. Biochar was effective for not only organic pollutants but also inorganic pollutants. Mohan et al. (2014) showed that biochar produced oak wood and oak bark were useful for the remediation of cadmium and lead. Lu et al. (2012) suggested that lead sorption to biochar was affected by pH, as the lead was precipitated as lead phosphate silicate.

As mentioned above, the heterogeneity of biochar led to adverse effects or unexpected results; however, there are enormous advantages of using biochar in the environment. However, to effectively use biochar as a positive biosorbent and for carbon sequestration, the complex relationship between production and utilization should be fully understood. Without fundamental knowledge of the mechanism and behavior of biochar, unexpected side effects in the environment may result. Consequently, fully understanding the fundamental characteristics of biochar is essential for its utilization in the real environment.

1.3. Ionizable pollutants in the environments

Organic pollutants in the soil environment are defined as harmful molecules to living organisms with resistance to chemical, biological, and photolytic degradation (Reid et al. 2000). Owing to their persistency, organic

Fig. 1-1. Present study topic of Biochar (Ahmad et al., 2014).



pollutants were accumulated with various adverse effects on human health and the ecosystem (Kelsey and Alexander 1997; Kester et al. 2005). Identified by fluctuations in the proton concentration, there are specific molecules that change their molecular charge, called ionizable organic pollutants (IOPs), which result in protonation or deprotonation (Tülp et al. 2009; Xiao and Pignatello 2014). Organic acids are primarily negatively charged at a certain pH value above their negative logarithmic acid dissociation constant (pK_a) owing to deprotonation, whereas they are neutrally charged below their pK_a (An and Dultz 2007). On the contrary, organic bases at pH values above their pK_a owing to protonation, while they are positively charged below their pK_a (Stapleton et al. 1994). The behaviors and fates of IOPs were governed not only by pH conditions but also by ionic strength, cation valence and type, anion valence and type, and content of organic matter in the surrounding environment; thus, the remediation strategies of IOPs should fully assess the various environmental factors described above.

Inorganic pollutants consist of oxidized elements and chemical compounds, in which two or more chemical elements are made from lack of organic carbon structure (Wilcox and Solutions 2005). These inorganic pollutants are ubiquitous because they are present not only in solid and liquid phases but also in the gas phase at ambient temperatures (Sommers and Sposito 1985). Owing to phase transition and chemical transformation, the effective remediation of inorganic pollutants is now easily addressed (Pletsch et al. 1999; Alcántara et al. 2012; Rezanian et al. 2015), and excessive amounts have been exposed in the environment due to the onset of rapid industrialization with extensive anthropogenic activity (Song et al. 2017). Heavy metals are representative inorganic pollutants, whereby most of the heavy metals on Earth are located in the lithosphere; however, anthropogenic activities such as mining and infrastructure construction have exposed the heavy metals in the

pedosphere. In general, heavy metals are present as positively charged molecules under oxidizing conditions in the pedosphere and hydrosphere, which causes severe oxidizing stress to living organisms (Gupta et al. 1996; Lim et al. 2008). However, some heavy metals and metalloids react with oxygen in the environment, assuming a negatively charged state with more than oxygen (Hesterberg 1998; Mondal et al. 2006). The majority of oxyanions are essential such as phosphate, sulfate, carbonate, and nitrate; however, toxic oxyanions also exist, causing a severe environmental threat to the ecosystem, such as arsenate, selenite, and antimonate. Based on the redox potential, the oxyanions are transformed to reduced species, and the electrochemical properties and toxicity are changed. In the soil and water environment, cationic heavy metals and anionic oxyanions co-exist at various concentrations and compositions; thus, it is important to stabilize their affinity to soil components and reduce their activity and bioavailability. Based on elemental or molecular charges, the transformation of inorganic pollutants species varies with respect to pH, owing to protonation or deprotonation; heavy metals in a soil environment are less stabilized under low pH conditions, whereas they are easily immobilized at high pH by sorption on the negatively charged surface and precipitation with hydroxyl ions (Farrah and Pickering 1979). The charge of oxyanions under high pH conditions typically increases through deprotonation (Kailasam and Rosenberg 2012); meanwhile, opposite sorption trends were observed compared with those of cationic heavy metals. Therefore, understanding the behavior of ionizable pollutants under fluctuating environmental conditions is important to adequately interpret their fate in the natural environment; however, difficulties remain because of the numerous environmental factors governing the behaviors and fates of these ionizable pollutants. In addition, such complex interactions remain problematic because of limitations of analytical measurements in heterogeneous environments.

1.4. Identification of sorption mechanisms

Many previous studies have attempted to identify the sorption mechanism of environmental pollutants on biochar using a traditional sorption isotherm (Cao et al. 2009; Zhang et al. 2013c; Venegas et al. 2015), which can be expressed as a function of sorbate concentration, such as organic or inorganic pollutants, on the biochar at constant temperatures. Several theoretical isotherms have been used to explain the sorption mechanism indirectly; for example, a Langmuir isotherm assumes monolayer sorption of a single sorbate on a single sorption site (Zhang et al. 2013a), whereas Freundlich isotherm is most suitable for empirical data, assuming of energetic surface heterogeneity (Yao et al. 2013). The Dubinin–Radushkevich isotherm is another empirical model described for non-ideal sorption at heterogeneous surfaces (Pinto et al. 2010). Thus, a comparison of the fitting results obtained from sorption isotherms can enable the prediction of the sorption mechanism; however, such sorption isotherms supply only indirect; thus, it is difficult to identify the binding affinity during sorption.

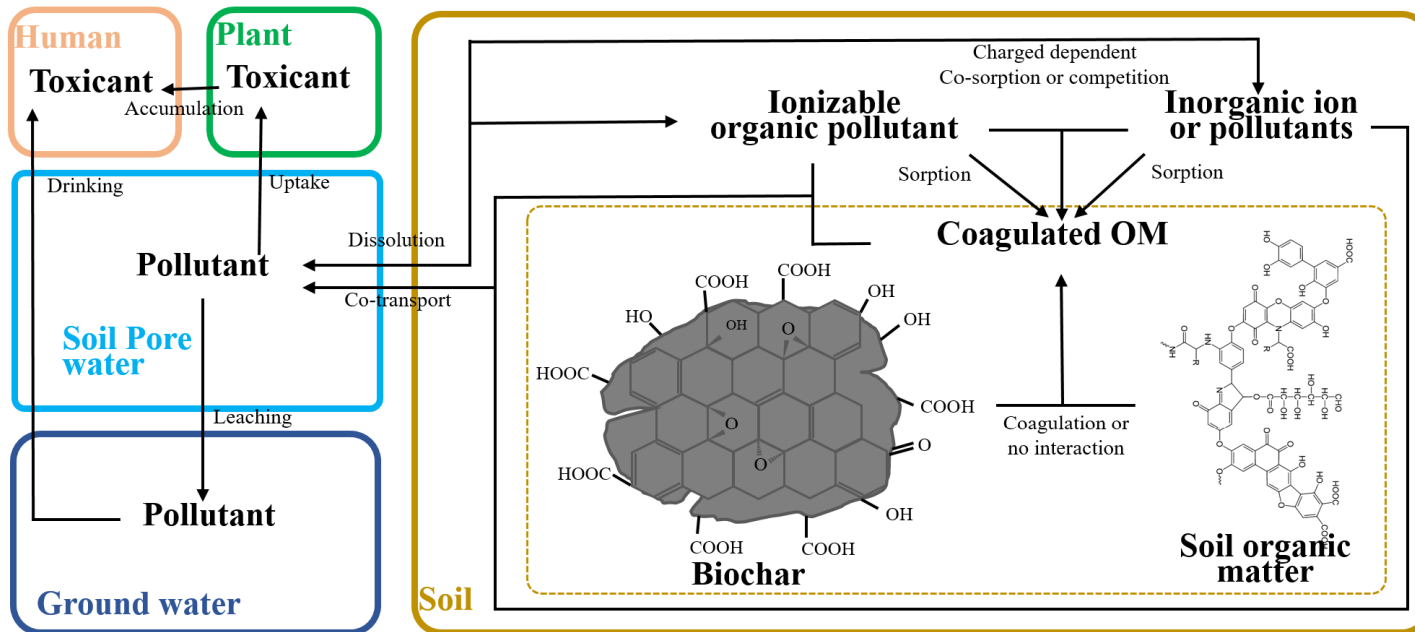
Recently, spectroscopy has been widely used to reveal the interaction of environmental pollutants in the biochar (Xu et al. 2011; Chia et al. 2012; Fan et al. 2018). Based on the wavelength of light, there are several spectroscopies that have enabled us to identify sorption mechanisms, namely, X-ray- and infrared-based spectroscopies. Fourier-transform infrared spectroscopy (FTIR) is equipped with to determine several factors, such as attenuated total reflection and diffuse reflectance, whereas photoacoustic spectroscopy is used to represent the structural configuration of both the biochar and the interaction of environmental pollutants at the interface between the biochar and liquid phases (Minnes et al. 2017). X-ray absorption near edge structure and extended X-ray absorption fine structure are effective techniques in identifying the electrochemical structure of the surrounding atoms. X-ray photoelectron

spectra (XPS) are used to confirm the quantitative measure of elemental composition for biochar interacting with environmental pollutants, in which its results determine the binding states between biochar and environmental pollutants (Atom and Konno 2016). X-ray fluorescence (XRF) spectrometry is used to analyze the concentration of the inorganic elements of biochar, while X-ray diffraction (XRD) provides results regarding the crystallographic structure, chemical composition, and physical characteristics of biochar after pollutant sorption (Chatterjee et al. 2016). Not just light-based techniques but also electron-based measurements are useful in identifying the porous structure of biochar. Field emission scanning electron microscopy (SEM) utilizing an energy dispersive X-ray spectroscopy detector allows the morphology and elemental composition of biochar interacting with chemical compounds to be analyzed (Rades et al. 2014). All the analytical techniques have advantages and disadvantages; thus, only limited information is provided with a single measurement technique. Consequently, it is essential to combine the data from various analytical techniques to verify the results, diminishing the disadvantages of individual measurement. To do so, this study has attempted to identify the sorption mechanisms and behaviors of organic and inorganic pollutants on biochar with observations from several aspects.

1.5. Aims of dissertation

The remediation of environmental pollutants using biochar has received considerable attention because biochar is an eco-friendly and cost-effective bio-sorbent. However, unexpected results have frequently been reported in previous biochar studies, since the physicochemical characteristics of biochar have not been fully addressed. Variations in the production of biochar cause a significant difference in the physicochemical characteristics of biochar; thus, is challenging to establish a standard procedure for characterization.

Fig. 1-2. Schematic illustration of environment pollutants behavior in the soil environment.



Despite the great potential of biochar for the remediation of organic and inorganic pollutants, its appropriate use as a bio-sorbent under various surrounding environmental conditions has not yet been comprehensively characterized. Therefore, it is necessary to understand the interaction of organic and inorganic pollutants with biochar under various environmental conditions for the further utilization of biochar as a bio-sorbent.

Thus, this review aims to provide comprehensive insight into the fundamental interactions of organic and inorganic pollutants with biochar produced at different pyrolysis temperatures under various environmental conditions. The provided literature review summarizes the previous studies regarding the variation of the physicochemical characteristics of biochar under surrounding environmental conditions, sorption of organic and inorganic pollutants to biochar, and the reason why environmental change is crucial for the sorption studies. The physicochemical characteristics of biochar produced at pyrolysis temperatures of 400 and 700 °C (B400 and B700) were fully examined with modern analytics to better understand their impacts on the sorption mechanism. Simazine as an organic pollutant, cadmium as a cationic heavy metal, and arsenate as an anionic oxyanion were selected, and their sorption mechanisms were comprehensively interpreted to understand the fundamental sorption mechanism and estimate their behaviors and fates for further implication in soil and water environments. Based on these results and interpretation, biochar should receive a great amount of attention in the effort to maximize the sorption capacity and affinity for pollutant stabilization in the soils and minimize unexpected outcomes resulting from the misunderstanding of the fundamental characteristics of biochar.

References

- Ahmad M, Rajapaksha AU, Lim JE, Zhang M, Bolan N, Mohan D, Vithanage M, Lee SS, Ok YS (2014) Biochar as a sorbent for contaminant management in soil and water: A review. *Chemosphere* 99:19–33. doi: 10.1016/j.chemosphere.2013.10.071
- Al-Wabel MI, Al-Omran A, El-Naggar AH, Nadeem M, Usman ARA (2013) Pyrolysis temperature induced changes in characteristics and chemical composition of biochar produced from conocarpus wastes. *Bioresour Technol* 131:374–379. doi: 10.1016/j.biortech.2012.12.165
- Alcántara MT, Gómez J, Pazos M, Sanromán MA (2012) Electrokinetic remediation of lead and phenanthrene polluted soils. *Geoderma* 173–174:128–133. doi: 10.1016/j.geoderma.2011.12.009
- An JH, Dultz S (2007) Adsorption of tannic acid on chitosan-montmorillonite as a function of pH and surface charge properties. *Appl Clay Sci* 36:256–264. doi: 10.1016/j.clay.2006.11.001
- Angin D (2013) Effect of pyrolysis temperature and heating rate on biochar obtained from pyrolysis of safflower seed press cake. *Bioresour Technol* 128:593–597. doi: 10.1016/j.biortech.2012.10.150
- Atom C, Konno H (2016) X-Ray Photoelectron Spectroscopy Learn more about X-Ray Photoelectron Spec- X-ray Photoelectron Spectroscopy
- Barrow CJ (2012) Biochar: Potential for countering land degradation and for improving agriculture. *Appl Geogr* 34:21–28. doi: 10.1016/j.apgeog.2011.09.008
- Buss W, Mašek O, Graham M, Wüst D (2015) Inherent organic compounds in biochar-Their content, composition and potential toxic effects. *J Environ Manage* 156:150–157. doi: 10.1016/j.jenvman.2015.03.035
- Cantrell KB, Hunt PG, Uchimiya M, Novak JM, Ro KS (2012) Impact of pyrolysis temperature and manure source on physicochemical characteristics of biochar. *Bioresour Technol* 107:419–428. doi: 10.1016/j.biortech.2011.11.084
- Cao X, Ma L, Gao B, Harris W (2009) Dairy-manure derived biochar effectively sorbs lead and atrazine. *Environ Sci Technol* 43:3285–3291. doi: 10.1021/es803092k
- Cha JS, Park SH, Jung SC, Ryu C, Jeon JK, Shin MC, Park YK (2016) Production and utilization of biochar: A review. *J Ind Eng Chem* 40:1–15. doi: 10.1016/j.jiec.2016.06.002
- Chatterjee AK, Material C, Dioxide T, Pattern D (2016) X-Ray Diffraction Learn more about X-Ray Diffraction X-Ray Diffraction
- Chen B, Chen Z (2009) Sorption of naphthalene and 1-naphthol by biochars of orange peels with different pyrolytic temperatures. *Chemosphere* 76:127–133. doi: 10.1016/j.chemosphere.2009.02.004
- Chen B, Zhou D, Zhu L (2008) Transitional adsorption and partition of nonpolar and polar aromatic contaminants by biochars of pine needles with different pyrolytic temperatures. *Environ Sci Technol* 42:5137–5143. doi: 10.1021/es8002684
- Chen J, Zhu D, Sun C (2007) Effect of heavy metals on the sorption of hydrophobic organic compounds to wood charcoal. *Environ Sci Technol* 41:2536–2541. doi:

10.1021/es062113+

- Chen T, Zhang YY, Wang H, Lu W, Zhou Z, Zhang YY, Ren L (2014) Influence of pyrolysis temperature on characteristics and heavy metal adsorptive performance of biochar derived from municipal sewage sludge. *Bioresour Technol* 164:47–54. doi: 10.1016/j.biortech.2014.04.048
- Chia CH, Gong B, Joseph SD, Marjo CE, Munroe P, Rich AM (2012) Imaging of mineral-enriched biochar by FTIR, Raman and SEM-EDX. *Vib Spectrosc* 62:248–257. doi: 10.1016/j.vibspec.2012.06.006
- Czimczik CI, Masiello CA (2007) Controls on black carbon storage in soils. *Global Biogeochem Cycles* 21:1–8. doi: 10.1029/2006GB002798
- Domingues RR, Trugilho PF, Silva CA, De Melo ICNA, Melo LCA, Magriotis ZM, Sánchez-Monedero MA (2017) Properties of biochar derived from wood and high-nutrient biomasses with the aim of agronomic and environmental benefits. *PLoS One* 12:1–19. doi: 10.1371/journal.pone.0176884
- Fan Q, Sun J, Chu L, Cui L, Quan G of chemical oxidation on surface oxygen-containing functional groups and adsorpti, Yan J, Hussain Q, Iqbal M (2018) Effects of chemical oxidation on surface oxygen-containing functional groups and adsorption behavior of biochar. *Chemosphere* 207:33–40. doi: 10.1016/j.chemosphere.2018.05.044
- Fang Q, Chen B, Lin Y, Guan Y (2014) Aromatic and hydrophobic surfaces of wood-derived biochar enhance perchlorate adsorption via hydrogen bonding to oxygen-containing organic groups. *Environ Sci Technol* 48:279–288. doi: 10.1021/es403711y
- Farrar H, Pickering WF (1979) pH effects in the adsorption of heavy metal ions by clays. *Chem Geol* 25:317–326. doi: 10.1016/0009-2541(79)90063-9
- Gupta SK, Vollmer MK, Krebs R (1996) The importance of mobile, mobilisable and pseudo total heavy metal fractions in soil for three-level risk assessment and risk management. *Sci Total Environ* 178:11–20. doi: 10.1016/0048-9697(95)04792-1
- Han L, Qian L, Yan J, Chen M (2016) Contributions of different biomass components to the sorption of 1,2,4-trichlorobenzene under a series of pyrolytic temperatures. *Chemosphere* 156:262–271. doi: 10.1016/j.chemosphere.2016.04.031
- Hesterberg D (1998) Biogeochemical cycles and processes leading to changes in mobility of chemicals in soils. *Agric Ecosyst Environ* 67:121–133. doi: 10.1016/S0167-8809(97)00110-2
- Inyang M, Dickenson E (2015) The potential role of biochar in the removal of organic and microbial contaminants from potable and reuse water: A review. *Chemosphere* 134:232–240. doi: 10.1016/j.chemosphere.2015.03.072
- Inyang MI, Gao B, Yao Y, Xue Y, Zimmerman A, Mosa A, Pullammanappallil P, Ok YS, Cao X (2016) A review of biochar as a low-cost adsorbent for aqueous heavy metal removal. *Crit Rev Environ Sci Technol* 46:406–433. doi: 10.1080/10643389.2015.1096880
- Kailasam V, Rosenberg E (2012) Oxyanion removal and recovery using silica polyamine composites. *Hydrometallurgy* 129–130:97–104. doi:

10.1016/j.hydromet.2012.08.010

- Kelsey JW, Alexander M (1997) Declining bioavailability and inappropriate estimation of risk of persistent compounds. *Environ Toxicol Chem* 16:582–585. doi: 10.1897/1551-5028(1997)016<0582:DBAIEO>2.3.CO;2
- Kester GB, Brobst RB, Carpenter A, Chaney RL, Rubin AB, Schoof RA, Taylor DS (2005) Risk characterization, assessment, and management of organic pollutants in beneficially used residual products. *J Environ Qual* 34:80–90
- Kloss S, Zehetner F, Dellantonio A, Hamid R, Ottner F, Liedtke V, Schwanninger M, Gerzabek MH, Soja G (2012) Characterization of Slow Pyrolysis Biochars: Effects of Feedstocks and Pyrolysis Temperature on Biochar Properties. *J Environ Qual* 41:990. doi: 10.2134/jeq2011.0070
- Kookana RS, Sarmah AK, Van Zwieten L, Krull E, Singh B (2011) Biochar application to soil. agronomic and environmental benefits and unintended consequences, 1st edn. Elsevier Inc.
- Lehmann J (2007) A handful of carbon. *Nature* 447:143–144. doi: 10.1038/447143a
- Lehmann J, Gaunt J, Rondon M (2006) Bio-char sequestration in terrestrial ecosystems - A review. *Mitig Adapt Strateg Glob Chang* 11:403–427. doi: 10.1007/s11027-005-9006-5
- Lim HS, Lee JS, Chon HT, Sager M (2008) Heavy metal contamination and health risk assessment in the vicinity of the abandoned Songcheon Au-Ag mine in Korea. *J Geochemical Explor* 96:223–230. doi: 10.1016/j.gexplo.2007.04.008
- Lu GY, Ikeya K, Watanabe A (2016) Size distribution of carbon layer planes in biochar from different plant type of feedstock with different heating temperatures. *Chemosphere* 163:252–258. doi: 10.1016/j.chemosphere.2016.07.106
- Lu H, Zhang W, Yang Y, Huang X, Wang S, Qiu R (2012) Relative distribution of Pb 2+ sorption mechanisms by sludge-derived biochar. *Water Res* 46:854–862. doi: 10.1016/j.watres.2011.11.058
- Matovic D (2011) Biochar as a viable carbon sequestration option: Global and Canadian perspective. *Energy* 36:2011–2016. doi: 10.1016/j.energy.2010.09.031
- Mimmo T, Panzacchi P, Baratieri M, Davies CA, Tonon G (2014) Effect of pyrolysis temperature on miscanthus (*Miscanthus × giganteus*) biochar physical, chemical and functional properties. *Biomass and Bioenergy* 62:149–157. doi: 10.1016/j.biombioe.2014.01.004
- Minnes R, Nissinmann M, Maizels Y, Gerlitz G, Katzir A, Raichlin Y (2017) Using Attenuated Total Reflection-Fourier Transform Infra-Red (ATR-FTIR) spectroscopy to distinguish between melanoma cells with a different metastatic potential. *Sci Rep* 7:1–7. doi: 10.1038/s41598-017-04678-6
- Mohan D, Kumar H, Sarswat A, Alexandre-Franco M, Pittman CU (2014a) Cadmium and lead remediation using magnetic oak wood and oak bark fast pyrolysis biochars. *Chem Eng J* 236:513–528. doi: 10.1016/j.cej.2013.09.057
- Mohan D, Sarswat A, Ok YS, Pittman CU (2014b) Organic and inorganic contaminants removal from water with biochar, a renewable, low cost and sustainable adsorbent - A critical review. *Bioresour Technol* 160:191–202. doi: 10.1016/j.biortech.2014.01.120

- Mondal P, Majumder CB, Mohanty B (2006) Laboratory based approaches for arsenic remediation from contaminated water: Recent developments. *J Hazard Mater* 137:464–479. doi: 10.1016/j.jhazmat.2006.02.023
- Mosa A, El-Ghamry A, Tolba M (2018) Functionalized biochar derived from heavy metal rich feedstock: Phosphate recovery and reusing the exhausted biochar as an enriched soil amendment. *Chemosphere* 198:351–363. doi: 10.1016/j.chemosphere.2018.01.113
- Mukome FND, Zhang X, Silva LCR, Six J, Parikh SJ (2013) Use of chemical and physical characteristics to investigate trends in biochar feedstocks. *J Agric Food Chem* 61:2196–2204. doi: 10.1021/jf3049142
- Nanda S, Mohanty P, Pant KK, Naik S, Kozinski JA, Dalai AK (2013) Characterization of North American Lignocellulosic Biomass and Biochars in Terms of their Candidacy for Alternate Renewable Fuels. *Bioenergy Res* 6:663–677. doi: 10.1007/s12155-012-9281-4
- Oleszczuk P, Joško I, Kuśmierz M (2013) Biochar properties regarding to contaminants content and ecotoxicological assessment. *J Hazard Mater* 260:375–382. doi: 10.1016/j.jhazmat.2013.05.044
- Pinto ML, Mestre AS, Carvalho AP, Pires J (2010) Comparison of methods to obtain micropore size distributions of carbonaceous materials from CO₂ adsorption based on the Dubinin-radushkevich isotherm. *Ind Eng Chem Res* 49:4726–4730. doi: 10.1021/ie100080r
- Pletsch M, De Araujo BS, Charlwood B V. (1999) Novel biotechnological approaches in environmental remediation research. *Biotechnol Adv* 17:679–687. doi: 10.1016/S0734-9750(99)00028-2
- Qin J, Chen Q, Sun M, Sun P, Shen G (2017) Pyrolysis temperature-induced changes in the catalytic characteristics of rice husk-derived biochar during 1,3-dichloropropene degradation. *Chem Eng J* 330:804–812. doi: 10.1016/j.cej.2017.08.013
- Qu T, Guo W, Shen L, Xiao J, Zhao K (2011) Experimental study of biomass pyrolysis based on three major components: Hemicellulose, cellulose, and lignin. *Ind Eng Chem Res* 50:10424–10433. doi: 10.1021/ie1025453
- Rades S, Hodoroaba VD, Salge T, Wirth T, Lobera MP, Labrador RH, Natte K, Behnke T, Gross T, Unger WES (2014) High-resolution imaging with SEM/T-SEM, EDX and SAM as a combined methodical approach for morphological and elemental analyses of single engineered nanoparticles. *RSC Adv* 4:49577–49587. doi: 10.1039/c4ra05092d
- Rajkovich S, Enders A, Hanley K, Hyland C, Zimmerman AR, Lehmann J (2012) Corn growth and nitrogen nutrition after additions of biochars with varying properties to a temperate soil. *Biol Fertil Soils* 48:271–284. doi: 10.1007/s00374-011-0624-7
- Reid BJ, Jones KC, Semple KT (2000) Bioavailability of persistent organic pollutants in soils and sediments - A perspective on mechanisms, consequences and assessment. *Environ Pollut* 108:103–112. doi: 10.1016/S0269-7491(99)00206-7
- Rezania S, Ponraj M, Talaiekhosani A, Mohamad SE, Md Din MF, Taib SM, Sabbagh F, Sairan FM (2015) Perspectives of phytoremediation using water hyacinth for

- removal of heavy metals, organic and inorganic pollutants in wastewater. *J Environ Manage* 163:125–133. doi: 10.1016/j.jenvman.2015.08.018
- Ronsse F, van Hecke S, Dickinson D, Prins W (2013) Production and characterization of slow pyrolysis biochar: Influence of feedstock type and pyrolysis conditions. *GCB Bioenergy* 5:104–115. doi: 10.1111/gcbb.12018
- Shaaban A, Se SM, Dimin MF, Juoi JM, Mohd Husin MH, Mitan NMM (2014) Influence of heating temperature and holding time on biochars derived from rubber wood sawdust via slow pyrolysis. *J Anal Appl Pyrolysis* 107:31–39. doi: 10.1016/j.jaap.2014.01.021
- Sommers LE, Sposito G (1985) Chemical models of inorganic pollutants in soils. *Crit Rev Environ Control* 15:1–24. doi: 10.1080/10643388509381725
- Song B, Zeng G, Gong J, Liang J, Xu P, Liu Z, Zhang Y, et al (2017) Evaluation methods for assessing effectiveness of in situ remediation of soil and sediment contaminated with organic pollutants and heavy metals. *Environ Int* 105:43–55. doi: 10.1016/j.envint.2017.05.001
- Stapleton MG, Sparks DL, Dentel SK (1994) Sorption of Pentachlorophenol to HDTMA-Clay as a Function of Ionic Strength and pH. *Environ Sci Technol* 28:2330–2335. doi: 10.1021/es00062a017
- Sun F, Lu S (2014) Biochars improve aggregate stability, water retention, and pore-space properties of clayey soil. *J Plant Nutr Soil Sci* 177:26–33. doi: 10.1002/jpln.201200639
- Tan X, Liu Y, Zeng G, Wang X, Hu X, Gu Y, Yang Z (2015) Application of biochar for the removal of pollutants from aqueous solutions. *Chemosphere* 125:70–85. doi: 10.1016/j.chemosphere.2014.12.058
- Tang J, Zhu W, Kookana R, Katayama A (2013) Characteristics of biochar and its application in remediation of contaminated soil. *J Biosci Bioeng* 116:653–659. doi: 10.1016/j.jbiosc.2013.05.035
- Tülp HC, Fenner K, Schwarzenbach RP, Goss KU (2009) pH-dependent sorption of acidic organic chemicals to soil organic matter. *Environ Sci Technol* 43:9189–9195. doi: 10.1021/es902272j
- Vaccari FP, Baronti S, Lugato E, Genesio L, Castaldi S, Fornasier F, Miglietta F (2011) Biochar as a strategy to sequester carbon and increase yield in durum wheat. *Eur J Agron* 34:231–238. doi: 10.1016/j.eja.2011.01.006
- Venegas A, Rigol A, Vidal M (2015) Viability of organic wastes and biochars as amendments for the remediation of heavy metal-contaminated soils. *Chemosphere* 119:190–198. doi: 10.1016/j.chemosphere.2014.06.009
- Wilcox JB, Solutions E (2005) Learn more about Inorganic Compound Electrical and Thermal Solutions Sources and Types of Inorganic Pollu- tants
- Windeatt JH, Ross AB, Williams PT, Forster PM, Nahil MA, Singh S (2014) Characteristics of biochars from crop residues: Potential for carbon sequestration and soil amendment. *J Environ Manage* 146:189–197. doi: 10.1016/j.jenvman.2014.08.003
- Woolf D, Amonette JE, Street-Perrott FA, Lehmann J, Joseph S (2010) Sustainable biochar to mitigate global climate change. *Nat Commun* 1:1090–1091. doi: 10.1038/ncomms1053

- Xiao F, Pignatello JJ (2014) Effect of adsorption nonlinearity on the ph-adsorption profile of ionizable organic compounds. *Langmuir* 30:1994–2001. doi: 10.1021/la403859u
- Xiao X, Chen B, Chen Z, Zhu L, Schnoor JL (2018) Insight into Multiple and Multilevel Structures of Biochars and Their Potential Environmental Applications: A Critical Review. *Environ Sci Technol* 52:5027–5047. doi: 10.1021/acs.est.7b06487
- Xie T, Reddy KR, Wang C, Yargicoglu E, Spokas K (2015) Characteristics and applications of biochar for environmental remediation: A review. *Crit Rev Environ Sci Technol* 45:939–969. doi: 10.1080/10643389.2014.924180
- Xu R kou, Xiao S cheng, Yuan J hua, Zhao A zhen (2011) Adsorption of methyl violet from aqueous solutions by the biochars derived from crop residues. *Bioresour Technol* 102:10293–10298. doi: 10.1016/j.biortech.2011.08.089
- Yao H, Lu J, Wu J, Lu Z, Wilson PC, Shen Y (2013) Adsorption of fluoroquinolone antibiotics by wastewater sludge biochar: Role of the sludge source. *Water Air Soil Pollut* 224:. doi: 10.1007/s11270-012-1370-7
- Yuan Y, Macquarrie DJ (2015) Microwave Assisted Acid Hydrolysis of Brown Seaweed *Ascophyllum nodosum* for Bioethanol Production and Characterization of Alga Residue. *ACS Sustain Chem Eng* 3:1359–1365. doi: 10.1021/acssuschemeng.5b00094
- Zhang G, Zhang Q, Sun K, Liu X, Zheng W, Zhao Y (2011) Sorption of simazine to corn straw biochars prepared at different pyrolytic temperatures. *Environ Pollut* 159:2594–2601. doi: 10.1016/j.envpol.2011.06.012
- Zhang K, Chen B, Mao J, Zhu L, Xing B (2018) Water clusters contributed to molecular interactions of ionizable organic pollutants with aromatized biochar via Π -PAHB: Sorption experiments and DFT calculations. *Environ Pollut* 240:342–352. doi: 10.1016/j.envpol.2018.04.083
- Zhang M, Gao B, Varnoosfaderani S, Hebard A, Yao Y, Inyang M (2013a) Preparation and characterization of a novel magnetic biochar for arsenic removal. *Bioresour Technol* 130:457–462. doi: 10.1016/j.biortech.2012.11.132
- Zhang X, Wang H, He L, Lu K, Sarmah A, Li J, Bolan NS, Pei J, Huang H (2013b) Using biochar for remediation of soils contaminated with heavy metals and organic pollutants. *Environ Sci Pollut Res* 20:8472–8483. doi: 10.1007/s11356-013-1659-0
- Zhao L, Cao X, Mašek O, Zimmerman A (2013) Heterogeneity of biochar properties as a function of feedstock sources and production temperatures. *J Hazard Mater* 256–257:1–9. doi: 10.1016/j.jhazmat.2013.04.015
- Zhao L, Cao X, Zheng W, Scott JW, Sharma BK, Chen X (2016) Copyrolysis of Biomass with Phosphate Fertilizers to Improve Biochar Carbon Retention, Slow Nutrient Release, and Stabilize Heavy Metals in Soil. *ACS Sustain Chem Eng* 4:1630–1636. doi: 10.1021/acssuschemeng.5b01570
- Zheng W, Guo M, Chow T, Bennett DN, Rajagopalan N (2010) Sorption properties of greenwaste biochar for two triazine pesticides. *J Hazard Mater* 181:121–126. doi: 10.1016/j.jhazmat.2010.04.103

(This page intentionally left blank)

CHAPTER 2. LITERATURE REVIEW

List of contents	2-1
Abstract	2-2
2.1. Introduction	2-3
2.2. Physicochemical characteristics of biochar	2-6
2.2.1. Molecular structures	2-7
2.2.2. Surface area	2-8
2.2.3. Porosity	2-8
2.2.4. pH, point of zero net charge, EC and ash contents	2-11
2.2.5. Elemental composition and atomic ratio	2-12
2.2.6. Oxygen containing acidic functional groups	2-16
2.2.7. Inorganic contents	2-19
2.3. Biochar as universal sorbent	2-20
2.3.1. Remediation of organic pollutants	2-20
2.3.2. Remediation of inorganic pollutants	2-24
2.4. Unexpected results in remediation of pollutants	2-27
2.4.1. Perspective in physicochemical characteristics of biochar	2-27
2.4.2. Perspective in environmental factors	2-28
2.4.3. Perspective in analytics for biochar characterization	2-30
2.5. Conclusions	2-31
Reference	2-32

Abstract

Biochar is a carbonaceous material produced from feedstocks through pyrolysis. It has received a considerable attention as a universal sorbent for organic and inorganic pollutants; however, its effect has demonstrated a variety of results, owing to the variation in the physicochemical characteristics of biochar and pollutants under fluctuating environmental conditions. With increasing pyrolysis temperature, biochar exhibits a deformed porous structure, in which aromatic carbon sheets are condensed in an aligned turbostratic structure with a large surface area and porosity. The pH, point of zero net charge, electrical conductivity (EC), and ash content of biochar increase due to the deposition of alkali salts by the progressive thermal decomposition of feedstocks. Furthermore, the behavior of pollutants differ based on surrounding environmental conditions, as the ionizable organic pollutants changed with the pK_a , and the increase in the ionic valence of heavy metals and oxyanions is influenced by the interaction with hydrogen or hydroxyl ions in aqueous solutions. Consequently, unexpected results occur in the remediation of pollutants to biochar under varying environmental conditions. This review aims to provide an overview of the changing physicochemical characteristics of biochar to evaluate as a biosorbent, and discuss the reasons for the unexpected results from the perspectives of biochar characteristics, environmental factors, and measurement technology. We believe that lab-scale studies for identifying the sorption mechanisms between biochar and pollutants are essential for designing remediation strategies more effectively by controlling the bioavailability and leachability in real environments.

Keywords

Physicochemical characteristics, Biochar, Sorption, Ionizable pollutants, pH

2.1. Introduction

Biochar is carbon-rich material produced from feedstocks, such as wood, leaves, or manure through pyrolysis under oxygen deficient conditions (Lehmann 2007a; Yuan et al. 2011). Variations in feedstocks type and pyrolysis temperature cause different physicochemical characteristics of biochar (Kloss et al. 2012; Ronsse et al. 2013; Mimmo et al. 2014), since the thermal decomposition of molecular structure in feedstocks occurs at specific pyrolysis temperatures (Chen et al. 2008; Phuong et al. 2015). Despite the use of the same feedstocks for the production of biochar, the physicochemical characteristics of biochar vary with the pyrolysis temperatures used in the production. For example, pine needle biochar produced at lower pyrolysis temperatures has an amorphous aliphatic fraction; however, with increasing pyrolysis temperature, this biochar exhibits an increasing aromatic fraction with a condensed aromatic core (Chen et al. 2008). This is because the cellulose and lignin in plant biomass are degraded at 220–315 °C and at > 400 °C, respectively (Qu et al. 2011; Mimmo et al. 2014). *Miscanthus* biochar increase in carbon content and specific surface area with increasing pyrolysis temperatures, owing to progressive thermal decomposition (Mimmo et al. 2014; Elmay et al. 2015); meanwhile, oxygen containing acidic functional groups and positively charged surface area were decreased (Lee et al. 2018). Not only does plant derived biochar have different physicochemical characteristics compared with biochar produced from animal manure, but it also contains a larger inorganic fraction (Zhang et al. 2013b). Such various physicochemical characteristics during the production of biochar would cause a problem as a biosorbent because the sorption capacity and affinity of biochar would not be uniform for the remediation of pollutants.

The remediation of polluted soil and water environments with organic and inorganic molecules is an urgent problem, as pollution is a direct threat to

human health (Wasi et al. 2013; Abdel-Shafy and Mansour 2016). However, solving the problem of pollution is challenging because both biochar and pollutants undergo transition and transformation with changes in environmental conditions, such as pH, ion composition, temperature, and redox conditions. Furthermore, pollutants can interact with various elements in soil and water environments, resulting in a variety of sorption behavior. Organic acids such as 2,4-D, benzoic acid, and chlorinated phenols have a neutral charge below pK_a (Uchimiya et al. 2012), whereas they are negatively charged at pH above pK_a , owing to deprotonation. Meanwhile, the organic base, composed of simazine and triazine, is positively charged below pK_a because of protonation, while it has a neutral charge above pK_a (Lee et al. 2018). Heavy metals are typically known as positively charged ions under neutral pH conditions; thus, they would be transported from soil to water with uptake by organisms, resulting in oxidative stress. Under alkali conditions, heavy metals could be precipitated with hydroxyl ions, whereas molecular structures would be transformed in the presence of other negatively charged elements in the soil and water (Basualto et al. 2006; Boparai et al. 2013). Oxyanions are negatively charged molecules formed with oxygen, and phosphate and arsenate (As(V)) are representative oxyanion species. Phosphate is well known as an essential element for plant growth, whereas As(V) is considered a notorious oxyanion because of its complex fate in soil and water environments. Under oxic conditions, As(V) coexists with H_3AsO_4 , $H_2AsO_4^-$, $HAsO_4^{2-}$, and AsO_4^{3-} due to have three pK_a (Kong et al. 2017); it also transforms to arsenite (As(III)), which is a reduced form of As(V) and is frequently reported as residing in the suboxic and anoxic conditions of soils. Consequently, oxyanions could be precipitated with positively charged elements or sorbed with the positively charged surface of soil and water components. As such, their behavior depends on the surrounding environmental conditions, such as pH, redox potential, and ion composition.

Of the various remediation technologies for pollutants, sorption, which occurs as the sorbate (organic and inorganic pollutants) is attached to the sorbent, is the most traditional and effective technique (El-Geundi 1991; Dąbrowski 2001). There are numerous studies on the sorption of pollutants, and sorbent is typically used to reduce the mobility and bioavailability of pollutants in soil and water. For example, calcite, a soil mineral produced from natural substances, has been shown to efficiently sorb arsenate (Sø et al. 2008); in addition, phyllosilicates, metal oxides, and synthetic organo–mineral complexes are effective sorbents for arsenate and phosphate (Violante and Pigna 2002). Soil organic matter is well known as sorbents for organic pollutants. Humin, which is the insoluble fraction of soil organic components, is valuable for reducing the capacity of sulfamethazine (Guo et al. 2017); meanwhile, humic or fulvic acid, which is the soluble fraction of soil organic components, is effective in managing europium (Tan et al. 2008). Recently, synthesized polymers, such as carbon nanotubes and activated carbon, have been frequently used for remediation of pollutant (Abdel-Halim and Al-Deyab 2011). Multiwall carbon nanotubes have been shown to diminish the amounts of capacity for pyrene, phenanthrene, and naphthalene (Yang et al. 2006), while activated carbon has demonstrated a comparative effect in reducing heavy metal concentration (Pyrzyńska and Bystrzejewski 2010).

Biochar is the most effective eco-friendly and cost-effective sorbent for environmental pollutants in soil and aqueous environments (Ahmad et al. 2014), resulting in heterogeneous physicochemical characteristics (Sun et al. 2011a; Yao et al. 2011; Deng et al. 2017). There are numerous studies regarding the sorption of biochar with pollutants. For example, the sorption amount of organic pollutants to biochar produced from woodchip were decreased in Minnesota soil (Spokas et al. 2009); in addition, pine needle biochar amended to the soil was shown to enhance the sorption of polycyclic aromatic

hydrocarbons (Chen and Yuan 2011). However, biochar pyrolyzed at temperatures of 200–700 °C (100 °C interval) demonstrated different levels of effectiveness for the sorption of phthalic acid esters because of differences in the polar and aliphatic domains of biochar (Sun et al. 2012). The sorption of heavy metals were also immobilized by the biochar produced from plant biomass (Park et al. 2013), and the sorption of ammonium, nitrate, and phosphate to biochar pyrolyzed from corn stover and oak wood increased owing to the deposition of minerals on the surface of biochar (Hollister et al. 2013). The remediation efficiency of pollutants varied in biochar, as the physicochemical characteristics of biochar govern the sorption mechanisms; however, this has not yet been comprehensively detailed. Therefore, it is important to understand not only the physicochemical characteristics of biochar but also the ionizable species of pollutants under fluctuating environmental conditions to estimate the sorption capacity and affinity in soil and water environments.

This review summarizes the diversity in the physicochemical characteristics of biochar by feedstocks type and pyrolysis temperature, the effectiveness of biochar as biosorbents for organic and inorganic pollutants in soil or water environments, and the unexpected results for the remediation of pollutants.

2.2. Physicochemical characteristics of biochar

Each biochar has distinctive physicochemical characteristics owing to the variety of constituent and molecular structures in feedstocks (Mukome et al. 2013; Xu et al. 2014; Xie et al. 2015). Biochar derived from animal biomass has more enrichment mineral content, along with higher electric conductivity and ash contents, as compared with biochar produced from plant biomass (Uchimiya and Hiradate 2014). Plant biochar has an abundance in organic

carbon content due to the contents of cellulose, hemicellulose, and lignin (Xu et al. 2014). However, the variation in the physicochemical characteristics of biochar with increasing pyrolysis temperatures demonstrates a similar tendency, regardless of the type of feedstocks (Singh and Cowie 2010; Ronsse et al. 2013).

2.2.1. Molecular structures

With increasing pyrolysis temperature, vulnerable organic components in feedstocks are released by thermal decomposition (Qu et al. 2011; Mimmo et al. 2014). The molecular structure of feedstocks, which exhibits a higher fraction of aromatic carbon and a highly disordered amorphous structure, is developed through conjugated aromatic carbon sheets and an aligned turbostratic structure (Fig. 2-1). The further progressive thermal decomposition of biomass led to a graphite structure (Chen et al. 2007; Mimmo et al. 2014). Phuong et al. (2015) demonstrated that the structure formation of rice husk and rice straw were amorphous, whereas the biochar was characterized as having a graphite-like structure confirmed by SEM analysis. Gómez-Zorrilla Martín et al. (2013) reported that the higher pyrolysis temperature resulted in the disappearance of crystalline cellulose in the wood biomass, indicating the absence of an amorphous structure. The result of this was the formation of a graphite structure with improved layer assignment, as demonstrated by SEM and XRD analysis. Bekiaris et al. (2016) observed the structural transformation of biochar with increasing pyrolysis temperature using FTIR spectra; they noted that the peaks corresponded to the O-H stretching vibration, with the asymmetric and symmetric C-H stretching vibrations diminished; meanwhile, the C=C stretching vibration in aromatic structures was increased, regardless of feedstocks type.

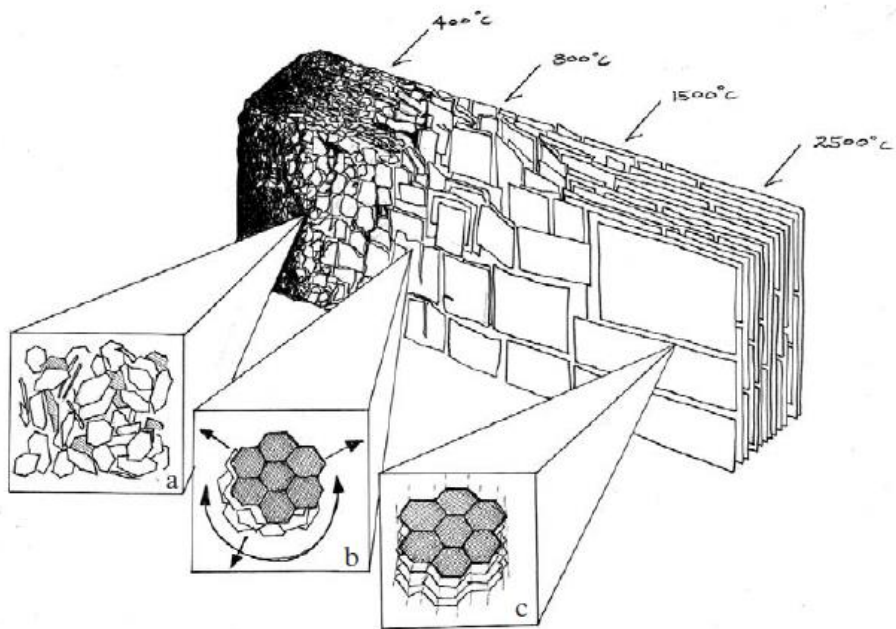
2.2.2. Surface area

The surface area of biochar is controlled by the pyrolysis temperature, since the volatile materials in feedstocks are decomposed with increasing pyrolysis temperature (Zhao et al. 2013; Domingues et al. 2017). Progressive thermal decomposition caused the formation of channel structures with a larger pore structure and increased surface area (Mukherjee et al. 2011; Sigmund et al. 2016). Lua et al. (2004) used Brunauer–Emmett–Teller (BET) analysis to show that the surface area of biochar produced pistachio-nut shells increased with pyrolysis temperature owing to the evolution of volatile materials in the feedstocks, resulting in an increase in the pore structure. Cantrell et al. (2012) showed that the most drastic increase in surface area of animal manure biochar was demonstrated by biochar produced at pyrolysis temperature of 700 °C due to the higher thermal degradation of organic molecules in the feedstocks. Although various types of feedstocks were used for biochar production, the change in the surface area with increasing pyrolysis temperature was consistent, regardless of feedstocks used; meanwhile, the biochar produced from plant biomass exhibited a greater surface area than the biochar produced from animal residues (Zhao et al. 2013; Shaaban et al. 2014; Domingues et al. 2017).

2.2.3. Porosity

The pyrolysis temperature determines not only the surface area but also the porosity, as these physical characteristics of biochar are governed by the thermal decomposition of organic volatiles in the feedstocks. The pore size distribution was correlated to the porosity and surface areas, as most of the contribution to the surface area came from the micro-pores (> 1.5 nm) of biochar, according to Gai et al. (2014). Furthermore, nano-pores (< 1.5 nm) were converted to micropores with increasing pyrolysis temperature, since the

Fig. 2-1 Schematic illustration for evolution of porous structures with increasing pyrolysis temperature. This figure is from the previous Dwonie et al (2012) study, it is included for better understanding the molecular scale transformation of biochar structure.



nano-pores collapsed between the adjacent pores, resulting in an increase in pore structures (Özçimen and Ersoy-Meriçboyu 2010; Sigmund et al. 2016). Angin (2013) showed that the BET surface area and micro-pore volume of biochar changed with increasing pyrolysis temperature and heating rate. Chen et al. (2014) showed that the pore size and pore volume of municipal sewage sludge biochar increased with increasing pyrolysis temperature, and Ahmad et al. (2012) demonstrated that a higher surface area and pore volume of biochar yielded greater sorption capacity of trichloroethylene. In addition, plant biomass biochar pyrolyzed at higher pyrolysis temperatures, which exhibited a higher BET surface area and micro-pores, were more effective in the sorption of heavy metal in the soil (Uchimiya et al. 2011b). Consequently, the porosity and surface area are critical factors that govern the capacity of biochar for the remediation of pollutants and retention of nutrients.

2.2.4. pH, point of zero net charge, electrical conductivity (EC) and ash contents

The chemical composition of feedstocks changes with increasing pyrolysis temperature, as oxygen containing functional groups are eliminated while alkali salts accumulate on the biochar (Uchimiya et al. 2011b; Al-Wabel et al. 2013; Singh et al. 2017). The oxygen containing functional groups are known as carboxylic, lactonic, and phenolic acidic groups (Tsechansky and Graber 2014; Essandoh et al. 2015), whereas the alkali salts are soluble salts, carbonates, metal oxides, hydroxides, and silicates (Okuno et al. 2005; Singh et al. 2010). Both oxygen containing functional groups and alkali salts contribute to the fundamental chemical characteristics of biochar, such as pH, point of zero net charge (PZNC), electrical conductivity (EC), and ash content (Usman et al. 2015; Tag et al. 2016) (Table 2-1). Lehmann (2007) showed that the pH of biochar increased with pyrolysis temperature, with a dramatic increase observed at pyrolysis temperature of 500 °C, since the maximum

thermal decomposition occurs in agricultural biomass at that temperature. Mukherjee et al. (2011) showed that the increasing pH with pyrolysis temperature was caused by the depletion of oxygen containing acidic functional groups accompanied by decreasing PZNC (Chen et al. 2014; Zhang et al. 2015). Gai et al. (2014) indicated that the EC and ash content of the four types of biochar increased with increasing pyrolysis temperature, because the volatile materials in the feedstocks were decomposed through consistent progressive thermal decomposition by the remaining salts. Yuan et al. (2015) also indicated that the pH, EC, and ash content of biochar produced from sewage sludge increased with pyrolysis temperature, resulting in an increase in the basic functional groups and the deposition of alkali salts (Usman et al. 2015). Therefore, these variations in the fundamental chemical characteristics of biochar affect not only the remediation of pollutant behavior but also the soil fertility by nutrient retention (Sun et al. 2011a; Essandoh et al. 2015). Furthermore, understanding the effect of fundamental chemical characteristics of biochar were important for biochar utilization (van Zwieten et al. 2010; Singh et al. 2017).

2.2.5. Elemental composition and atomic ratio

Volatile materials and oxygen containing acidic functional groups in feedstocks were released to the atmosphere during the production of biochar with increasing pyrolysis temperature (Fang et al. 2014; Luo et al. 2015); meanwhile, the carbon structure is maintained and aligned with turbostratic structures. This is confirmed by the variation of atomic ratios such as (O+N)/C, H/C, and O/C, reflective of the polarization, carbonization, and hydrophilization, respectively (Nguyen et al. 2007; Xiao et al. 2016). Al-Wabel et al. (2013) demonstrated that the elemental composition and the concentration of oxygen, hydrogen, and sulfur of biochar produced from conocarpus waste

Fig. 2-2 Van Krevelen diagram of various biochar derived from various feedstocks under different pyrolysis temperature. The gray symbols indicated the previous study according to Ahmad et al. (2014) and colored symbols represented the updated results in the other previous studies.

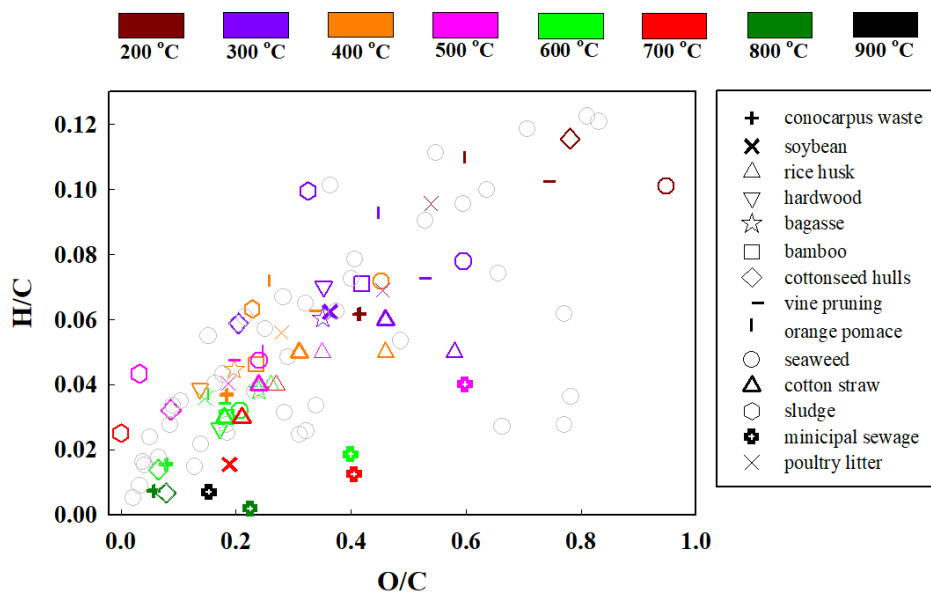


Table 2-1 Ash and elemental contents of biochar produced under various feedstocks and pyrolysis temperatures.

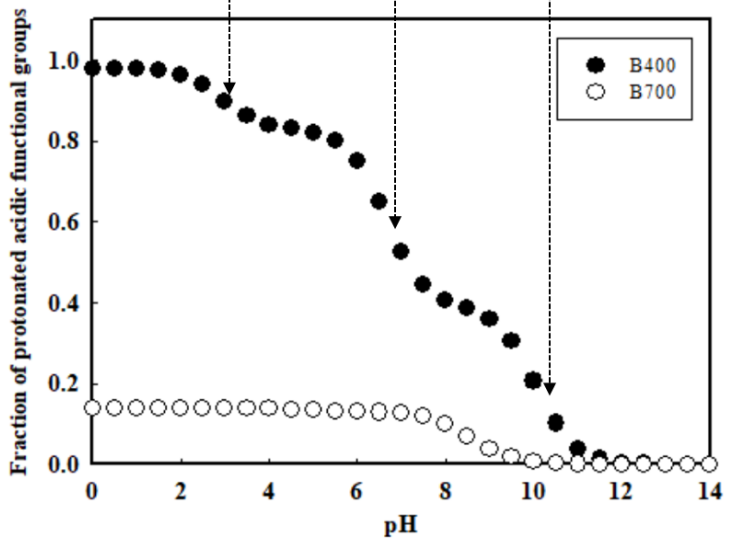
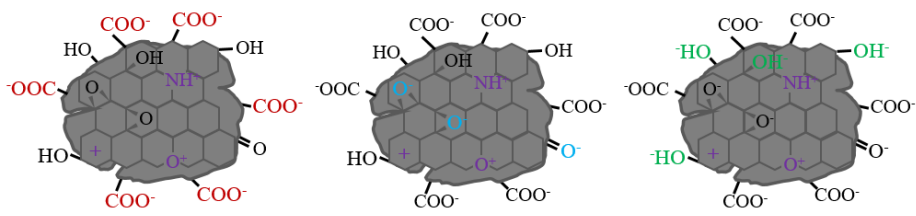
Feedstocks	Pyrolysis temperature (°C)	Ash (%)	Elemental contents (g kg ⁻¹)						References
			Na	K	Ca	Mg	P	Fe	
Poultry litter	350	9.3	1.14	1.24	0.61	0.53	-	-	Tag et al. (2016)
	300	12.8	1.71	1.55	0.25	0.19	-	-	
	350	18.4	2.50	1.82	0.02	0.03	-	-	
	500	21.8	2.88	2.76	0.01	0.02	-	-	
	600	29.3	3.10	3.29	0.01	0.04	-	-	
Sewage sludge	300	65.8	-	7.47	20.6	6.19	38.8	34.5	Yuan et al. (2015)
	400	75.5	-	8.99	22.7	6.96	42.7	38.4	
	500	80.6	-	10.1	23.9	7.47	44.7	40.8	
	600	83.8	-	13.3	24.0	7.86	45.1	41.7	
	700	86.8	-	16.6	25.8	8.06	49.2	43.1	
Municipal sewage	500	74.2	1.17	8.52	59.3	14.7	18.2	31.1	Chen et al. (2014)
	600	77.9	1.72	8.50	62.7	15.5	18.8	33.6	
	700	81.5	1.38	9.94	64.4	16.4	20.4	35.3	
	800	83.9	1.93	9.29	65.8	16.6	19.3	35.8	
	900	88.1	3.42	8.68	69.6	17.5	20.2	37.2	
Vine pruning	250	5.0	0.06	0.06	0.07	0.03	-	-	Tag et al. (2016)
	300	6.8	0.08	0.07	0.04	0.02	-	-	
	350	8.3	0.08	0.07	0.04	0.02	-	-	
	500	10.6	0.10	0.08	0.02	0.02	-	-	
	600	11.5	0.14	0.11	0.01	0.01	-	-	
Palm tree	300	14.4	4.0	21.8	48.5	15.3	-	-	Usman et al. (2015)
	400	16.3	4.2	21.7	60.4	15.7	-	-	
	500	19.7	4.8	22.3	58.1	19.3	-	-	
	600	20.7	5.3	25.8	77.7	19.0	-	-	
	700	21.1	5.0	26.9	76.5	19.2	-	-	
	800	21.4	5.8	27.1	80.8	20.2	-	-	
Orange pomace	350	6.7	0.03	0.03	0.11	0.03	-	-	Tag et al. (2016)
	300	9.4	0.05	0.06	0.03	0.01	-	-	
	350	11.3	0.06	0.06	0.02	0.01	-	-	
	500	14.2	0.07	0.07	0.01	0.01	-	-	
	600	16.3	0.10	0.10	0.01	0.00	-	-	
Seaweed	250	22.9	2.17	3.24	0.87	0.07	-	-	Tag et al. (2016)
	300	28.7	2.86	3.73	0.75	0.06	-	-	
	350	33.4	2.90	4.12	0.22	0.08	-	-	
	500	40.0	3.33	4.51	0.21	0.08	-	-	
	600	42.7	4.29	5.49	0.16	0.08	-	-	
Sugar cane straw	400	11.3	-	15.0	6.8	1.9	1.1	-	Melo et al. (2013)
	500	11.7	-	19.0	7.4	2.4	1.2	-	
	600	13.1	-	18.0	9.1	2.6	1.1	-	
	700	13.2	-	22.0	9.5	2.8	1.1	-	

decreased with increasing pyrolysis temperature, whereas the carbon content increased, causing a decrease in the (O+N)/C, H/C, and O/C ratios due to the release of volatile materials from the feedstocks. Xu et al. (2014) explained that the contents of nitrogen, hydrogen, and oxygen in manure derived biochar decreased with increasing pyrolysis temperature owing to the volatilization of organic materials in the manure biomass, followed by the decrease in (O+N)/C, H/C, and O/C. Although different types of feedstocks were used for biochar production, the variation in elemental composition was identical with increasing pyrolysis temperature, since the volatile organic material in the feedstocks was released through progressive thermal decomposition (Mukome et al. 2013).

2.2.6. Oxygen containing acidic functional groups

During the decomposition of volatile organic materials in feedstocks, oxygen containing acidic functional groups were also released with increasing pyrolysis temperature, which decreased the area of the hydrophilic surface; meanwhile, the hydrophobic surface experienced opposite behavior (Kloss et al. 2012; Shaaban et al. 2014; Fan et al. 2018). The acidic functional groups on surface of biochar are generally known as carboxylic, lactonic, and phenolic, and their abundance is determined by the chemical composition in feedstocks (Mukherjee et al. 2011; Fidel et al. 2013). The abundance of acidic functional groups decreases with increasing pyrolysis temperature (Fig. 2-3) and exhibits an identical pattern to those of various types of feedstocks (Chun et al. 2004; Suliman et al. 2016). The qualification and quantification of acidic functional groups on biochar surface were conducted by Boehm titration methods (Boehm 1994; Contescu et al. 1997), quantifying carboxylic, lactonic, and phenolic acidic functional groups through titration with three different bases (NaHCO_3 , Na_2CO_3 , and NaOH) (Fidel et al.

Fig. 2-3 Variation of charged surface of biochar with increasing pH by deprotonated acidic functional groups (e.g., carboxylic, lactonic, and phenolic) on biochar surface.



2013; Tsechansky and Graber 2014). Suliman et al. (2016) showed that the carboxylic, lactonic, and phenolic acidic functional groups of plant biomass biochar decreased with increasing pyrolysis temperature, owing to the release of volatile materials in the plant biomass, in agreement with the XPS result. Suliman et al. (2016) also indicated that the carboxylic, lactonic, and phenolic acidic functional groups on the surface of biochar produced from cow manure decreased with increasing pyrolysis temperature, which might be demonstrated by the decarboxylation, dehydration, and oxidation of feedstocks during thermal decomposition. Uchimiya et al. (2011a) insisted that the carboxyl and phenolic functional groups on biochar surface played an important role in the sorption of heavy metals, owing to the providing the ligand surface. In addition, the charges of carboxylic, lactonic, and phenolic functional groups on the biochar surface changed with respective logarithmic acid dissociation constant (pK_a) (Leon and Radovic 1991), and the variation of the surrounding pH condition could affect the surface charge of biochar due to the deprotonation of acidic functional groups as well as ionizable pollutants with increasing pH (Kloss et al. 2012; Bian et al. 2015). Therefore, the variation of the charged species for acidic functional groups was important for identifying sorption mechanisms between biochar and ionizable pollutant toward a better understanding the sorption behavior (Uchimiya et al. 2011a; Pardo et al. 2016).

2.2.7. Inorganic contents

The contents of inorganic components in biochar were determined by the fundamental chemical composition of the feedstocks employed for biochar production (Kloss et al. 2012). Reportedly, animal derived biochar has greater inorganic content than plant-derived biochar (Cantrell et al. 2012; Uchimiya and Hiradate 2014). Furthermore, inorganics greater accumulated in biochar pyrolyzed at higher temperatures owing to the progressive release of volatile

organic materials (Wang 2017; Huang et al. 2018a). Zhao et al. (2013) showed that the cation contents of biochar produced from both pig manure and wheat straw increased with pyrolysis temperature, whereas the cation concentration of wheat straw biochar was lower than the concentration of pig manure biochar using XRF results (Mohan et al. 2014a). Ding et al. (2014) demonstrated that lead sorption to biochar produced bagasse was controlled by cation exchange and complexation between the biochar and the lead ion. This is because the biochar exhibited greater cation sorption capacity with increasing pyrolysis temperature. Huang et al. (2018) explained that the cadmium sorption mechanism to biochar derived from chicken manure was determined from complexation, precipitation, and cation exchange between the mineral contents of biochar and cadmium ion. Thus, the sorption capacity of cadmium varied with pH condition as a result of the change in both the charged species of cadmium and charged surface of biochar, resulting in the deprotonation of the acidic functional groups (An and Dultz 2007; Zarzycki and Rosso 2018). Consequently, studies characterizing the interaction between biochar and ionizable pollutants under varied environmental conditions are essential for revealing the sorption mechanisms more accurately.

2.3. Biochar as Universal Sorbent

2.3.1. Remediation of organic pollutants

Biochar has been used universally as a sorbent to decrease the bioavailability of organic pollutants in soil and aqueous environments. Because of its effectiveness and cost savings, biochar has received remarkable attention since 2000, and numerous studies are still in progress to characterize the heterogeneity of physicochemical characteristics during the production of biochar. Since, the sorption of pollutants to biochar is controlled by the heterogeneity of its physicochemical characteristics. Under sorption isotherm

Table 2-2 Summary of the sorption isotherm parameters and matrix involved in sorption of organic pollutants produced from various feedstocks at different pyrolysis temperature (PT). The K_F is a constant related to sorption capacity.

Organic pollutant	Feedstocks	PT (°C)	Matrix	K_F	References
Atrazine	pig manure	300	water, soil, biochar	7.38	Ren et al. (2018)
Atrazine	wood chip	450	water, biochar	541	Zheng et al. (2010)
Catechol	oak	250	water, biochar	5014	Kasozi et al. (2010)
		400		1495	
		650		11384	
Catechol	pine	250	water, biochar	1212	Kasozi et al. (2010)
		400		305	
		650		2901	
Catechol	grass	250	water, biochar	6768	Kasozi et al. (2010)
		400		4230	
		650		23624	
Fluridone	grass	200	water, soil, biochar	0.15	Sun et al. (2011)
		300		44.2	
		400		606.1	
		500		437.4	
		600		554	
Fluridone	wood	200	water, soil, biochar	0.38	Sun et al. (2011)
		300		35.2	
		400		342.2	
		500		126.9	
		600		405.9	
Naphthalene	pine needle	100	water, biochar	219.8	Chen et al. (2008)
		200		1086.4	
		300		3118.9	
		400		16672.5	
		500		19319.7	
		600		12502.6	
		700		120781.4	
Naphthalene	orange peel	200	water, biochar	1698.2	Chen et al. (2009)
		300		4570.9	
		400		6760.8	
		500		1778.3	
		600		1412.5	
Naphthalene	pine wood	700	water, soil, biochar	58884.4	Chen et al. (2012)
		150		152.4	
		250		2722.7	
		350		10543.9	
		500		58076.4	
Phenanthrene	poultry litter	400	water, biochar	281.8	Sun et al. (2011)
	wheat straw	400		120.2	
Phenanthrene	sawdust	350	water, soil, biochar	0.35	Zhang et al. (2010)
		700		2.10	
Simazine	corn straw	100	water, biochar	124	Zhang et al. (2011)
		200		574	
		300		2669	
		400		1618	
		500		3133	
Simazine	wood chip	450	water, biochar	514	Zheng et al. (2010)
	miscanthus	400		803.3	

Table 2-3 Summary of the sorption isotherm parameters and matrix involved in sorption of inorganic pollutants produced from various feedstocks at different pyrolysis temperatures (PTs).

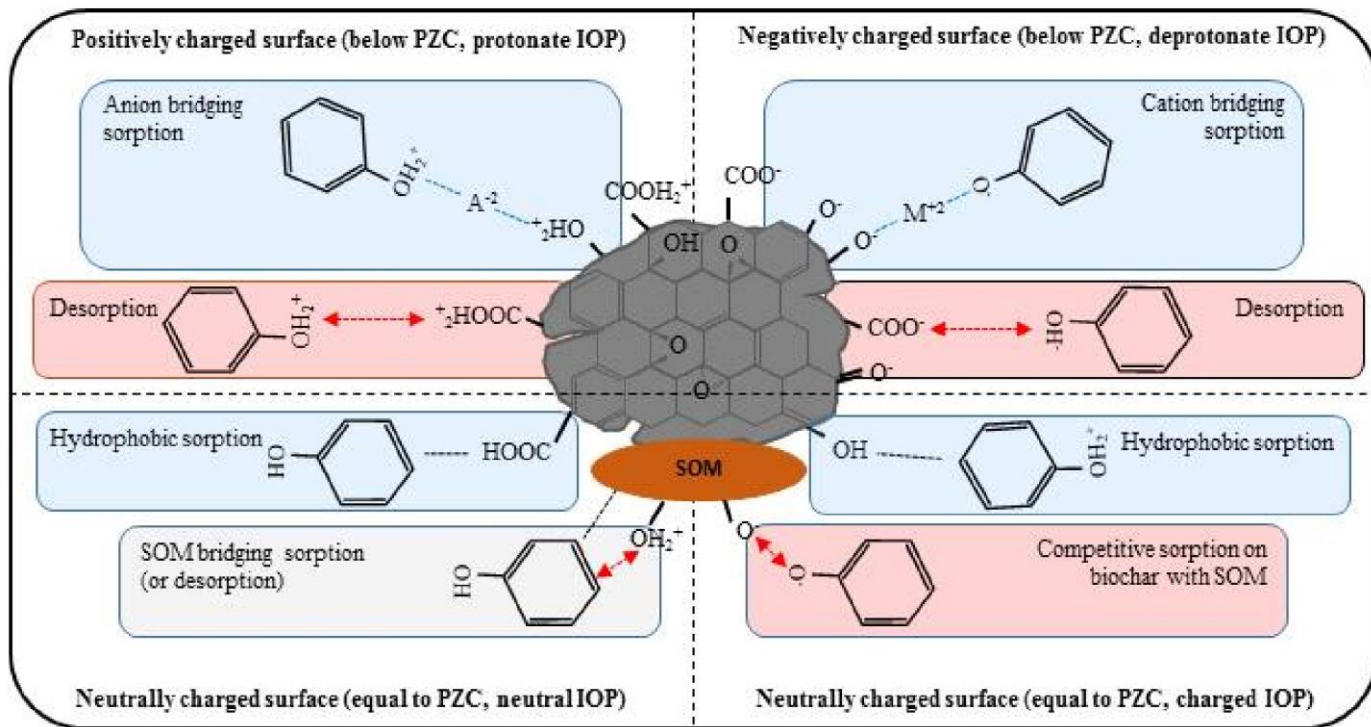
Inorganic pollutant	Feedstocks	PT (°C)	Better fit isotherm	Isotherm parameter	References
Arsenate	municipal waste	400	Langmuir	0.0172	Jin et al. (2014)
		500		0.1763	
		600		0.1300	
Arsenate	perilla leave	300	Langmuir	0.0277	Niazi et al. (2017)
		700		0.0519	
Arsenate	oak wood	500	Langmuir	0.0280	Zama et al. (2017)
Arsenite	peanut shell	350	Freundlich	0.0017	
		450		0.0011	
		550		0.0013	
Arsenite	mulberry wood	650	Langmuir	0.0008	
		350		0.0001	Zama et al. (2017)
		550		0.000394	
Cadmium	peanut shell	650	Freundlich	0.0004	
		350		0.0002	Zama et al. (2017)
		450		0.0007	
Cadmium	corn cobs	550	Langmuir	0.0005	
		650		0.0014	
		350		0.322	Zama et al. (2017)
Cadmium	dairy manure	450	Langmuir	0.588	
		550		0.416	
		650		0.526	
Cadmium	poultry manure	200	Langmuir	0.285	Xu et al. (2013)
		350		Freundlich	
Cadmium	poultry manure	350	Freundlich	0.0001	Zama et al. (2017)
		450		0.0001	
		550		0.0005	
Copper	corn straw	600	Langmuir	0.1970	Chen et al. (2011)
		450		0.1068	
Copper	dairy manure	200	Langmuir	0.762	Xu et al. (2013)
		350		Freundlich	
Lead	buckwheat	350	Freundlich	0.0005	Zama et al. (2017)
		450		0.0005	
		550		0.0006	
		650		0.0010	
Lead	corn cobs	350	Freundlich	0.0006	Zama et al. (2017)
		450		0.0003	
		550		0.0002	
		650		0.0002	
Lead	dairy manure	200	Langmuir	0.641	Cao et al. (2009)
		350		0.452	
Lead	poultry manure	350	Freundlich	0.0006	Zama et al. (2017)
		450		0.0007	
		550		0.0008	
		650		0.0008	
Phosphate	sugar cane	300	Langmuir	0.0724	Trazzi et al. (2016)
		500		0.1271	
		700		0.1391	
Phosphate	miscanthus	300	Langmuir	0.0868	Trazzi et al. (2016)
		500		0.1524	
		700		0.1695	

studies (Table 2-2), Cao et al. (2009) confirmed that dairy manure biochar affected the sorption ability of atrazine, Chen et al. (2008) showed that biochar produced from pine needles was effective in the sorption of naphthalene, nitrobenzene, and 1, 3-dinitrobenzene in an aqueous solution, and Chen and Chen (2009) showed that the orange peel biochar with increasing pyrolysis temperature enhanced the sorption ability of naphthalene and 1-naphthol through pore filling mechanisms. Based on these studies, the expectation of a promising effectiveness of biochar in the soil environment has risen, whereby soils were amended with biochar for the remediation of environmental pollutants to improve soil health and fertility. Yu et al. (2009) indicated that the plant uptake of carbofuran and chlorpyrifos were reduced in soil amended with the biochar pyrolyzed at 850 °C. Sarmah et al. (2010) revealed that the biochar retained the estrogenic steroid hormone and its primary metabolite in the farm soil. Yu et al. (2010) also showed that the soil amended with biochar enhanced the sorption of the pesticide pyrimethanil, and the sorption capacity was increased in the biochar at higher pyrolysis temperature. Zhang et al. (2010) reported that the soil amendment of biochar derived from *Pinus radiata* improved the sorption of phenanthrene. The sorption of phenanthrene to biochar pyrolyzed at higher temperatures was more affordable owing to the higher porosity and surface area. However, despite the considerable sorption ability of biochar toward organic pollutants, the fundamental physicochemical characteristics of biochar responsible for the sorption mechanisms are still not understood comprehensively; this is due not only to the heterogeneity of the physicochemical characteristics of biochar but also the heterogeneous matrix of the soil, which consists of organic matter, phyllosilicates, and metal (hydro)oxides, along with water and air together.

2.3.2 Remediation of inorganic pollutants

Organic pollutants as well as inorganic pollutants were sorbed by biochar to reduce the mobility and bioavailability in aqueous and soil environments (Table 2-3). Cao et al. (2009) confirmed that the sorption of lead to biochar produced from dairy manure was effective under aqueous conditions. Liu and Zhang (2009) also found that the remediation of lead using biochar derived plant biomass showed an effective decrease through a physical endothermic process, and Uchimiya et al. (2010) revealed that the mobility of copper, cadmium, nickel, and lead was effectively decreased by the surface sorption and partitioning mechanisms, resulting from the application of biochar produced broiler litter. Furthermore, the sorption studies using biochar in the soil matrix were also conducted to assess the ability of remediation for the oxyanions. Steiner et al. (2008) confirmed that the nitrogen retention and plant uptake increased in the soil amended with biochar. Hartley et al. (2009) found that the application of *Miscanthus* biochar in arsenic polluted soils were affected by the enhanced arsenic mobility, which also enhanced the availability of phosphorus due to competition on the sorption site. Ding et al. (2010) indicated that the retention of ammonium nitrogen was elevated with the application of biochar produced from bamboo biomass to the soil through the resulting cation exchange. Namgay et al. (2010) demonstrated that the mobility of arsenic, cadmium, copper, lead, and zinc in soil decreased with the application of biochar. In contrast, the mineral content in biochar was decreased owing to the fluctuation of the surrounding environment; this mineral content would serve as a fertilizer or toxicant in the soil environment. Brockhoff et al. (2010) showed that the mineral nutrition in the soil amended with biochar increased owing to the released nitrogen from the biochar. Warren et al. (2009) determined that the biochar produced from animal bone could serve as a potential phosphorus fertilizer due to the dissolution of the phosphorus in this biochar. Therefore, the production of biochar for the remediation of inorganic

Fig. 2-4 Schematic illustration of interaction between biochar and ionizable environmental pollutants under changing environmental factors (e.g., pH, cationic and anionic valence, and organic matter).



pollutants should consider not only the fundamental physicochemical characteristics of biochar but also the environmental conditions, because the physicochemical characteristics of biochar and chemical species are complexly controlled by the fluctuation of the surrounding environment.

2.4. Unexpected results in remediation of pollutants

2.4.1. Perspectives in physicochemical characteristics of biochar

Biochar exhibits various physicochemical characteristics, which are mainly determined by the conditions during the pyrolysis and types of feedstocks (Lehmann 2007a; Özçimen and Ersoy-Meriçboyu 2010). This indicates that identical samples of feedstocks used for biochar production would exhibit disparate physicochemical characteristics owing to the difference in pyrolysis temperatures (Luo et al. 2015; Han et al. 2016). If identical feedstocks with identical pyrolysis temperatures were employed for biochar production, it would still produce distinct physicochemical characteristics due to the lack of standardization in biochar production methods worldwide (Cha et al. 2016; Suliman et al. 2016; Domingues et al. 2017). Consequently, the factors contributing to the sorption mechanisms of biochar and a fundamental understanding of physicochemical characteristics are still unclear, demonstrating the controversial results regarding the effectiveness of remediation (Zhang et al. 2010; Sun et al. 2011b). Both Namgay et al. (2010) and Park et al. (2011) demonstrated cadmium sorption to green waste biochar pyrolyzed at 550 °C, and the difference in the amount of sorption capacity was due to the individual heterogeneous physicochemical characteristics of biochar under different soil environmental conditions. Jiang et al. (2012a and 2012b) indicated that the amount of lead sorption on rice straw biochar produced at pyrolysis temperature of 300 °C showed contradictory results because of the heterogeneous physicochemical characteristics of biochar under various soils. The amount of

sorption capacity of lead and atrazine on dairy manure biochar pyrolyzed at 200 and 350 °C were studied by Cao et al. (2009) and Cao and Harris (2010), who indicated identical results for the lead sorption, in which more sorption showed in biochar produced at 350 °C; meanwhile, the atrazine sorption results were contradictory. Despite the identical biochar and environmental pollutants employing in studies, the sorption of 1,3-dinitrobenzene was found to greater on pine needle biochar pyrolyzed at 300 °C in the study of Chen et al. (2012) compared with their previous study in 2008. The sorption capacity of naphthalene and 1-naphthol to orange peel biochar produced at 300 °C was higher in the study of Chen and Chen (2009) than that from their study in 2012. Likewise, Gomez-Eyles et al. (2011) and Freddo et al. (2012) showed different sorption capacity of polycyclic aromatic hydrocarbons (PAHs) in hardwood biochar produced at 600 °C, owing to differences in the matrix. Although biochar has great effectiveness in remediation both organic and inorganic environmental pollutants, many studies have shown controversial results for the remediation of environmental pollutants, owing to the lack of an accurate and comprehensive examination of the physicochemical characteristics of biochar.

2.4.2. Perspectives in environmental factors

In the biochar studies for pollutant remediation, the physicochemical characteristics of biochar related to the corresponding sorption mechanism have not been fully revealed under various environmental conditions (Park et al. 2017; Lee et al. 2018). Under fluctuating environmental conditions, not only do the physicochemical characteristics of biochar change but also the ionizable pollutants themselves, causing a diversity of the sorption mechanisms between the biochar and the pollutants. Tong et al. (2011) showed that the sorption capacity of copper to crop straw biochar increased with increasing pH through the electrostatic attraction owing to the more negatively charged surface of

biochar by the deprotonation of acidic functional groups on biochar. Oh et al. (2012) conducted the fluoride sorption to orange peel biochar, and found that the sorption changed with increasing pH due to the variation of the interaction between biochar and the acidic functional groups. Harvey et al. (2011) indicated that the interaction of biochar with potassium and cadmium varied with pH; the sorption of potassium took place predominantly on deprotonated acidic functional groups *via* ion exchange, while the sorption of cadmium exhibited cation- π bonding mechanisms with soft ligands such as C=O and an electron-rich domain on the aromatic structure. By changing the pH, the species of ionizable sulfamethazine (SMT) with increasing pH also changed in accordance with pK_a ($pK_{a1} = 2.28$, $pK_{a2} = 7.42$); the amount of sorption capacity to biochar varied such that positively charged SMT under acidic conditions interacted with biochar through π - π electron donor acceptor interaction, whereas negatively charged SMT in alkali condition reacted with positively charged surface of biochar *via* H-bonding mechanism (Teixidó et al. 2011).

Not only the pH but also various environmental factors, such as ionic strength, ion composition, and mineral and organic matter affect the sorption mechanism of organic and inorganic environmental pollutants, since these factors induce changes in both the physicochemical characteristics of biochar and the environmental pollutant species (Lian et al. 2014; Wang et al. 2015; Ahmed et al. 2017). Qiu et al. (2009) showed that the sorption of brilliant blue to biochar increased with ionic strength, while the sorption of rhodamine B fluctuated. Yao et al. (2011) studied that retention of phosphate decreased, since the complexation between biochar and phosphate was interrupted by other anion species such as chlorine, nitrate, and carbonate. Cui et al. (2011) showed that the amount of phosphate sorption capacity was less under persistent ferrihydrite conditions owing to the interaction of biochar with ferrihydrite.

Therefore, it is essential to understand the interaction between biochar and environmental pollutants under a variety of changing environmental factors to better estimate the fate and behavior of pollutants in real environments.

2.4.3. Perspectives in analytics for biochar characterization

Before the current level of development in biochar studies, the sorption studied was mainly conducted through sorption isotherm models, such as the Freundlich and Langmuir isotherms (Allen et al. 1988; Khan et al. 1995), and the specific interactions between biochar and pollutants were not specifically interpreted (Zheng et al. 2010). However, in recent studies, the sorption mechanisms have been characterized using various analytical methods to better understand the real interaction between biochar and pollutants under its surrounding environments. This has enabled the observation of such phenomena from several perspectives to verify results. Based on these results, it is possible to explain the interaction of biochar with the pollutants. Chia et al. (2012) demonstrated that the component and morphology of biochar were obtained using FTIR, Raman spectroscopy, SEM-EDS, and XPS. Huang et al. (2018b) showed the structural transformation between metal ion in biochar and ofloxacin using FTIR. Zhang et al. (2015) confirmed the complex interaction of biochar with cadmium by SEM-EDS and XRD, and Dong et al. (2011) explained the sorption of chromium to biochar using the FTIR and XPS results. Thus, in the future, studies on the sorption mechanisms will explore more definitively the interaction between biochar and pollutants on the basis of traditional sorption isotherm results, along with various analytical methods, to reveal more concrete and direct evidence. The development of analytics will become more critical in the accurate interpretation of phenomena for sorption mechanisms in real environments.

2.5. Conclusions

Biochar is known as a universal sorbent owing to its heterogeneous physicochemical characteristics, which are caused by variations in feedstocks under diverse pyrolysis temperatures; this heterogeneity is the reason for the unpredictability of the results for the remediation of environmental pollutants. As both the physicochemical characteristics of biochar and species of ionizable pollutants were changed by surrounding environmental conditions. The surface charge of biochar was more negatively charged with increasing pH, owing to the deprotonation of oxygen containing acidic functional groups; in this case, the inorganic content also releases from the biochar surface by changing the pH and ionic strength. The behavior of charged pollutants was controlled by electrochemical properties such as pK_a and ionic valence. Consequently, the sorption mechanisms of biochar with ionizable pollutants should be comprehensively examined by changing the environmental factors such as pH, ionic strength, and the presence of cations, anions, and organic matter. For this purpose, lab-scale studies to identifying the sorption mechanisms between biochar and environmental pollutants under varying with environmental factors are essential for the estimation of the interaction in real environments. Therefore, a fundamental understanding of the physicochemical characteristics of biochar and comprehensive interpretation of the sorption mechanisms under various environmental conditions would help in the estimation of the behavior and fate of biochar with pollutant in soil and water environments.

References

- Abdel-Halim, E.S., and S.S. Al-Deyab. 2011. Removal of heavy metals from their aqueous solutions through adsorption onto natural polymers. *Carbohydr. Polym.* 84(1): 454–458. doi: 10.1016/j.carbpol.2010.12.001.
- Abdel-Shafy, H.I., and M.S.M. Mansour. 2016. A review on polycyclic aromatic hydrocarbons: Source, environmental impact, effect on human health and remediation. *Egypt. J. Pet.* 25(1): 107–123. doi: 10.1016/j.ejpe.2015.03.011.
- Ahmad, M., S.S. Lee, X. Dou, D. Mohan, J.K. Sung, et al. 2012. Effects of pyrolysis temperature on soybean stover- and peanut shell-derived biochar properties and TCE adsorption in water. *Bioresour. Technol.* 118: 536–544. doi: 10.1016/j.biortech.2012.05.042.
- Ahmad, M., A.U. Rajapaksha, J.E. Lim, M. Zhang, N. Bolan, et al. 2014. Biochar as a sorbent for contaminant management in soil and water: A review. *Chemosphere* 99: 19–33. doi: 10.1016/j.chemosphere.2013.10.071.
- Ahmed, M.B., J.L. Zhou, H.H. Ngo, W. Guo, M.A.H. Jahir, et al. 2017. Single and competitive sorption properties and mechanism of functionalized biochar for removing sulfonamide antibiotics from water. *Chem. Eng. J.* 311: 348–358. doi: 10.1016/j.cej.2016.11.106.
- Al-Wabel, M.I., A. Al-Omran, A.H. El-Naggar, M. Nadeem, and A.R.A. Usman. 2013. Pyrolysis temperature induced changes in characteristics and chemical composition of biochar produced from conocarpus wastes. *Bioresour. Technol.* 131: 374–379. doi: 10.1016/j.biortech.2012.12.165.
- Allen, S.J., G. McKay, and K.Y.H. Khader. 1988. Multi-component sorption isotherms of basic dyes onto peat. *Environ. Pollut.* 52(1): 39–53. doi: 10.1016/0269-7491(88)90106-6.
- An, J.H., and S. Dultz. 2007. Adsorption of tannic acid on chitosan-montmorillonite as a function of pH and surface charge properties. *Appl. Clay Sci.* 36(4): 256–264. doi: 10.1016/j.clay.2006.11.001.
- Angin, D. 2013. Effect of pyrolysis temperature and heating rate on biochar obtained from pyrolysis of safflower seed press cake. *Bioresour. Technol.* 128: 593–597. doi: 10.1016/j.biortech.2012.10.150.
- Basualto, C., M. Poblete, J. Marchese, A. Ochoa, A. Acosta, et al. 2006. Extraction of cadmium from aqueous solutions by emulsion liquid membranes using a stirred transfer cell contactor. *J. Braz. Chem. Soc.* 17(7): 1347–1354. doi: 10.1590/S0103-50532006000700023.
- Bekiaris, G., C. Peltre, L.S. Jensen, and S. Bruun. 2016. Using FTIR-photoacoustic spectroscopy for phosphorus speciation analysis of biochars. *Spectrochim. Acta - Part A Mol. Biomol. Spectrosc.* 168: 29–36. doi: 10.1016/j.saa.2016.05.049.
- Bian, Y., Z. Bian, J. Zhang, A. Ding, S. Liu, et al. 2015. Adsorption of cadmium ions from aqueous solutions by activated carbon with oxygen-containing functional groups. *Chinese J. Chem. Eng.* 23(10): 1705–1711. doi: 10.1016/j.cjche.2015.08.031.
- Boehm, H.P. 1994. Some aspects of the surface chemistry of carbon blacks and other carbons. *Carbon N. Y.* 32(5): 759–769. doi: 10.1016/0008-6223(94)90031-0.
- Boparai, H.K., M. Joseph, and D.M. O'Carroll. 2013. Cadmium (Cd²⁺) removal by nano zerovalent iron: Surface analysis, effects of solution chemistry and surface complexation modeling. *Environ. Sci. Pollut. Res.* 20(9): 6210–6221. doi:

- 10.1007/s11356-013-1651-8.
- Brockhoff, S.R., N.E. Christians, R.J. Killorn, R. Horton, and D.D. Davis. 2010. Physical and mineral-nutrition properties of sand-based turfgrass root zones amended with biochar. *Agron. J.* 102(6): 1627–1631. doi: 10.2134/agronj2010.0188.
- Cantrell, K.B., P.G. Hunt, M. Uchimiya, J.M. Novak, and K.S. Ro. 2012. Impact of pyrolysis temperature and manure source on physicochemical characteristics of biochar. *Bioresour. Technol.* 107: 419–428. doi: 10.1016/j.biortech.2011.11.084.
- Cao, X., and W. Harris. 2010. Properties of dairy-manure-derived biochar pertinent to its potential use in remediation. *Bioresour. Technol.* 101(14): 5222–5228. doi: 10.1016/j.biortech.2010.02.052.
- Cao, X., L. Ma, B. Gao, and W. Harris. 2009. Dairy-manure derived biochar effectively sorbs lead and atrazine. *Environ. Sci. Technol.* 43(9): 3285–3291. doi: 10.1021/es803092k.
- Cha, J.S., S.H. Park, S.C. Jung, C. Ryu, J.K. Jeon, et al. 2016. Production and utilization of biochar: A review. *J. Ind. Eng. Chem.* 40: 1–15. doi: 10.1016/j.jiec.2016.06.002.
- Chen, B., and Z. Chen. 2009. Sorption of naphthalene and 1-naphthol by biochars of orange peels with different pyrolytic temperatures. *Chemosphere* 76(1): 127–133. doi: 10.1016/j.chemosphere.2009.02.004.
- Chen, Z., B. Chen, D. Zhou, and W. Chen. 2012. Bisolute sorption and thermodynamic behavior of organic pollutants to biomass-derived biochars at two pyrolytic temperatures. *Environ. Sci. Technol.* 46(22): 12476–12483. doi: 10.1021/es303351e.
- Chen, B., and M. Yuan. 2011. Enhanced sorption of polycyclic aromatic hydrocarbons by soil amended with biochar. *J. Soils Sediments* 11(1): 62–71. doi: 10.1007/s11368-010-0266-7.
- Chen, T., Y.Y. Zhang, H. Wang, W. Lu, Z. Zhou, et al. 2014. Influence of pyrolysis temperature on characteristics and heavy metal adsorptive performance of biochar derived from municipal sewage sludge. *Bioresour. Technol.* 164: 47–54. doi: 10.1016/j.biortech.2014.04.048.
- Chen, B., D. Zhou, and L. Zhu. 2008. Transitional adsorption and partition of nonpolar and polar aromatic contaminants by biochars of pine needles with different pyrolytic temperatures. *Environ. Sci. Technol.* 42(14): 5137–5143. doi: 10.1021/es8002684.
- Chen, J., D. Zhu, and C. Sun. 2007. Effect of heavy metals on the sorption of hydrophobic organic compounds to wood charcoal. *Environ. Sci. Technol.* 41(7): 2536–2541. doi: 10.1021/es062113+.
- Chia, C.H., B. Gong, S.D. Joseph, C.E. Marjo, P. Munroe, et al. 2012. Imaging of mineral-enriched biochar by FTIR, Raman and SEM-EDX. *Vib. Spectrosc.* 62: 248–257. doi: 10.1016/j.vibspec.2012.06.006.
- Chun, Y., G. Sheng, G.T. Chiou, and B. Xing. 2004. Compositions and sorptive properties of crop residue-derived chars. *Environ. Sci. Technol.* 38(17): 4649–4655. doi: 10.1021/es035034w.
- Contescu, A., C. Contescu, K. Putyera, and J.A. Schwarz. 1997. Surface acidity of carbons characterized by their continuous pK distribution and Boehm titration. *Carbon N. Y.* 35(1): 83–94. doi: 10.1016/S0008-6223(96)00125-X.

- Cui, H.J., M.K. Wang, M.L. Fu, and E. Ci. 2011. Enhancing phosphorus availability in phosphorus-fertilized zones by reducing phosphate adsorbed on ferrihydrite using rice straw-derived biochar. *J. Soils Sediments* 11(7): 1135–1141. doi: 10.1007/s11368-011-0405-9.
- Dąbrowski, A. 2001. Adsorption - From theory to practice. *Adv. Colloid Interface Sci.* 93(1–3): 135–224. doi: 10.1016/S0001-8686(00)00082-8.
- Deng, H., D. Feng, J. xiong He, F. ze Li, H. mei Yu, et al. 2017. Influence of biochar amendments to soil on the mobility of atrazine using sorption-desorption and soil thin-layer chromatography. *Ecol. Eng.* 99: 381–390. doi: 10.1016/j.ecoleng.2016.11.021.
- Ding, W., X. Dong, I.M. Ime, B. Gao, and L.Q. Ma. 2014. Pyrolytic temperatures impact lead sorption mechanisms by bagasse biochars. *Chemosphere* 105: 68–74. doi: 10.1016/j.chemosphere.2013.12.042.
- Ding, Y., Y.X. Liu, W.X. Wu, D.Z. Shi, M. Yang, et al. 2010. Evaluation of biochar effects on nitrogen retention and leaching in multi-layered soil columns. *Water. Air. Soil Pollut.* 213(1–4): 47–55. doi: 10.1007/s11270-010-0366-4.
- Domingues, R.R., P.F. Trugilho, C.A. Silva, I.C.N.A. De Melo, L.C.A. Melo, et al. 2017. Properties of biochar derived from wood and high-nutrient biomasses with the aim of agronomic and environmental benefits. *PLoS One* 12(5): 1–19. doi: 10.1371/journal.pone.0176884.
- Dong, X., L.Q. Ma, and Y. Li. 2011. Characteristics and mechanisms of hexavalent chromium removal by biochar from sugar beet tailing. *J. Hazard. Mater.* 190(1–3): 909–915. doi: 10.1016/j.jhazmat.2011.04.008.
- El-Geundi, M.S. 1991. Colour removal from textile effluents by adsorption techniques. *Water Res.* 25(3): 271–273. doi: 10.1016/0043-1354(91)90006-C.
- Elmay, Y., Y. Le Brech, L. Delmotte, A. Dufour, N. Brosse, et al. 2015. Characterization of *Miscanthus* pyrolysis by DRIFTS, UV Raman spectroscopy and mass spectrometry. *J. Anal. Appl. Pyrolysis* 113: 402–411. doi: 10.1016/j.jaap.2015.03.004.
- Essandoh, M., B. Kunwar, C.U. Pittman, D. Mohan, and T. Mlsna. 2015. Sorptive removal of salicylic acid and ibuprofen from aqueous solutions using peine wood fast pyrolysis biochar. *Chem. Eng. J.* 265: 219–227. doi: 10.1016/j.cej.2014.12.006.
- Fan, Q., J. Sun, L. Chu, L. Cui, G. of chemical oxidation on surface oxygen-containing functional groups and adsorpti Quan, et al. 2018. Effects of chemical oxidation on surface oxygen-containing functional groups and adsorption behavior of biochar. *Chemosphere* 207: 33–40. doi: 10.1016/j.chemosphere.2018.05.044.
- Fang, Q., B. Chen, Y. Lin, and Y. Guan. 2014. Aromatic and hydrophobic surfaces of wood-derived biochar enhance perchlorate adsorption via hydrogen bonding to oxygen-containing organic groups. *Environ. Sci. Technol.* 48(1): 279–288. doi: 10.1021/es403711y.
- Fidel, R.B., D.A. Laird, and M.L. Thompson. 2013. Evaluation of Modified Boehm Titration Methods for Use with Biochars. *J. Environ. Qual.* 42(6): 1771. doi: 10.2134/jeq2013.07.0285.
- Freddo, A., C. Cai, and B.J. Reid. 2012. Environmental contextualisation of potential toxic elements and polycyclic aromatic hydrocarbons in biochar. *Environ. Pollut.* 171: 18–24. doi: 10.1016/j.envpol.2012.07.009.

- Gai, X., H. Wang, J. Liu, L. Zhai, S. Liu, et al. 2014. Effects of feedstock and pyrolysis temperature on biochar adsorption of ammonium and nitrate. *PLoS One* 9(12): 1–19. doi: 10.1371/journal.pone.0113888.
- Gomez-Eyles, J.L., T. Sizmur, C.D. Collins, and M.E. Hodson. 2011. Effects of biochar and the earthworm *Eisenia fetida* on the bioavailability of polycyclic aromatic hydrocarbons and potentially toxic elements. *Environ. Pollut.* 159(2): 616–622. doi: 10.1016/j.envpol.2010.09.037.
- Gómez-Zorrilla Martín, S., A. Riera-Mestre, R. Pujol Farriols, D. Leiva Pedraza, S. Jordán Lucas, et al. 2013. Suspected acute pulmonary embolism in patients with and without cancer: Alternative diagnoses. *Emergencias* 25(2): 92–98.
- Guo, X., X. Shen, M. Zhang, H. Zhang, W. Chen, et al. 2017. Sorption mechanisms of sulfamethazine to soil humin and its subfractions after sequential treatments. *Environ. Pollut.* 221: 266–275. doi: 10.1016/j.envpol.2016.11.073.
- Han, L., L. Qian, J. Yan, and M. Chen. 2016. Contributions of different biomass components to the sorption of 1,2,4-trichlorobenzene under a series of pyrolytic temperatures. *Chemosphere* 156: 262–271. doi: 10.1016/j.chemosphere.2016.04.031.
- Hartley, W., N.M. Dickinson, P. Riby, and N.W. Lepp. 2009. Arsenic mobility in brownfield soils amended with green waste compost or biochar and planted with *Miscanthus*. *Environ. Pollut.* 157(10): 2654–2662. doi: 10.1016/j.envpol.2009.05.011.
- Harvey, O.R., B.E. Herbert, R.D. Rhue, and L.J. Kuo. 2011. Metal interactions at the biochar-water interface: Energetics and structure-sorption relationships elucidated by flow adsorption microcalorimetry. *Environ. Sci. Technol.* 45(13): 5550–5556. doi: 10.1021/es104401h.
- Hollister, C.C., J.J. Bisogni, and J. Lehmann. 2013. Ammonium, nitrate, and phosphate sorption to and solute leaching from biochars prepared from corn stover (*zea mays* l.) and oak wood (*quercus* spp.). *J. Environ. Qual.* 42(1): 137–144. doi: 10.2134/jeq2012.0033.
- Huang, F., L.Y. Gao, J.H. Deng, S.H. Chen, and K.Z. Cai. 2018a. Quantitative contribution of Cd²⁺ adsorption mechanisms by chicken-manure-derived biochars. *Environ. Sci. Pollut. Res.* 25(28): 28322–28334. doi: 10.1007/s11356-018-2889-y.
- Huang, P., C. Ge, D. Feng, H. Yu, J. Luo, et al. 2018b. Effects of metal ions and pH on ofloxacin sorption to cassava residue-derived biochar. *Sci. Total Environ.* 616–617: 1384–1391. doi: 10.1016/j.scitotenv.2017.10.177.
- Jiang, T.Y., J. Jiang, R.K. Xu, and Z. Li. 2012. Adsorption of Pb(II) on variable charge soils amended with rice-straw derived biochar. *Chemosphere* 89(3): 249–256. doi: 10.1016/j.chemosphere.2012.04.028.
- Khan, S.A., Riaz-ur-Rehman, and M.A. Khan. 1995. Sorption of strontium on bentonite. *Waste Manag.* 15(8): 641–650. doi: 10.1016/0956-053X(96)00049-9.
- Kloss, S., F. Zehetner, A. Dellantonio, R. Hamid, F. Ottner, et al. 2012. Characterization of Slow Pyrolysis Biochars: Effects of Feedstocks and Pyrolysis Temperature on Biochar Properties. *J. Environ. Qual.* 41(4): 990. doi: 10.2134/jeq2011.0070.
- Kong, Y., J. Kang, J. Shen, Z. Chen, and L. Fan. 2017. Influence of humic acid on the removal of arsenate and arsenic by ferric chloride: effects of pH, As/Fe ratio, initial As concentration, and co-existing solutes. *Environ. Sci. Pollut. Res.*

- 24(3): 2381–2393. doi: 10.1007/s11356-016-7994-1.
- Lee, S., J. Han, and H.M. Ro. 2018. Interpreting the pH-dependent mechanism of simazine sorption to *Miscanthus* biochar produced at different pyrolysis temperatures for its application to soil. *Korean J. Chem. Eng.* 35(7): 1468–1476. doi: 10.1007/s11814-018-0054-4.
- Lehmann, J. 2007a. A handful of carbon. *Nature* 447(7141): 143–144. doi: 10.1038/447143a.
- Lehmann, J. 2007b. Bio-energy in the black. *Front. Ecol. Environ.* 5(7): 381–387. doi: 10.1890/1540-9295(2007)5[381:BITB]2.0.CO;2.
- Leon, C.A., and L.R. Radovic. 1991. Influence of Oxygen Functional Groups on the Performance of Carbon-Supported Catalysts. *Mater. Sci.*: 1007–1014.
- Lian, F., B. Sun, Z. Song, L. Zhu, X. Qi, et al. 2014. Physicochemical properties of herb-residue biochar and its sorption to ionizable antibiotic sulfamethoxazole. *Chem. Eng. J.* 248: 128–134. doi: 10.1016/j.cej.2014.03.021.
- Liu, Z., and F.S. Zhang. 2009. Removal of lead from water using biochars prepared from hydrothermal liquefaction of biomass. *J. Hazard. Mater.* 167(1–3): 933–939. doi: 10.1016/j.jhazmat.2009.01.085.
- Lua, A.C., T. Yang, and J. Guo. 2004. Effects of pyrolysis conditions on the properties of activated carbons prepared from pistachio-nut shells. *J. Anal. Appl. Pyrolysis* 72(2): 279–287. doi: 10.1016/j.jaap.2004.08.001.
- Luo, L., C. Xu, Z. Chen, and S. Zhang. 2015. Properties of biomass-derived biochars: Combined effects of operating conditions and biomass types. *Bioresour. Technol.* 192: 83–89. doi: 10.1016/j.biortech.2015.05.054.
- Mimmo, T., P. Panzacchi, M. Baratieri, C.A. Davies, and G. Tonon. 2014. Effect of pyrolysis temperature on miscanthus (*Miscanthus × giganteus*) biochar physical, chemical and functional properties. *Biomass and Bioenergy* 62(0): 149–157. doi: 10.1016/j.biombioe.2014.01.004.
- Mohan, D., H. Kumar, A. Sarswat, M. Alexandre-Franco, and C.U. Pittman. 2014. Cadmium and lead remediation using magnetic oak wood and oak bark fast pyrolysis bio-chars. *Chem. Eng. J.* 236: 513–528. doi: 10.1016/j.cej.2013.09.057.
- Mukherjee, A., A.R. Zimmerman, and W. Harris. 2011. Surface chemistry variations among a series of laboratory-produced biochars. *Geoderma* 163(3–4): 247–255. doi: 10.1016/j.geoderma.2011.04.021.
- Mukome, F.N.D., X. Zhang, L.C.R. Silva, J. Six, and S.J. Parikh. 2013. Use of chemical and physical characteristics to investigate trends in biochar feedstocks. *J. Agric. Food Chem.* 61(9): 2196–2204. doi: 10.1021/jf3049142.
- Namgay, T., B. Singh, and B.P. Singh. 2010. Influence of biochar application to soil on the availability of As, Cd, Cu, Pb, and Zn to maize (*Zea mays* L.). *Aust. J. Soil Res.* 48(6–7): 638–647. doi: 10.1071/SR10049.
- Nguyen, T.H., H.H. Cho, D.L. Poster, and W.P. Ball. 2007. Evidence for a pore-filling mechanism in the adsorption of aromatic hydrocarbons to a natural wood char. *Environ. Sci. Technol.* 41(4): 1212–1217. doi: 10.1021/es0617845.
- Oh, T.K., B. Choi, Y. Shinogi, and J. Chikushi. 2012. Effect of pH conditions on actual and apparent fluoride adsorption by biochar in aqueous phase. *Water. Air. Soil Pollut.* 223(7): 3729–3738. doi: 10.1007/s11270-012-1144-2.
- Okuno, T., N. Sonoyama, J.I. Hayashi, C.Z. Li, C. Sathe, et al. 2005. Primary release of alkali and alkaline earth metallic species during the pyrolysis of pulverized

- biomass. *Energy and Fuels* 19(5): 2164–2171. doi: 10.1021/ef050002a.
- Özçimen, D., and A. Ersoy-Meriçboyu. 2010. Characterization of biochar and bio-oil samples obtained from carbonization of various biomass materials. *Renew. Energy* 35(6): 1319–1324. doi: 10.1016/j.renene.2009.11.042.
- Pardo, B., N. Ferrer, J. Sempere, and R. Gonzalez-Olmos. 2016. A key parameter on the adsorption of diluted aniline solutions with activated carbons: The surface oxygen content. *Chemosphere* 162: 181–188. doi: 10.1016/j.chemosphere.2016.07.066.
- Park, J.H., G.K. Choppala, N.S. Bolan, J.W. Chung, and T. Chuasavathi. 2011. Biochar reduces the bioavailability and phytotoxicity of heavy metals. *Plant Soil* 348(1–2): 439–451. doi: 10.1007/s11104-011-0948-y.
- Park, J.H., G. Choppala, S.J. Lee, N. Bolan, J.W. Chung, et al. 2013. Comparative Sorption of Pb and Cd by Biochars and Its Implication for Metal Immobilization in Soils. *Water, Air, Soil Pollut.* 224(12). doi: 10.1007/s11270-013-1711-1.
- Park, C.M., J. Han, K.H. Chu, Y.A.J. Al-Hamadani, N. Her, et al. 2017. Influence of solution pH, ionic strength, and humic acid on cadmium adsorption onto activated biochar: Experiment and modeling. *J. Ind. Eng. Chem.* 48(2016): 186–193. doi: 10.1016/j.jiec.2016.12.038.
- Phuong, H.T., M.A. Uddin, and Y. Kato. 2015. Characterization of biochar from pyrolysis of rice husk and rice straw. *J. Biobased Mater. Bioenergy* 9(4): 439–446. doi: 10.1166/jbmb.2015.1539.
- Pyrzyńska, K., and M. Bystrzejewski. 2010. Comparative study of heavy metal ions sorption onto activated carbon, carbon nanotubes, and carbon-encapsulated magnetic nanoparticles. *Colloids Surfaces A Physicochem. Eng. Asp.* 362(1–3): 102–109. doi: 10.1016/j.colsurfa.2010.03.047.
- Qiu, Y., Z. Zheng, Z. Zhou, and G.D. Sheng. 2009. Effectiveness and mechanisms of dye adsorption on a straw-based biochar. *Bioresour. Technol.* 100(21): 5348–5351. doi: 10.1016/j.biortech.2009.05.054.
- Qu, T., W. Guo, L. Shen, J. Xiao, and K. Zhao. 2011. Experimental study of biomass pyrolysis based on three major components: Hemicellulose, cellulose, and lignin. *Ind. Eng. Chem. Res.* 50(18): 10424–10433. doi: 10.1021/ie1025453.
- Ronsse, F., S. van Hecke, D. Dickinson, and W. Prins. 2013. Production and characterization of slow pyrolysis biochar: Influence of feedstock type and pyrolysis conditions. *GCB Bioenergy* 5(2): 104–115. doi: 10.1111/gcbb.12018.
- Sarmah, A.K., P. Srinivasan, R.J. Smernik, M. Manley-Harris, M.J. Antal, et al. 2010. Retention capacity of biochar-amended New Zealand dairy farm soil for an estrogenic steroid hormone and its primary metabolite. *Aust. J. Soil Res.* 48(6–7): 648–658. doi: 10.1071/SR10013.
- Shaaban, A., S.M. Se, M.F. Dimin, J.M. Juoi, M.H. Mohd Husin, et al. 2014. Influence of heating temperature and holding time on biochars derived from rubber wood sawdust via slow pyrolysis. *J. Anal. Appl. Pyrolysis* 107: 31–39. doi: 10.1016/j.jaap.2014.01.021.
- Sigmund, G., T. Hüffer, T. Hofmann, and M. Kah. 2016. Biochar total surface area and total pore volume determined by N₂ and CO₂ physisorption are strongly influenced by degassing temperature. *Sci. Total Environ.* d. doi: 10.1016/j.scitotenv.2016.12.023.
- Singh, B.P., and A. Cowie. 2010. The mean turnover time of biochar in soil varies

- depending on biomass source and pyrolysis temperature. *Proc. 19th World Congr. Soil Sci. Soil Solut. a Chang. world, Brisbane, Aust. 1-6 August 2010. Symp. 2.2.2 Dyn. Org. Mater. soils (August): 235–238.*
- Singh, B., M.M. Dolk, Q. Shen, and M. Camps-Arbestain. 2017. Biochar pH, electrical conductivity and liming potential. *Biochar A Guid. to Anal. Methods (June 2018): 23–38.* doi: 10.13040/IJPSR.0975-8232.5(2).607-1.
- Singh, B., B.P. Singh, and A.L. Cowie. 2010. Characterisation and evaluation of biochars for their application as a soil amendment. *Aust. J. Soil Res. 48(6–7): 516–525.* doi: 10.1071/SR10058.
- Sø, H.U., D. Postma, R. Jakobsen, and F. Larsen. 2008. Sorption and desorption of arsenate and arsenite on calcite. *Geochim. Cosmochim. Acta 72(24): 5871–5884.* doi: 10.1016/j.gca.2008.09.023.
- Spokas, K.A., W.C. Koskinen, J.M. Baker, and D.C. Reicosky. 2009. Impacts of woodchip biochar additions on greenhouse gas production and sorption/degradation of two herbicides in a Minnesota soil. *Chemosphere 77(4): 574–581.* doi: 10.1016/j.chemosphere.2009.06.053.
- Steiner, C., B. Glaser, W.G. Teixeira, J. Lehmann, W.E.H. Blum, et al. 2008. Nitrogen retention and plant uptake on a highly weathered central Amazonian Ferralsol amended with compost and charcoal. *J. Plant Nutr. Soil Sci. 171(6): 893–899.* doi: 10.1002/jpln.200625199.
- Suliman, W., J.B. Harsh, N.I. Abu-Lail, A.M. Fortuna, I. Dallmeyer, et al. 2016. Influence of feedstock source and pyrolysis temperature on biochar bulk and surface properties. *Biomass and Bioenergy 84: 37–48.* doi: 10.1016/j.biombioe.2015.11.010.
- Sun, K., J. Jin, M. Keiluweit, M. Kleber, Z. Wang, et al. 2012. Polar and aliphatic domains regulate sorption of phthalic acid esters (PAEs) to biochars. *Bioresour. Technol. 118: 120–127.* doi: 10.1016/j.biortech.2012.05.008.
- Sun, K., M. Keiluweit, M. Kleber, Z. Pan, and B. Xing. 2011a. Sorption of fluorinated herbicides to plant biomass-derived biochars as a function of molecular structure. *Bioresour. Technol. 102(21): 9897–9903.* doi: 10.1016/j.biortech.2011.08.036.
- Sun, K., K. Ro, M. Guo, J. Novak, H. Mashayekhi, et al. 2011b. Sorption of bisphenol A, 17 α -ethinyl estradiol and phenanthrene on thermally and hydrothermally produced biochars. *Bioresour. Technol. 102(10): 5757–5763.* doi: 10.1016/j.biortech.2011.03.038.
- Tag, A.T., G. Duman, S. Ucar, and J. Yanik. 2016. Effects of feedstock type and pyrolysis temperature on potential applications of biochar. *J. Anal. Appl. Pyrolysis 120: 200–206.* doi: 10.1016/j.jaap.2016.05.006.
- Tan, X.L., X.K. Wang, H. Geckeis, and T.H. Rabung. 2008. Sorption of Eu(III) on humic acid or fulvic acid bound to hydrous alumina studied by SEM-EDS, XPS, TRLFS, and batch techniques. *Environ. Sci. Technol. 42(17): 6532–6537.* doi: 10.1021/es8007062.
- Teixidó, M., J.J. Pignatello, J.L. Beltrán, M. Granados, and J. Peccia. 2011. Speciation of the ionizable antibiotic sulfamethazine on black carbon (Biochar). *Environ. Sci. Technol. 45(23): 10020–10027.* doi: 10.1021/es202487h.
- Tong, X.J., J.Y. Li, J.H. Yuan, and R.K. Xu. 2011. Adsorption of Cu(II) by biochars generated from three crop straws. *Chem. Eng. J. 172(2–3): 828–834.* doi: 10.1016/j.cej.2011.06.069.

- Tsechansky, L., and E.R. Graber. 2014. Methodological limitations to determining acidic groups at biochar surfaces via the Boehm titration. *Carbon N. Y.* 66: 730–733. doi: 10.1016/j.carbon.2013.09.044.
- Uchimiya, M., S.C. Chang, and K.T. Klasson. 2011a. Screening biochars for heavy metal retention in soil: Role of oxygen functional groups. *J. Hazard. Mater.* 190(1–3): 432–441. doi: 10.1016/j.jhazmat.2011.03.063.
- Uchimiya, M., and S. Hiradate. 2014. Pyrolysis temperature-dependent changes in dissolved phosphorus speciation of plant and manure biochars. *J. Agric. Food Chem.* 62(8): 1802–1809. doi: 10.1021/jf4053385.
- Uchimiya, M., I.M. Lima, K. Thomas Klasson, S. Chang, L.H. Wartelle, et al. 2010. Immobilization of heavy metal ions (Cu II, Cd II, Ni II, and Pb II) by broiler litter-derived biochars in water and soil. *J. Agric. Food Chem.* 58(9): 5538–5544. doi: 10.1021/jf9044217.
- Uchimiya, M., L.H. Wartelle, and V.M. Boddu. 2012. Sorption of triazine and organophosphorus pesticides on soil and biochar. *J. Agric. Food Chem.* 60(12): 2989–2997. doi: 10.1021/jf205110g.
- Uchimiya, M., L.H. Wartelle, K.T. Klasson, C.A. Fortier, and I.M. Lima. 2011b. Influence of pyrolysis temperature on biochar property and function as a heavy metal sorbent in soil. *J. Agric. Food Chem.* 59(6): 2501–2510. doi: 10.1021/jf104206c.
- Usman, A.R.A., A. Abduljabbar, M. Vithanage, Y.S. Ok, M.M.M. Ahmad, et al. 2015. Biochar production from date palm waste: Charring temperature induced changes in composition and surface chemistry. *J. Anal. Appl. Pyrolysis* 115: 392–400. doi: 10.1016/j.jaap.2015.08.016.
- Violante, A., and M. Pigna. 2002. Competitive sorption of arsenate and phosphate on different clay minerals and soils. *Soil Sci. Soc. Am. J.* 66(6): 1788–1796.
- Wang, L. 2017. Surface Properties and Chemical Composition of Corncob and Miscanthus Biochars : Effects of Production Temperature Surface Properties and Chemical Composition of Corncob and Miscanthus Biochars : Effects of Production Temperature and Method. (November). doi: 10.1080/10426910802679196.
- Wang, B., J. Lehmann, K. Hanley, R. Hestrin, and A. Enders. 2015. Adsorption and desorption of ammonium by maple wood biochar as a function of oxidation and pH. *Chemosphere* 138: 120–126. doi: 10.1016/j.chemosphere.2015.05.062.
- Warren, G.P., J.S. Robinson, and E. Someus. 2009. Dissolution of phosphorus from animal bone char in 12 soils. *Nutr. Cycl. Agroecosystems* 84(2): 167–178. doi: 10.1007/s10705-008-9235-6.
- Wasi, S., S. Tabrez, and M. Ahmad. 2013. Toxicological effects of major environmental pollutants: An overview. *Environ. Monit. Assess.* 185(3): 2585–2593. doi: 10.1007/s10661-012-2732-8.
- Xiao, X., Z. Chen, and B. Chen. 2016. H/C atomic ratio as a smart linkage between pyrolytic temperatures, aromatic clusters and sorption properties of biochars derived from diverse precursory materials. *Sci. Rep.* 6(October 2015): 22644. doi: 10.1038/srep22644.
- Xie, T., K.R. Reddy, C. Wang, E. Yargicoglu, and K. Spokas. 2015. Characteristics and applications of biochar for environmental remediation: A review. *Crit. Rev. Environ. Sci. Technol.* 45(9): 939–969. doi: 10.1080/10643389.2014.924180.
- Xu, D., Y. Zhao, K. Sun, B. Gao, Z. Wang, et al. 2014. Cadmium adsorption on plant-

- and manure-derived biochar and biochar-amended sandy soils: Impact of bulk and surface properties. *Chemosphere* 111: 320–326. doi: 10.1016/j.chemosphere.2014.04.043.
- Yang, K., X. Wang, L. Zhu, and B. Xing. 2006. Competitive sorption of pyrene, phenanthrene, and naphthalene on multiwalled carbon nanotubes. *Environ. Sci. Technol.* 40(18): 5804–5810. doi: 10.1021/es061081n.
- Yao, Y., B. Gao, M. Inyang, A.R. Zimmerman, X. Cao, et al. 2011. Removal of phosphate from aqueous solution by biochar derived from anaerobically digested sugar beet tailings. *J. Hazard. Mater.* 190(1–3): 501–507. doi: 10.1016/j.jhazmat.2011.03.083.
- Yu, X., L. Pan, G. Ying, and R.S. Kookana. 2010. Enhanced and irreversible sorption of pesticide pyrimethanil by soil amended with biochars. *J. Environ. Sci.* 22(4): 615–620. doi: 10.1016/S1001-0742(09)60153-4.
- Yu, X.Y., G.G. Ying, and R.S. Kookana. 2009. Reduced plant uptake of pesticides with biochar additions to soil. *Chemosphere* 76(5): 665–671. doi: 10.1016/j.chemosphere.2009.04.001.
- Yuan, H., T. Lu, H. Huang, D. Zhao, N. Kobayashi, et al. 2015. Influence of pyrolysis temperature on physical and chemical properties of biochar made from sewage sludge. *J. Anal. Appl. Pyrolysis* 112: 284–289. doi: 10.1016/j.jaap.2015.01.010.
- Yuan, J.H., R.K. Xu, and H. Zhang. 2011. The forms of alkalis in the biochar produced from crop residues at different temperatures. *Bioresour. Technol.* 102(3): 3488–3497. doi: 10.1016/j.biortech.2010.11.018.
- Zarzycki, P., and K.M. Rosso. 2018. Surface Charge Effects on Fe(II) Sorption and Oxidation at (110) Goethite Surfaces. *J. Phys. Chem. C* 122(18): 10059–10066. doi: 10.1021/acs.jpcc.8b02099.
- Zhang, H., K. Lin, H. Wang, and J. Gan. 2010. Effect of *Pinus radiata* derived biochars on soil sorption and desorption of phenanthrene. *Environ. Pollut.* 158(9): 2821–2825. doi: 10.1016/j.envpol.2010.06.025.
- Zhang, P., H. Sun, L. Yu, and T. Sun. 2013. Adsorption and catalytic hydrolysis of carbaryl and atrazine on pig manure-derived biochars: Impact of structural properties of biochars. *J. Hazard. Mater.* 244–245: 217–224. doi: 10.1016/j.jhazmat.2012.11.046.
- Zhang, F., X. Wang, D. Yin, B. Peng, C. Tan, et al. 2015. Efficiency and mechanisms of Cd removal from aqueous solution by biochar derived from water hyacinth (*Eichornia crassipes*). *J. Environ. Manage.* 153: 68–73. doi: 10.1016/j.jenvman.2015.01.043.
- Zhao, L., X. Cao, O. Mašek, and A. Zimmerman. 2013. Heterogeneity of biochar properties as a function of feedstock sources and production temperatures. *J. Hazard. Mater.* 256–257: 1–9. doi: 10.1016/j.jhazmat.2013.04.015.
- Zheng, W., M. Guo, T. Chow, D.N. Bennett, and N. Rajagopalan. 2010. Sorption properties of greenwaste biochar for two triazine pesticides. *J. Hazard. Mater.* 181(1–3): 121–126. doi: 10.1016/j.jhazmat.2010.04.103.
- van Zwieten, L., S. Kimber, S. Morris, K.Y. Chan, A. Downie, et al. 2010. Effects of biochar from slow pyrolysis of papermill waste on agronomic performance and soil fertility. *Plant Soil* 327(1): 235–246. doi: 10.1007/s11104-009-0050-x.

CHAPTER 3. INTERPRETING THE pH-DEPENDENT MECHANISM OF SIMAZINE SORPTION TO *MISCANTHUS* BIOCHAR PRODUCED AT DIFFERENT PYROLYSIS TEMPERATURES FOR ITS APPLICATION TO SOIL

List of contents	3-1
Abstract	3-2
3.1. Introduction	3-3
3.2. Materials and methods	3-6
3.2.1. Physicochemical characteristics of biochar	3-6
3.2.2. Batch sorption experiments	3-7
3.2.2.1. Sorption kinetics	3-8
3.2.2.2. Degradation kinetics.....	3-8
3.2.2.3. Speciation.....	3-9
3.2.2.4. Sorption isotherm.....	3-9
3.2.2.5. Sorption isotherm for Scatchard plot analysis.....	3-10
3.2.2.6. Simazine analysis	3-10
3.2.3. Data analysis and fitting	3-11
3.3. Results and disussion	3-13
3.3.1. Physicochemical characteristics of biochar	3-13
3.3.2. Structural transformation of biochar	3-17
3.3.3. Sorption kinetics, speciation, and degradation.....	3-18
3.3.4. Sorption isotherm	3-27
3.3.5. Scatchard plot analysis of simazine sorption	3-29
3.3.6. Sorption mechanism	3-34
3.4. Conclusions	3-37
Reference	3-39

Abstract

Biochar has received considerable attention as an eco-friendly bio-sorbent; however, multifarious characteristics caused by pyrolysis and feedstock pose difficulties in its application. The pH-dependent sorption of the pesticide simazine on *Miscanthus* biochar produced at two pyrolysis temperatures (400 and 700 °C; hereafter B400 and B700) was characterized. The specific surface area (SSA) of the micro- and nano-pores, elemental composition, surface acidity and infrared spectra were determined. The SSA was greater in B700 than in B400, and the former had greater SSA in micro-pores and lower SSA in nano-pores than the latter. During pyrolysis, the single-bond structures of the feedstock were converted to aromatic structures, and further pyrolysis led to ligneous structures. Alterations in pore structure and concave-up Scatchard plot corroborated the presence of two sorption mechanisms: electrostatic attractions (S_{es}) and hydrophobic attractions (S_{hp}). Decreases in maximum sorption in the q_{max-L} with increasing pH was due to decreased S_{es} via deprotonation of carboxylic groups on biochar, while those in the q_{max-H} with increasing pyrolysis temperature was due to decreased S_{hp} resulting from pore structure deformation. Our approach, which addresses the pH-dependence of charge density of sorbate and sorbent, could help provide better understanding of the behavior of simazine.

Keywords

Simazine, *Miscanthus* biochar, pyrolysis temperature, pH-dependent sorption, Scatchard plot

3.1. Introduction

Biochar is a carbon-rich material produced through pyrolysis of various feedstocks under diverse circumstances (Lehmann 2007a), and has received increased attention because of its applications to wastewater treatment, global warming mitigation, soil fertility improvement, pollution remediation, agricultural waste recycling and carbon sequestration (Atkinson et al. 2010; van Zwieten et al. 2010; Li et al. 2016). Therefore, many attempts have been made to study biochar application; however, unexpected or inconsistent results frequently occurred in *in situ* application, while laboratory experiments showed great potential (Kloss et al. 2014; Xu et al. 2016). Main causes of discrepancies arise from abstruse characteristics and a lack of understanding of the fundamental mechanism (Kloss et al. 2012; Zhao et al. 2013).

Recent studies showed that feedstocks and pyrolysis predominantly determine biochar characteristics (Chen et al. 2008; Mukherjee et al. 2011). Of various pyrolysis parameters, pyrolysis temperature is a key factor that governs the characteristics of biochar (Zhao et al. 2013) because thermal decomposition of specific molecular structures needs specific temperatures (Qu et al. 2011; Mimmo et al. 2014). Previous studies revealed that dramatic changes in the biochar structure occurs at the certain pyrolysis temperature, and the change significantly affects the biochar characteristics (Lehmann 2007b; Chen et al. 2008; Zhang et al. 2011). Therefore, thermal decomposition determines not only pore-geometry and specific surface area (SSA) but also distinctive hydrophobic and hydrophilic surfaces (Song and Guo 2012; Budai et al. 2014; Han et al. 2016a).

Structural and chemical transformations during pyrolysis render biochar a promising biosorbent for inorganic/organic pollutants. High sorption capacity of biochar is due to the presence of oxygenated functional groups and inorganic residue fractions for inorganic pollutants (Cao et al. 2009; Uchimiya

et al. 2011; Qian and Chen 2013; Xu and Chen 2015) and associated with aromatic composition of its porous structures for organic pollutants (Ahmad et al. 2012; Oleszczuk et al. 2012). Since the nature of surface charge is due to the presence of acidic/basic functional groups in biochar, it is a function of solution-pH and point of zero net charge (PZNC) of the sorbent (Zhao et al. 2015). Therefore, knowledge of pH-dependent sorption is a prerequisite to understanding the sorption mechanism for inorganic/organic pollutants (Uchimiya et al. 2010; Jia et al. 2013a). Despite extensive investigations, the mechanisms responsible for the effect of solution-pH on the sorption of sorbates to sorbents are not well-understood due to their heterogeneity.

Changes in acidic functional groups on the surface of activated carbons can lead to significant changes in the sorption mechanisms for organic pollutants (Jia et al. 2013a; Wang et al. 2013). Therefore, acidic and basic functional groups present on biochar surface play a central role by attracting charged ions (Uchimiya et al. 2011) or repelling hydrophobic organic pollutants (Fang et al. 2014). Since oxygen containing carboxylic, lactonic, and phenolic functional groups are particularly responsible for sorption behavior of biochar (Leon and Radovic 1991), knowledge of the effects of changes in these functional groups on sorption mechanisms will contribute to understanding of the interaction of organic pollutants with various types of biochar.

Simazine [2-chloro-4,6-bis(ethylamino)-s-triazine] is an herbicide that has lone-pair electrons in its structure. Recent evidence suggests that simazine has posed threats to ground and surface water quality (Flores et al. 2009; Silva and Iyer 2014) due to its low solubility in water and comparative nonvolatility (Whitacre 2010). Under acidic pH conditions below the negative logarithmic acid dissociation constant (pK_a), simazine is positively charged due to protonation. Otherwise, it behaves as a neutral organic pollutant under the pH above pK_a (Celis et al. 2010; Weber 2010). When the pH is lower than

PZNC, the sorbent surface is positively charged and the degree of protonation decreases with increasing pH; otherwise, the surface is negatively charged (Yang et al. 2004). Therefore, the behavior of simazine across the environmental pH range is necessary to study mechanistic simazine sorption to the surface of a sorbent that has a certain PZNC.

Sorption mechanisms between inorganic sorbates and metal-based sorbent can be determined using X-ray- and electron-based methods (Betts et al. 2013; Fang et al. 2016); however, these methods are not applicable to sorption between organic pollutants and organic sorbents because organic pollutants are easily decomposed under the radiation of X-rays and electrons (Grubb 1974). As alternatives, several theoretical isotherms have been employed to interpret the sorption mechanisms: Langmuir, Freundlich and Dubinin-Radushkevich isotherms. Particularly, the Dubinin-Radushkevich isotherm can formulate adsorption following a pore filling mechanism to predict sorption at homogeneous and heterogeneous surfaces (Liu and Chen 2015). Therefore, comparison of the fitting results obtained from sorption isotherms can enable prediction of sorption mechanisms of an organic sorbate onto the homogeneous or heterogeneous surface of the sorbent.

Our objectives were to identify differences in the physicochemical characteristics of *Miscanthus* biochar produced at two different pyrolysis temperatures, predict the behaviors of simazine in the environment, interpret the pH-dependent mechanism of simazine sorption to biochar using three isotherm models and Scatchard plot analysis, and present a comprehensive approach to assessing and predicting the fate and behavior of simazine.

3.2. Material and methods

3.2.1. Physicochemical characteristics of biochar

Two types of biochar were produced from a *Miscanthus* feedstock at

different pyrolysis temperatures (400 and 700 °C) (hereafter, B400 and B700), which is before and after pyrolysis temperature of 500 °C, where the dramatic change was observed in the previous studies (Lehmann 2007b; Chen et al. 2008; Zhang et al. 2011). The heating rate was approximately 10 °C min⁻¹ and the target temperatures were maintained for one hour for complete pyrolysis under N₂ gas purging. The biochar was ball-milled (MM400, Retsch, Germany) and sieved through a 106-µm mesh to minimize size-effects (Zheng et al. 2010). Size fractionation using Analysette 3 pro (Fritsch, Germany) to identify the fraction of < 25 µm, 25-53 µm and 53-106 µm was performed. The SSA of biochar was determined using the Brunauer-Emmett-Teller isotherm with two gas adsorbates: N₂ (ASAP 2010, Micromeritics, USA) for nano-pores (<1.5 nm) and CO₂ (BELSORP-mini II, Microtrac BEL, Japan) for both nano- and micro-pores (>1.5 nm) (Mukherjee et al. 2011; Sigmund et al. 2016). The PZNC was determined using the pH drift method (Yang et al. 2004).

Carbon (C), hydrogen (H), nitrogen (N), and sulfur (S) were analyzed using an elemental analyzer (Flash 2000, Thermo, USA). Oxygen (O) was calculated by subtracting each percent of C, H, N and S from 100 % (Chen et al. 2008). Acidic functional groups of biochar were determined by the Boehm's titration (Boehm 1994; Fidel et al. 2013). Biochar was pretreated with dilute HCl (pH 2) to minimize side-effects (Contescu et al. 1997), and then added to each 20 mL of three bases of 0.05 M solutions (NaHCO₃, Na₂CO₃, and NaOH) on a flask-shaker at 160 rpm for 24 h. Each mix was centrifuged using a MF-600 centrifuge (Hanil, Korea) at 4000 rpm for 40 min. Ten milliliters of each supernatant was back-titrated with 0.01 M HCl using an automatic titrator (702 SM Titrino, Metrohm, Switzerland). Yield content was calculated by dividing the weight of biochar after pyrolysis by the weight of feedstocks before pyrolysis. Ash content was estimated by the combustion method, which

measured the residual weight after heating at 750 °C (Cao and Harris 2010; Stefaniuk and Oleszczuk 2015).

Fourier-transform infrared (FT-IR) spectra of feedstocks and its derived biochar were obtained using an IR Tracer-100 FT-IR spectrometer (Shimadzu, Japan) equipped with a MIRacle attenuated total reflectance (ATR) accessory (Piketech, USA) with a ZnSe crystal plate at an incidence angle of 45° (Mimmo et al. 2014). The resolution was set to 4 cm⁻¹, and the spectral range covered the 4000-650 cm⁻¹. Sixty-four scans were collected for each measurement, and ATR correction and smoothing were applied to minimize the difference in penetration depth. Concentration of inorganic elements were measured using an X-ray fluorescence (XRF) spectrometer (S4 Pioneer, Bruker, USA) with power settings of 4 kW under a helium purge. Apparent density of biochar was measured following the ASTM D-285 procedure.

3.2.2. Batch sorption experiments

Four batch experiments were conducted: sorption kinetics, degradation kinetics, speciation, and sorption isotherms. All reagents were purchased from Sigma-Aldrich (USA), and concentrations of simazine and CaCl₂ were 5 mg L⁻¹ (maximum solubility) and 0.05 M, respectively (Zheng et al. 2010). The pH was daily adjusted with 0.1 M HCl or 0.1 M NaOH for degradation kinetics, and with 1 M HCl or 1 M NaOH to sorption isotherms. Each sample was allowed to equilibrate in a 30 mL amber glass vial with a Teflon-lined cap on a vial-shaker at 160 rpm after 81 h under room temperature (controlled to 25 °C), and each mix was filtered through a 0.45-µm nylon membrane filter. For sample extraction, 2 mL of hexane was injected into 10 mL of each filtrate. One milliliter of supernatant was transferred into a 2 mL amber vial with a rubber cap for GC analysis. All experiments were performed in triplicate.

3.2.2.1. Sorption kinetics

The sorption kinetics was measured without pH adjustment. A concentrated simazine solution was prepared by mixing 5 mL of a standard stock solution with methanol (20 mg L⁻¹) and distilled water (15 mL) in the vial to make 5 mg L⁻¹ as the initial simazine concentration. The simazine solution was mixed with 0.2 g of biochar, and the suspension was allowed to equilibrate in a 30 mL amber glass vial with a Teflon-lined cap on a vial-shaker (DS-300L, Dasol, Korea) at 160 rpm without adjusting the pH. The mixture was shaken for 0.5, 1, 2, 6, 12, 24, 48, 72, 96 and 185 h under room temperature (controlled to 25 °C). Each mix was filtered through a 0.45- μ m nylon membrane filter. For sample extraction, 2 mL of hexane was injected into 10 mL of each filtrate. One milliliter of supernatant was transferred into a 2 mL amber vial with a rubber cap for GC analysis (Method S6). All experiments were performed in triplicate.

3.2.2.2. Degradation kinetics

The pH-dependent simazine degradation was measured across pH ranges from 1 to 12 to obtain time-course variations in simazine concentration. A concentrated simazine solution was prepared by mixing 5 mL of a standard stock solution with methanol (20 mg L⁻¹) and distilled water (15 mL) in the vial to make 5 mg L⁻¹ as the initial concentration. The pH was adjusted daily with 0.1 M HCl or 0.1 M NaOH. The simazine solution was allowed to equilibrate in a 30 mL amber glass vial with a Teflon-lined cap on a vial-shaker (DS-300L, Dasol, Korea) at 160 rpm under controlled room temperature (25 °C) conditions. The initial pH values were set at 1, 2, 4, 6, 8, 10, 11 and 12, and the sample was collected at 1, 12, 24 and 81 h. The pH was measured at the start and end of each pH-run without adjusting the pH during agitation. For sample extraction, the pH of solution was adjusted to pH 7 to minimize speciation effect on extraction, and 2 mL of hexane was injected into 10 mL of each filtrate. One

milliliter of supernatant was transferred into a 2 mL amber vial with a rubber cap for GC analysis. All experiments were performed in triplicate.

3.2.2.3. Speciation

The pH-dependent speciation of simazine was measured from pH 2 to 12 (2 pH intervals). A concentrated simazine solution was prepared by mixing 5 mL of a standard stock solution with methanol (20 mg L^{-1}) and distilled water (15 mL) in the vial to make 5 mg L^{-1} as the initial concentration. The simazine solution was allowed to equilibrate in a 30 mL amber glass vial with a Teflon-lined cap on a vial-shaker (DS-300L, Dasol, Korea) at 160 rpm under controlled room temperature ($25 \text{ }^{\circ}\text{C}$) conditions. I performed two sets of triplicate for the hexane extraction. The pH in a set of triplicate was adjusted to pH 7, and the pH of another set of triplicate was not readjusted. Two mL of hexane was injected into 10 mL of each filtrate. One milliliter of supernatant was transferred into a 2 mL amber vial with a rubber cap for GC analysis. One set adjusted to pH 7 was used for analysis of the total concentration of simazine, and the other set with no pH adjustment was for the concentration of neutral simazine.

3.2.2.4. Sorption isotherm

Five milliliters of simazine stock solution (20 mg L^{-1}) and 5 mL of 0.2 M CaCl_2 were mixed with different concentrations ($2.5, 5, 7.5, \text{ and } 10 \text{ g L}^{-1}$) of biochar. The mix was allowed to equilibrate in a 30 mL amber glass vial with a Teflon-lined cap on a vial-shaker (DS-300L, Dasol, Korea) at 160 rpm under controlled room temperature ($25 \text{ }^{\circ}\text{C}$) conditions. The pH of the sample was adjusted daily to 3, 5.5 and 9 using 1 M HCl or 1 M NaOH. For sample extraction, the pH of solution was adjusted to pH 7 to minimize speciation effect on extraction, and 2 mL of hexane was injected into 10 mL of each filtrate.

One milliliter of supernatant was transferred into a 2 mL amber vial with a rubber cap for GC analysis. All experiments were performed in triplicate.

3.2.2.5. Sorption isotherm for Scatchard plot analysis

The simazine stock solution (20 mg L⁻¹), distilled water and the background solution (0.2 M CaCl₂) were mixed up to make different concentration of simazine (0.5, 1, 2, 3, 4 and 5 mg L⁻¹) with constant ionic strength (0.05 M CaCl₂). The mix was allowed to equilibrate in a 30 mL amber glass vial containing 0.2 g of the biochar with a Teflon-lined cap on a vial-shaker (DS-300L, Dasol, Korea) at 160 rpm under controlled room temperature (25 °C) conditions. The samples were shaken for 81 h, and the pH was daily readjusted using 1 M HCl or 1 M NaOH. The target pH of the sample was 3.5 and 7.5. For sample extraction, the pH of solution was adjusted to pH 7 to minimize speciation effect on extraction, and 2 mL of hexane was injected into 10 mL of each filtrate. One milliliter of supernatant was transferred into a 2 mL amber vial with a rubber cap for GC analysis. All experiments were performed in triplicate.

3.2.2.6. Simazine analysis

Samples were injected into a gas chromatograph equipped with a micro-electron capture detector (GC- μ ECD) (6890N, Agilent Technologies Inc., USA). A silica capillary column (HP-5, 0.32 mm i.d. x 30 m x 0.25 μ m) was used (Morgante et al. 2012). The inlet temperature was maintained at 250 °C and operated in split-mode with a 1 mL sample injection-volume using an autosampler. The GC oven-temperature was initially set to 50 °C with a hold-time of 1 min, and then raised to 150 °C at 20 °C min⁻¹ with a hold-time of 4 min, to 230 °C at 3 °C min⁻¹ with a hold-time of 1 min and finally to 300 °C at 10 °C min⁻¹ with a final hold-time of 2.5 min. Total analysis-time per sample

was 50 min, and the retention-time was 19 min. The μ ECD was kept at 300 °C. All calibrations were performed in ChemStation (Agilent, USA).

3.2.3. Data analysis and fitting

A formulation that simulate simazine speciation was proposed based on the Henderson-Hasselbach equation (1) (Gunasekara et al. 2007), and 1.7 was used for the pK_a of simazine (Gunasekara et al. 2007).

$$pH = pK_a + \log([S]/[HS^+]) \quad (1)$$

where [S] and [HS⁺] are the concentrations of neutral and protonated simazine (mol L⁻¹), respectively. Concentration of simazine sorbed (q_{eq} , mg kg⁻¹) were calculated from differences between the initial and equilibrium concentrations in solution (2):

$$q_{eq} = \frac{(C_0 - C_{eq}) \times V}{m} \quad (2)$$

where C_0 and C_{eq} are the initial and equilibrium concentrations of simazine (mg L⁻¹) in solution, and m (kg) and V (L) are the mass of sorbent and volume of solution, respectively.

Percent simazine recovery (3) was obtained by extracting the sorbed simazine using methanol (Morgante et al. 2012), and 98-103% (data excluded).

$$Recovery = \frac{(C_{eq} + C_{ex})}{C_0} \times 100 \quad (3)$$

where C_{ex} is the concentration (mg L⁻¹) after methanol-extracted.

A first-order kinetics (4) was applied to describe the degradation of simazine (Bersanetti et al. 2005).

$$\ln C_t = \ln C_0 - k_{dg} \cdot t \quad (4)$$

where C_t is the concentration (mg L⁻¹) at time t (h) and k_{dg} is the rate constant (mg L⁻¹h⁻¹) at $1/t$. Isotherm results at pH values (3, 6 and 9) were fitted to the

Langmuir, Freundlich, and Dubinin-Radushkevich isotherm (Foo and Hameed 2010; Liu and Chen 2015).

The Langmuir model is expressed as follows:

$$q_{eq} = \frac{q_{max} \cdot K_L \cdot C_{eq}}{(1 + K_L \cdot C_{eq})} \quad (5)$$

where K_L is a constant ($L \text{ mg}^{-1}$) related to energy, and q_{max} is the maximum sorption capacity (mg kg^{-1}).

The Freundlich model is expressed as follows:

$$q_{eq} = K_F \cdot C_{eq}^{\frac{1}{n}} \quad (6)$$

where K_F ($\text{mg kg}^{-1}(\text{mg L}^{-1})^{-n}$) and $1/n$ are the equilibrium constants indicative of the sorption capacity and intensity, respectively.

The Dubinin-Radushkevich model, which describes non-ideal adsorption by heterogeneous surface energies, is expressed as follows (Dabrowski 2001):

$$q_{eq} = q_{max} \cdot e^{(-\beta \cdot F^2)} \quad (7)$$

$$F = R \cdot T \cdot \ln \left(1 + \frac{1}{C_{eq}} \right) \quad (8)$$

where β is related to mean sorption energy ($\text{mol}^2 \text{kJ}^{-2}$), F is the Polanyi potential, R is the gas law constant ($\text{kJ mg}^{-1} \text{K}^{-1}$), and T is absolute temperature (K). This model serves as a proxy to check whether sorption follows physisorption or chemisorption. The E_s indicates the free energy changes (kJ mol^{-1}) when one mole of ions is transferred into infinite space from its sorbent space during sorption, serving as a criterion to distinguish between physisorption and chemisorption (9).

$$E_s = \frac{1}{\sqrt{2 \cdot \beta}} \quad (9)$$

To compare the applicability of the model, the percent normalized standard deviation (Δq) was calculated as follows (Mihaly Cozmuta et al. 2012):

$$\Delta q = 100 \times \sqrt{\frac{\sum_{i=1}^n \left[\left(\frac{q_{exp} - q_{cal}}{q_{exp}} \right)_i \right]^2}{n-1}} \quad (10)$$

where q_{exp} and q_{cal} are measured and calculated amount of simazine sorbed on biochar (mg kg^{-1}) for the number of experimental points (n).

Scatchard plot (11) is used to evaluate the affinities of binding sites for a particular sorption (Gezici et al. 2005; Pehlivan et al. 2008).

$$\frac{q_{eq}}{c_{eq}} = -\left(\frac{1}{K_{ds}}\right)q_{eq} + \frac{q_{max}}{K_{ds}} \quad (11)$$

where K_{ds} is the dissociation constant (mg L^{-1}) of the binding site. Lower K_{ds} indicates involvement of more active sites for sorption (Pehlivan et al. 2008). A plot that deviates from linearity means the presence of more than one type of binding site, while a linear plot assumes that the binding sites are identical and independent (Gezici et al. 2007; Liu and Chen 2015).

3.3. Results and discussion

3.3.1. Physicochemical characteristics of biochar

The SSA was estimated at $5.6 \text{ m}^2 \text{ g}^{-1}$ for micro-pores and $191.6 \text{ m}^2 \text{ g}^{-1}$ for nano-pores in B400, and 236.3 and $293.5 \text{ m}^2 \text{ g}^{-1}$, respectively, in B700 (Table 3-1). Previous investigations on *Miscanthus* biochar reported that SSA of micro-pores ranged from 2.4 to $381.5 \text{ m}^2 \text{ g}^{-1}$, and sharply increased in pyrolysis temperature range between 400 and $600 \text{ }^\circ\text{C}$ (Kim et al. 2013). Luo et al. (2015) and Han et al. (2016b) ascribed this SSA increase to progressive volatilization of cellulose, hemicellulose and lignin as temperature increased, since volatilization causes formation of channel structures with larger pore-size, increasing total SSA. The result of size fractionation for $< 25 \text{ }\mu\text{m}$, $25\text{-}53 \text{ }\mu\text{m}$ and $53\text{-}106 \text{ }\mu\text{m}$ were 14.7 , 52.8 and 32.5% for B400 while 15.6 , 62.0 and 22.4% for B700, respectively.

Numerous studies on biochar have related some molar elemental ratios such as (O+N)/C, H/C and O/C to polarization, carbonization and hydrophilization, respectively (Chen and Chen 2009; Chen et al. 2012a). In this study, B400 had a (O+N)/C of 0.28, O/C of 0.27 and H/C of 0.60, whereas B700 had 0.19, 0.18 and 0.17, respectively, due to increased C and decreased H, N, O and S contents (Keiluweit et al. 2010), indicating decreased polarization and hydrophilization and increased carbonization with increasing pyrolysis temperature. Previous studies have shown that *Miscanthus* biochar produced at 400 °C had a (O+N)/C ranging between 0.26 and 0.48, O/C between 0.26 and 0.48, and H/C between 0.05 and 0.09, while those produced at 700 °C had the respective ratios ranged from 0.08 to 0.09, 0.07 to 0.08, and was 0.02 (Budai et al. 2014; Trazzi et al. 2016). The yield and Ash content were 31.0 and 8.8 for B400 while it was 26.0 and 11.6 for B700, respectively.

The PZNC was determined as 8.8 for B400 and 10.0 for B700, thus indicating that more alkalines, metal oxides and minerals were released from the latter, causing the development of more positively charged sites at a given pH (Al-Wabel et al. 2013). Since solution-pH determines its net surface charge, biochar can have positively and negatively charged surfaces for hydrophilic interactions at a given pH (As 2010). This means that net surface charge of B400 and B700 are positive at circumneutral pH, with more positive charges at the surface of the latter. The acidities of B400 and B700 were measured at 0.150 and 0.013 mmol g⁻¹ for carboxylic acid groups, 0.167 and 0.125 mmol g⁻¹ for lactonic acid groups, and 0.421 and 0.013 mmol g⁻¹ for phenolic acid groups, respectively, and the decrease in the acidity of surface functional groups with increasing pyrolysis temperature was due to volatilization of oxygen containing structures

Table 3-1 Physicochemical characteristics of *Miscanthus* biochar produced at two pyrolysis temperatures at 400 °C (B400) and 700 °C (B700).

Biochar	Specific surface area ^a (m ² g ⁻¹)		Elemental composition ^c (%)					Atomic ratio			Acidic functional group ^d (mmol g ⁻¹)				PZNC ^e	Yield (%)	Ash ^f (%)
	Micro-pores ^b	Nano-pores ^b	C	H	O	N	S	(O+N)/CH/C	O/C	Carboxylic	Lactonic	Phenolic	Total				
B400	5.6	191.6	70.5	3.5	25.4	0.6	0.02	0.28	0.60	0.27	0.150	0.167	0.421	0.74	8.8	31.0	8.8
B700	236.3	57.2	79.2	1.1	19.3	0.4	0.02	0.19	0.17	0.18	0.013	0.125	0.013	0.15	10.0	26.0	11.6

^aSpecific surface area (SSA) was estimated based on the results obtained from BET isotherms using N₂ (N₂-BET) and CO₂ (CO₂-BET).

^bThe SSA of micropores was equal to the N₂-BET results, while that of nanopores was calculated by subtracting the CO₂-BET results from the N₂-BET results.

^cElemental composition was measured using an elemental analyzer, and the atomic ratio was calculated.

^dAcidic functional groups were measured by Boehm titration.

^eThe point of zero net charge (PZNC) was estimated by the pH drift method.

^fAsh content was estimated by the combustion method.

Table 3-2 X-ray fluorescence (XRF) spectroscopy results of dried *Miscanthus* and biochar produced at 400 °C (B400) and 700 °C (B700).

Components	Dried <i>Miscanthus</i>	B400	B700
	Weight percent (%)		
CH ₂	99.9	97.0	95.7
Si	0.60	1.61	2.35
K	0.05	0.68	0.98
Ca	0.11	0.22	0.30
P	0.04	0.17	0.23
Mg	0.05	0.15	0.22
S	0.02	0.04	0.05
Al	0.01	0.03	0.05
Fe	0.01	0.02	0.03
Cl	0.08	0.02	0.06
Mn	0.01	0.02	0.02
Zn	0.00	0.00	0.01

(Chun et al. 2004; Song and Guo 2012). The XRF results of B400 and B700 revealed that each concentration of Si, K, Ca, P, Mg, S, Al and Fe was below 1%. Concentrations of Si were 0.60% for biochar feedstock, 1.61% for B400 and 2.35% for B700, as a result of Si-accumulation due to pyrolysis.

3.3.2. Structural transformation of biochar

Compared with biochar feedstock, the bands representing vibrations for polysaccharide, aliphatic, ester, phenol and carbohydrate structures disappeared during pyrolysis, while those indicating double bonds of aromatic C=C (1596 cm^{-1}) and carbonyl C=O (1695 cm^{-1}) (Chen et al. 2008) appeared in B400 but completely disappeared in B-700 (Fig. 3-1), leaving only lignin C=C (1540 cm^{-1}) and Si-containing structures ($1200\text{-}900\text{ cm}^{-1}$). Relative intensities of biochar peaks were lower at higher pyrolysis temperature ($700\text{ }^{\circ}\text{C}$) due to the formation of ring-structured lignin C=C and concomitant decreases in carbonyl C=O and aromatic C=C (Fig. 3-1), creating larger pores (Table 3-1). This was corroborated by the scanning electron photomicrograph (SEM) images (Fig. 3-2). It was observed that the decrease of acidity of surface functional group with increasing pyrolysis temperature, and the structural transformation to aromatic structure led such result (Table 3-1).

In both biochar, the band indicating Si-O-Si and Si-O vibrations appeared at 1094 cm^{-1} (Xu and Chen 2015). The XRF spectrograms of biochar also corroborated Si-accumulation and mineral deposits (Table 3-2). Xiao et al. (2014) reported an accumulation of Si-containing structures and a concurrent decrease in single bonds among C, S and O atoms in biochar with increasing pyrolysis temperature. Therefore, it inferred that pyrolysis caused conversion of single-bond structures of *Miscanthus* feedstock into aromatic structures with Si-accumulation. Further pyrolysis to $700\text{ }^{\circ}\text{C}$ led to the formation of ligneous structures with mineral salt deposits, increasing SSA due to the increase in

micro-pore (larger pore) volumes (Fig. 3-2 and Table 3-1). Apparent density of biochar increases with increasing activation during pyrolysis due to the collapse of pores (Ding et al. 2014), and was 0.43 Mg m^{-3} for B400 and 0.48 Mg m^{-3} for B700. The SEM photomicrographs (Fig. 3-2) and XRF spectrograms (Table 3-2) supported the accumulation of mineral salts on biochar surface, suggesting a probable contribution of mineral surface moieties of biochar to simazine sorption. However, since sorption distribution coefficients (K_d) for triazine onto mineral surfaces in the literature were very low (Clausen et al. 2001) and the mineral fractions of our *Miscanthus* biochar were low (3.0% for B400 and 4.3% for B700) (Table 3-2), and it disregarded the contribution of mineral surfaces of biochar to the sorption of simazine.

3.3.3. Sorption kinetics, speciation, and degradation

Although sorption equilibrium was reached within 24 h for both biochar (Fig. 3-3), and all batch experiments were conducted for 81 h to guarantee the achievement of equilibrium under various experimental conditions. The mole ratio of neutral to protonated simazine species was 0.60 at pH 1.9, and increased to near unity at pH 5; this increasing pattern fitted well to theoretical calculation using the Henderson-Hasselbalch equation (Fig. 3-4). Rates of simazine degradation (k_{dg}) were 0.012 at pH 1.0 and 0.032 h^{-1} at pH 12.1, while its degradation did not occur across the two pH extremes ($2.0 \leq \text{pH} \leq 10.0$) (Fig. 3-4). Therefore, degradation and protonation of simazine was disregarded across working pH ranges ($3.5 \leq \text{pH} \leq 10$).

Simazine degrades abiotically through chemical and photolytic processes (Rahman and Holland 1985); however, the possibility of photodegradation was disregarded by encapsulation of simazine samples with airtight amber vials. Simazine remains stable in neutral pH range, but becomes

Fig. 3-1 Stacked ATR FT-IR spectra of dried *Miscanthus* and biochar produced at 400 °C (B400) and 700 °C (B700). Arrows and numbers indicate the frequency of the vibration mode in the molecular structure.

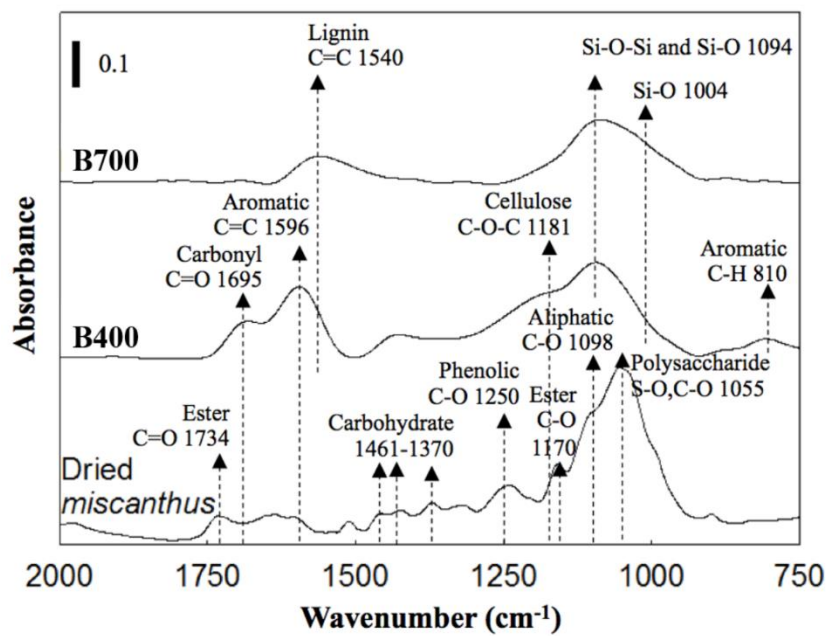


Fig. 3-2 Scanning electron micrographs of *Miscanthus* biochar produced at 400 °C (B400) and 700 °C (B700). All images were recorded with a probe current of 15.5 kV.

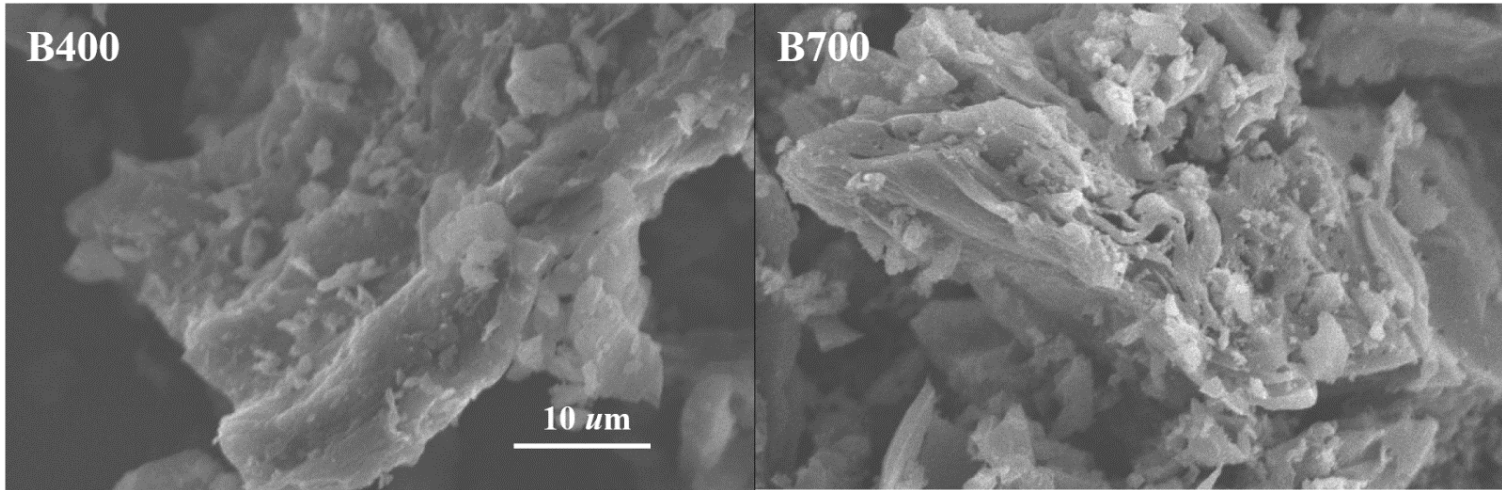


Fig. 3-3 Sorption kinetics of simazine to *Miscanthus* biochar produced at 400 °C (B400; solid circle) and 700 °C (B700; open circle). The initial pH of simazine solution was 4.5, and the final pH of the mixture was 7.9 for B400 and 9.6 for B700. The initial concentration of simazine was 5 mg L⁻¹.

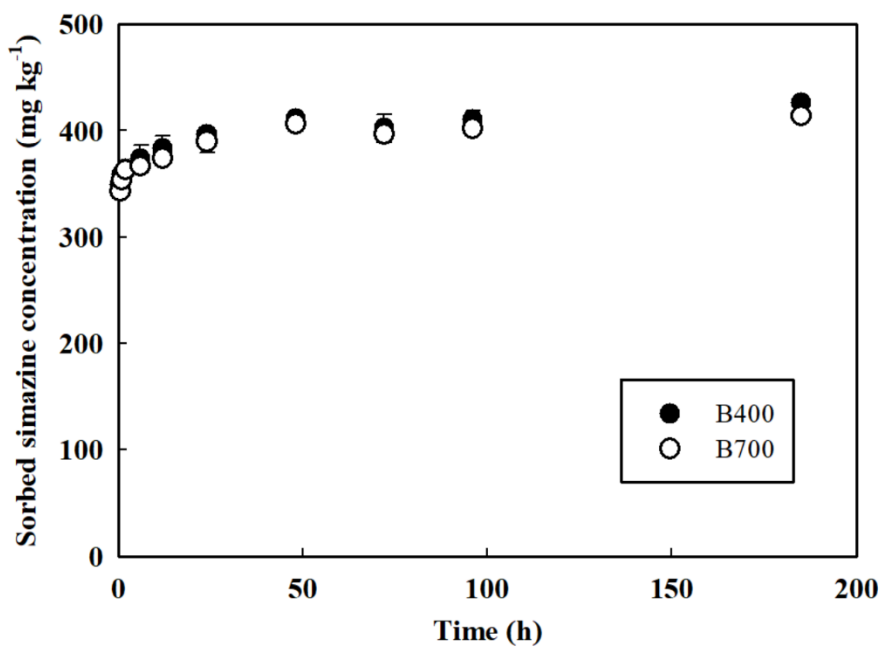
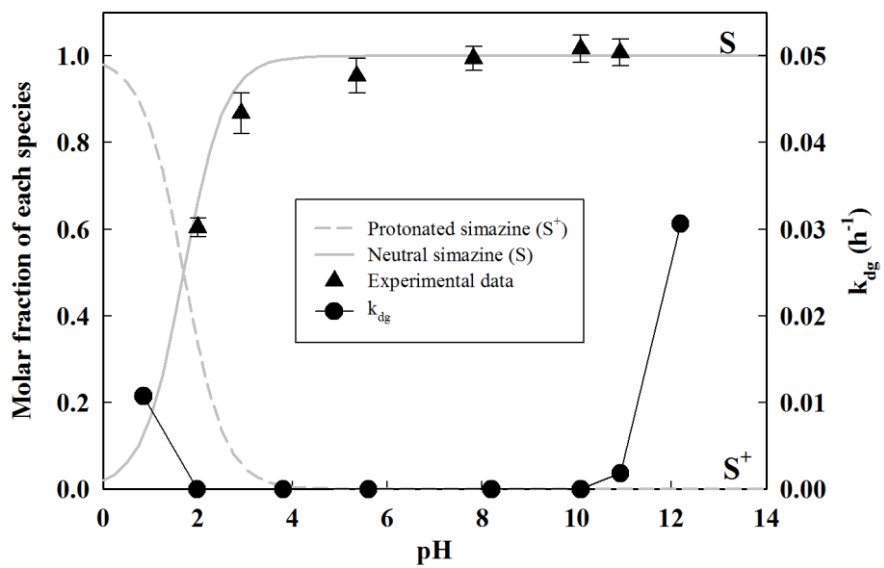


Fig. 3-4 Molar fraction of protonated (gray dashed line) and neutral (gray solid line) simazine calculated using the Henderson-Hasselbach equation and of neutral simazine obtained from batch experiments (solid triangle) as a function of solution pH and the first-order degradation kinetics (k_{dg}) of simazine estimated by varying the pH (solid circle with a line).



unstable under extremely acidic or alkaline conditions. Simazine has been known to undergo hydrolytic dechlorination due to protonation of lone-pair electrons on the N atom in the aromatic ring structure and subsequent cleavage of C-Cl bond due to electron deficiency under acidic conditions and to the direct nucleophilic substitution of Cl by OH under alkaline conditions (Armstrong et al. 1967; Burkhard and Guth 1981).

3.3.4. Sorption isotherm

Equilibrium sorption data were fitted to the Langmuir and Freundlich isotherms to identify the sorption mechanisms of simazine onto biochar, and to the Dubinin-Radushkevich isotherm to estimate E_s . Fitted isotherm parameters indicated that simazine sorption data obtained at three set pH values of 3, 6 and 9 fitted best to the Freundlich model (Fig. 3-5) in terms of average R^2 and Δq (Table 3-3). In this pH region, simazine molecule remains undegraded, while surface acidity of biochar changes at pH 4-5 due to its carboxylic acid groups and at pH 7-8 due to its lactonic acid groups (Leon and Radovic 1991). The fitted result indicated that the simazine sorption on the biochar in this study was more explainable by the heterogeneous adsorption with the Freundlich and the Dubinin-Radushkevich isotherm than the Langmuir isotherm, which assumes monolayer adsorption on the homogeneous solid surface.

From the Dubinin-Radushkevich isotherm plots, the isotherm constant β was calculated as 0.1021 for B400 and 0.1392 for B700; the maximum sorption capacity (q_{max}) was 1154.5 and 856.9 mg kg⁻¹, respectively. The corresponding mean free energy (E_s) was calculated as 1.72-2.92 kJ mol⁻¹ for B400 and 1.46-2.54 kJ mol⁻¹ for B700, thus indicating that the sorption of simazine to biochar followed a physisorption. Relatively high values of E_s indicate enthalpy-related sorption, while relatively low values indicate entropy-related sorption (Liu and Chen 2015). If E_s lies between 0-8 kJ mol⁻¹, the

sorption process follows physisorption, while a value of E_s between 8-16 kJ mol⁻¹ indicates chemisorption (Melvin et al. 2015). In general, q_{max} and E_s decreased with increasing pH and pyrolysis temperature, while the isotherm constant increased (Table 3-3). Based on the results, it infer that the sorption of simazine occurs at heterogeneous sorption sites of biochar surface with a non-uniform distribution of sorption energy, and this inference was well predicted by the results of previous studies (Cao et al. 2009; Zheng et al. 2010).

Decrease in K_F (a proxy of sorption capacity) of the Freundlich model from 1104 to 546 for B400 and from 643 to 427 in B700 with increasing pH (Table 3-3) indicated that the sorption capacity of biochar would vary with pH, posing a challenge to our presumption that hydrophobic interactions would be a dominant process for simazine sorption to biochar surface. To date, few attempts have been made to predict the pH-dependent sorption-behavior of organic pollutants on biochar surface. Yang et al. (2004) reported that the maximum sorption of diuron occurred at pH 2.5, while ametryne showed its maximum sorption at pH 4.0. Zheng et al. (2010) demonstrated that simazine sorption gradually decreased with increasing pH. Jia et al. (2013) observed that K_F of oxytetracycline sorption to maize-straw-derived biochar varied with solution-pH. Previous investigations on the sorption of organic pollutants with ionizable functional groups suggested that their sorption capacity decreases with increasing pH due to electrostatic repulsion between ionizable organic pollutants and biochar (Lingamdinne et al. 2015; Rajapaksha et al. 2015). In our study, however, neutral simazine remained undegraded over a wide pH range from 3 to 10 (Fig. 3-4).

Contrary to our presumption that the sorption capacity of biochar would increase due to an increase in SSA (Chen and Chen 2009; Chen et al. 2012b), our results obviously showed that the mean value of the parameters related to sorption capacity (K_F and q_{max}) of biochar decreased with increasing

pyrolysis temperatures (Table 3-3), while SSA increased (Table 3-1). In particular, the values of K_F and q_{max} also decreased (Table 3-3) as more pH-dependent sorption sites were deprotonated with increasing pH and pyrolysis temperature (Ping et al. 2014), resulting in decreased sorption of neutral simazine (Fig. 3-5).

3.3.5 Scatchard plot analysis of simazine sorption

Estimates of the fitted values of E_s (Table 3-3) indicated simazine sorption followed an entropy-related physisorption. Concave-upward Scatchard plots indicated the presence of two classes of binding sites with differing K_{ds} and/or involvement of at least two sorption processes (Fig. 3-6). Nonlinear Scatchard plots indicate involvement of more than one sorption process (Gezici et al. 2007). The nonlinearity may imply the presence of two types of binding sites having different affinities for the simazine sorption. For that reason, two sorption types were calculated, where has lower sorption range (type-L) and higher sorption range (type-H). The suffix after K_{ds} and q_{max} indicate the sorption types.

Increasing pH increased K_{ds-L} from 0.007 to 0.105 mg L⁻¹ and q_{max-L} from 287.5 to 296.5 mg kg⁻¹ for B400, and from 0.027 to 0.048 mg L⁻¹ and from 313.5 to 355.1 mg kg⁻¹ for B700. However, K_{ds-H} increased in B400 but decreased in B700, while q_{max-H} decreased (Fig. 3-6). In contrast, increasing pyrolysis temperature decreased K_{ds-H} from 0.242 to 0.196 mg L⁻¹ and q_{max-H} from 558.8 to 511.9 mg kg⁻¹; however, K_{ds-L} responded oppositely to pH, while q_{max-L} increased (Fig. 3-6). From these relationships, it infers that pH affected simazine sorption more in the lower sorption-range, while sorption affinity of biochar decreased as pH increased. In contrast, pyrolysis temperature affected more in the higher sorption-range, lowering q_{max} and raising sorption affinity of biochar at higher pyrolysis temperature. Therefore, it deduced that K_{ds-L}

responded sensitively to pH in the lower sorption- range that causes change in the electrostatic field, while K_{ds-H} was responsible for simazine sorption associated with changes in surface and pore-structure modification caused by pyrolysis temperature changes (Table 3-1) in the higher sorption-range. Therefore, increases in pH decreased K_{ds-L} more in B400 than in B700 (Table 3-1), while increases in pyrolysis temperature decreased K_{ds-H} more at higher pH than at lower pH. Estimates of the fitted K_{ds} and q_{max} indicated that the maximum sorption (the sum of q_{max-L} and q_{max-H}) of simazine decreased as pH and/or pyrolysis temperature increased (Fig. 3-5).

Three possible binding mechanisms are involved in the sorption of simazine onto biochar surface: van der Waals (vdW) forces, π - π electron donor-acceptor (EDA) interactions, and weak H-bonding (Zhu et al. 2004). Based on the Scatchard plot analysis, it could ascribe strong electrostatic attraction (S_{es}) to a dominant sorption mechanism in the lower sorption-range (Park et al. 2017), and a relatively weak hydrophobic attraction (S_{hp}) to another process that governs in the higher sorption-range (Xu et al. 2007), since the EDA or H-bonding interactions are responsible for S_{es} and the vdW interactions explain S_{hp} (Gauthier et al. 1987; Krichko and Gagarin 1990). As consequences, two types of binding sites of biochar responded independently to changing pH and/or pyrolysis temperature.

3.3.6. Sorption mechanism

Based on the physicochemical characteristics of biochar and batch sorption results, it addresses two questions about simazine sorption in response to changes in pH and pyrolysis temperature. The first question is the causal relationships for decrease q_{max} with increasing pH (Fig. 3-6). At pH 3.6 or 3.8 (almost pK_a+2), simazine behaves as a neutral molecule, causing strong S_{hp} with positively charged biochar while weakening the contribution of S_{es} . Increases

Fig. 3-5 Fitting of the Freundlich isotherm to each dataset of simazine sorption obtained at three set pH values [3.0 (circle), 5.5 (rectangle) and 9 (triangle)] for (a) B400 and (b) B700.

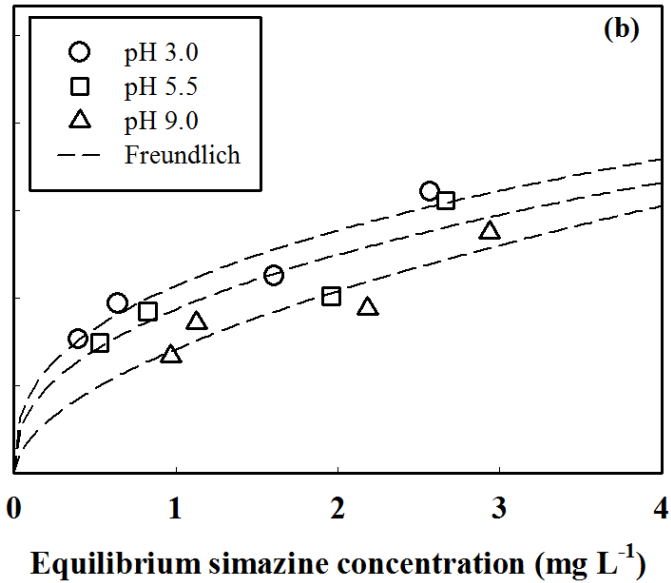
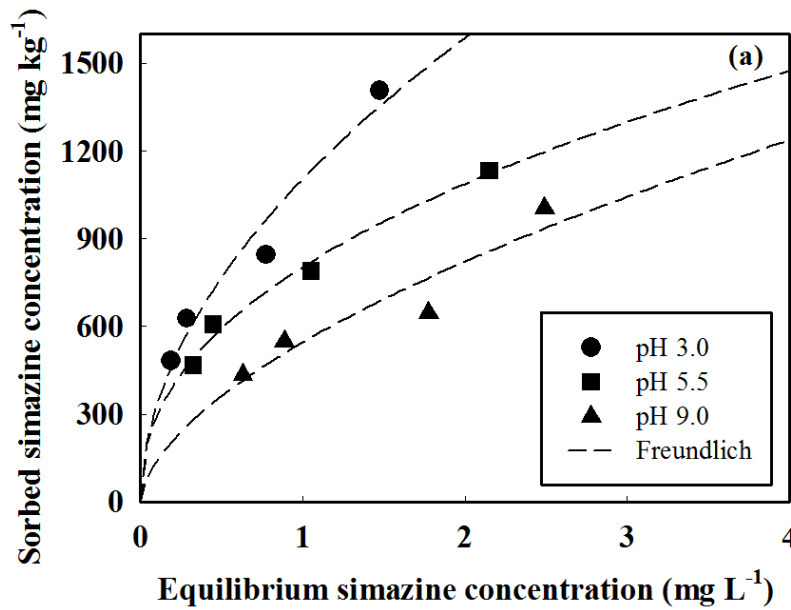


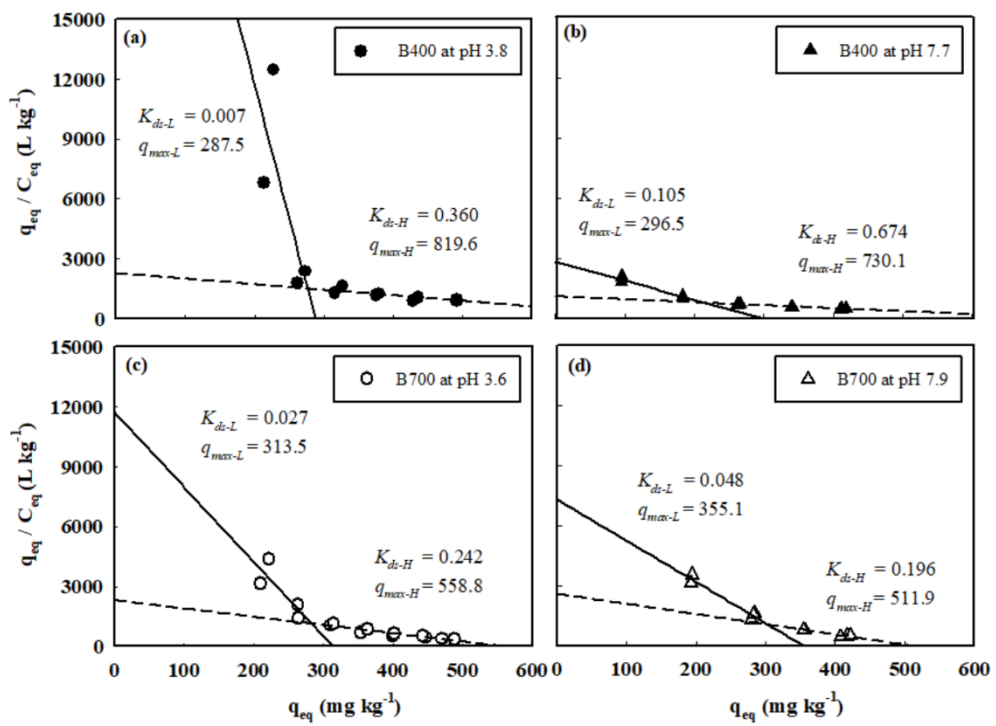
Table 3-3 Isotherm parameters for sorption of simazine on the *Miscanthus* biochar produced pyrolysis temperature at 400 °C (B400) and 700 °C (B700). The biochar dosage was 2.5, 5.0, 7.5 and 10 g L⁻¹ with 5 mg L⁻¹ simazine for 81 h of agitation using vial-shaker (DS-300L, Dasol, Korea) at 160 rpm under room temperature (controlled to 25 °C). The target pH was 3.0, 5.5 and 9.0, and the pH was daily adjusted with 1M HCl or 1M NaOH. The value in parentheses indicates the standard error of isotherm fitting.

Biochar	pH	Langmuir isotherm				Freundlich isotherm				Dubinin-Radushkevich isotherm				
		K_L	q_{max}	R^2	Δq	K_F	$1/n$	R^2	Δq	β	q_{max}	E_s	R^2	Δq
B400	3.0	1.44	1939	0.90	16.3	1104	0.523	0.96	10.3	0.059	1361	2.92	0.83	18.7
	(0.02)	(0.85)	(520)			(63.0)	(0.09)			(0.02)	(212)			
	5.5	1.43	1452	0.96	7.42	803.3	0.438	0.99	5.35	0.079	1122	2.52	0.91	10.3
	(0.26)	(0.41)	(170)			(21.3)	(0.04)			(0.02)	(105)			
	9.0	0.50	1665	0.85	14.5	546.2	0.590	0.88	12.5	0.169	980.5	1.72	0.76	16.8
	(0.03)	(0.41)	(733)			(62.8)	(0.16)			(0.07)	(161)			
B700	3.0	1.67	1089	0.85	11.7	643.0	0.372	0.91	9.10	0.078	894.8	2.54	0.78	13.3
	(0.02)	(0.89)	(194)			(41.9)	(0.09)			(0.03)	(108)			
	5.5	1.21	1078	0.73	16.3	563.1	0.412	0.79	14.6	0.105	844.8	2.18	0.66	17.4
	(0.57)	(0.96)	(312)			(69.2)	(0.16)			(0.06)	(136)			
	9.0	0.47	1315	0.81	13.3	426.8	0.551	0.84	12.4	0.235	831.0	1.46	0.75	14.5
	(0.21)	(0.37)	(540)			(61.2)	(0.17)			(0.10)	(127)			

in pH to 7.7 or 7.9 induces deprotonation of acidic carboxylic groups, decreasing sorption affinity of biochar to neutral simazine due to increased negative charge densities on biochar surface, which therefore decreases q_{max} due to increased electrostatic and/or hydrophobic repulsion (Chen and Chen 2009). However, despite increased K_{ds-L} , q_{max-L} slightly increased, indicating the presence of attractive electrostatic interactions as surface negativity increased (Qiu et al. 2009). This phenomenon was corroborated by the experimental sorption data that were fitted to the Freundlich model (Fig. 3-5). Therefore, it concluded that pH is a major factor that governs simazine sorption through S_{es} that controls deprotonation of acidic functional groups of biochar and protonation of simazine.

Second, q_{max} decreased with increasing pyrolysis temperature (Table 3-3) while SSA increased (Table 3-1). This observation was not consistent with previous results that the sorption of organic pollutants to biochar increased as SSA increased (Chen and Chen 2009; Chen et al. 2012a). In this study, SSA increased with pore-size enlargement due to pore-structure deformation during pyrolysis as pyrolysis temperature increased (Table 3-1). Increase in pyrolysis temperature induced deformation of smaller pores to more open-structured larger pores that may provide more accessible sorption sites (Table 3-1), leading to increased biochar sorption affinity at a given pH. However, increases in pyrolysis temperature decreased maximum sorption over a higher sorption-range (q_{max-H}) while the affinity of biochar for simazine increased, indicating possible unstable simazine sorption favoring desorption in large micro-pores prior to sorption-desorption equilibrium. Lian et al. (2011) observed that during the sorption/desorption process, desorption of organic pollutants was less hindered in relatively smaller nano-pores with turbostratic and partly compartmentalized structures. However, simazine sorption to biochar in lower

Fig. 3-6 Scatchard plot (y-axis: the ratio of biochar-bound simazine to free simazine, q_{eq}/C_{eq} ; x- axis: q_{eq}) showing two types of sorption mechanism between simazine and biochar obtained at: (a) pH = 3.8 (solid circle) and (b) pH = 7.7 (solid triangle) for B400, and (c) pH = 3.6 (open circle) and (d) pH = 7.9 (open triangle) for B700. Data points represent experimental results. Solid lines represent electrostatic interaction; dashed lines denote hydrophobic interaction.



sorption-range (q_{max-L}) increased with pyrolysis temperature (Fig. 3-6), and this increase was due to S_{es} (Lian et al. 2011). However, pyrolysis temperature - induced deformation of pore-structure resulted in overall decrease in q_{max} , and this deduction agreed well with experimental sorption data (Fig. 3-5). Therefore, pyrolysis temperature is a dominant factor that governs simazine sorption through S_{hp} due to deformation of smaller pores to open-structured pores.

3.4. Conclusions

I hypothesized that pH would determine the surface charge density of biochar and simazine that alters the response of simazine sorption, and this response would vary with pyrolysis temperature. Pyrolysis resulted in conversion of single bond structures of *Miscanthus* feedstock into aromatic structures with Si-accumulation, and further pyrolysis at 700 °C led to the formation of ligneous structures with mineral salt deposits and increased SSA due to an increase in micro-pore. Alterations in pore-structures and surface-minerals of biochar with concave-upward Scatchard plots corroborated the existence of at least two dominant sorption mechanisms with multiple types of binding sites: strong sorption process due to electrostatic attraction and weak sorption process *via* hydrophobic attraction. Overall, q_{max} decreased as pH and pyrolysis temperature increased. Decreases in q_{max-L} with increasing pH could be explained by decreases in S_{es} due to progressive deprotonation of acidic functional groups, decreasing positively charged surface at biochar. However, decreases in q_{max-H} with increasing pyrolysis temperature was due to decreases in S_{hp} , resulting from progressive deformation of pore-structure. The results confirmed our hypothesis that solution-pH and pyrolysis temperature differently affect the sorption of simazine containing lone-pair electrons onto the surface of biochar with variable surface charge density. There are numerous studies to amend the biochar in the soil environment for sequestering the

carbon, improving the soil physical property, holding the nutrients and decomposing the organic pollutants. Many promising results have showed up so far, but the fundamental and crucial mechanisms have not fully understood yet. Based on this study, one step forward to understand the feasible mechanism between organic pollutants and biochar under various pH conditions, and it would be applicable to estimate the transport and degradation phenomena of organic pollutant in the presence of biochar under soil environment.

References

- Ahmad M, Lee SS, Dou X, Mohan D, Sung JK, Yang JE, Ok YS (2012) Effects of pyrolysis temperature on soybean stover- and peanut shell-derived biochar properties and TCE adsorption in water. *Bioresour Technol* 118:536–544. doi: 10.1016/j.biortech.2012.05.042
- Al-Wabel MI, Al-Omran A, El-Naggar AH, Nadeem M, Usman ARA (2013) Pyrolysis temperature induced changes in characteristics and chemical composition of biochar produced from conocarpus wastes. *Bioresour Technol* 131:374–379. doi: 10.1016/j.biortech.2012.12.165
- Armstrong DE, Chesters G, Harris RF (1967) Atrazine Hydrolysis in Soil. *Soil Sci Soc Am J* 31:61. doi: 10.2136/sssaj1967.03615995003100010019x
- As (2010) pH-dependent mineral release and surface properties of corn straw biochar agronomic implications. *Environ Sci Technol* 44:9318–9323
- Atkinson CJ, Fitzgerald JD, Hips NA (2010) Potential mechanisms for achieving agricultural benefits from biochar application to temperate soils: A review. *Plant Soil* 337:1–18. doi: 10.1007/s11104-010-0464-5
- Bersanetti PA, Almeida RMRG, Barboza M, Araújo MLGC, Hokka CO (2005) Kinetic studies on clavulanic acid degradation. *Biochem Eng J* 23:31–36. doi: 10.1016/j.bej.2004.10.007
- Betts AR, Chen N, Hamilton JG, Peak D (2013) Rates and mechanisms of Zn²⁺ adsorption on a meat and bonemeal biochar. *Environ Sci Technol* 47:14350–14357. doi: 10.1021/es4032198
- Boehm HP (1994) Some aspects of the surface chemistry of carbon blacks and other carbons. *Carbon N Y* 32:759–769. doi: 10.1016/0008-6223(94)90031-0
- Budai A, Wang L, Gronli M, Strand LT, Antal MJ, Abiven S, Dieguez-alonso A, Anca-couce A, Rasse DP (2014) Surface Properties and Chemical Composition of Corn cob and Miscanthus Biochars: Effects of Production Temperature and Method
- Burkhard N, Guth JA (1981) Chemical hydrolysis of 2-chloro-4,6-bis(alkylamino)-1,3,5-triazine herbicides and their breakdown in soil under the influence of adsorption. *Pestic Sci* 12:45–52. doi: 10.1002/ps.2780120107
- Cao X, Harris W (2010) Properties of dairy-manure-derived biochar pertinent to its potential use in remediation. *Bioresour Technol* 101:5222–5228. doi: 10.1016/j.biortech.2010.02.052
- Cao X, Ma L, Gao B, Harris W (2009) Dairy-manure derived biochar effectively sorbs lead and atrazine. *Environ Sci Technol* 43:3285–3291. doi: 10.1021/es803092k

- Celis R, Cornejo J, Hermosín MC, Koskinen WC (2010) Sorption-Desorption of Atrazine and Simazine by Model Soil Colloidal Components. *Soil Sci Soc Am J* 61:436. doi: 10.2136/sssaj1997.03615995006100020010x
- Chen B, Chen Z (2009) Sorption of naphthalene and 1-naphthol by biochars of orange peels with different pyrolytic temperatures. *Chemosphere* 76:127–133. doi: 10.1016/j.chemosphere.2009.02.004
- Chen B, Zhou D, Zhu L (2008) Transitional adsorption and partition of nonpolar and polar aromatic contaminants by biochars of pine needles with different pyrolytic temperatures. *Environ Sci Technol* 42:5137–5143. doi: 10.1021/es8002684
- Chen Z, Chen B, Chiou CT (2012a) Fast and slow rates of naphthalene sorption to biochars produced at different temperatures. *Environ Sci Technol* 46:11104–11111. doi: 10.1021/es302345e
- Chen Z, Chen B, Zhou D, Chen W (2012b) Bisolute sorption and thermodynamic behavior of organic pollutants to biomass-derived biochars at two pyrolytic temperatures. *Environ Sci Technol* 46:12476–12483. doi: 10.1021/es303351e
- Chun Y, Sheng G, Chiou GT, Xing B (2004) Compositions and sorptive properties of crop residue-derived chars. *Environ Sci Technol* 38:4649–4655. doi: 10.1021/es035034w
- Clausen L, Fabricius I, Madsen L (2001) Adsorption of pesticides onto quartz, calcite, kaolinite, and alpha-alumina. *J Environ Qual* 30:846–857. doi: 10.2134/jeq2001.303846x
- Contescu A, Contescu C, Putyera K, Schwarz JA (1997) Surface acidity of carbons characterized by their continuous pK distribution and Boehm titration. *Carbon N Y* 35:83–94. doi: 10.1016/S0008-6223(96)00125-X
- Da browski A (2001) Adsorption - From theory to practice. *Adv Colloid Interface Sci* 93:135–224. doi: 10.1016/S0001-8686(00)00082-8
- Ding W, Dong X, Ime IM, Gao B, Ma LQ (2014) Pyrolytic temperatures impact lead sorption mechanisms by bagasse biochars. *Chemosphere* 105:68–74. doi: 10.1016/j.chemosphere.2013.12.042
- Fang Q, Chen B, Lin Y, Guan Y (2014) Aromatic and hydrophobic surfaces of wood-derived biochar enhance perchlorate adsorption via hydrogen bonding to oxygen-containing organic groups. *Environ Sci Technol* 48:279–288. doi: 10.1021/es403711y
- Fang S, Tsang DCW, Zhou F, Zhang W, Qiu R (2016) Stabilization of cationic and anionic metal species in contaminated soils using sludge-derived biochar. *Chemosphere* 149:263–271. doi: 10.1016/j.chemosphere.2016.01.060
- Fidel RB, Laird DA, Thompson ML (2013) Evaluation of Modified Boehm Titration Methods for Use with Biochars. *J Environ Qual* 42:1771. doi: 10.2134/jeq2013.07.0285

- Flores C, Morgante V, González M, Navia R, Seeger M (2009) Adsorption studies of the herbicide simazine in agricultural soils of the Aconcagua valley, central Chile. *Chemosphere* 74:1544–1549. doi: 10.1016/j.chemosphere.2008.10.060
- Foo KY, Hameed BH (2010) Insights into the modeling of adsorption isotherm systems. *Chem Eng J* 156:2–10. doi: 10.1016/j.cej.2009.09.013
- Gauthier TD, Seitz WR, Grant CL (1987) Effects of Structural and Compositional Variations of Dissolved Humic Materials on Pyrene Koc Values. *Environ Sci Technol* 21:243–248. doi: 10.1021/es00157a003
- Gezici O, Kara H, Ersöz M, Abali Y (2005) The sorption behavior of a nickel-insolubilized humic acid system in a column arrangement. *J Colloid Interface Sci* 292:381–391. doi: 10.1016/j.jcis.2005.06.009
- Gezici O, Kara H, Yanik S, Ayyildiz HF, Kucukkolbasi S (2007) Investigating sorption characteristics of copper ions onto insolubilized humic acid by using a continuously monitored solid phase extraction technique. *Colloids Surfaces A Physicochem Eng Asp* 298:129–138. doi: 10.1016/j.colsurfa.2006.12.007
- Grubb DT (1974) Radiation damage and electron microscopy of organic polymers. *J Mater Sci* 9:1715–1736. doi: 10.1007/BF00540772
- Gunasekara AS, Troiano J, Goh KS, Tjeerdema RS (2007) Chemistry and fate of simazine. *Rev Environ Contam Toxicol* 189:1–23. doi: 10.1007/978-0-387-35368-5_1
- Han L, Qian L, Yan J, Chen M (2016a) Contributions of different biomass components to the sorption of 1,2,4-trichlorobenzene under a series of pyrolytic temperatures. *Chemosphere* 156:262–271. doi: 10.1016/j.chemosphere.2016.04.031
- Han L, Qian L, Yan J, Chen M (2016b) Contributions of different biomass components to the sorption of 1,2,4-trichlorobenzene under a series of pyrolytic temperatures. *Chemosphere* 156:262–271. doi: 10.1016/j.chemosphere.2016.04.031
- Jia M, Wang F, Bian Y, Jin X, Song Y, Kengara FO, Xu R, Jiang X (2013a) Effects of pH and metal ions on oxytetracycline sorption to maize-straw-derived biochar. *Bioresour Technol* 136:87–93. doi: 10.1016/j.biortech.2013.02.098
- Jia M, Wang F, Bian Y, Jin X, Song Y, Kengara FO, Xu R, Jiang X (2013b) Effects of pH and metal ions on oxytetracycline sorption to maize-straw-derived biochar. *Bioresour Technol* 136:87–93. doi: 10.1016/j.biortech.2013.02.098
- Keiluweit M, Nico PS, Johnson M, Kleber M (2010) Dynamic molecular structure of plant biomass-derived black carbon (biochar). *Environ Sci Technol* 44:1247–1253. doi: 10.1021/es9031419
- Kim WK, Shim T, Kim YS, Hyun S, Ryu C, Park YK, Jung J (2013) Characterization of cadmium removal from aqueous solution by biochar produced from a giant

- Miscanthus at different pyrolytic temperatures. *Bioresour Technol* 138:266–270. doi: 10.1016/j.biortech.2013.03.186
- Kloss S, Zehetner F, Dellantonio A, Hamid R, Ottner F, Liedtke V, Schwanninger M, Gerzabek MH, Soja G (2012) Characterization of Slow Pyrolysis Biochars: Effects of Feedstocks and Pyrolysis Temperature on Biochar Properties. *J Environ Qual* 41:990. doi: 10.2134/jeq2011.0070
- Kloss S, Zehetner F, Oburger E, Buecker J, Kitzler B, Wenzel WW, Wimmer B, Soja G (2014) Trace element concentrations in leachates and mustard plant tissue (*Sinapis alba* L.) after biochar application to temperate soils. *Sci Total Environ* 481:498–508. doi: 10.1016/j.scitotenv.2014.02.093
- Krichko AA, Gagarin SG (1990) New ideas of coal organic matter chemical structure and mechanism of hydrogenation processes. *Fuel* 69:885–891. doi: 10.1016/0016-2361(90)90236-J
- Lehmann J (2007a) A handful of carbon. *Nature* 447:143–144. doi: 10.1038/447143a
- Lehmann J (2007b) Bio-energy in the black. *Front Ecol Environ* 5:381–387. doi: 10.1890/1540-9295(2007)5[381:BITBJ]2.0.CO;2
- Leon CA, Radovic LR (1991) Influence of Oxygen Functional Groups on the Performance of Carbon-Supported Catalysts. *Mater Sci* 1007–1014
- Li F, Shen K, Long X, Wen J, Xie X, Zeng X, Liang Y, Wei Y, Lin Z, Huang W, Zhong R (2016) Preparation and characterization of biochars from *eichornia crassipes* for cadmium removal in aqueous solutions. *PLoS One* 11:7–9. doi: 10.1371/journal.pone.0148132
- Lian F, Huang F, Chen W, Xing B, Zhu L (2011) Sorption of apolar and polar organic contaminants by waste tire rubber and its chars in single- and bi-solute systems. *Environ Pollut* 159:850–857. doi: 10.1016/j.envpol.2011.01.002
- Lingamdinne LP, Roh H, Choi YL, Koduru JR, Yang JK, Chang YY (2015) Influencing factors on sorption of TNT and RDX using rice husk biochar. *J Ind Eng Chem* 32:178–186. doi: 10.1016/j.jiec.2015.08.012
- Liu H, Chen W (2015) Magnetic mesoporous imprinted adsorbent based on Fe₃O₄-modified sepiolite for organic micropollutant removal from aqueous solution. *RSC Adv* 5:27034–27042. doi: 10.1039/c5ra00985e
- Luo L, Xu C, Chen Z, Zhang S (2015) Properties of biomass-derived biochars: Combined effects of operating conditions and biomass types. *Bioresour Technol* 192:83–89. doi: 10.1016/j.biortech.2015.05.054
- Melvin SS, M EAA, Chidambaram R (2015) Biosorption of Cr(VI) by *Ceratocystis paradoxa* MSR2 Using isotherm modelling, kinetic study and optimization of batch parameters using response surface methodology. *PLoS One* 10:1–23. doi: 10.1371/journal.pone.0118999
- Mihaly Cozmuta L, Mihaly Cozmuta A, Peter A, Nicula C, Bakatula Nsimba E, Tutu H (2012) The influence of pH on the adsorption of lead by Na-clinoptilolite:

- Kinetic and equilibrium studies. *Water SA* 38:269–278. doi: 10.4314/wsa.v38i2.13
- Mimmo T, Panzacchi P, Baratieri M, Davies CA, Tonon G (2014) Effect of pyrolysis temperature on miscanthus (*Miscanthus × giganteus*) biochar physical, chemical and functional properties. *Biomass and Bioenergy* 62:149–157. doi: 10.1016/j.biombioe.2014.01.004
- Morgante V, Flores C, Fadic X, González M, Hernández M, Cereceda-Balic F, Seeger M (2012) Influence of microorganisms and leaching on simazine attenuation in an agricultural soil. *J Environ Manage* 95:S300–S305. doi: 10.1016/j.jenvman.2011.06.045
- Mukherjee A, Zimmerman AR, Harris W (2011) Surface chemistry variations among a series of laboratory-produced biochars. *Geoderma* 163:247–255. doi: 10.1016/j.geoderma.2011.04.021
- Oleszczuk P, Hale SE, Lehmann J, Cornelissen G (2012) Activated carbon and biochar amendments decrease pore-water concentrations of polycyclic aromatic hydrocarbons (PAHs) in sewage sludge. *Bioresour Technol* 111:84–91. doi: 10.1016/j.biortech.2012.02.030
- Park CM, Han J, Chu KH, Al-Hamadani YAJ, Her N, Heo J, Yoon Y (2017) Influence of solution pH, ionic strength, and humic acid on cadmium adsorption onto activated biochar: Experiment and modeling. *J Ind Eng Chem* 48:186–193. doi: 10.1016/j.jiec.2016.12.038
- Pehlivan E, Yanik BH, Ahmetli G, Pehlivan M (2008) Equilibrium isotherm studies for the uptake of cadmium and lead ions onto sugar beet pulp. *Bioresour Technol* 99:3520–3527. doi: 10.1016/j.biortech.2007.07.052
- Ping L, Zhuoxin Y, Jianfeng L, Qiang J, Yaofang D, Qiaohui F, Wangsuo W (2014) The immobilization of U(vi) on iron oxyhydroxides under various physicochemical conditions. *Environ Sci Process Impacts* 16:2278–2287. doi: 10.1039/c4em00301b
- Qian L, Chen B (2013) Dual role of biochars as adsorbents for aluminum: The effects of oxygen-containing organic components and the scattering of silicate particles. *Environ Sci Technol* 47:8759–8768. doi: 10.1021/es401756h
- Qiu Y, Zheng Z, Zhou Z, Sheng GD (2009) Effectiveness and mechanisms of dye adsorption on a straw-based biochar. *Bioresour Technol* 100:5348–5351. doi: 10.1016/j.biortech.2009.05.054
- Qu T, Guo W, Shen L, Xiao J, Zhao K (2011) Experimental study of biomass pyrolysis based on three major components: Hemicellulose, cellulose, and lignin. *Ind Eng Chem Res* 50:10424–10433. doi: 10.1021/ie1025453
- Rahman A, Holland PT (1985) Persistence and mobility of simazine in some new zealand soils. *New Zeal J Exp Agric* 13:59–65. doi: 10.1080/03015521.1985.10426059

- Rajapaksha AU, Vithanage M, Ahmad M, Seo DC, Cho JS, Lee SE, Lee SS, Ok YS (2015) Enhanced sulfamethazine removal by steam-activated invasive plant-derived biochar. *J Hazard Mater* 290:43–50. doi: 10.1016/j.jhazmat.2015.02.046
- Sigmund G, Hüffer T, Hofmann T, Kah M (2016) Biochar total surface area and total pore volume determined by N₂ and CO₂ physisorption are strongly influenced by degassing temperature. *Sci Total Environ* d: doi: 10.1016/j.scitotenv.2016.12.023
- Silva M, Iyer P (2014) Toxicity endpoint selections for a simazine risk assessment. *Birth Defects Res B Dev Reprod Toxicol* 101:308–324. doi: 10.1002/bdrb.21114
- Song W, Guo M (2012) Quality variations of poultry litter biochar generated at different pyrolysis temperatures. *J Anal Appl Pyrolysis* 94:138–145. doi: 10.1016/j.jaap.2011.11.018
- Stefaniuk M, Oleszczuk P (2015) Characterization of biochars produced from residues from biogas production. *J Anal Appl Pyrolysis* 115:157–165. doi: 10.1016/j.jaap.2015.07.011
- Trazzi PA, Leahy JJ, Hayes MHB, Kwapinski W (2016) Adsorption and desorption of phosphate on biochars. *J Environ Chem Eng* 4:37–46. doi: 10.1016/j.jece.2015.11.005
- Uchimiya M, Chang S, Klasson KT (2011) Screening biochars for heavy metal retention in soil: Role of oxygen functional groups. *J Hazard Mater* 190:432–441. doi: 10.1016/j.jhazmat.2011.03.063
- Uchimiya M, Lima IM, Thomas Klasson K, Chang S, Wartelle LH, Rodgers JE (2010) Immobilization of heavy metal ions (CuII, CdII, NiII, and PbII) by broiler litter-derived biochars in water and soil. *J Agric Food Chem* 58:5538–5544. doi: 10.1021/jf9044217
- van Zwieten L, Kimber S, Morris S, Chan KY, Downie A, Rust J, Joseph S, Cowie A (2010) Effects of biochar from slow pyrolysis of papermill waste on agronomic performance and soil fertility. *Plant Soil* 327:235–246. doi: 10.1007/s11104-009-0050-x
- Wang J, Wang F, Yao J, Guo H, Blake RE, Choi MMF, Song C (2013) Effect of pH and temperature on adsorption of dimethyl phthalate on carbon nanotubes in aqueous phase. *Anal Lett* 46:379–393. doi: 10.1080/00032719.2012.713067
- Weber JB (2010) Adsorption of s-Triazines by Montmorillonite As a Function of pH and Molecular Structure I. *Soil Sci Soc Am J* 34:401. doi: 10.2136/sssaj1970.03615995003400030017x
- Whitacre DM (2010) Reviews of Environmental Contamination and Toxicology. 202:1–52. doi: 10.1007/978-1-4419-1157-5

- Xiao X, Chen B, Zhu L (2014) Transformation, morphology, and dissolution of silicon and carbon in rice straw-derived biochars under different pyrolytic temperatures. *Environ Sci Technol* 48:3411–3419. doi: 10.1021/es405676h
- Xu G, Zhang Y, Sun J, Shao H (2016) Negative interactive effects between biochar and phosphorus fertilization on phosphorus availability and plant yield in saline sodic soil. *Sci Total Environ*. doi: 10.1016/j.scitotenv.2016.06.079
- Xu Y, Chen B (2015) Organic carbon and inorganic silicon speciation in rice-bran-derived biochars affect its capacity to adsorb cadmium in solution. *J Soils Sediments* 15:60–70. doi: 10.1007/s11368-014-0969-2
- Xu Z, Kuang D, Liu L, Deng Q (2007) Selective adsorption of norfloxacin in aqueous media by an imprinted polymer based on hydrophobic and electrostatic interactions. *J Pharm Biomed Anal* 45:54–61. doi: 10.1016/j.jpba.2007.05.024
- Yang Y, Chun Y, Shang G, Huang M (2004) pH-dependence of pesticide adsorption by wheat-residue-derived black carbon. *Langmuir* 20:6736–6741. doi: 10.1021/la049363t
- Zhang G, Zhang Q, Sun K, Liu X, Zheng W, Zhao Y (2011) Sorption of simazine to corn straw biochars prepared at different pyrolytic temperatures. *Environ Pollut* 159:2594–2601. doi: 10.1016/j.envpol.2011.06.012
- Zhao L, Cao X, Mašek O, Zimmerman A (2013) Heterogeneity of biochar properties as a function of feedstock sources and production temperatures. *J Hazard Mater* 256–257:1–9. doi: 10.1016/j.jhazmat.2013.04.015
- Zhao L, Cao X, Zheng W, Wang Q, Yang F (2015) Endogenous minerals have influences on surface electrochemistry and ion exchange properties of biochar. *Chemosphere* 136:133–139. doi: 10.1016/j.chemosphere.2015.04.053
- Zheng W, Guo M, Chow T, Bennett DN, Rajagopalan N (2010) Sorption properties of greenwaste biochar for two triazine pesticides. *J Hazard Mater* 181:121–126. doi: 10.1016/j.jhazmat.2010.04.103
- Zhu D, Hyun S, Pignatello JJ, Lee LS (2004) Evidence for π - π electron donor-acceptor interactions between π -donor aromatic compounds and π -acceptor sites in soil organic matter through pH effects on sorption. *Environ Sci Technol* 38:4361–4368. doi: 10.1021/es035379e

(This page intentionally left blank)

CHAPTER 4. INTERACTIVE EFFECT OF pH AND CATION VALENCE IN BACKGROUND ELECTROLYTE SOLUTIONS ON SIMAZINE SORPTION TO *MISCANTHUS* BIOCHAR PRODUCED AT TWO DIFFERENT PYROLYSIS TEMPERATURES

List of contents	4-1
Abstract	4-2
4.1. Introduction	4-3
4.2. Materials and methods	4-6
4.2.1. Physicochemical characteristics of biochar	4-6
4.2.2. SCD and morphological characteristics of biochar	4-8
4.2.3. Sorption isotherm experiment	4-9
4.2.4. Data calculation and fitting	4-10
4.2.5. Statistical analysis	4-12
4.3. Results and disussion	4-12
4.3.1. Physicochemical characteristics of biochar	4-12
4.3.2. SCD of biochar	4-19
4.3.3. Effect of pH and CV in background electrolyte solutions	4-20
4.3.4. Effect of pore structures of biochar	4-29
3.3.5. Environmental effects of biochar on IOP remediation	4-30
4.4. Conclusions	4-32
Reference	4-35

Abstract

Biochar has considerable sorption efficiency for organic pollutants; however, effect of physicochemical characteristics and their alteration by environmental conditions on the sorption mechanism is still unknown. The pH-dependent sorption of simazine on *Miscanthus* biochar produced at two pyrolysis temperatures (400 and 700 °C; hereafter B400 and B700) was investigated under two different electrolytes and interpreted the sorption mechanism. The surface charge density (SCD) decreased more in B400 than in B700 at higher pH due to more deprotonation of acidic functional groups (AFGs), but greater decreases were observed in B700 than in B400 from pH 2 to pH 3 as a result of alkali salts deposition. The decrease in K_F with increasing pH showed that simazine sorption decreased as van der Waals forces because surface of biochar carried a greater negative SCD, which repulse simazine molecules due to the enhanced deprotonation of AFGs. At a given pH, K_F was lower in CaCl_2 than in NaCl due to the formation of larger metal-biochar complexes, resulting in enhanced blocking of pores available for simazine sorption. Knowledge of the pH-dependence of SCD and accessibility of biochar pores could help better interpret the behavior of simazine-like pollutants in soil and aquatic environments.

Keywords

Simazine, Electrolyte, Biochar, Sorption, Isotherm, pH, Cation Valence

4.1. Introduction

Biochar is a carbonaceous material produced through pyrolysis of various forms of feedstocks under oxygen limited conditions (Lehmann 2007a; Qiu et al. 2009), resulting in diverse physicochemical characteristics. Feedstocks and pyrolysis temperature are key factors that determine the physicochemical characteristics of biochar (Zhao et al. 2013; Zielińska et al. 2015), since thermal decomposition of specific molecular structures in feedstocks requires specific pyrolysis temperatures (Qu et al. 2011; Mimmo et al. 2014). As cellulose degrades at 220-315 °C, hemicellulose degrades at 315-400 °C and lignin degrades at >400 °C (Qu et al. 2011; Mimmo et al. 2014) during pyrolysis, increased pyrolysis temperature causes an increase in aromatic C structures on the surface of plant-derived biochar (Elmay et al. 2015) due to progressive polymerization (Domingues et al. 2017). As a result, biochar produced by pyrolysis at different pyrolysis temperatures will have different specific surface area (SSA) and surface hydrophilicity/hydrophobicity properties; thus, biochar can serve as a cost-effective (Angin 2013; Méndez et al. 2013), environmentally sound solution in the effective remediation of organic pollutants under various environmental conditions (Cao and Harris 2010; Zhang et al. 2013b). However, the efficiency of remediation using biochar has not been fully investigated or understood in terms of the interactions of organic pollutants with various types of biochar due to insufficient knowledge of the physicochemical characteristics of biochar; thus, adverse effects or unprecedented results have frequently been reported in recent investigations (Tang et al. 2013; Cely et al. 2014; Kumari et al. 2014). Therefore, understanding the sorption mechanisms of biochar for organic pollutants in relation to the physicochemical characteristics of biochar is a prerequisite for interpreting the interactions between organic pollutants and biochar in real environments.

Under various environmental conditions, the relationship between the physicochemical characteristics of biochar and sorption mechanisms may vary, depending mainly on pH and background electrolyte, and this difference in turn affects the interactions of organic pollutants with biochar (Zheng et al. 2010; Lian et al. 2014). Acidic functional groups (AFGs) on the surface of biochar are mainly responsible for the remediation of organic pollutants (Uchimiya et al. 2011; Vu et al. 2017), and their concentrations can be measured by Boehm titration, which quantifies carboxylic, lactonic and phenolic acidic groups (Boehm 1994). Since each oxygen containing AFG has a negative logarithmic acid dissociation constant (pK_a), when the pH is higher than the pK_a , it is negatively charged due to deprotonation (Reddad et al. 2002; Rahman and Islam 2009). Moreover, the surface charge density (SCD) of biochar becomes more negative with increasing pH, since further increases in pH deprotonate carboxylic ($pK_a \approx 4.4$), lactonic ($pK_a \approx 8.2$) and phenolic ($pK_a \approx 10$) acidic groups (Leon and Radovic 1991). When the pH is lower than the point of zero net charge (PZNC), the surface of biochar is positively charged, and the degree of protonation decreases with increasing pH; otherwise, the surface is negatively charged (Graber 2010; Pignatello et al. 2011). As a consequence, charged biochar can repel neutral organic pollutants but attract charged organic pollutants (Dong et al. 2011; Zheng et al. 2013). Concurrently, charged biochar can interact with background electrolytes, which affect the ionic atmosphere of the solution, to achieve electrostatic stabilization (Chen et al. 2017). Therefore, understanding the behavior of simazine and biochar across an environmental pH range with varying background electrolytes is necessary to study the mechanism of simazine sorption to the surface of biochar. However, despite current knowledge regarding the effect of pH and background electrolytes on the sorption mechanism, the interactions of simazine molecules on the surface

of biochar remain largely unknown due to the heterogeneity of biochar (Zheng et al. 2010).

Simazine [2-chloro-4,6-bis(ethylamino)-s-triazine] is an herbicide that has lone-pair electrons in its nitrogen containing heterocyclic structure and inhibits the photosynthetic electron transport process in annual grasses and broadleaf weeds (Silva and Iyer 2014). Due to its remarkably efficient weed control, simazine has been widely used as a nonselective herbicide since its introduction in 1956 (Gunasekara et al. 2007). However, recent evidence has shown that simazine poses threats to the environment and to human health because of its persistence and accumulation, resulting from its low solubility and non-volatility (Gunasekara et al. 2007); triazines can cause hormonal disruption and damage to the kidneys and thyroid (Trentacoste et al. 2001; USEPA 2006). Therefore, the removal or remediation of simazine from polluted soils is urgent; nevertheless, the pH-dependence of the sorption mechanism of simazine to biochar needs to be better understood to properly assess the risks and threats from the environmental problems associated with simazine under natural environmental conditions. At pH values below its pK_a of 1.7 (Gunasekara et al. 2007), simazine, which is an organic base, is positively charged due to protonation, while it is neutral above this pK_a (Weber 2010); thus, the sorption mechanisms of simazine to biochar are pH-dependent. Therefore, knowledge of the behavior of simazine and biochar across at least the surrounding environmental pH and background electrolyte conditions is essential to interpret the sorption mechanisms of simazine to biochar and develop suitable remediation technology for real environments.

It hypothesized that changes in pyrolysis temperature alter the surface morphology and charge characteristics of biochar and that the pyrolysis temperature-driven sorption behavior of biochar varies with pH, cation valence (CV) and their interaction in background electrolyte solution, thus changing the

sorption capacity and mechanism of simazine sorption to biochar. Here, this hypothesis was tested by interpreting the effects of pH, CV and their interactions on pyrolysis temperature-driven simazine sorption. To this end, batch sorption isotherms of simazine to *Miscanthus* biochar produced at two different pyrolysis temperatures (400 and 700 °C) was conducted under different pH and CV conditions in background electrolyte solutions; fitted the experimental sorption data to sorption isotherm models; measured the SCD and morphological characteristics of biochar before and after treatment; analyzed the effect of pH, CV and their interaction on simazine sorption to biochar.

4.2. Material and methods

4.2.1. physicochemical characteristics of biochar

Biochar was produced from *Miscanthus* feedstock at different pyrolysis temperatures (400 and 700 °C) (hereafter, B400 and B700, respectively) to distinguish the physicochemical characteristics based on thermal decomposition, which occurred below or above a pyrolysis temperature of 500 °C (Lehmann 2007b; Chen et al. 2008; Zhang et al. 2011). The rate of heating was approximately 10 °C min⁻¹, and the target temperatures were maintained for 1 h for the completion of pyrolysis under N₂ gas purging. Biochar was ball-milled (MM400, Retsch, Germany) and sieved through a 106-µm mesh to minimize the size effects (Zheng et al. 2010). The SSA was determined using the Brunauer-Emmett-Teller (BET) isotherm with N₂ and CO₂ gas adsorbates because N₂ (ASAP 2010, Micromeritics, USA) is sorbed only on micro-pores (>1.5 nm), while CO₂ (BELSORP-mini II, Microtrac BEL, Japan) is sorbed on both micro- and nano-pores (<1.5 nm) (Sigmund et al. 2016). Biochar particles were separated into three fractions (<25, 25-53 and 53-106 µm) using Analysette 3 pro (Fritsch, Germany). The mass percent of carbon (C), hydrogen (H), nitrogen (N) and sulfur (S) was analyzed using an elemental

analyzer (Flash 2000, Thermo, USA), and that of O (oxygen) was calculated by subtracting %C, %H, %N and %S from 100%.

The AFGs was determined by Boehm titration (Mukherjee et al. 2011; Wang et al. 2014). Since the results of Boehm titration can be affected by dissolved salts, biochar was pretreated with dilute HCl at pH 2 for 3 days followed by washing with deionized water until the AgNO_3 test for Cl^- ions was negative and then oven dried at 80 °C for 24 h (Contescu et al. 1997). After pretreatment, biochar (0.2 g) was added to 20 mL of 0.05 M of three base solutions (NaHCO_3 , Na_2CO_3 and NaOH) for 24 h and shaken on a flask shaker at 160 rpm (DS-300L, Dasol, Korea). Then, biochar suspension was separated by centrifugation (MF-600 plus, Hanil, Korea) for 40 min at 4000 rpm. Ten milliliters of the supernatant was back-titrated with 0.01 M HCl using an automatic titrator (702 SM Titrino, Metrohm, Switzerland). The AFGs were estimated on the assumption that 0.05 M NaHCO_3 neutralizes carboxyl groups, 0.05 M Na_2CO_3 neutralizes carboxyl and lactonic groups, and 0.05 M NaOH neutralizes carboxyl, lactonic and phenolic groups.

Ash content of biochar was estimated by the combustion method, in which the residual weight was measured after heating at 750 °C for 6 h (Zhang et al. 2013a). The electrical conductivity (EC) and pH were measured in a 1:20 (w/v) biochar/water suspension with an EC meter (Orion 3 star, Thermo, USA) and a pH meter (Orion 3 star, Thermo, USA) after shaking for 1.5 h (Rajkovich et al. 2012). The PZNC was determined using the pH drift method (Yang et al. 2004). Approximately 60 mg of biochar was mixed with 20 mL of 0.05 M CaCl_2 , and the pH was adjusted using 0.5 M HCl or 0.5 M NaOH. Then, the sample was shaken for 24 h on a flask shaker at 160 rpm. The pH was measured with a pH meter and plotted against the initial pH, with the PZNC taken at the equal point between the initial and final pH. The concentration of inorganic elements was analyzed using X-ray fluorescence (XRF) (S4 Pioneer, Bruker, USA).

4.2.2. SCD and morphological characteristics of biochar

All reagents were purchased from Sigma-Aldrich (St. Louis, MO, USA). The SCD of biochar was measured by the potentiometric titration method (Szekeres and Tomb acz 2012). To achieve complete protonation of AFGs, biochar (1 g) was added to 100 mL of 0.05 M CaCl₂ solution in a 250 mL Duran laboratory glass bottle sealed with a PTFE cap, and the mixture was equilibrated by shaking on a vial shaker (DS-300L, Dasol, Korea) at 160 rpm for 3 days at 25 ± 0.5 °C. During equilibration, the suspension was adjusted daily to pH 2 using 1 M HCl solution, and then 0.01 M NaOH solution (titrant) was added dropwise to the acidic suspension (pH 2) using an automatic titrator to raise the pH to 11. The volume of titrant consumed and the corresponding pH were recorded in 10 s intervals during the titration. A blank titration was repeated without biochar to correct for the volume of titrant consumed. The SCD, $\delta_{0,H}$ (C m⁻²), was calculated from the points on the titration curve as follows:

$$\Gamma_{H^+} + \Gamma_{OH^-} = \frac{C_{NaOH}(V_b - V_a)}{s \cdot \gamma \cdot V} \quad (1)$$

$$\delta_{0,H} = F(\Gamma_{H^+} + \Gamma_{OH^-}) \quad (2)$$

where Γ_{H^+} and Γ_{OH^-} (mol m⁻²) are the concentrations of H⁺ and OH⁻ on the surface of biochar, respectively, C_{NaOH} (mol L⁻¹) is the concentration of titrant, V_b and V_a (L) are the volumes of titrant added in the blank and analyte (biochar) titrations, respectively, s (m² kg⁻¹) is the SSA, γ (kg L⁻¹) is the mass concentration, V (L) is the total volume of the solution, and F (C mol⁻¹) is the Faraday constant.

The morphology and elemental composition of biochar after simazine sorption at different pH values and CVs in background electrolyte solutions were analyzed with a field emission-scanning electron microscope (FE-SEM) (AURIGA, Carl Zeiss, Germany) equipped with an energy dispersive X-ray

spectroscopy (EDS) detector (Bruker Nano GmbH, Berlin, Germany). For FE-SEM analysis, biochar samples were placed in a forced-air oven (DS-80-2, Dasol, Korea) at 80 °C for at least 48 h and then mounted on an aluminum stub using double-sided conductive copper tape. The microscope was operated at an accelerating voltage of 10 kV, and the working distance was set at 10 nm from the final lens at varying magnifications.

4.2.3. Sorption isotherm experiment

All reagents were purchased from Sigma-Aldrich (St. Louis, MO, USA), and an aqueous standard solution of simazine was prepared by diluting the simazine stock solution in methanol (99.8% purity) (Zheng et al. 2010). Five milliliters of the simazine stock solution (20 mg L⁻¹) was mixed with 10 mL of 0.2 M NaCl or 0.1 M CaCl₂ solution and biochar (0.2 g) in a 30 mL amber glass vial with a Teflon-lined cap to prevent photodegradation of simazine (Gunasekara et al. 2007). The pH was adjusted to 3.5, 7.5 and 10 using 1 M HCl or 1 M NaOH, and distilled water was added to make a total volume of 20 mL; the final solution contained simazine (5 mg L⁻¹, the maximum solubility), NaCl (0.1 M) and CaCl₂ (0.05 M). Each sample was equilibrated by shaking on a flask shaker at 160 rpm for 81 h at 25 ± 0.5 °C, and the pH was readjusted daily during equilibration. Each mixture was filtered through a 0.45-µm nylon membrane filter to separate simazine from biochar matrix. For the determination of simazine concentrations, 10 mL of each filtrate was shaken vigorously after adding 2 mL of hexane, and one milliliter of supernatant was transferred to a 2 mL amber vial with a rubber cap for GC analysis. To ensure the quality of the data collection (accuracy and precision), all batch sorption experiments were performed in triplicate according to the US Environmental Protection Agency (US EPA) (USEPA 1998).

The simazine concentration was measured using a gas chromatograph with micro-electron capture detector (GC- μ ECD) (6890N, Agilent Technologies Inc., USA) with a silica capillary column (HP-5, 0.32 mm i.d. x 30 m x 0.25 μ m) (Morgante et al. 2012). The inlet and detector temperatures were 250 °C and 300 °C, respectively, and the carrier gas was N₂ with a flow rate of 1.2 mL min⁻¹ under constant flow mode. The oven temperature was set as follows: initial temperature of 50 °C (held for 1 min), 20 °C min⁻¹ to 150 °C (held for 4 min), 3 °C min⁻¹ to 230 °C (held for 1 min), and finally 10 °C min⁻¹ to 300 °C (held for 5 min). The total analysis time per sample was 50 min, and the retention time for simazine was 19 min. All calibrations were performed in ChemStation (Agilent, USA). To guarantee the stability of GC- μ ECD measurements, the instrument calibration was performed by analyzing the standard simazine solutions and plotting the relative response factors of analyte in each batch sorption experiment.

4.2.4. Data calculation and fitting

The concentration of simazine sorbed on biochar (q_{eq} , mg kg⁻¹) was calculated from the difference between the initial and equilibrium concentrations of simazine in solution:

$$q_{eq} = \frac{(C_0 - C_{eq}) \times V}{m} \quad (3)$$

where C_0 and C_{eq} are the initial and equilibrium concentrations of simazine (mg L⁻¹) in solution, respectively, V is the volume of solution (L), and m is the mass of biochar (kg).

The sorption isotherm results constructed at pH 3.5, 7.5 and 10 were fitted to the Langmuir and Freundlich isotherm models to simulate the sorption process of simazine to biochar (Wang et al. 2014; Rajapaksha et al. 2015). The

Langmuir model, which describes ideal monolayer adsorption, is expressed as follows:

$$q_{eq} = \frac{q_{max} \cdot K_L \cdot C_{eq}}{(1 + K_L \cdot C_{eq})} \quad (4)$$

where q_{max} is the maximum sorption capacity (mg kg⁻¹) and K_L is a constant related to energy (L mg⁻¹). The linear form of the Freundlich model, which describes nonideal sorption in multilayers and is based on heterogeneous surfaces with non-uniform distribution energy, is expressed as follows:

$$\log q_{eq} = \log K_F + \frac{1}{n} \log C_{eq} \quad (5)$$

where K_F is the equilibrium constant indicating sorption capacity (mg kg⁻¹(mg L⁻¹)⁻ⁿ) and $1/n$ is the sorption intensity.

To assess the applicability of the sorption isotherm model, the percent normalized standard deviation (Δq) was calculated as follows (El-Kamash et al. 2005; Mihaly Cozmuta et al. 2012):

$$\Delta q = 100 \times \sqrt{\frac{\sum_{i=1}^n \left[\left(\frac{q_{exp} - q_{cal}}{q_{exp}} \right)_i \right]^2}{n-1}} \quad (6)$$

where q_{exp} and q_{cal} are the measured and estimated amounts of simazine sorbed on biochar for each data point (mg kg⁻¹), respectively, and n is the number of experimental measurement data points.

4.2.5. Statistical analysis

Data were analyzed using the general linear model (GLM) procedure in SPSS software (SPSS Inc., Version 25.0, Chicago, IL, USA). The effects of two factors (pH and CV) and their interaction on the fitting parameters for the Freundlich and Langmuir isotherms were evaluated for each biochar, B400 and B700. Two-way analysis of variance (ANOVA) of a completely randomized design with three replications per treatment was performed to test for significant differences among the treatment means within each factor and for

interactions between factors. The least significance difference (LSD) test at the significance level of $p < 0.05$ was used to separate means.

4.3. Results and discussion

4.3.1. physicochemical characteristics of biochar

The SSA was estimated at $5.6 \text{ m}^2 \text{ g}^{-1}$ for micro-pores and $191.6 \text{ m}^2 \text{ g}^{-1}$ for nano-pores in B400, and $236.3 \text{ m}^2 \text{ g}^{-1}$ and $57.2 \text{ m}^2 \text{ g}^{-1}$, respectively, in B700 (Table 4-1). Previous investigations on *Miscanthus* biochar reported that SSA of biochar increased with increasing pyrolysis temperature (Cao and Harris 2010; Zielińska and Oleszczuk 2015). The SSA of micro-pores of this biochar sharply increased from 10.97 to $443.92 \text{ m}^2 \text{ g}^{-1}$ by increasing pyrolysis temperature from $300 \text{ }^\circ\text{C}$ to $700 \text{ }^\circ\text{C}$, while that of nano-pores gradually decreased from 110.83 to $11.04 \text{ m}^2 \text{ g}^{-1}$ (Abdul et al. 2017). An increase in SSA of micro-pores with a concurrent decrease in SSA of nano-pores with increasing pyrolysis temperature can be explained by progressive volatilization of specific molecular structures such as cellulose, hemicellulose and lignin, leading to formation of channel structures of larger pore-size and thereby increasing the quantity of micro-pores (Qu et al. 2011; Han et al. 2016). The percentage of particles having a given equivalent diameter ($<25 \text{ }\mu\text{m}$, $25\text{-}53 \text{ }\mu\text{m}$ and $53\text{-}106 \text{ }\mu\text{m}$) was 14.7, 52.8 and 32.5% for B400, and 5.6, 62.0 and 22.4% for B700, respectively.

Some atomic ratios could be used to characterize the aromaticity, hydrophobicity and polarity of biochar (Zheng et al. 2010), and the ratio of $(\text{O}+\text{N})/\text{C}$, O/C and H/C can be proxies of polarization, carbonization and hydrophilization of biochar, respectively (Essandoh et al. 2015; Li et al. 2017). In this study, the ratios of the corresponding values at higher pyrolysis temperature (B700) were lower than those at lower pyrolysis temperature (B400) (Table 4-1). In other words, the ratio of $(\text{O}+\text{N})/\text{C}$, O/C and H/C of

Table 4-1 Physicochemical characteristics of *Miscanthus* biochar pyrolyzed at two temperatures of 400 °C (B400) and 700 °C (B700).

Biochar	Specific surface area ^a (m ² g ⁻¹)		Elemental composition ^c (%)					Atomic ratio ^c			Acidic functional groups ^d (mmol g ⁻¹) ^d			Ash ^e	EC ^f	pH ^f	PZNC ^g
	Micro-pores ^b	Nano-pores ^b	C	H	O	N	S	(O+N)/C	H/C	O/C	Carboxylic	Lactonic	Phenolic	%	(dS m ⁻¹)		
B400	5.6	191.6	70.5	3.5	25.4	0.6	0.02	0.28	0.60	0.27	0.150	0.167	0.421	8.80	0.21	9.0	8.84
B700	236.3	57.2	79.2	1.1	19.3	0.4	0.02	0.19	0.17	0.18	0.013	0.125	0.013	11.6	0.53	10.5	10.0

^aSpecific surface area (SSA) was estimated based on the results obtained from BET isotherms using N₂ (N₂-BET) and CO₂ (CO₂-BET).

^bThe SSA of micropores was equal to the N₂-BET results, while that of nanopores was calculated by subtracting the CO₂-BET results from the N₂-BET results.

^cElemental composition was measured using an elemental analyzer, and the atomic ratio was calculated.

^dAcidic functional groups were measured by Boehm titration.

^eAsh content was estimated by the combustion method.

^fEC and pH were measured with an EC meter and a pH meter, respectively.

^gThe point of zero net charge (PZNC) was estimated by the pH drift method.

Miscanthus biochar decreased from 0.28 to 0.19, 0.27 to 0.18 and 0.60 to 0.17, respectively, as a result of increased C and decreased H, O, N and S contents. With the decrease in the ratio of (O+N)/C, O/C and H/C, it inferred that polarity and the hydrophilicity of biochar decreased while aromaticity increased due to increased carbonization (Uchimiya et al. 2011; Wang et al. 2019). Previous investigations have reported that *Miscanthus* biochar produced at 400 °C had the atomic ratio of (O+N)/C, O/C and H/C ranged from 0.26 to 0.48, 0.26 to 0.48 and 0.05 to 0.09, while the respective ratios of biochar produced at 700 °C ranged from 0.08 to 0.09 and 0.07 to 0.08, and were 0.02 (Kloss et al. 2012; Lian et al. 2014; Vu et al. 2017).

The transformation of feedstocks during pyrolysis alters the molecular structures of biochar in various ways (Boehm 1994) and further modifies its properties through thermal degradation of easily decomposable oxygen containing molecular structures (Boehm 1994; Reddad et al. 2002). With an increase in pyrolysis temperature, the ash content increased from 8.8 (B400) to 11.6% (B700), and the EC increased from 0.21 to 0.53 dS m⁻¹ (Tables 4-1 and 4-2). The ash content of biochar increased due to the release of volatiles (Wang et al. 2019), while the EC increased as a result of non-volatiles remaining after pyrolysis (Gai et al. 2015). Therefore, the ash content indicates the concentration of inorganic constituents, while the EC represents total concentration of dissolved salts or total amount of dissolved ions resulting from thermal decomposition of feedstocks (Angin 2013; Domingues et al. 2017). From those relations, it infer that inorganic and alkali salts that were combined with the volatile biomass structures containing C, H, O, and N began to separate from the agricultural biochar feedstocks and that more nonvolatile inorganic and alkali salts were deposited more in B700 during thermal decomposition (Cao and Harris 2010; Méndez et al. 2013). As more alkali salts were deposited at higher pyrolysis temperature, the pH of B700 (10.5) was higher than that of

B400 (9.0). Since solution-pH determines the net surface charge of the sorbent, biochar can have positively and negatively charged surfaces for hydrophilic interactions at a given pH (Silber et al. 2010). This means that the net surface charge of B400 and B700 is positive at circumneutral pH, with more positive charges at the surface of the latter (Lee et al. 2018).

The acidity of B400 and B700 was measured at 0.150 and 0.013 mmol g⁻¹ for carboxylic acid groups, 0.167 and 0.125 mmol g⁻¹ for lactonic acid groups, and 0.421 and 0.013 mmol g⁻¹ for phenolic acid groups, respectively, as observed in our previous study (Lee et al. 2018), and the decrease in the acidity of surface functional groups with increasing pyrolysis temperature was due to volatilization of oxygen containing structures (Sun et al. 2011; Kumari et al. 2014). The results of XRF spectra confirmed more deposition of inorganic salts in B700 than in B400 (Table 4-2). Concentrations of Si were 1.61% for B400 and 2.35% for B700, as a result of Si-accumulation due to pyrolysis, which were higher than those of biochar feedstock (0.60%). However, concentrations of K, Ca, P, Mg, S, Al and Fe in both biochar were below 1%.

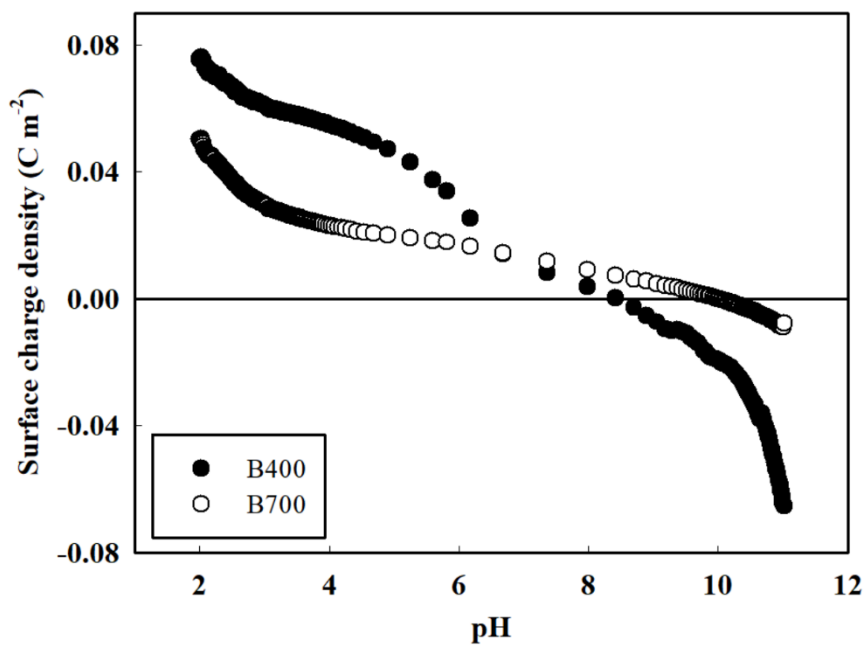
4.3.2. SCD of biochar

The positive SCD of *Miscanthus* biochar decreased from 0.08 to -0.06 C m⁻² for B400 and from 0.05 to -0.01 C m⁻² for B700 as pH increased (Fig. 4-1). The positive biochar SCD was associated with the concentration of oxygen containing AFGs; progressive thermal decomposition caused polarization and hydrophilization of biochar (Essandoh et al. 2015; Xiao and Pignatello 2016), resulting in a decreased proportion of AFGs and SCD in B700 (Table 4-1). In both B400 and B700, the SCD remarkably decreased at pH values of 4 to 5, 7 to 8, and above 10 (Fig. 4-1), which corresponded to the pK_a values of carboxylic ($pK_a = 4\sim 5$), lactonic ($pK_a = 7\sim 8$) and phenolic ($pK_a = 10$) functional

Table 4-2 XRF results of dried *Miscanthus* and biochar pyrolyzed at two temperatures of 400 °C (B400) and 700 °C (B700).

Components	Dried <i>Miscanthus</i>	B400	B700
Mass percent (%)			
CH ₂	99.9	97.0	95.7
Si	0.60	1.61	2.35
K	0.05	0.68	0.98
Ca	0.11	0.22	0.30
P	0.04	0.17	0.23
Mg	0.05	0.15	0.22
S	0.02	0.04	0.05
Al	0.01	0.03	0.05
Fe	0.01	0.02	0.03
Cl	0.08	0.02	0.06
Mn	0.01	0.02	0.02
Zn	0.00	0.00	0.01

Fig. 4-1 Surface charge density (SCD) of *Miscanthus* biochar produced at two pyrolysis temperatures of 400 °C (B400) and 700 °C (B700) as a function of pH determined by potentiometric titration in 0.05 M CaCl₂ solution.



groups, respectively (Leon and Radovic 1991). However, a decrease in SCD of biochar was also observed in the pH range between 2 and 3, in which the pK_a values of surface AFGs are not applicable; this decrease could be explained by the interaction of deposited alkali salts with H^+ ions in solution, leading to electrostatic stabilization (Li et al. 2017; Ruthenberg and Chang 2017). Kloss et al. (2012) and Tran et al. (2017) reported that the positive SCD of biochar decreased with increasing pH and that the decreasing effect was diminished with increasing pyrolysis temperature as a result of a reduction in deprotonated surface AFGs, which reduced polarization and hydrophilization. Therefore, it believe that deprotonation of AFGs and deposition of alkali salts on the surface of biochar are the main causes of the reduction in SCD with increasing pH (Kloss et al. 2012; Li et al. 2017). In short, a greater reduction in the positive SCD of biochar at higher pH values was due to a progressive deprotonation of biochar AFGs in pH ranges that include the pK_a values of surface AFGs (Table 4-1) and to enhanced deposition of inorganic and alkali salts on the biochar.

4.3.3. Effect of pH and CV in background electrolyte solutions

The sorption isotherms constructed at pH values of 3.5, 7.5 and 10 under different background electrolyte conditions were fitted to the Langmuir and Freundlich isotherms (Fig. 4-2), and the fitting results indicated that the Freundlich model yielded a better fit of simazine sorption to biochar than the Langmuir model, as was evident from higher mean R^2 and lower mean Δq on the fitted parameters (Table 4-3). Yuan et al. (2011) showed that the Freundlich model well described the alteration in SCD due to protonation and/or deprotonation of AFGs on biochar surface in the sorption process of carbaryl and atrazine (Zhang et al. 2013b). Sun et al. (2011) reported that the interaction of fluridone with biochar was altered by changes in pH due to the alteration in the SCD of biochar, which affects the sorption mechanism in terms of H-

bonding and/or van der Waals forces. Therefore, the pH-dependent sorption mechanism of simazine on biochar in terms of the physicochemical characteristics of biochar were interpreted, since electrostatic interactions between H-bonding and hydrophobic interactions such as van der Waals forces and pore-filling mechanisms create heterogeneity in biochar (Zhang et al. 2011).

As pH increased from 3.5 to 10, the constant K_F decreased from 645.7 to 501.2 in 0.1 M NaCl solution (ionic strength = 0.1) and from 537.0 to 363.1 in 0.1 M CaCl₂ solution (ionic strength = 0.15) for B400, while their counterparts for B700 decreased from 501.2 to 338.8 and from 537.0 to 275.4, respectively (Table 4-3). A decrease in K_F with increasing pH could be explained by the decrease in sorption strength between sorbate and sorbent (Wang and Lemley 2006), since an increase in the negativity of the SCD of biochar due to progressive deprotonation of AFGs at a pH above 1.7 (the pK_a of simazine) (Chen et al. 2017) increases electrostatic repulsion with neutral simazine molecules (Uchimiya et al. 2011; Fang et al. 2014). Wang and Lemley (2006) observed a decrease in the sorption strength of ametryn to soil with increasing pH due to enhanced electrostatic repulsion (lower K_F), and Rajapaksha et al. (2015) demonstrated that K_F (a proxy of sorption capacity) of sulfamethazine sorption decreased with increasing pH as electrostatic repulsion increased.

Even though lower K_F was expected for B400 due to its lower SSA and to more deprotonation at the surface (Table 4-1), K_F of B700 for simazine sorption was invariably lower than the corresponding value of B400 at a given pH and CV, indicating that CV-driven alterations in pore space morphology may predominate over pH-driven deprotonation of AFGs at the surface acidic sites. Therefore, it is inferred that the reduction of simazine sorption can be predominantly attributed to greater blocking of the entrance to internal pores due to the formation of larger metal-biochar complexes (Narasimha Rao and

Mathew 1995; Persson 2010), even though progressive deprotonation with increasing pH increases electrostatic repulsion between neutral simazine molecules and biochar (Kim et al. 2016; Peng et al. 2016). In addition, decreases in K_F with increasing pH were greater in Ca^{2+} electrolyte than in Na^+ electrolyte for both B400 and B700 (Table 4-3), indicating that Ca^{2+} ions compete with simazine molecules to a greater extent for the binding sites of biochar than Na^+ ions. Changing CV from Na^+ to Ca^{2+} caused the formation of larger metal-biochar complexes that blocks to a greater extent the entrance of internal pores (Fig. 4-3).

An increase in CV resulted in a decrease in K_F of biochar at a given pH and pyrolysis temperature, with a greater decrease at higher pH values (Table 4-3). However, CV-driven changing patterns of K_F with pH were different between B400 and B700. The patterns of decreasing K_F with increasing pH were parallel under both electrolyte conditions for B400; however, the two patterns crossed at the middle pH (7.5) for B700, indicating a significant interactive effect of pH and CV on K_F for B700 (Fig. 4-2). The K_F values of B700 in Ca^{2+} solution were higher at pH 3.5 and lower at pH 10 than their counterparts in Na^+ solution. On the other hand, pH affected the strength of simazine sorption ($1/n$), while CV did not. However, a significant interaction between pH and CV was observed for B700 but not for B400 (Table 4-3). Lee et al. (2018) identified that at least two dominant sorption mechanisms of simazine occur at multiple types of binding sites on biochar: a strong sorption process due to electrostatic attraction in the lower sorption range and a weak sorption process *via* hydrophobic attraction in the higher sorption range.

Overall, an increase in CV lowered K_F , and the corresponding decrease at a given pH was greater for B700 than for B400. This phenomenon can be explained by the formation of larger metal-biochar complexes (Fig. 4-3) that blocks to a greater extent the entrances of the intramolecular pore spaces

available for simazine sorption (Narasimha Rao and Mathew 1995; Persson 2010) at more deprotonated (negatively charged) acidic sites on biochar (Table 4-1) (Dong et al. 2011). Previous studies have shown that the physicochemical characteristics of a sorbent are altered by changing the background electrolyte ions. Largeot et al. (2008) demonstrated that the size (hydrated radius) of the background electrolyte changed the pore size of biochar-derived carbon by affecting the formation of metal complexes, and Gabelich et al. (2002) showed that the effective SSA of clay available for sorption was lower than that measured by using BET analysis due to the interactions of carbon with background electrolyte ions. Therefore, it could infer that environmental factors such as pH and CV in background electrolyte solutions affect the strength and mechanism of simazine sorption at the surface of biochar by altering the physicochemical characteristics of biochar. Therefore, I concluded that progressive deprotonation of AFGs on the surface of biochar with increasing pH and the blockage of biochar intra-pores by the deposition of metal complexes due to increasing CV may be the main mechanism for a decrease in K_F in response to increasing pH and CV in background electrolytes.

4.3.4. Effect of pore structure of biochar on simazine sorption

As pH increased from 3.5 to 10, the deposition of Na^+ or Ca^{2+} on the surface of biochar increased for the two types of biochar (Fig. 4-3); the concentrations of the relevant ions increased from 0.67 to 3.69 in NaCl solution and 0.41 to 1.56 in CaCl_2 solution for B400 and from 0.24 to 0.56 and 0.29 to 0.54 for B700 in the corresponding electrolyte solutions, respectively (Table 4-4). An increase in Na^+ or Ca^{2+} on the surface of biochar can interrupt the sorption of simazine due to the formation of metal-biochar complexes, since negative surface charge developed from progressive deprotonation of AFGs

Fig. 4-2 Simazine sorption isotherms fitted to the linear Freundlich model in 0.1 M NaCl (rectangles) and 0.05 M CaCl₂ (triangles) for B400 (a-c, indicated on the left side with solid symbols) and B700 (d-f, indicated on the right side with open symbols) at three pH values of 3.5, 7.5 and 10. The mixture was agitated at 160 rpm for 81 h at room temperature of 25 ± 0.5 °C.

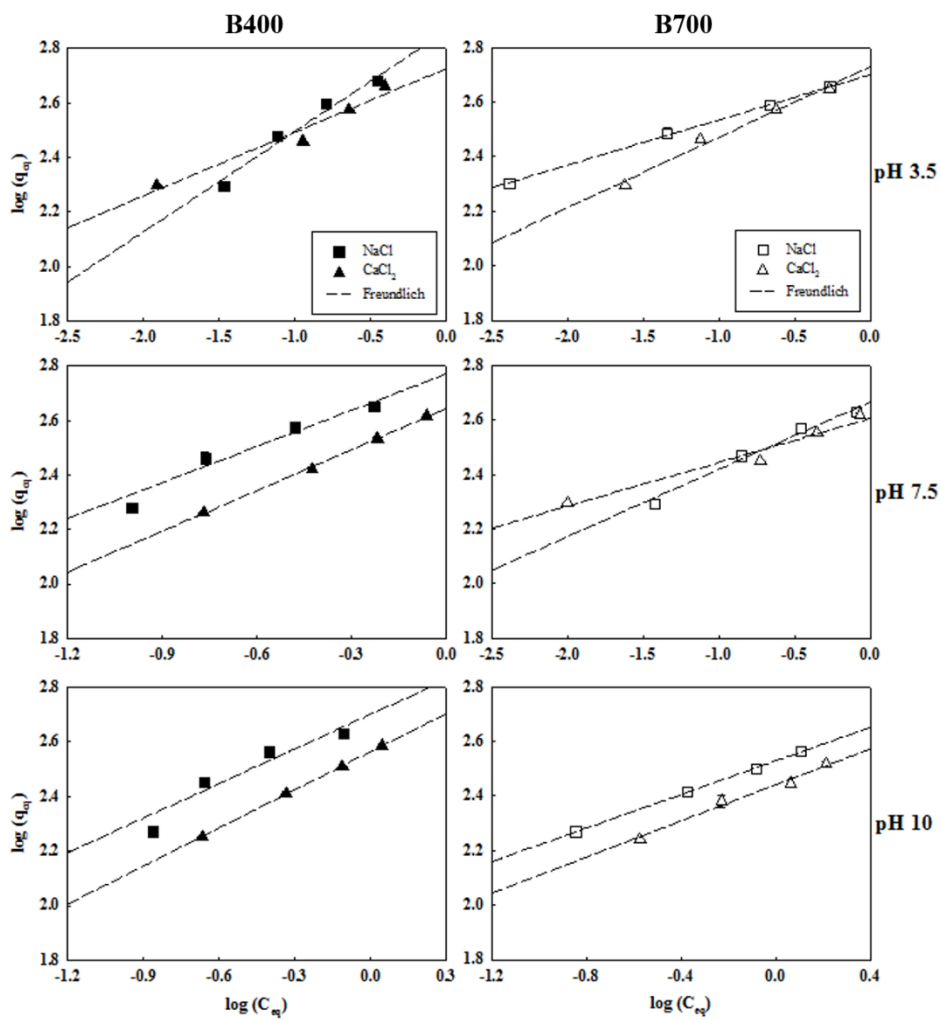


Table 4-3 Linear Freundlich and Langmuir sorption isotherm parameters for simazine sorption on *Miscanthus* biochar produced at two pyrolysis temperatures of 400 °C (B400) and 700 °C (B700) obtained at three pH values in 0.1 M NaCl and 0.05 M CaCl₂ solutions, with the results of two-way analysis of variance (ANOVA) showing the significance of the effects of two factors and their interaction on each isotherm parameter. The mixture was shaken at 160 rpm for 81 h at 25 ± 0.5 °C.

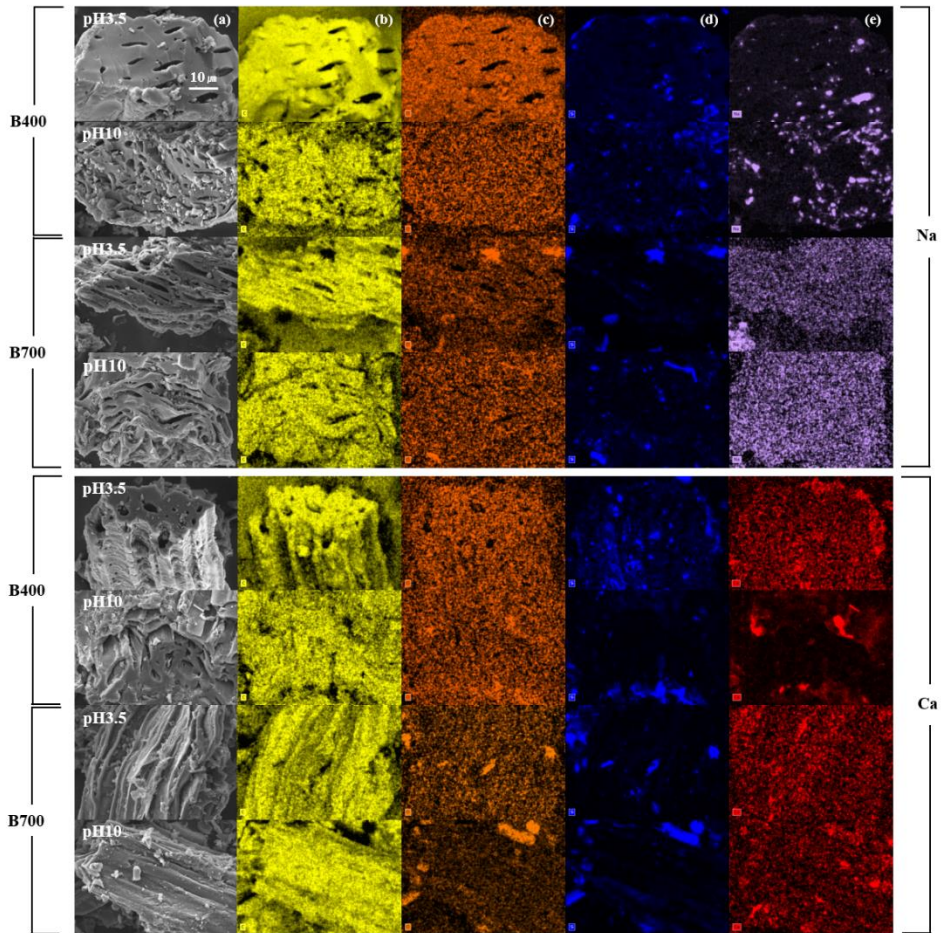
Biochar	Cation valence	pH	Linear Freundlich isotherm			Langmuir isotherm				
			$\log K_F$	$1/n$	R^2	Δq	K_L	q_{max}	R^2	Δq
B400	Na ⁺	3.5	2.81 (0.03)	0.36 (0.03)	0.96	1.6	14.7 (1.2)	565.6 (15.7)	0.99	4.5
		7.5	2.77 (0.03)	0.44 (0.04)	0.94	1.5	5.2 (0.5)	593.3 (22.9)	0.99	6.1
		10	2.70 (0.03)	0.42 (0.05)	0.91	1.7	4.4 (0.5)	557.4 (3.90)	0.98	6.1
	Ca ²⁺	3.5	2.73 (0.02)	0.23 (0.02)	0.96	1.9	46.0 (20.3)	423.3 (33.6)	0.76	23.3
		7.5	2.64 (0.00)	0.50 (0.01)	1.00	1.1	2.2 (0.3)	615.6 (36.2)	0.98	8.5
		10	2.56 (0.00)	0.47 (0.01)	1.00	0.3	1.9 (0.2)	552.2 (27.4)	0.98	4.5
ANOVA										
Cation valence			***	n.s.		n.s.	n.s.			
pH			***	**		n.s.	**			
Cation valence x pH			n.s.	n.s.		n.s.	**			
B700	Na ⁺	3.5	2.70 (0.02)	0.17 (0.01)	0.99	0.4	137.0 (53.6)	413.1 (25.3)	0.75	15.6
		7.5	2.67 (0.01)	0.25 (0.02)	0.97	0.8	16.2 (2.3)	444.2 (14.8)	0.96	6.9
		10	2.53 (0.00)	0.31 (0.00)	1.00	0.3	4.5 (0.7)	413.5 (18.9)	0.98	6.6
	Ca ²⁺	3.5	2.73 (0.02)	0.26 (0.01)	0.99	1.0	27.2 (3.7)	453.5 (14.6)	0.97	8.8
		7.5	2.60 (0.01)	0.16 (0.01)	0.96	1.6	73.9 (23.3)	368.1 (17.3)	0.75	24.7
		10	2.44 (0.01)	0.33 (0.02)	0.97	1.1	2.8 (0.5)	384.8 (18.7)	0.94	6.8
ANOVA										
Cation valence			**	n.s.		n.s.	n.s.			
pH			***	**		n.s.	n.s.			
Cation valence x pH			**	*		n.s.	n.s.			

***: significant at $p < 0.001$ level; **: significant at $p < 0.01$ level; *: significant at $p < 0.05$ level; n.s.: not significant ($p > 0.05$).

Table 4-4 FE-SEM/EDS elemental analysis results for two types of biochar produced at 400 and 700 °C (B400 and B700) obtained after simazine sorption at pH 3.5 and 10 in 0.1 M NaCl or 0.05 M CaCl₂ solutions.

Biochar	Cation valence	pH	Elemental concentration (%)			
			C	O	Si	Na ⁺ or Ca ²⁺
B400	Na ⁺	3.5	73.1±22.4	24.0±8.05	2.24±0.14	0.67 ± 0.19
		10	68.3±21.4	23.3±8.46	4.65±0.14	3.69 ± 0.72
	Ca ²⁺	3.5	72.9±22.7	25.3±9.03	1.41±0.19	0.41 ± 0.12
		10	69.0±21.4	27.7±9.59	1.77±0.17	1.56 ± 0.24
B700	Na ⁺	3.5	77.7±24.1	19.2±6.83	2.87±0.33	0.24 ± 0.12
		10	80.3±25.0	17.6±6.67	1.52±0.19	0.56 ± 0.18
	Ca ²⁺	3.5	80.3±25.0	16.9±6.39	2.49±0.26	0.29 ± 0.11
		10	74.9±23.3	19.0±7.00	5.53±0.65	0.54 ± 0.13

Fig. 4-3 FE-SEM/EDS images of (a) morphology (black), (b) C (yellow), (c) O (orange), (d) Si (blue), and (e) Na (purple) or Ca (red) for two types of biochar produced at 400 and 700 °C (B400 and B700, respectively), obtained after simazine sorption at pH 3.5 and 10 in 0.1 M NaCl or 0.05 M CaCl₂ solutions.



interact with cations in electrolyte solutions. This causes the blocking of the pore spaces available for simazine sorption in response to increasing pH and CV in the background electrolyte solution, resulting in different sizes of hydrated radii in the ionic atmosphere of the solution (Nguyen et al. 2007; Powell et al. 2011). The SEM morphology images showed the accumulation of Na^+ or Ca^{2+} on the biochar surface to a greater extent with increasing pH and CV (Fig. 4-3). In particular, the amount of simazine sorbed on biochar was higher in Na^+ electrolyte solution than in Ca^{2+} electrolyte solution (Fig. 4-2).

Despite higher deposition of Na^+ or Ca^{2+} on B400 than on B700 (Fig. 4-3), since the formation of metal-biochar complexes was greater in B400 than in B700 due to higher concentration of AFGs on the surface, the sorption of simazine was also greater in B400 (Fig. 4-2). This relationship can be explained by the fact that the pores of B700, which had more large pores available for simazine sorption (Table 4-1), was more blocked than those of B400, as a result of increased pore-filling mechanism (Borchardt et al. 2013). For this reason, less amount of simazine was sorbed on B700 than on B400 despite its higher SSA (Table 4-1). Therefore, it confirmed that the amount of simazine sorbed on biochar is a function of altered physicochemical characteristics of biochar under varying pH and CV conditions in a background electrolyte solution. Under circumneutral pH regions in soil-water systems, the neutral species of simazine may bind mainly to the hydrophobic sorption sites of biochar through van der Waals forces and the pore-filling mechanisms; however, it can bind to its hydrophilic sorption sites through intermolecular interactions such as H-bonding (a relatively minor mechanism) (Herwig et al. 2001).

4.3.5 Environmental effects of biochar on ionizable organic pollutant remediation

In general, the sorption of ionizable organic pollutants to biochar involves three possible mechanisms: π - π electron donor-acceptor (EDA) interactions, van der Waals forces and weak H-bonding (Herwig et al. 2001; Zhu et al. 2004). EDA interactions describe the binding of electron-donor molecules (organic pollutants) to electron-acceptor sites (aromatic C in biochar) (Zhang et al. 2013b), while H-bonding occurs between positively charged organic pollutants and the negatively charged surface of biochar (Zhang et al. 2013b) and van der Waals forces involve the binding of sorbate molecules to biochar without covalent or ionic bonding (Liu et al. 2012). In our previous study, two types of biochar binding sites responded independently to changing pH and/or pyrolysis temperature were found: strong sorption occurred in the lower sorption range due to EDA and/or H-bonding interactions, and relatively weak sorption occurred in the higher sorption range due to van der Waals forces (Lee et al. 2018).

However, the relative contribution of each of these mechanisms to the sorption of ionizable organic pollutants, such as simazine, to biochar varies with environmental factors such as pH and CV in the background electrolyte solution, since these factors alter the physicochemical characteristics and SCD of biochar and ionizable organic molecules, as observed in this study. Therefore, it can explain the mechanisms for simazine sorption to biochar in terms of pH and CV and their interactions. Under the acidic pH conditions below its PZNC, the positively charged surface of biochar interacts with neutral simazine molecules *via* H-bonding, van der Waals forces and the pore-filling mechanism. However, an increase in pH causes more electrostatic repulsion of neutral simazine due to more deprotonation of AFGs at respective pK_a . On the other hand, changing to a higher CV in a background electrolyte solution can lead to greater blocking of the entrance to intra-structural pores due to the formation of larger metal-biochar complexes. Therefore, decreased sorption capacity (K_F) of biochar for

simazine in both B400 and B700 as pH and CV increased (Table 4-3) were observed due to increased repulsive van der Waals forces and pore-filling mechanism.

As pH and CV of the surrounding electrolytic solution affect the morphological and physicochemical characteristics of biochar, it is presumed that the behavior of simazine sorption to biochar and the relative contribution of each factor and their interactions to K_F of biochar for simazine were different between B400 and B700. In this study, K_F of biochar was invariably lower in B700 than in B400 at any combination of the levels of two factors (Table 4-3), even though the former had higher SSA and lower AFGs than the latter (Table 4-1). Besides, even though greater decreases in K_F for simazine were expected for B400 due to more deprotonation at the surface acidic sites and to its lower SSA, the entire sorption capacity (K_F) was lower in B700. From these relations, it can be deduced that CV-driven pore-filling mechanisms predominate over pH-driven repulsive van der Waals forces in controlling the sorption affinity and capacity of biochar for simazine, when pH and CV are concerned.

Therefore, the physicochemical characteristics of biochar should be considered in order to effectively control ionizable organic pollutants that are positively, negatively or neutrally charged depending on protonation or deprotonation (de Ridder et al. 2010; Pignatello et al. 2011). For example, the negatively charged surface of biochar due to progressive deprotonation of surface AFGs with increasing pH above its PZNC attracts cation species or positively charged ionizable organic pollutants to achieve electrostatic stabilization but repulses negatively or neutrally charged ionizable organic pollutants through electrostatic repulsion (Pignatello et al. 2011; Fang et al. 2014; Lian et al. 2014). In addition, our results clearly revealed that CV of the background electrolyte solution is another key factor affecting the pH-dependent sorption of ionizable organic molecules to a variable-charge sorbent.

Thus, an understanding of the physicochemical characteristics and charge behavior of biochar and ionizable organic pollutants under various environmental conditions is a prerequisite to assessing the efficacy of remediation and its environmental risks in real environments such as soils and nearby waters.

4.4. Conclusions

I hypothesized that pH and CV in a background electrolyte solution would determine the behavior of the sorption of simazine (containing lone-pair electrons) to biochar (carrying variable SCD) by altering the charge behavior and surface morphology of biochar, and the sorption response would be different depending on pyrolysis temperature because pyrolysis temperature governs pore space morphology and surface charge behavior of biochar. For this hypothesis were tested by interpreting the effects of pH, CV and their interactions on pyrolysis temperature-driven simazine sorption. Fitting of experimental data of simazine sorption to the Freundlich model obviously showed that K_F of biochar for simazine decreased as pH and CV increased due respectively to increased electrostatic repulsion for neutral simazine molecules with increasing pH and (predominantly) to more inhibition of internal pore entrances with increasing CV. The pH-driven decreases in K_F were greater with Ca^{2+} ions (higher CV), while CV-driven decreases were greater at higher pH values. However, invariably lower K_F of biochar in B700 than in B400 was observed at any given combination of the levels of pH and CV, even though higher K_F was expected for the former from its higher SSA and lower AFGs at the surface, and this discrepancy means that increasing CV contributes to a greater extent to decreased K_F than increasing pH. From these relations, it deduced that CV-driven alterations in pore space and surface morphology predominate over pH-driven van der Waals forces in controlling the sorption

affinity and capacity of biochar for simazine, where pH and CV are concerned. The results confirmed our hypothesis by revealing that changing CV alters surface coverage available for simazine sorption and the blocking of the entrance to internal pore space while pH governs protonation/deprotonation of AFGs, and that CV predominates over pH in controlling the behavior of simazine (containing lone-pair electrons) sorption to biochar (carrying variable SCD). Therefore, this approach and findings will contribute to a more comprehensive understanding of the sorption mechanisms and behavior of ionizable organic pollutants (variable-charge sorbates) to the surface of biochar (variable-charge sorbent) and help better interpret their environmental occurrence, behavior, transport and fate under natural soils and nearby water environments.

References

- Abdul G, Zhu X, Chen B (2017) Structural characteristics of biochar-graphene nanosheet composites and their adsorption performance for phthalic acid esters. *Chem Eng J* 319:9–20. doi: 10.1016/j.cej.2017.02.074
- Angin D (2013) Effect of pyrolysis temperature and heating rate on biochar obtained from pyrolysis of safflower seed press cake. *Bioresour Technol* 128:593–597. doi: 10.1016/j.biortech.2012.10.150
- Boehm HP (1994) Some aspects of the surface chemistry of carbon blacks and other carbons. *Carbon N Y* 32:759–769. doi: 10.1016/0008-6223(94)90031-0
- Borchardt L, Oschatz M, Paasch S, Kaskel S, Brunner E (2013) Interaction of electrolyte molecules with carbon materials of well-defined porosity: characterization by solid-state NMR spectroscopy. *Phys Chem Chem Phys* 15:15177. doi: 10.1039/c3cp52283k
- Cao X, Harris W (2010) Properties of dairy-manure-derived biochar pertinent to its potential use in remediation. *Bioresour Technol* 101:5222–5228. doi: 10.1016/j.biortech.2010.02.052
- Cely P, Tarquis AM, Paz-Ferreiro J, Méndez A, Gascó G (2014) Factors driving the carbon mineralization priming effect in a sandy loam soil amended with different types of biochar. *Solid Earth* 5:585–594. doi: 10.5194/se-5-585-2014
- Chen B, Zhou D, Zhu L (2008) Transitional adsorption and partition of nonpolar and polar aromatic contaminants by biochars of pine needles with different pyrolytic temperatures. *Environ Sci Technol* 42:5137–5143. doi: 10.1021/es8002684
- Chen M, Wang D, Yang F, Xu X, Xu N, Cao X (2017) Transport and retention of biochar nanoparticles in a paddy soil under environmentally-relevant solution chemistry conditions. *Environ Pollut* 230:540–549. doi: 10.1016/j.envpol.2017.06.101
- Contescu A, Contescu C, Putyera K, Schwarz JA (1997) Surface acidity of carbons characterized by their continuous pK distribution and Boehm titration. *Carbon N Y* 35:83–94. doi: 10.1016/S0008-6223(96)00125-X
- de Ridder DJ, Villacorte L, Verliefde ARD, Verberk JQJC, Heijman SGJ, Amy GL, van Dijk JC (2010) Modeling equilibrium adsorption of organic micropollutants onto activated carbon. *Water Res* 44:3077–3086. doi: 10.1016/j.watres.2010.02.034
- Domingues RR, Trugilho PF, Silva CA, De Melo ICNA, Melo LCA, Magriotis ZM, Sánchez-Monedero MA (2017) Properties of biochar derived from wood and high-nutrient biomasses with the aim of agronomic and environmental benefits. *PLoS One* 12:1–19. doi: 10.1371/journal.pone.0176884
- Dong X, Ma LQ, Li Y (2011) Characteristics and mechanisms of hexavalent chromium removal by biochar from sugar beet tailing. *J Hazard Mater* 190:909–915. doi: 10.1016/j.jhazmat.2011.04.008
- El-Kamash AM, Zaki AA, El Geleel MA (2005) Modeling batch kinetics and thermodynamics of zinc and cadmium ions removal from waste solutions using synthetic zeolite A. *J Hazard Mater* 127:211–220. doi: 10.1016/j.jhazmat.2005.07.021

- Elmay Y, Brech Y Le, Delmotte L, Dufour A, Brosse N, Gadiou R (2015) Characterization of Miscanthus pyrolysis by DRIFTS, UV Raman spectroscopy and mass spectrometry. *J Anal Appl Pyrolysis* 113:402–411. doi: 10.1016/j.jaap.2015.03.004
- Essandoh M, Kunwar B, Pittman CU, Mohan D, Mlsna T (2015) Sorptive removal of salicylic acid and ibuprofen from aqueous solutions using peine wood fast pyrolysis biochar. *Chem Eng J* 265:219–227. doi: 10.1016/j.cej.2014.12.006
- Fang Q, Chen B, Lin Y, Guan Y (2014) Aromatic and hydrophobic surfaces of wood-derived biochar enhance perchlorate adsorption via hydrogen bonding to oxygen-containing organic groups. *Environ Sci Technol* 48:279–288. doi: 10.1021/es403711y
- Gabelich CJ, Tran TD, Suffet IH “Mel” (2002) Electrosorption of Inorganic Salts from Aqueous Solution Using Carbon Aerogels. *Environ Sci Technol* 36:3010–3019. doi: 10.1021/es0112745
- Gai C, Li Y, Peng N, Fan A, Liu Z (2015) Co-liquefaction of microalgae and lignocellulosic biomass in subcritical water. *Bioresour Technol* 185:240–245. doi: 10.1016/j.biortech.2015.03.015
- Graber ER (2010) pH-Dependent Mineral Release and Surface Properties of Cornstraw Biochar : Agronomic Implications. 44:9318–9323
- Gunasekara AS, Troiano J, Goh KS, Tjeerdema and RS, Tjeerdema RS (2007) Chemistry and Fate of Simazine. *Rev Environ Contam Toxicol* 202:1–52. doi: 10.1007/978-1-4419-1157-5
- Han L, Qian L, Yan J, Chen M (2016) Contributions of different biomass components to the sorption of 1,2,4-trichlorobenzene under a series of pyrolytic temperatures. *Chemosphere* 156:262–271. doi: 10.1016/j.chemosphere.2016.04.031
- Herwig U, Klumpp E, Narres HD, Schwuger MJ (2001) Physicochemical interactions between atrazine and clay minerals. *Appl Clay Sci* 18:211–222. doi: 10.1016/S0169-1317(01)00024-2
- Kim E, Jung C, Han J, Her N, Park CM, Jang M, Son A, Yoon Y (2016) Sorptive removal of selected emerging contaminants using biochar in aqueous solution. *J Ind Eng Chem* 36:364–371. doi: 10.1016/j.jiec.2016.03.004
- Kloss S, Zehetner F, Dellantonio A, Hamid R, Ottner F, Liedtke V, Schwanninger M, Gerzabek MH, Soja G (2012) Characterization of Slow Pyrolysis Biochars: Effects of Feedstocks and Pyrolysis Temperature on Biochar Properties. *J Environ Qual* 41:990. doi: 10.2134/jeq2011.0070
- Kumari KGID, Moldrup P, Paradelo M, De Jonge LW (2014) Phenanthrene sorption on biochar-amended soils: Application rate, aging, and physicochemical properties of soil. *Water Air Soil Pollut* 225: . doi: 10.1007/s11270-014-2105-8
- Largeot C, Portet C, Chmiola J, Taberna PL, Gogotsi Y, Simon P (2008) Relation between the ion size and pore size for an electric double-layer capacitor. *J Am Chem Soc* 130:2730–2731. doi: 10.1021/ja7106178
- Lee S, Han J, Ro HM (2018) Interpreting the pH-dependent mechanism of simazine sorption to Miscanthus biochar produced at different pyrolysis temperatures for

- its application to soil. *Korean J Chem Eng* 35:1468–1476. doi: 10.1007/s11814-018-0054-4
- Lehmann J (2007a) A handful of carbon. *Nature* 447:143–144. doi: 10.1038/447143a
- Lehmann J (2007b) Bio-energy in the black. *Front Ecol Environ* 5:381–387. doi: 10.1890/1540-9295(2007)5[381:BITB]2.0.CO;2
- Leon CA, Radovic LR (1991) Influence of Oxygen Functional Groups on the Performance of Carbon-Supported Catalysts. *Mater Sci* 1007–1014
- Li X, Jiang L, Li L, Yan Y (2017) Effects of HF etching on nanoindentation response of ion-exchanged aluminosilicate float glass on air and tin sides. *J Mater Sci* 52:4367–4377. doi: 10.1007/s10853-016-0684-z
- Lian F, Sun B, Song Z, Zhu L, Qi X, Xing B (2014) Physicochemical properties of herb-residue biochar and its sorption to ionizable antibiotic sulfamethoxazole. *Chem Eng J* 248:128–134. doi: 10.1016/j.cej.2014.03.021
- Liu W, Carrasco J, Santra B, Michaelides A, Scheffler M, Tkatchenko A (2012) Benzene adsorbed on metals: Concerted effect of covalency and van der Waals bonding. *Phys Rev B - Condens Matter Mater Phys* 86:1–6. doi: 10.1103/PhysRevB.86.245405
- Méndez A, Terradillos M, Gascó G (2013) Physicochemical and agronomic properties of biochar from sewage sludge pyrolysed at different temperatures. *J Anal Appl Pyrolysis* 102:124–130. doi: 10.1016/j.jaap.2013.03.006
- Mihaly Cozmuta L, Mihaly Cozmuta A, Peter A, Nicula C, Bakatula Nsimba E, Tutu H (2012) The influence of pH on the adsorption of lead by Na-clinoptilolite: Kinetic and equilibrium studies. *Water SA* 38:269–278. doi: 10.4314/wsa.v38i2.13
- Mimmo T, Panzacchi P, Baratieri M, Davies CA, Tonon G (2014) Effect of pyrolysis temperature on miscanthus (*Miscanthus × giganteus*) biochar physical, chemical and functional properties. *Biomass and Bioenergy* 62:149–157. doi: 10.1016/j.biombioe.2014.01.004
- Morgante V, Flores C, Fadic X, González M, Hernández M, Cereceda-Balic F, Seeger M (2012) Influence of microorganisms and leaching on simazine attenuation in an agricultural soil. *J Environ Manage* 95:S300–S305. doi: 10.1016/j.jenvman.2011.06.045
- Mukherjee A, Zimmerman AR, Harris W (2011) Surface chemistry variations among a series of laboratory-produced biochars. *Geoderma* 163:247–255. doi: 10.1016/j.geoderma.2011.04.021
- Narasimha Rao S, Mathew PK (1995) Effects of exchangeable cations on hydraulic conductivity of a marine clay. *Clays Clay Miner* 43:433–437. doi: 10.1346/CCMN.1995.0430406
- Nguyen TH, Cho HH, Poster DL, Ball WP (2007) Evidence for a pore-filling mechanism in the adsorption of aromatic hydrocarbons to a natural wood char. *Environ Sci Technol* 41:1212–1217. doi: 10.1021/es0617845
- Peng P, Lang YH, Wang XM (2016) Adsorption behavior and mechanism of pentachlorophenol on reed biochars: PH effect, pyrolysis temperature, hydrochloric acid treatment and isotherms. *Ecol Eng* 90:225–233. doi: 10.1016/j.ecoleng.2016.01.039

- Persson I (2010) Hydrated metal ions in aqueous solution: How regular are their structures? *Pure Appl Chem* 82:1901–1917. doi: 10.1351/PAC-CON-09-10-22
- Pignatello JJ, Ni JZ, Xing BS (2011) Adsorption of aromatic carboxylate ions to charcoal black carbon is accompanied by release of hydroxide ion. *Abstr Pap Am Chem Soc* 242:9240–9248
- Powell MR, Cleary L, Davenport M, Shea KJ, Siwy ZS (2011) Electric-field-induced wetting and dewetting in single hydrophobic nanopores. *Nat Nanotechnol* 6:798–802. doi: 10.1038/nnano.2011.189
- Qiu Y, Zheng Z, Zhou Z, Sheng GD (2009) Effectiveness and mechanisms of dye adsorption on a straw-based biochar. *Bioresour Technol* 100:5348–5351. doi: 10.1016/j.biortech.2009.05.054
- Qu T, Guo W, Shen L, Xiao J, Zhao K (2011) Experimental study of biomass pyrolysis based on three major components: Hemicellulose, cellulose, and lignin. *Ind Eng Chem Res* 50:10424–10433. doi: 10.1021/ie1025453
- Rahman MS, Islam MR (2009) Effects of pH on isotherms modeling for Cu(II) ions adsorption using maple wood sawdust. *Chem Eng J* 149:273–280. doi: 10.1016/j.cej.2008.11.029
- Rajapaksha AU, Vithanage M, Ahmad M, Seo DC, Cho JS, Lee SE, Lee SS, Ok YS (2015) Enhanced sulfamethazine removal by steam-activated invasive plant-derived biochar. *J Hazard Mater* 290:43–50. doi: 10.1016/j.jhazmat.2015.02.046
- Rajkovich S, Enders A, Hanley K, Hyland C, Zimmerman AR, Lehmann J (2012) Corn growth and nitrogen nutrition after additions of biochars with varying properties to a temperate soil. *Biol Fertil Soils* 48:271–284. doi: 10.1007/s00374-011-0624-7
- Reddad Z, Gerente C, Andres Y, Le Cloirec P (2002) Adsorption of several metal ions onto a low-cost biosorbent: Kinetic and equilibrium studies. *Environ Sci Technol* 36:2067–2073. doi: 10.1021/es0102989
- Ruthenberg K, Chang H (2017) Acidity: Modes of characterization and quantification. *Stud Hist Philos Sci Part A* 65–66:121–131. doi: 10.1016/j.shpsa.2017.04.003
- Sigmund G, Hüffer T, Hofmann T, Kah M (2016) Biochar total surface area and total pore volume determined by N₂ and CO₂ physisorption are strongly influenced by degassing temperature. *Sci Total Environ* d: doi: 10.1016/j.scitotenv.2016.12.023
- Silber A, Levkovitch I, Graber ER (2010) PH-dependent mineral release and surface properties of cornstraw biochar: Agronomic implications. *Environ Sci Technol* 44:9318–9323. doi: 10.1021/es101283d
- Silva M, Iyer P (2014) Toxicity endpoint selections for a simazine risk assessment. *Birth Defects Res Part B - Dev Reprod Toxicol* 101:308–324. doi: 10.1002/bdrb.21114
- Sun K, Keiluweit M, Kleber M, Pan Z, Xing B (2011) Sorption of fluorinated herbicides to plant biomass-derived biochars as a function of molecular structure. *Bioresour Technol* 102:9897–9903. doi: 10.1016/j.biortech.2011.08.036

- Szekeres M, Tombác E (2012) Surface charge characterization of metal oxides by potentiometric acid-base titration, revisited theory and experiment. *Colloids Surfaces A Physicochem Eng Asp* 414:302–313. doi: 10.1016/j.colsurfa.2012.08.027
- Tang J, Zhu W, Kookana R, Katayama A (2013) Characteristics of biochar and its application in remediation of contaminated soil. *J Biosci Bioeng* 116:653–659. doi: 10.1016/j.jbiosc.2013.05.035
- Tran HN, You SJ, Chao HP (2017) Insight into adsorption mechanism of cationic dye onto agricultural residues-derived hydrochars: Negligible role of π - π interaction. *Korean J Chem Eng* 34:1708–1720. doi: 10.1007/s11814-017-0056-7
- Trentacoste S V, Friedmann AS, Youker RT, Breckenridge CB, Zirkin BR (2001) Atrazine effects on testosterone levels and androgen-dependent reproductive organs in peripubertal male rats. *J Androl* 22:142–148. doi: 10.1002/j.1939-4640.2001.tb02164.x
- Uchimiya M, Chang SC, Klasson KT (2011) Screening biochars for heavy metal retention in soil: Role of oxygen functional groups. *J Hazard Mater* 190:432–441. doi: 10.1016/j.jhazmat.2011.03.063
- USEPA (2006) Triazine Cumulative Risk Assessment. 67
- USEPA (1998) Fate, transport and transformation test guidelines - Sediment and soil adsorption/desorption isotherm. 18
- Vu TM, Trinh VT, Doan DP, Van HT, Nguyen TV, Vigneswaran S, Ngo HH (2017) Removing ammonium from water using modified corncob-biochar. *Sci Total Environ* 579:612–619. doi: 10.1016/j.scitotenv.2016.11.050
- Wang J, Liu H, Yang S, Zhang J, Zhang C, Wu H (2014) Physicochemical characteristics and sorption capacities of heavy metal ions of activated carbons derived by activation with different alkyl phosphate triesters. *Appl Surf Sci* 316:443–450. doi: 10.1016/j.apsusc.2014.07.206
- Wang Q, Lemley AT (2006) Reduced adsorption of ametryn in clay, humic acid, and soil by interaction with ferric ion under fenton treatment conditions. *J Environ Sci Heal - Part B Pestic Food Contam Agric Wastes* 41:223–236. doi: 10.1080/03601230500354766
- Wang Y, Qiu L, Zhu M, Sun G, Zhang T, Kang K (2019) Comparative Evaluation of Hydrothermal Carbonization and Low Temperature Pyrolysis of *Eucommia ulmoides* Oliver for the Production of Solid Biofuel. *Sci Rep* 9:1–11. doi: 10.1038/s41598-019-38849-4
- Weber JB (2010) Adsorption of s-Triazines by Montmorillonite As a Function of pH and Molecular Structure1. *Soil Sci Soc Am J* 34:401. doi: 10.2136/sssaj1970.03615995003400030017x
- Xiao F, Pignatello JJ (2016) Effects of Post-Pyrolysis Air Oxidation of Biomass Chars on Adsorption of Neutral and Ionizable Compounds. *Environ Sci Technol* 50:6276–6283. doi: 10.1021/acs.est.6b00362
- Yang Y, Chun Y, Shang G, Huang M (2004) pH-dependence of pesticide adsorption by wheat-residue-derived black carbon. *Langmuir* 20:6736–6741. doi: 10.1021/la049363t

- Yuan JH, Xu RK, Zhang H (2011) The forms of alkalis in the biochar produced from crop residues at different temperatures. *Bioresour Technol* 102:3488–3497. doi: 10.1016/j.biortech.2010.11.018
- Zhang G, Zhang Q, Sun K, Liu X, Zheng W, Zhao Y (2011) Sorption of simazine to corn straw biochars prepared at different pyrolytic temperatures. *Environ Pollut* 159:2594–2601. doi: 10.1016/j.envpol.2011.06.012
- Zhang P, Sun H, Yu L, Sun T (2013a) Adsorption and catalytic hydrolysis of carbaryl and atrazine on pig manure-derived biochars: Impact of structural properties of biochars. *J Hazard Mater* 244–245:217–224. doi: 10.1016/j.jhazmat.2012.11.046
- Zhang X, Wang H, He L, Lu K, Sarmah A, Li J, Bolan NS, Pei J, Huang H (2013b) Using biochar for remediation of soils contaminated with heavy metals and organic pollutants. *Environ Sci Pollut Res* 20:8472–8483. doi: 10.1007/s11356-013-1659-0
- Zhao L, Cao X, Mašek O, Zimmerman A (2013) Heterogeneity of biochar properties as a function of feedstock sources and production temperatures. *J Hazard Mater* 256–257:1–9. doi: 10.1016/j.jhazmat.2013.04.015
- Zheng H, Wang Z, Zhao J, Herbert S, Xing B (2013) Sorption of antibiotic sulfamethoxazole varies with biochars produced at different temperatures. *Environ Pollut* 181:60–67. doi: 10.1016/j.envpol.2013.05.056
- Zheng W, Guo M, Chow T, Bennett DN, Rajagopalan N (2010) Sorption properties of greenwaste biochar for two triazine pesticides. *J Hazard Mater* 181:121–126. doi: 10.1016/j.jhazmat.2010.04.103
- Zhu D, Hyun S, Pignatello JJ, Lee LS (2004) Evidence for π - π electron donor-acceptor interactions between π -donor aromatic compounds and π -acceptor sites in soil organic matter through pH effects on sorption. *Environ Sci Technol* 38:4361–4368. doi: 10.1021/es035379e
- Zielińska A, Oleszczuk P (2015) Evaluation of sewage sludge and slow pyrolyzed sewage sludge-derived biochar for adsorption of phenanthrene and pyrene. *Bioresour Technol* 192:618–626. doi: 10.1016/j.biortech.2015.06.032
- Zielińska A, Oleszczuk P, Charmas B, Skubiszewska-Zięba J, Pasiieczna-Patkowska S (2015) Effect of sewage sludge properties on the biochar characteristic. *J Anal Appl Pyrolysis* 112:201–213. doi: 10.1016/j.jaap.2015.01.025

(This page intentionally left blank)

CHAPTER 5. COMPREHENSIVE INTERPRETATION FOR THE SORPTION MECHANISMS OF Cd²⁺ and As(V) WITH *MISCANTHUS* BIOCHAR USING SCANNING ELECTRON MICROSCOPY, X-RAY DIFFRACTION AND PHOTOEMISSION SPECTROSCOPY

List of contents	5-1
Abstract	5-2
5.1. Introduction	5-3
5.2. Materials and methods	5-6
5.2.1. Physicochemical characteristics of biochar	5-6
5.2.2. Sorption kinetics and isotherm	5-6
5.2.3. Chemical modeling	5-8
5.2.4. X-ray diffraction and photoemission spectroscopy	5-8
5.2.5. Scanning electron microscopy	5-9
5.3. Results and disussion	5-10
5.3.1. Physicochemical characteristics of biochar	5-10
5.3.2. Sorption isotherm	5-12
5.3.3. Possible precipitation modeling using visual MINTEQ.....	5-22
5.3.4. Characterization of crystallized precipitated using XRD	5-25
5.3.5. Surface complexation and precipitation determined by XPS	5-29
5.3.5.1. C, O and Si as biochar structure	5-29
5.3.5.2. Sorption of background Na ⁺ and Ca ²⁺ ion	5-38
5.3.5.3. Sorption mechanism of Cd ²⁺ and As(V)	5-40
5.3.6. Distinctive sorption mechanism between Cd ²⁺ and As(V)	5-51
5.4. Conclusions	5-56
Reference	5-58

Abstract

Heavy metal pollution poses detrimental threats to ecosystems and human life, and biochar has received increasing attention as a biosorbent. However, the underlying sorption mechanisms of biochar for heavy metals that takes into account the alterations in biochar's physicochemical and surface charge characteristics caused by environmental conditions is still unclear. Here, pH-dependent batch sorption experiments of two contrasting heavy metals (cationic cadmium (Cd^{2+}) and oxyanionic arsenate (As(V))) to *Miscanthus* biochar produced at two pyrolysis temperatures (400 and 700 °C) were conducted, and the sorption mechanism was interpreted using scanning electron microscopy, X-ray diffraction and photoemission spectroscopy. Partitioning and outer-sphere complexation are sorption mechanisms for both Cd^{2+} and As(V) irrespective of pH; however, inner-sphere complexation with acidic functional groups (AFGs) and precipitation as otavite predominate at higher pH values for Cd^{2+} , while hydrophobic attraction of reduced As molecules and electrostatic cation bridging complexation with multivalent ions at deprotonated AFGs are predominant for As(V) . The pH-dependent sorption results showed that the sorption capacity was higher at higher pH for both Cd^{2+} and As(V) and that the sorption capacity of As(V) was even lower than that of Cd^{2+} . This unexpected phenomenon can be explained by the reduced As(V) by electrons from the biochar and by the difference in charge density of As(V) with basic functional groups (BFGs) on biochar surface. These findings pose a significant challenge to more comprehensive understanding of the sorption behavior of inorganic pollutants to biochar, and help better explain the environmental fate and behavior in natural soil and water systems.

Keywords

Cadmium, Arsenate, *Miscanthus* biochar, Pyrolysis temperature, pH-dependent

5.1. Introduction

Cadmium (Cd) is a problematic cationic heavy metal since it is released by various industrial processes, exhibits high levels of toxicity and accumulates in organisms, causing oxidative stress (Yu et al. 2006; Wills et al. 2008). In contrast, arsenic (As) is an anionic toxic metalloid deposited into soil from preservatives, pesticides and antibiotics (Sø et al. 2008) and mainly exists as arsenate (As(V)) in soil. The oxyanion species of As disrupts phosphate metabolism in organisms due to the similar electrochemical properties between oxyanionic As and phosphate (Chun-xi et al. 2007). Thus, the removal and remediation of cationic Cd and anionic As(V) in soil and water systems are important issues worldwide affecting the security of human health and ecosystems. However, it is not easy to remove these species together because of their opposite characteristic sorption patterns in soil components, which are mainly attributed to their charge difference. Cationic Cd mainly exists as Cd^{2+} in the soil environment, and it is easily sorbed on the negatively charged surface of soil components or precipitated with background ions (Basualto et al. 2006; Boparai et al. 2013), while redox conditions govern the species transformation of As. As(V) is the most prevalent form under oxic conditions, and soil pH governs the protonation of H_3AsO_4 , H_2AsO_4^- , HAsO_4^{2-} or AsO_4^{3-} (Kong et al. 2017). Both Cd^{2+} and As(V) have been reported to be present at trace levels in contaminated soils, and it is essential to minimize their bioavailability and leachability to block their transport to plants, animals and humans. Therefore, understanding the behavior of Cd^{2+} and As(V) across a range of surrounding environmental conditions, such as pH and the presence of inorganic compounds, is essential to decrease the risks to human health and ecosystems.

Biochar is a carbon-rich material obtained from various feedstocks through pyrolysis under oxygen-limited conditions, and it has received great attention worldwide as an alternative sorbent for nutrients and toxic molecules

and as a substrate for carbon sequestration (Nanda et al. 2013). Many factors during pyrolysis govern the characteristics of the biochar that is produced, and the pyrolysis temperature (PT) is one of the crucial factors determining the physicochemical characteristics of biochar. Increasing PT commonly causes a higher aromatic carbon content, higher concentrations of alkaline species and more developed pore structures, while lower concentrations of acidic functional groups (AFGs) have been found on the surface of biochars produced at higher PTs (Uchimiya and Hiradate 2014; Wang 2017). AFGs include carboxylic, lactic and phenolic groups, while the reported basic functional groups (BFGs) include pyridinium groups, oxonium groups and protonated aromatic rings (Lawrinenko and Laird 2015). Both types of functional groups affect the sorption mechanism of charged molecules such as heavy metals, metalloids, pesticides and salts (Ahmad et al. 2014) because the surface charge of biochar is governed by the protonation and deprotonation of BFGs and AFGs. Under acidic conditions, the surface charge of biochar is positive due to the combination of deprotonation of BFGs and protonation of AFGs. With increasing pH above the pK_a of AFGs (carboxylic $pK_a \approx 4.4$, lactic $pK_a \approx 8.2$, and phenolic $pK_a \approx 10$), the surface charge of biochar becomes more negative due to deprotonation (Leon and Radovic 1991; Silber et al. 2010), but no pK_b for BFGs has previously been reported. In addition, deformation of the pore structure by thermal decomposition will change the sorption mechanism (Lee et al. 2020). However, the sorption mechanisms of heavy metals and oxyanions remain to be clarified by molecular-scale observations.

The development of analytical techniques and theoretical calculations has enabled us to observe sorption mechanisms at the molecular scale by comparing experimental and theoretical results. Many X-ray-based techniques and electron microscopy techniques have shown us the properties of such reactions at the molecular scale; however, it is not easy to interpret the results

of various analytical techniques and theoretical calculations because their analysis and interpretation pose an excessive burden. For example, X-ray fluorescence (XRF) and X-ray diffraction (XRD) provide us with the elemental composition and crystal structure of major components, while X-ray photoelectron spectroscopy (XPS) can be used to observe the binding energy of both amorphous and crystal structures at the surface at the depth of a few nanometers. Scanning electron microscopy (SEM) captures the physical characteristics of pore structures, and chemical modeling provides theoretical estimations of precipitation and complexation. Comparisons among these techniques and comparisons with traditional sorption isotherms could lead to increased accuracy and prove the real sorption mechanism, and a comprehensive understanding is essential for revealing the further implications of biochar in real soil, where both cationic and anionic pollutants are present together.

Therefore, the objective of this study was to elucidate the sorption mechanisms of cationic Cd^{2+} and anionic As(V) to biochar produced from *Miscanthus* pyrolyzed at two different PTs (400 and 700 °C). To do so, the physicochemical characteristics of the biochars were evaluated, traditional isotherm models were tested, theoretical chemical modeling was employed, and the results from X-ray-based techniques and electron microscopy were comprehensively interpreted to assess the behavior of Cd^{2+} and As(V) in real environments.

5.2. Material and methods

5.2.1. Physicochemical characteristics of biochar

Two types of biochar were produced from *Miscanthus* at the two different PTs of 400 and 700 °C (hereafter, B400 and B700) based on previous studies (Usman et al. 2015; Lee et al. 2018) that showed dramatic changes in

the physicochemical characteristics of biochar due to thermal decomposition (Lehmann 2007; Chen et al. 2008; Zhang et al. 2011). The biochar samples were ball-milled (MM400, Retsch, Germany) and sieved through a 106- μm mesh to minimize size effects (Zheng et al. 2010). The specific surface area, major elemental composition (C, N, H, O and S, determined by elemental analyzer), minor elemental composition (determined by XRF), AFGs (measured by the Boehm titration method) (Boehm 1994), surface charge density (determined by using potentiometric titration) (Szekeres and Tombácz 2012), and point of zero net charge (PZNC, determined by the pH drift method) (Yang et al. 2004) were previously measured and employed for this study.

5.2.2. Sorption kinetics and isotherm

The sorption kinetics study was performed to evaluate the time required for equilibrium adsorption of Cd^{2+} and As(V) without pH adjustment. Two hundred milligrams of biochar was mixed with 20 mL of 1 mM CdCl_2 and Na_2HAsO_4 in 100 mM NaCl as a background solution in a 30 mL amber glass vial with a Teflon-lined cap. The samples were allowed to equilibrate on a vial shaker (DS-300L, Dasol, Korea) at 160 rpm until the desired time (0.1, 0.5, 1, 2, 6, 12, 24, 48, 86 and 120 h) at room temperature (25 ± 2 °C). Samples were collected at the desired time and filtered through a 0.45- μm nylon membrane filter. Each aliquot was diluted for quantification of Cd^{2+} and As(V) using inductively coupled plasma optical emission spectroscopy (ICP-OES) (Icap-7200, Thermo, USA). All reagents were purchased from Sigma-Aldrich (St. Louis, MO, USA) at least 98% purity.

The sorption isotherm study was conducted to elucidate the sorption mechanisms of Cd^{2+} and As(V) with pH adjustment. Two hundred milligrams of biochar and 20 mL of different concentrations of CdCl_2 or Na_2HAsO_4 (1, 2, 3, 4, 5 and 10 mM) containing 100 mM NaCl as a background solution were

placed in a 30 mL amber glass vial with a Teflon-lined cap. The samples were allowed to equilibrate by shaking on a vial shaker at 160 rpm for 120 h; the equilibration time were defined by a kinetic study. The pH of the samples was adjusted to 3.5, 7.0 and 10 using 1 M HCl or 1 M NaOH during equilibration. The samples were filtered through a 0.45- μm nylon membrane filter. Each aliquot was diluted for quantification of Cd^{2+} and As(V) using ICP-OES. All experiments were performed in triplicate. The sorption isotherm results at pH 3.5, 7.0 and 10 were fitted to the Langmuir and Freundlich isotherms. The Langmuir sorption isotherm, which assumes monolayer adsorption on a sorbent, is expressed as follows:

$$q_{eq} = \frac{q_{max} \cdot K_L \cdot C_{eq}}{(1 + K_L \cdot C_{eq})} \quad (1)$$

where q_{eq} and q_{max} are the equilibrium and maximum sorbed concentrations of Cd^{2+} and As(V) on biochar (mmol g^{-1}), K_L is a constant related to energy (L mmol^{-1}), and C_{eq} is the equilibrium concentration of Cd^{2+} and As(V) in solution. The Freundlich sorption isotherm, which interprets multilayer sorption on a heterogeneous sorbent with nonuniform distribution energy, is expressed as follows:

$$q_{eq} = K_F \cdot C_{eq}^{1/n} \quad (2)$$

where K_F is a constant related to sorption capacity ($\text{mmol g}^{-1}(\text{mmol L}^{-1})^{-n}$) and $1/n$ is the sorption intensity.

5.2.3. Chemical modeling

Chemical modeling was conducted to calculate the equilibrium, speciation, solubility and precipitation of ions in an aqueous solution, and Visual MINTEQ ver. 3.1 (KTH, SEED, Sweden) that an extensive thermodynamic database were employed for the calculation. The dissolved ion concentrations of B400 and B700 from the kinetic study (listed in Table 5-3)

were used to develop chemical models of the background solutes. The software was used to calculate the saturation indices ($SI = \log_{10}(I_{AP}/K_{sp})$) of all the potential solid compounds at different pH values (pH 3.5, 7 and 10) and solute concentrations (0, 1, 2, 3, 5 and 10 mM). The compounds with relatively high supersaturation ratios ($SI \gg 0$) were assumed to be potential precipitates, and the potential precipitates were employed for further analysis in XRD and XPS.

5.2.4. X-ray diffraction and photoemission spectroscopy

XRD is an effective method for measuring abundant crystal structures (usually higher than 1%); thus, abundant precipitates can be identified from XRD results, but amorphous structures cannot be examined. For that reason, both XRD and XPS were employed to characterize the crystal structure and amorphous structure of the samples. The biochar samples after the sorption experiment were dried for XRD and XPS analysis; the 1 and 5 mM treatments were analyzed to identify the precipitates, while only the 1 mM treatment was analyzed by XPS to characterize the binding mechanisms of Cd^{2+} and As(V). XRD was conducted using a powder X-ray diffractometry instrument (D8, Advance, Bruker, Germany) operated at 40 kV and 20 mA. The data were collected over a 2θ range of $0-50^\circ$ using Cu-K α radiation at a scan rate of 2° min^{-1} (Cao and Harris 2010). The diffraction patterns were analyzed by using the American Mineralogist Crystal Structure Database (Downs and Hall-Wallace 2003) and compared with the Visual MINTEQ calculation results to confirm the mineralogical composition of the precipitates of B400 and B700 with Cd^{2+} and As(V).

XPS was performed to characterize the binding mechanisms of 1 mM Cd^{2+} and As(V) on B400 and B700 at pH 3.5, 7.0 and 10 using an AXIS-Hsi spectrometer (Kratos Analytical, Japan) equipped with a Mg K α X-ray source (Liao et al. 2012). A finely ground powder biochar sample from the sorption

isotherm experiment was fixed onto a metallic sample holder using double-sided Teflon tape. Survey scans were obtained within a binding energy range of 0–1200 eV with a pass energy of 100 eV and step size of 1 eV, and for the elemental regions (As, C, Ca, Cd, Na, O, and Si), a 20 eV pass energy and a 0.1 eV step size were used. The XPS spectra were analyzed and deconvoluted using the Gaussian–Lorentzian sum function with a 30% Gaussian–Lorentzian value to optimize the spectra using Avantage software (Thermo Scientific), and a Shirley background correction was carried out to remove background noise (Briggs and Seah 1990).

5.2.5. Scanning electron microscopy

The morphology and elemental composition of the biochars after sorption isotherm of Cd^{2+} and As(V) at different pH values were analyzed with a field emission-scanning electron microscope (FE-SEM) (AURIGA, Carl Zeiss, Germany) equipped with an energy dispersive X-ray spectroscopy (EDS) detector (Bruker Nano GmbH, Berlin, Germany). For FE-SEM analysis, biochar samples were placed in a forced-air oven (DS-80-2, Dasol, Korea) at 80 °C for at least 48 h and then mounted on an aluminum stub using double-sided conductive copper tape. The microscope was operated at an accelerating voltage of 10 kV, and the working distance was set at 10 nm from the final lens at varying magnifications.

5.3. Results and discussion

5.3.1. Physicochemical characteristics of biochar

BET isotherms using CO_2 and N_2 provide information on the pore structure of biochars due to the distinctive sorption characteristics of CO_2 and N_2 on nano- and micro-pores. The specific surface areas (SSAs) of B400 and B700 were estimated at 5.6 and 236.3 $\text{m}^2 \text{g}^{-1}$ for micro-pores and 191.6 and 57.2

$\text{m}^2 \text{g}^{-1}$ for nano-pores, respectively (Table 5-1). With increasing PT, a dramatic increase in micro-pores was observed, while the nano-pores decreased due to progressive thermal decomposition from nano-pore structures to micro-pore structures in the *Miscanthus* biochar; consequently, the total SSA of B400 and B700 were 197.2 and 293.5 $\text{m}^2 \text{g}^{-1}$, respectively. Previous investigations on *Miscanthus* biochar reported that the SSA of micro-pores ranged from 2.4 to 381.5 $\text{m}^2 \text{g}^{-1}$ (Kim et al. 2013a) and dramatically increased in the PT range between 400 and 600 °C due to the collapse of the nano-pore by progressive thermal decomposition (Kim et al. 2013b). Luo et al. (2015) and Lee et al. (2018) reported an SSA increase caused by the progressive volatilization of cellulose, hemicellulose and lignin with increasing PTs (Qu et al. 2011; Mimmo et al. 2014), since the progressive thermal decomposition of molecular structures causes the formation of channel structures with larger pore sizes. As a result, the total SSA increases (Cantrell et al. 2012; Kloss et al. 2012; Zhao et al. 2013); this results may also be responsible for the increased hydrophobic surface area of B700 compared with that of B400 (Shaaban et al. 2014; Peng et al. 2016).

The surface charge density (SCD) of B400 was 0.0577, 0.0082 and -0.0192 C m^{-2} at pH 3.5, 7.0 and 10, while it was 0.0256, 0.0118 and -0.0007 C m^{-2} for B700, respectively (Fig. 5-1). The SCD of B400 was more positively charged than that of B700, and the change in SCD with increasing pH was more obvious in B400 than in B700. This difference occurred because oxygen containing AFGs, such as carboxylic, lactonic and phenolic groups, were more abundant in B400 than in B700 (Table 5-1); thus, increased pH caused the AFGs on the biochar to be more deprotonated at their corresponding pK_a values. Leon and Radovic (1991) indicated that the pK_a values of carboxylic, lactonic and phenolic groups were from 4 to 5, from 7 to 8, and approximately 10, respectively. From these different physicochemical characteristics of B400 and

Table 5-1. Physicochemical characteristics of *Miscanthus* biochar pyrolyzed at two temperatures of 400 °C (B400) and 700 °C (B700).

Biochar	Specific surface area ^a (m ² g ⁻¹)		Elemental composition ^c (%)					Atomic ratio ^c			Acidic functional groups ^d (mmol g ⁻¹)			Ash ^e	EC ^f	pH ^f	PZNC ^g
	Micro-pores ^b	Nano-pores ^b	C	H	O	N	S	(O+N)/C	H/C	O/C	Carboxylic	Lactonic	Phenolic	%	(dS m ⁻¹)		
B400	5.6	191.6	70.5	3.5	25.4	0.6	0.02	0.28	0.60	0.27	0.150	0.167	0.421	8.80	0.21	9.0	8.84
B700	236.3	57.2	79.2	1.1	19.3	0.4	0.02	0.19	0.17	0.18	0.013	0.125	0.013	11.6	0.53	10.5	10.0

^aSpecific surface area (SSA) was estimated based on the results obtained from BET isotherms using N₂ (N₂-BET) and CO₂ (CO₂-BET).

^bThe SSA of micropores was equal to the N₂-BET results, while that of nanopores was calculated by subtracting the CO₂-BET results from the N₂-BET results.

^cElemental composition was measured using an elemental analyzer, and the atomic ratio was calculated.

^dAcidic functional groups were measured by Boehm titration.

^eAsh content was estimated by the combustion method.

^fEC and pH were measured with an EC meter and a pH meter, respectively.

^gThe point of zero net charge (PZNC) was estimated by the pH drift method.

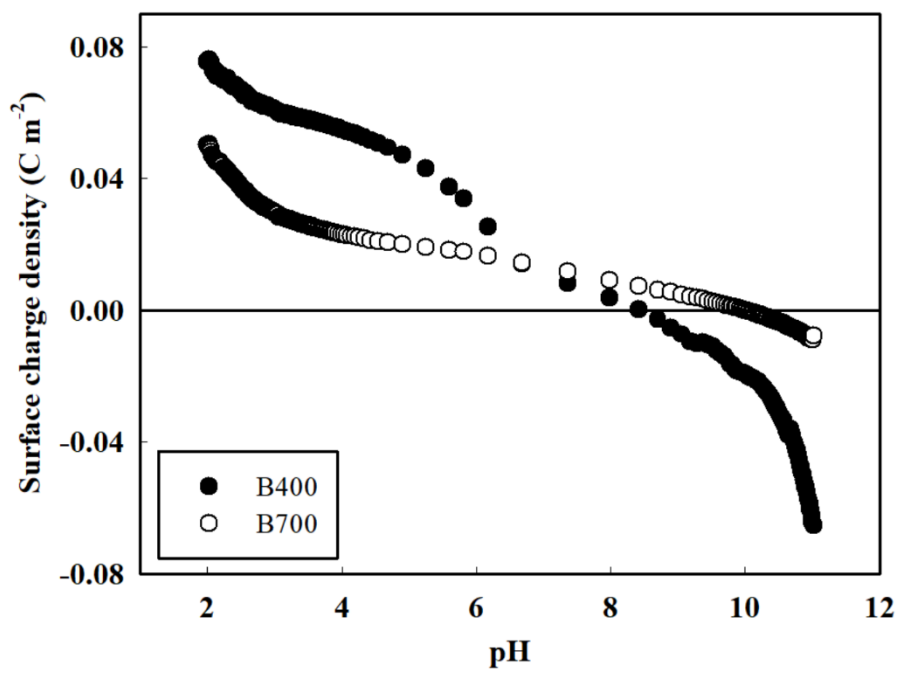
B700, the sorption behavior of Cd^{2+} and As(V) would be expected to show distinctly different sorption mechanisms as a function of pH.

5.3.2. Sorption isotherm

The equilibrium time for Cd^{2+} and As(V) sorption on B400 and B700 was preliminarily evaluated in the sorption kinetics study, and we concluded that 120 h was enough time to reach the equilibrium state for further sorption isotherm analysis (Fig. 5-2). The sorption isotherm study was conducted at pH values of 3.5, 7.0 and 10, and the results were fitted to the Langmuir and Freundlich isotherms to identify the sorption mechanisms of Cd^{2+} and As(V) to biochar (Table 5-2). The better fitting results were obtained using the Freundlich model than the Langmuir model in terms of the r^2 value (Fig. 5-3). Therefore, the pH-dependent sorption of Cd^{2+} and As(V) to biochar in this study was presumed to be multilayer sorption on the heterogeneous surface of biochar with a nonuniform distribution of energy (Ahmed et al. 2017; Huang et al. 2018).

The K_F of Cd^{2+} for B400 was 0.0012, 0.0617 and 32.38 at pH values of 3.5, 7.0 and 10, while it was 0.0041, 0.0442 and 193.7 for B700, respectively (Table 5-2). In addition, the $1/n$ values for both B400 and B700 in the Cd^{2+} treatments showed an interesting pattern in which $1/n$ was close to 1, which indicates a linear relationship between c_{eq} and q_{eq} except at neutral pH. When $1/n$ is close to 1, sorbent-sorbate interactions occur through partitioning (El-Kamash et al. 2005; Venegas et al. 2015), and the increase in K_F with increasing pH could be explained by the increase in sorption strength between Cd^{2+} and biochar (Wang and Lemley 2006; Uchimiya et al. 2010). At low pH, the sorption of Cd^{2+} was mainly attributed to partitioning into the porous structures of the biochar, which was confirmed by the fact that $1/n$ was close to 1 for both biochars. B700 showed a greater increase in K_F than B400 because

Fig. 5-1 Surface charge density (SCD) of *Miscanthus* biochar produced at two pyrolysis temperatures of 400 °C (B400) and 700 °C (B700) as a function of pH determined by potentiometric titration in 0.05 M CaCl₂ solution.



it had a more porous structure than B400 (Table 5-1). However, the $1/n$ value for Cd^{2+} at pH 7.0 (0.114 for B400 and 0.394 for B700) showed a more distinctive pattern than the $1/n$ value at pH 3.5, which indicates that an additional sorption mechanism was involved. This mechanism could be explained by the AFGs, which were more abundant in B400 than in B700 (Table 5-1). The contents of carboxyl and lactonic AFGs in B400 were 0.15 and 0.17 mmol g^{-1} , while those in B700 were 0.013 and 0.125 mmol g^{-1} , respectively. Based on the results, the sorption mechanism of Cd^{2+} at pH 7.0 mainly involved electrostatic attraction and covalent bonding between the negatively charged surface due to the deprotonated AFGs and Cd^{2+} , and the K_F of B400 was higher than that of B700 (Shafqat and Pierzynski 2014). The value of $1/n$ was significantly lower at pH 7 than at pH 3.5, which indicates that the limited sorption sites contributed to the sorption of Cd^{2+} . It was reasonable to presume that both partitioning in the porous structure and covalent bonding caused the distinctive sorption pattern at pH 7.

The sorption of Cd^{2+} at pH 10 showed a dramatic increase in K_F , and most of the Cd^{2+} was sorbed in B400 and B700. The K_F of B400 was lower than that of B700, which might imply that other sorption mechanisms dominated. With increasing pH, the biochar surface became more negatively charged due to the progressive deprotonation of AFGs on the biochar surface, and Cd^{2+} partitioned more into the porous structures of the biochar and sorbed through electrostatic attraction and complexation. In addition, anions in aqueous media would precipitate easily with Cd^{2+} and multi-valent cations, which were the various elements from the biochar surface. Thus, precipitation is presumed to be the dominant sorption mechanism under alkaline conditions. Overall, three possible sorption mechanisms of Cd^{2+} onto biochar were inferred: partitioning into porous structures, complexation with surface AFGs and precipitation. The

detailed processes were interpreted by advanced observation using XRD and XPS and by chemical modeling.

Unlike the Cd^{2+} sorption mechanism, As(V) showed a relatively simple sorption pattern. The K_F of As(V) for B400 was 0.0016, 0.0015 and 0.0114 at pH values of 3.5, 7.0 and 10, while it was 0.0045, 0.0051 and 0.0074 for B700, respectively (Table 5-2). In addition, the $1/n$ value close to 1 indicated that partitioning occurred in the sorption of As(V). However, the sorption strength of As(V) was not as favorable as that of Cd^{2+} , as indicated by the lower K_F of As(V) (0.0016-0.0114) than Cd^{2+} treatments (0.0012-193). The K_F of As(V) in both biochars showed similar results at pH 3.5 and 7.0, while a significant increase was observed at pH 10 compared with the results at low and neutral pH conditions. The SCD results confirmed that positively charged surfaces were abundant at pH 3.5 and 7.0, but the sorption capacity of As(V) was significantly lower than that of Cd^{2+} . The binding affinity of As(V) has been reported to be relatively high among those of oxyanions (Han et al., 2020). From previous studies, the sorption capacity of anions decreases with increasing pH due to the deprotonation of AFGs, but significant adsorption was observed in this study. Thus, the low K_F of As(V) compared with that of Cd^{2+} on the biochar surface, where a positively charged surface was prevalent, was not explainable. It was presumed that the biochar sorption sites for As(V) were not accessible because their molecular size or charge density was not suitable for As(V) retention. Additionally, OH^- , Cl^- and other anions in the aqueous phase compete with As(V) for the positively charged biochar surface. Based on this assumption, As(V) should not form inner-sphere complexes with the biochar surface; the details of this assumption were interpreted on the basis of the XPS results. Therefore, the As(V) sorption behavior could be explained by four possible mechanisms: partitioning into porous structures, precipitation with cations from inorganic biochar components, sorption on precipitates

Fig. 5-2 Kinetic study of the Cd^{2+} and As(V) sorption without controlling the pH conditions for 120 h. Two hundred milligrams of biochar was mixed with 20 mL of 1 mM CdCl_2 or 1 mM Na_2HAsO_4 with 100 mM NaCl as the background electrolyte. The final pH of Cd^{2+} was 6.4 and 6.8 for B400 and B700 and for As(V) it was 7.1 and 9.9 for B400 and B700, respectively.

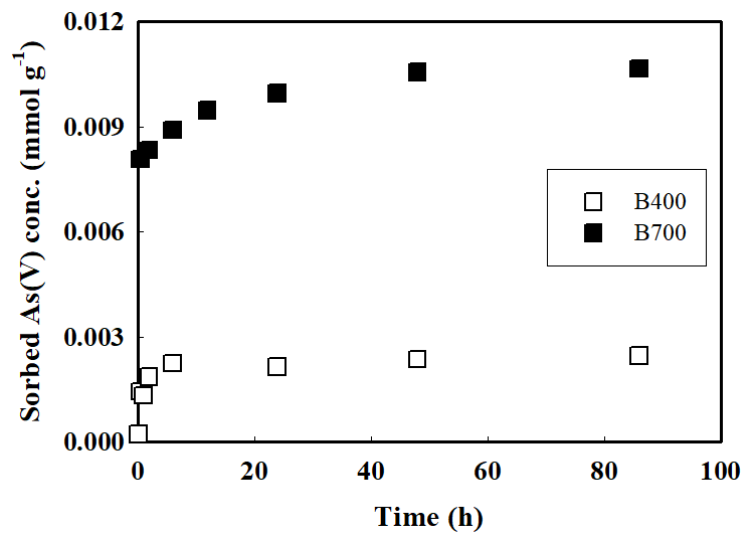
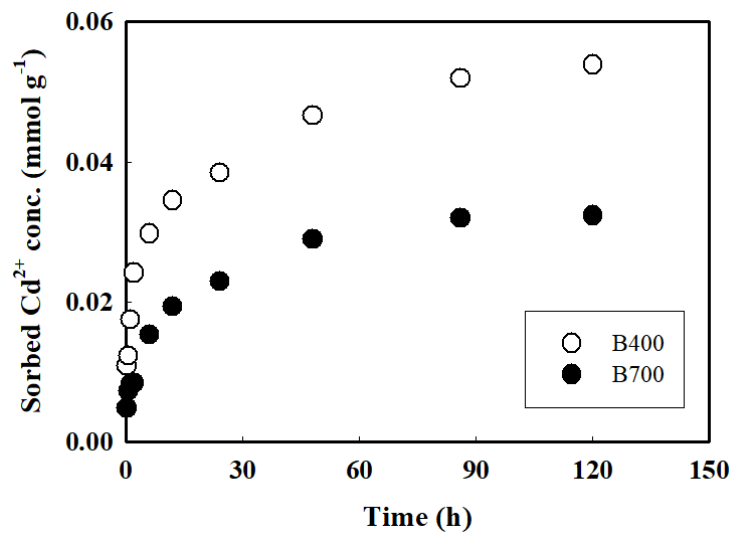


Fig. 5-3 Sorption isotherms of Cd^{2+} and As(V) at six concentrations (1, 2, 3, 4, 5, and 10 mM) and three pH values (3.5, 7.0 and 10) on B400 (a and c) and B700 (b and d). Error bars indicate the standard deviation of triplicate measurements. The dotted line indicates the fitting result of the Freundlich model, while the circles, rectangles and triangles indicate pH values of 3.5, 7.0 and 10, respectively.

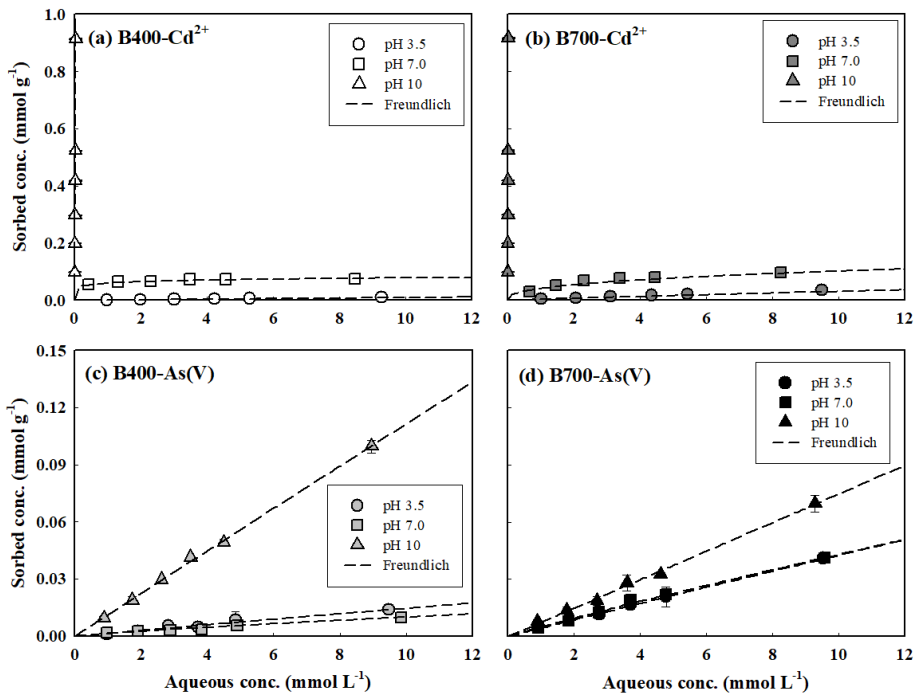


Table 5-2 Fitting results using the Freundlich isotherms for Cd²⁺ or As(V) sorption on *Miscanthus* biochar pyrolyzed at two temperatures of 400 °C (B400) and 700 °C (B700) under three pH conditions (3.5, 7.0 and 10). The mixture was agitated at 160 rpm for 120 h at room temperature (25 °C). The value of K_F is a constant related to sorption capacity (mmol g⁻¹(mmol L⁻¹)⁻ⁿ), and $1/n$ is the sorption intensity. The R^2 value means the correlation of determination of fitting.

Metals	Biochar	Freundlich isotherm			
		pH	K_F (mmol g ⁻¹)/ (mmol L ⁻¹) ^{1/n}	$1/n$	R^2
Cd ²⁺	B400	3.5	0.0012 (0.000)	0.9782 (0.0350)	0.996
		7.0	0.0617 (0.0018)	0.1137 (0.0209)	0.687
		10	32.3758 (2.3803)	1.0075 (0.0191)	0.997
	B700	3.5	0.0041 (00005)	0.9472 (0.0680)	0.947
		7.0	0.0442 (0.0021)	0.3935 (0.0306)	0.926
		10	193.6909 (58.7284)	1.3463 (0.0716)	0.975
As(V)	B400	3.5	0.0016 (0.0004)	0.9633 (0.1318)	0.842
		7.0	0.0015 (0.0003)	0.8293 (0.0892)	0.895
		10	0.0114 (0.0004)	0.9905 (0.0172)	0.997
	B700	3.5	0.0045 (0.0005)	0.9770 (0.0499)	0.975
		7.0	0.0051 (0.0003)	0.9270 (0.0311)	0.987
		10	0.0074 (0.0005)	1.0047 (0.0357)	0.983

through hydrophobic attraction, and sorption as bridging complexes with multi-valent ions. However, it is difficult to identify the sorption mechanism using sorption isotherms; thus, further XPS and XRD analyses were performed.

5.3.3. Possible precipitation modeling using visual MINTEQ

It is extremely difficult to determine possible precipitates using XPS and XRD because there are numerous candidates involved in precipitation. Thus, chemical modeling based on the background ion concentrations measured by ICP-OES was applied to calculate the possible precipitates, which are listed in Table 5-4. A total of 25 elements were quantified, but only 6 elements (Ca, K, Mg, Mn, Na and Si) were employed for the calculation (Table S3); the selected elements showed relatively high concentrations in the aqueous phase (> 0.01 mM) under neutral pH conditions. Regardless of the heavy metal treatment and biochar used, SiO_2 minerals were found at pH 3.5 and 7.0, and CaCO_3 minerals (aragonite, calcite and vaterite), chrysotile ($\text{Mg}_3(\text{Si}_2\text{O}_5)(\text{OH})_4$), dolomite ($\text{CaMg}(\text{CO}_3)_2$) and sepiolite ($\text{Mg}_4\text{Si}_6\text{O}_{15}(\text{OH})_2 \cdot 6\text{H}_2\text{O}$) were found at pH 10. In the Cd^{2+} treatment, otavite (CdCO_3) and $\text{Cd}(\text{OH})_2$ were calculated to be the possible precipitates on B400 and B700 at pH values of 7.0 and 10, while rhodochrosite (MnCO_3) and quartz (SiO_2) precipitated on B400 only at pH 10. For the As(V) treatment, $\text{Mn}_3(\text{AsO}_4)_2 \cdot 8\text{H}_2\text{O}$ was calculated to be the only As(V)-containing precipitate on B400 at pH 10. The possible complexes and precipitates from the visual MINTEQ calculation results were employed in further XRD and XPS analysis to interpret the sorption mechanisms of Cd^{2+} and As(V) as a function of pH.

5.3.4. Characterization of crystallized precipitates using X-ray diffraction

Two biochar samples before and after sorption experiments employing two concentration levels (1 and 5 mM) of Cd^{2+} and As(V) at three pH conditions

Table 5-3 Dissolved ion composition of B400 and B700 by inductively coupled plasma optical emission spectroscopy (ICP-OES) measurements. The bold elements were employed for visual MINTEQ calculation, in which the concentration was above 0.01 mM (concentrations less than 0.01 mM were not included for the calculation).

Element	B400 (mM)	B700 (mM)
K	2.630	3.197
Al	0.001	0.006
Ag	0.000	0.000
B	0.000	0.002
Ca	0.484	0.326
Co	0.000	0.000
Cr	0.000	0.000
Cu	0.000	0.000
Fe	0.001	0.001
Mg	0.219	0.095
Mn	0.011	0.001
Ni	0.001	0.001
Sb	0.000	0.000
Se	0.004	0.003
Ti	0.000	0.000
Tl	0.000	0.004
V	0.000	0.000
Zn	0.001	0.001
Si	0.552	0.206
Na	95.422	94.726

Table 5-4 Possible precipitates calculated using Visual MINTEQ software with dissolved concentrations of six major ions (Ca, K, Mg, Mn, Si and Na) with Cd²⁺ or As(V) ions at pH 3.5, 7.0 and 10. The listed precipitates were categorized because they exceeded saturation (saturation index: $(SI = \log_{10}(I_{AP}/K_{sp}) \gg 0)$). The calculation was conducted at pH intervals of 0.5, but 3 pH points are listed.

pH	B400		B700	
	1 mM Cd ²⁺	1 mM As(V)	1 mM Cd ²⁺	1 mM As(V)
3.5	SiO ₂ (Chalcedony, Cristobalite, Quartz)	SiO ₂ (Chalcedony, Cristobalite, Quartz)	SiO ₂ (Quartz)	SiO ₂ (Quartz)
7.0	SiO ₂ (Chalcedony, Cristobalite, Quartz) CdCO ₃ (Otavite)	SiO ₂ (Chalcedony, Cristobalite, Quartz)	SiO ₂ (Quartz) CdCO ₃ (Otavite)	SiO ₂ (Quartz)
10	CaCO ₃ (Aragonite, Calcite, Vaterite) Cd(OH) ₂ Mg ₃ (Si ₂ O ₅)(OH) ₄ (Chrysotile) CaMg(CO ₃) ₂ (Dolomite) MnCO ₃ (Rhodochrosite) CdCO ₃ (Otavite) SiO ₂ (Quartz) Mg ₄ Si ₆ O ₁₅ (O H) ₂ ·6H ₂ O (Sepiolite)	CaCO ₃ (Aragonite, Calcite, Vaterite) Mg ₃ (Si ₂ O ₅)(OH) ₄ (Chrysotile) CaMg(CO ₃) ₂ (Dolomite) Mn ₃ (AsO ₄) ₂ · 8H ₂ O (s) MnCO ₃ (Rhodochrosite) SiO ₂ (Quartz) Mg ₄ Si ₆ O ₁₅ (O H) ₂ ·6H ₂ O (Sepiolite)	CaCO ₃ (Aragonite, Calcite) Cd(OH) ₂ Mg ₃ (Si ₂ O ₅)(OH) ₄ (Chrysotile) CaMg(CO ₃) ₂ (Dolomite) CdCO ₃ (Otavite) Mg ₄ Si ₆ O ₁₅ (O H) ₂ · 6H ₂ O (Sepiolite)	CaCO ₃ (Aragonite, Calcite, Vaterite) Mg ₃ (Si ₂ O ₅)(OH) ₄ (Chrysotile) CaMg(CO ₃) ₂ (Dolomite) Mg ₄ Si ₆ O ₁₅ (O H) ₂ · 6H ₂ O (Sepiolite)

(3.5, 7.0 and 10) were measured by XRD, and the diffraction patterns are illustrated in Fig. 5-4. Four crystallized precipitates were identified for the 1 mM treatments, while three additional precipitates were observed for the 5 mM treatments. In both B400 and B700, SiO₂ (quartz) peaks at 26.65 and 20.87° (listed by intensity) appeared, while NaCl (halite) was identified in all treatments at 31.73, 45.49 and 27.39°. Except for quartz and halite, significant peaks were not observed in the Cd²⁺ treatments at pH 3.5 in either B400 or B700, which corresponded to the previous sorption isotherm results and subsequent XPS interpretation (Fig. 5-9).

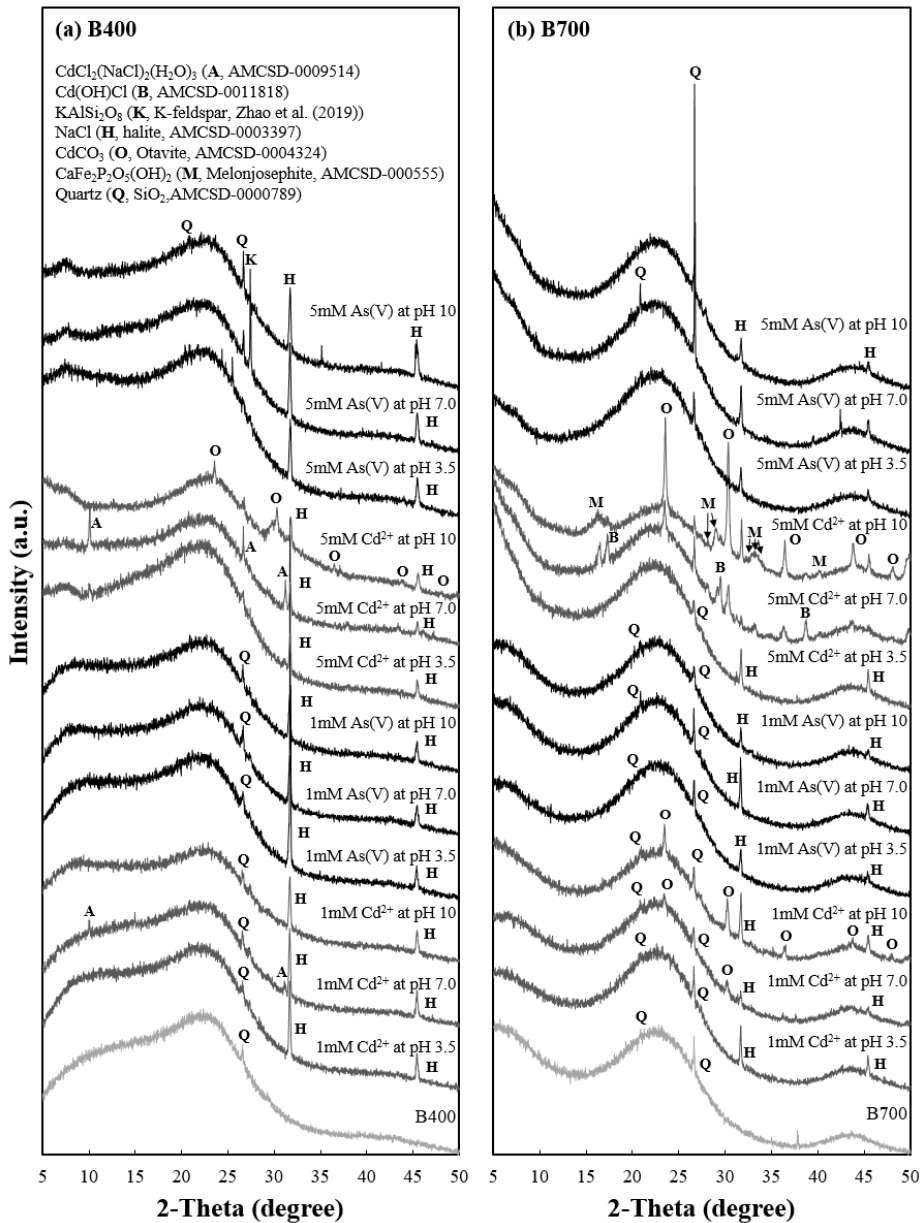
No precipitates other than quartz and halite were identified at pH 3.5 for either Cd²⁺ or As(V), while CdCl₂(NaCl)₂(H₂O)₃, Cd(OH)Cl, CaFe₂P₂O₅(OH)₂ (melonjosephite) and CdCO₃ (otavite) were identified in the Cd²⁺ treatments at pH 7 and 10. Small peaks corresponding to CdCl₂(NaCl)₂(H₂O)₃ (peaks at 31.14, 10.01 and 46.01°) were identified in B400 at pH 7.0 only, and the peak intensity in the 5 mM treatment was greater than that in the 1 mM treatment. Otavite was identified at 30.35, 23.56, 36.52, 43.92 and 49.60° in B400 and B700, and its intensity increased with increasing pH from 7.0 to 10. Additionally, with increasing Cd²⁺ concentration from 1 mM to 5 mM, additional precipitation of Cd(OH)Cl was observed at 17.27, 29.49, 38.72 and 49.83° at pH 7.0 in B700 only, and CaFe₂P₂O₅(OH)₂ (melonjosephite) was also observed at 29.26, 30.71, 34.17, 16.36, 28.00, 33.07, 37.80 and 33.82° at pH 10 in B700.

Significant peaks of As-containing precipitates, excluding quartz and halite, were not observed in the As(V) treatments for B400 and B700 at the investigated pH values. However, with increasing As(V) concentration from 1 mM to 5 mM, additional precipitation of KAlSi₃O₈ (K-feldspar) was observed in B400 at pH 7.0, and a dramatic increase in SiO₂ was shown in B700 at pH 7.0. These two peaks were unexpected; however, a similar diffraction pattern

was previously reported (Zhao et al. 2019). The quartz peaks were easily confirmed by comparing the intensity change; the peaks of K-feldspar at 27.41 and 27.49° overlapped, resembling a single peak.

It is difficult to quantify and compare the abundance of precipitates on the basis of XRD results, but general patterns can be explained. Halite was more abundant in B400 than B700, and it was also more abundant in the Cd²⁺ treatments at pH 3.5 and 10 than at pH 7, while the opposite pattern was observed for As(V). Increasing the Cd²⁺ concentration from 1 to 5 mM decreased the halite abundance. The SEM-EDS study showed different distributions of Na⁺ and Cl⁻ on the two biochars. Na⁺ and Cl⁻ were evenly distributed on the surface of B700, while they were observed as few-micrometer precipitates on B400 (Fig. 5-8). In addition, the atomic ratio of Cl/C increased in B400 with increasing pH, while the opposite pattern was observed for B700 (0.006 and 0.018 for B400 at pH 3.5 and 10; 0.002 and 0.001 for B700 at pH 3.5 and 10, respectively). This result could be explained by two factors: precipitation and surface charge density. As reported previously, B400 had more aggregated precipitates, while the precipitates of B700 were evenly distributed, which was the result of the diminished negatively charged AFGs. As a result, Cl⁻ was repelled less from the surface, and different precipitation patterns appeared on the two biochars. Although no concrete evidence has been suggested for this phenomenon, it aids in understanding the sorption behavior of As(V). The intensity of Si-containing minerals on both biochars was higher at neutral pH than under acidic and alkaline conditions, which implies the surface polymerization of silicate with dissolved ions at neutral pH (Qian and Chen 2013; Qian et al. 2013). Otavite had a greater intensity at alkaline pH and was more abundant in B700 than in B400 (Zhang et al. 2015). XRD patterns only reveal information about the crystallized structure, and XRD patterns

Fig. 5-4 X-ray diffraction patterns of B400 (a) and B700 (b) before the sorption experiment (light gray) and after sorption of Cd^{2+} (dark gray) and As(V) (black) at two different concentrations (1 and 5 mM) and three different pH values (3.5, 7.0 and 10). Seven crystal structures were identified and are listed with their codes from the American Mineralogist Crystal Structure Database (AMCSD). Capital letters indicate the positions of the major peaks of each crystal structure listed above.



should be explained with XPS results, which have information about both the amorphous and crystallized structures.

5.3.5 Surface complexation and precipitation determined by X-ray photoemission spectroscopy

XPS analysis was employed to determine both the amorphous and crystallized structures of biochar with Cd^{2+} or As(V) . Only the 1 mM Cd^{2+} and As(V) treatments were measured to focus on the peaks from surface complexation by excluding precipitates. However, no peaks were detected in the 1 mM As(V) treatments, so $\text{As}3p$ was additionally measured in the 5 mM As(V) treatments. The biochar structures of B400 and B700 were interpreted from $\text{C}1s$, $\text{O}1s$ and $\text{Si}2p$ spectra, and the background ions ($\text{Na}1s$ and $\text{Ca}2p$) and target metals (Cd and As) were analyzed.

5.3.5.1 C, O and Si in the biochar structure

Three $\text{C}1s$ peaks at 284.0, 285.5 and 288.2 eV were identified in B400, while 5 peaks at 284.5, 285.8, 286.5, 288.3 and 300.3 eV were observed in B700 (Fig. 3). The peaks at ~ 284.0 , ~ 285.5 , ~ 286.5 , ~ 288.2 and ~ 289.3 eV were assigned to aliphatic C-C , aromatic C=C , graphitic C=C , C=O and C-O , and carbonate, respectively (Fig. 5-5) (Severini et al. 2002; Tsaneva et al. 2014). These structures in B400 and B700 showed no significant differences regardless of the Cd^{2+} or As(V) treatment. From these results, structural transformation causing thermal decomposition with increasing PT was clearly demonstrated. Aliphatic C-C was abundant in B400, while aromatic and graphitic C=C were dominant in B700. Unlike previous studies of biochar, we separated the C=C peak into aromatic C=C and graphitic C=C because distinct results were obtained during the fitting process. The results clearly demonstrate the structural transformation of biochar by thermal decomposition.

On the surface of the *Miscanthus* biochar, Si was the most abundant inorganic element. The Si content was previously confirmed by XRF (1.61% for B400 and 2.35% for B700) (Lee et al. 2018), and it is essential to understand the Si2p spectra first before interpreting the O1s spectra due to the formation of SiO₂. Three Si2p peaks in both B400 and B700 were identified at ~100.2, ~101.7 and ~102.8 eV, and the peaks were deconvoluted into amorphous Si-(OH)_x, amorphous Si-O_x and crystallized Si-O₂, respectively. Due to the precipitation of Si on the surface of the biochars measured by SEM-EDS (Fig. 5-8), the intensity ratio of Si (intensity from precipitates/intensity from the surface) was slightly different, which might indicate the presence of evenly distributed amorphous Si-containing minerals on the surface and crystallized SiO₂ as a precipitate (Koshizaki et al. 1998). The increase in PT from 400 to 700 °C caused the crystallization of SiO₂ as macro particles from nanosized and evenly distributed surface precipitates (Qian et al. 2017). Consequently, the intensity of crystallized SiO₂ significantly differed between B400 and B700. However, the XRD results for quartz differed less than the XPS results between the two materials, which could be explained by the different X-ray penetration depths of the measurements since XPS is surface specific (less than 100 nm), while the depth measured by XRD is a few micrometers (Mourdikoudis et al. 2018).

Four O1s peaks were identified in both B400 and B700, but the peak positions were significantly shifted. The peaks of B400 were at 531.2, 532.4, 533.5 and 534.7 eV and were assigned to amorphous O_x-Si, crystallized O₂-Si and aliphatic O-C, aromatic O-C, and O=C, respectively (Fig. 5-5). The peaks of B700 were at 531.9, 532.8, 534.1 and 535.4 eV, corresponding to amorphous O_x-Si, crystallized O₂-Si and carbonate, aromatic O-C and O=C, and graphitic O-C, respectively. From the Si2p results, the O1s peaks at 531.2 and 531.9 eV

Fig. 5-5 High-resolution C1s (a and d), O1s (b and e) and Si2p (c and f) XPS spectra of the two biochars (B400 and B700) before the sorption experiment. Spectral components were obtained and subjected to peak deconvolution using Igor Pro 8 software and X-ray Photoelectron Spectroscopy Tools with the National Institute for Standards and Technology XPS database. White circles and black lines indicate experimental data and the fitting results, respectively. The small spectra in the fitting results indicate the components identified by deconvolution. All spectra were fitted to asymmetric Gaussian-Lorentzian functions (70% Gaussian and 30% Lorentzian).

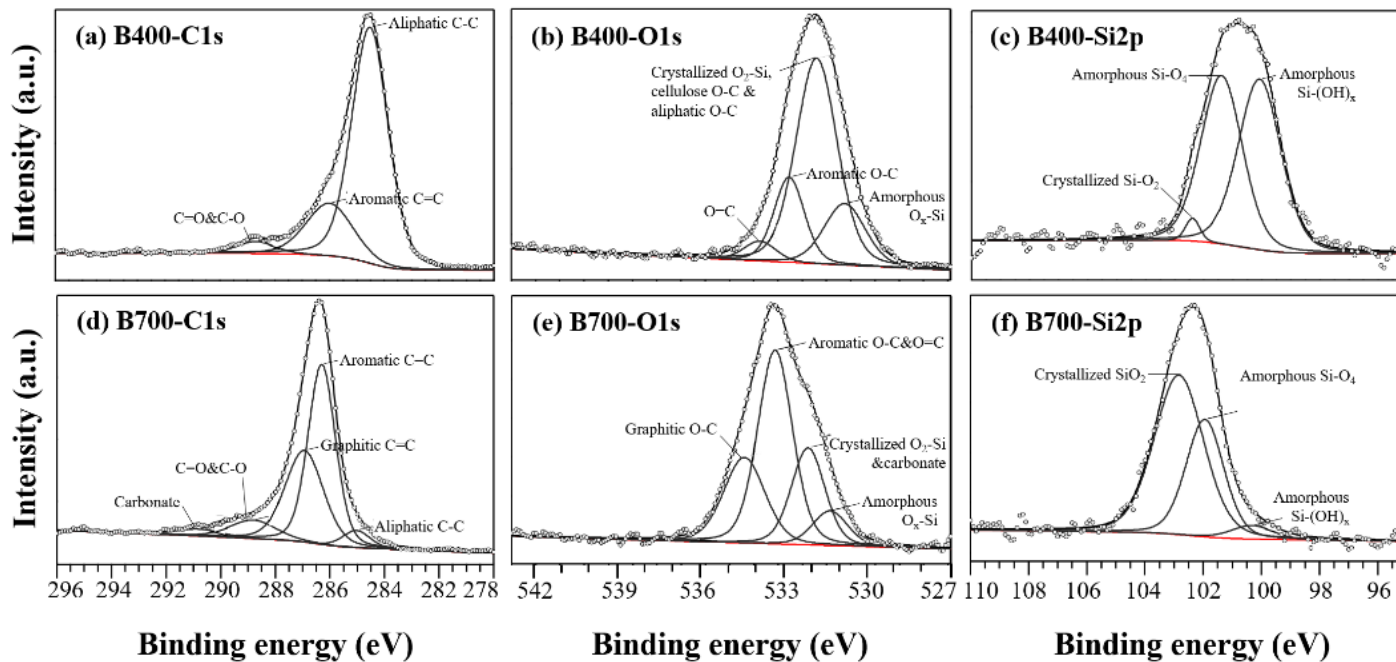


Fig. 5-6 High-resolution Na1s XPS spectra of two biochars (B400 and B700) after sorption experiments of Cd²⁺ and As(V) at pH 7.0 and 10. The spectra at pH 3.5 were not illustrated because no significant signals were observed. Spectral components were obtained and addressed by peak deconvolution using Igor Pro 8 software and X-ray Photoelectron Spectroscopy Tools with National Institute for Standards and Technology XPS database. White circles and black lines refer to experimental data and the fitting result, respectively. The small spectra in the fitting result indicate the components by deconvolution. All spectra were fitted to asymmetric Gaussian-Lorentzian functions (70% Gaussian and 30% Lorentzian).

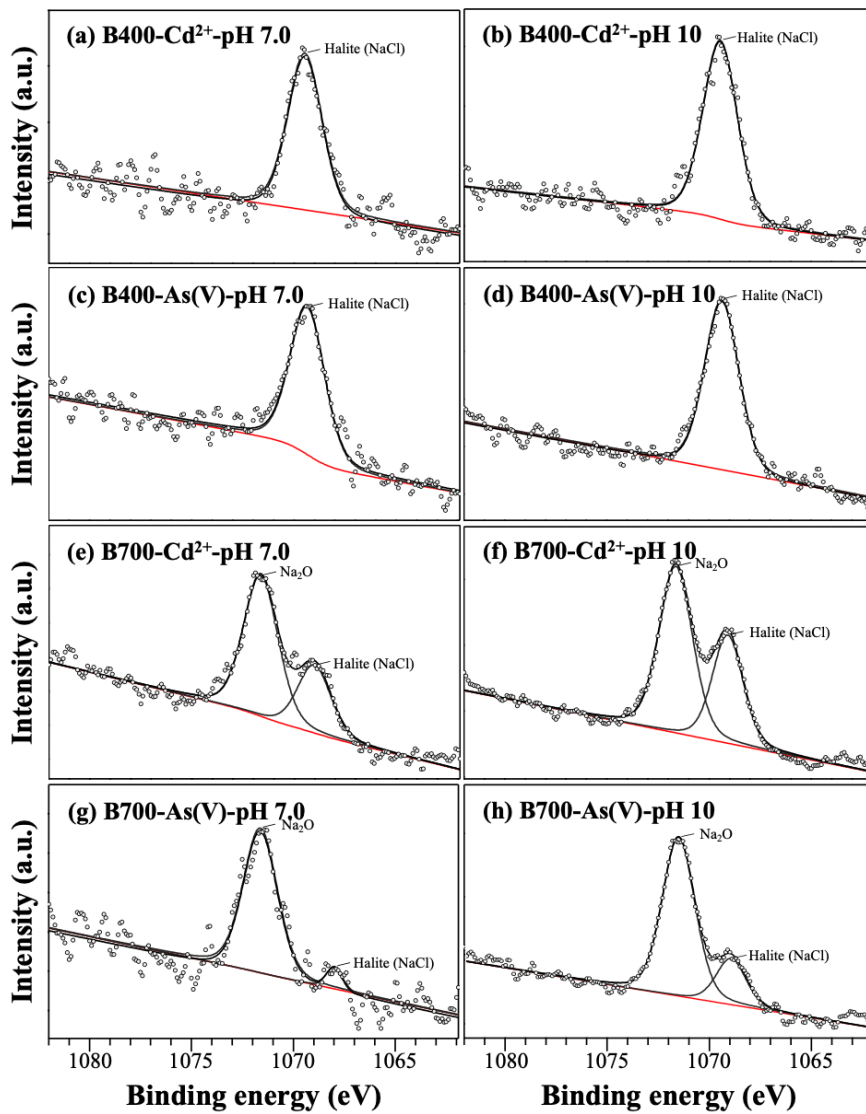
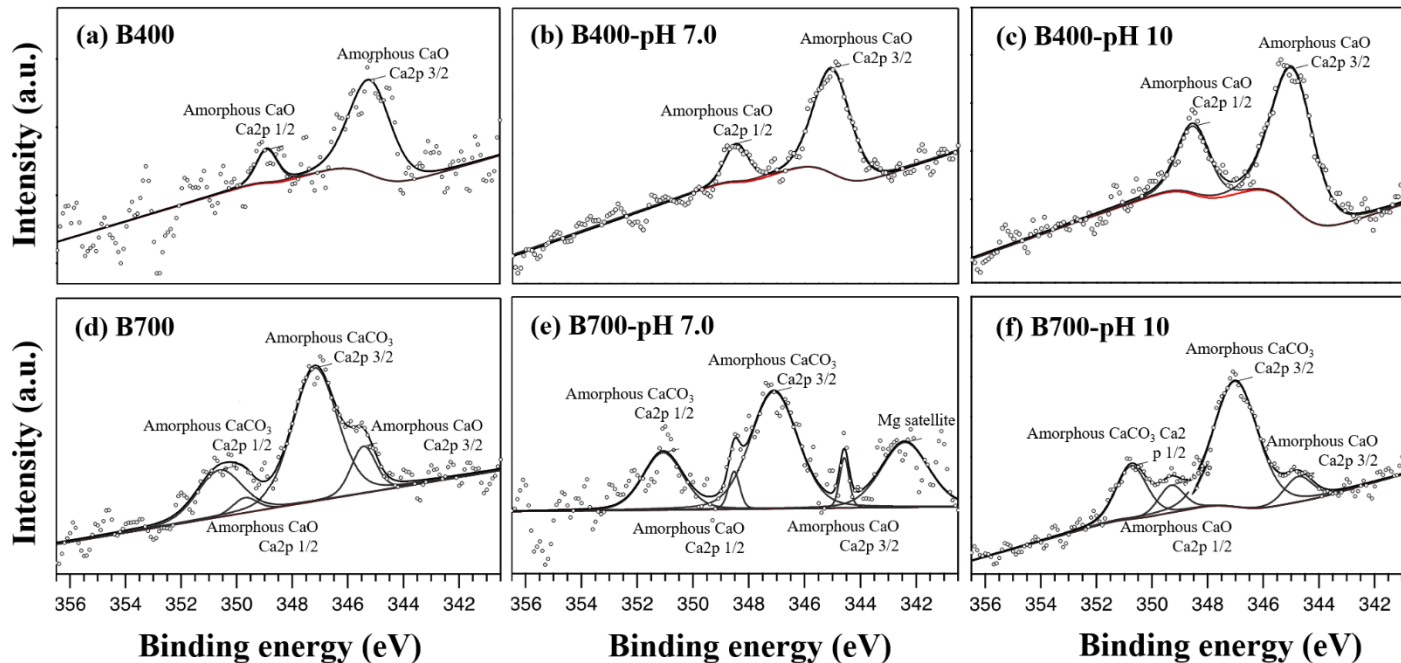


Fig. 5-7 High-resolution Ca2p XPS spectra of two biochar (B400 and B700) before the As(V) sorption experiment (a and d) and after the sorption experiment at pH 7.0 and 10. The spectra in the Cd²⁺ sorption experiment were not illustrated because no significant signals were observed. Spectral components were obtained and addressed by peak deconvolution using Igor Pro 8 software and X-ray Photoelectron Spectroscopy Tools with National Institute for Standards and Technology XPS database. White circles and black lines refer to experimental data and the fitting result, respectively. The small spectra in the fitting result indicate the components by deconvolution. All spectra were fitted to asymmetric Gaussian-Lorentzian functions (70% Gaussian and 30% Lorentzian).



were attributed to amorphous Si-(OH)_x and Si-O₄, and the peak shift in B700 was caused by the decrease in the amorphous Si-(OH)_x fraction while amorphous Si-O₄ remained. The peaks at 532.4 eV for B400 and 532.8 eV for B700 showed close positioning, but the composition was completely different because of the disappearance of aliphatic C-O and the high abundance of crystallized SiO₂ and carbonate. B400 showed a negligible abundance of crystallized SiO₂, while the peak of aliphatic C-O was significant. The peaks at 533.5 and 534.7 eV of B400 and the peaks at 534.1 and 535.4 eV of B700 were interpreted as aromatic C-O, C=O and graphitic C-O. The increase in PT dramatically decreased the amount of aliphatic C-C and increased the amount of aromatic and graphitic C=C, accompanied by increased aromatic and graphitic C-O. However, the oxygen concentration decreased from 25.3 to 19.2% according to elemental composition analysis (Table 5-1), but the oxygen containing C1s peaks increased, which could be due to the formation of aromatic and graphitic structures inside the biochar structure, where the remaining oxygen was mainly located on the surface.

5.3.5.2 Sorption of background Na⁺ and Ca²⁺ ions

Two Na1s peaks were observed, but no peaks were observed at pH 3.5 for either biochar (Fig. 5-6). A Na1s peak was observed at 1071.5 eV for B400, while the peak was located at 1071.5 and 1073.6 eV for B700 in the Cd²⁺ and As(V) treatments, and the peak intensity increased with increasing pH in both B400 and B700. At low pH, the sorption amount of Na⁺ ions to biochar was lower due to electrostatic repulsion with the positively charged surface of the biochar (Fig. 5-1). Thus, most Na⁺ ions existed in the solution phase and not on the surface or in the pore space of the biochar; as a result, no peak was observed at pH 3.5 regardless of Cd²⁺ or As(V) treatment. In contrast, a Na1s peak was observed at pH 7.0 and 10 in all treatments. A halite peak at 1071.5 eV was

observed due to the precipitation of Na^+ ions in the pore space of the biochar; the peak intensities for B400 were larger than those for B700, and they increased from pH 7.0 to pH 10, which could be caused by the deprotonation of AFGs and the pore space distribution. This result was not correlated with the peak intensities of halite in the XRD results, which could be explained by the difference in penetration depth for the two X-ray instruments (XRD and XPS) (Mourdikoudis et al. 2018) and the distribution of Na^+ on the biochar surface observed by SEM-EDS (Fig. 5-8). Unlike halite, the Na_2O peak at 1073.6 eV, based on a study from Savintsev et al. (2016) was only observed at pH 7.0 and 10 in B700 and at different ratios, which could not be explained by our knowledge. The Na_2O peak from Savintsev et al. (2016) was acquired under laser irradiation, but this experiment did not employ such conditions.

In the case of Ca2p, four peaks were observed, but with a different pattern. No peaks were identified in the Cd^{2+} treatments for either B400 or B700 under all pH conditions. The As(V) treatments at pH 3.5 also showed no peaks, while the biochars before the sorption experiment (B400 and B700) and As(V) treatment at pH 7.0 and 10 showed significant peaks (Fig. 5-7). Peaks at 345.0 and 348.2 eV were identified in the As(V) treatments for B400, while two additional peaks (347.2 and 350.4 eV) were observed in the As(V) treatments for B700. Ca2p showed a significant peak shift as the pH and PT increased, which indicates that Ca^{2+} sorption by the biochar involved a more complex sorption mechanism than did Na^+ sorption. The peaks at 345.0 and 348.2 eV were identified as 2p_{3/2} and 2p_{1/2} of CaO, while the peaks at 347.2 and 350.4 eV were previously reported as 2p_{3/2} and 2p_{1/2} of CaCO_3 according to the NIST database (Sosulnikov et al.). Both CaO and CaCO_3 were characterized as amorphous structures because they were not identified in the XRD analysis. The intensity of the peaks increased with increasing pH, implying that more CaO and CaCO_3 precipitated on the surface; this precipitation did not occur

under acidic conditions. However, the SEM-EDS observations confirmed the presence of Ca^{2+} on the biochar surface of both B400 and B700 under all pH conditions, while precipitation of Ca^{2+} was not confirmed by XPS under acidic pH conditions (Fig. 5-8). These results could be explained by the distribution of Ca^{2+} on the biochar surface observed by SEM-EDS. Na^+ precipitated as macrosized particles in B400, while it was evenly distributed in B700 at all pH conditions; however, Ca^{2+} was evenly distributed for both B400 and B700, and macrosized precipitates were identified with increasing pH. This process indirectly provided precipitation as CaO and CaCO_3 . Additionally, the 5 mM As(V) treatments showed similar results for Ca^{2+} as the 1 mM treatments, but the intensity was higher than that of the 1 mM treatments (data excluded). For these reasons, the sorption capacity of As(V) was significantly lower than that of Cd^{2+} under acidic conditions (Fig. 5-3), confirming that Ca^{2+} was not adsorbed on the biochar surface and existed as ions in the solution at low pH. Additionally, during the drying process for analysis, Ca^{2+} remained on the surface without precipitation; thus, an even distribution was possibly achieved. If Ca^{2+} were adsorbed on the biochar surface, As(V) would be more abundant on the surface through Ca-bridging complexes, but this process did not occur in this study.

5.3.5.3 Sorption mechanism of Cd^{2+} and As(V)

The XPS spectra of Cd3d and As3d are illustrated in Fig. 5-9 and Fig. 5-10 for B400 and B700 at pH 3.5, 7.0 and 10, but the concentrations differed (1 mM for the Cd^{2+} treatments and 5 mM for the As(V) treatments). This difference occurred because no significant peaks were observed in the As3d region (37-50 eV) for the 1 mM As(V) treatment, which was presumed to be due to the lower sorption capacity for As(V) than Cd^{2+} (approximately 10 times lower); thus, the 5 mM As(V) treatment was also measured using XPS. In the

case of Cd3d, 4 peaks were identified at pH 7 and 10, while no peaks were observed at pH 3.5. Two peaks at ~403.5 and ~410.5 eV were identified in B400, and two additional peaks at ~405.5 and ~412.0 eV were observed in B700. According to the NIST database, the peaks at 405.5 and 412.0 eV were from otavite, while the peaks at 403.5 and 410.5 eV were from the mononuclear bidentate sorption of CdO. Based on the XPS and XRD results, the peaks at ~405.5 and ~412.0 eV were from crystallized otavite, while the peaks at ~403.5 and ~410.5 eV were classified as amorphous CdO because otavite was detected by XRD, while CdO did not appear. Furthermore, the SEM-EDS results showed no aggregates of amorphous CdO, so this structure was evenly distributed; thus, Cd²⁺ formed complexes with AFGs. Therefore, it was reasonable to conclude that the first sorption mechanism of Cd²⁺ observed at 403.5 and 410.5 eV was mononuclear bidentate sorption as CdO in both B400 and B700 at pH 7.0 and 10. The second sorption mechanism, corresponding to the peaks at 405.5 and 412.0 eV, was attributed to precipitation as otavite, which was only detected in B700 at pH 7.0 and 10.

Unfortunately, no significant peak in the As3d region (37-50 eV) was observed for the two biochars after 1 mM As(V) sorption, but significant peaks were observed in the 5 mM As(V) treatments. Five peaks related to As(V) were identified, which were located at ~41.0, ~43.0, ~43.7, ~44.4 and 45.1 eV. The peaks at ~41.0, ~43.0 and ~43.7 eV were observed in B400 at pH 7 and 10 and were assigned to metallic zero valent As (As(0)), As(III) 3d_{5/2} and As(III) 3d_{3/2}, respectively, based on a previous study (Penke et al. 2017). Four peaks were measured in B700: two peaks at 43.0 and 43.7 eV were from As(III), and two additional peaks at ~44.4 and ~45.1 eV were characterized as As(V) 3d_{5/2} and As(V) 3d_{3/2}. Minor peaks were identified in both B400 and B700, and they were presumed to be Mn3p and Mg2p. The peak area of metallic As(O) in B400 increased, while that of As(III) decreased with increasing pH from 7.0 to 10.

Fig. 5-8 Field emission scanning electron microscope equipped with an energy dispersive X-ray spectroscopy (FE-SEM/EDS) image of biochar samples under two different pyrolysis temperatures (B400 and B700) at two pH values (3.5 and 10). The colored images represent the elemental distribution of C (yellow), O (orange), Si (blue), Na (light violet), Cl (violet), Ca (red), Al (green) and K (light blue) at the same scale using SEM-EDS measurements. The FE-SEM/EDS was operated at an accelerating voltage of 10 kV using SE2 mode. This FE-SEM/EDS graph was previously reported, but it was included here as supporting information for the convenience of readers.

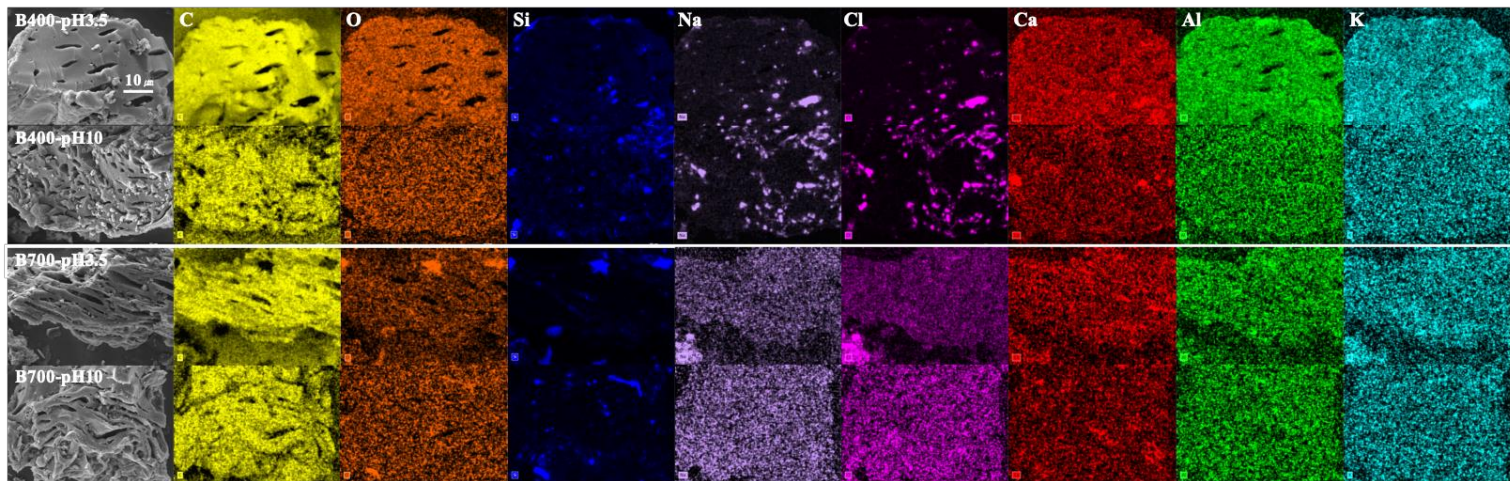


Fig. 5-9 High-resolution Cd3d XPS spectra of the two biochars (B400 and B700) at three different pH values (3.5, 7.0 and 10). Spectral components were obtained and identified by peak deconvolution using Igor Pro 8 software and X-ray Photoelectron Spectroscopy Tools with the National Institute for Standards and Technology XPS database. White circles and black lines indicate experimental data and the fitting results, respectively. The small spectra in the fitting results indicate the components identified by deconvolution. All spectra were fitted to asymmetric Gaussian-Lorentzian functions (70% Gaussian and 30% Lorentzian).

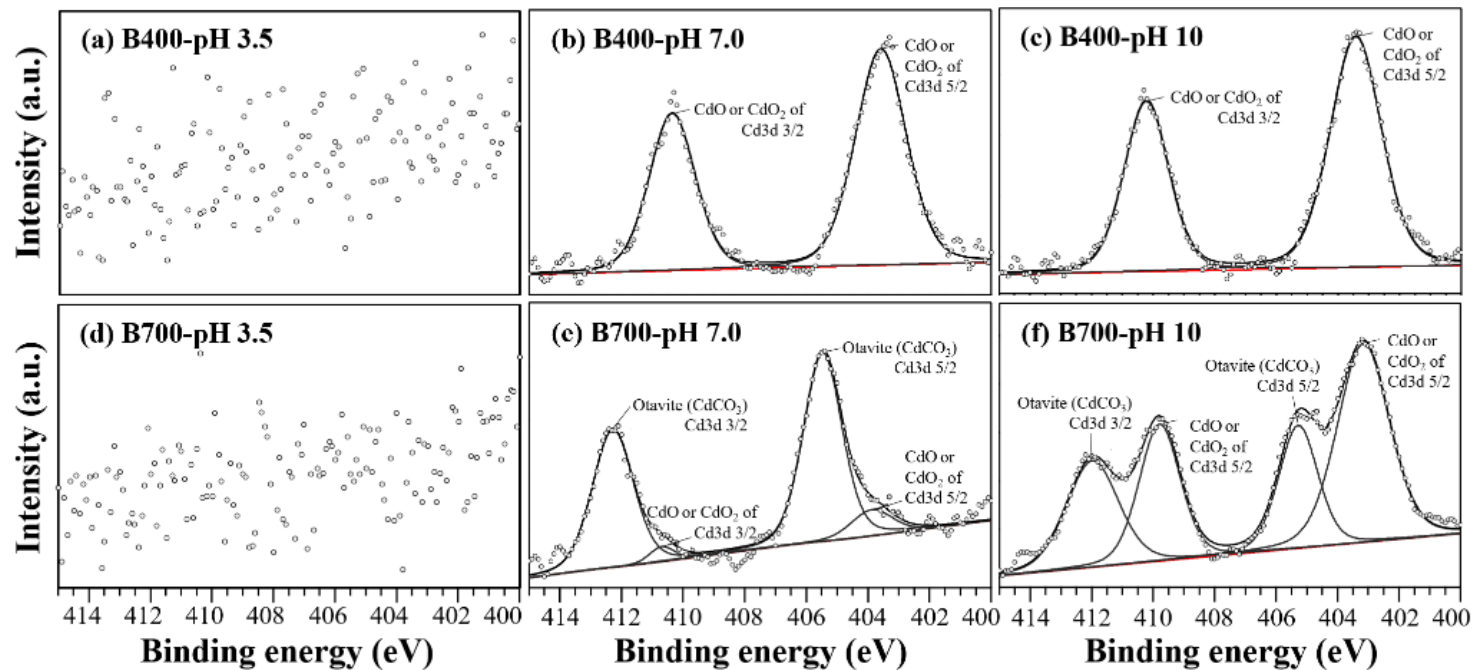
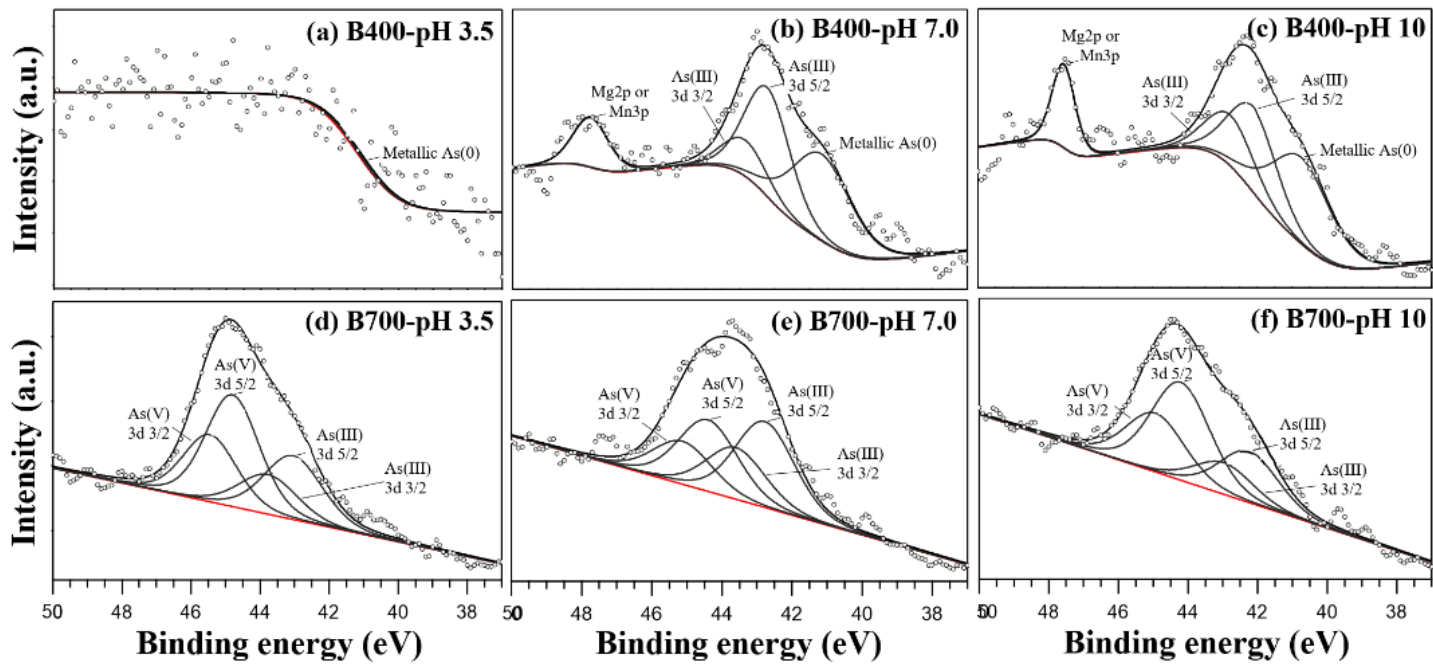


Fig. 5-10 High-resolution As3d XPS spectra of the two biochars (B400 and B700) at three different pH values (3.5, 7.0 and 10). Spectral components were obtained and identified by peak deconvolution using Igor Pro 8 software and X-ray Photoelectron Spectroscopy Tools with the National Institute for Standards and Technology XPS database. White circles and black lines indicate experimental data and the fitting results, respectively. The small spectra in the fitting results indicate the components identified by deconvolution. All spectra were fitted to asymmetric Gaussian-Lorentzian functions (70% Gaussian and 30% Lorentzian).



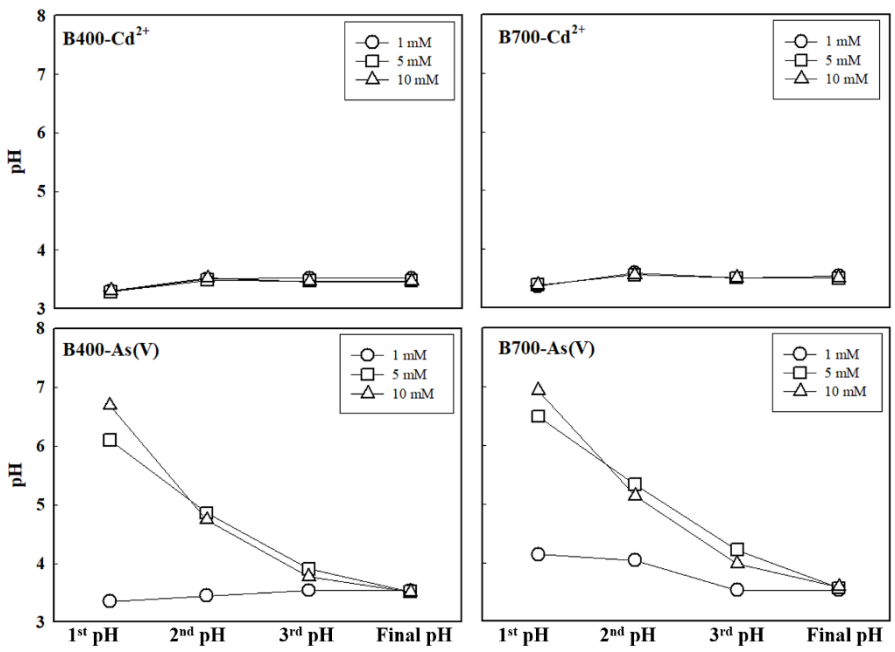
B700 showed different ratios between As(III) and As(V), and the ratios were similar at pH 3.5 and 10, while they were distinct at pH 7. For both biochars, amorphous As(V) was not observed under any pH conditions since it is difficult to characterize sorption mechanisms with XPS alone because the reduction and oxidation (redox) of As and spin-orbit splitting cause complexly overlapping XPS spectra. In addition, the formation of inner-sphere complexes would generally promote this complexity; however, there was no inner-sphere complexation, based on the low sorption capacity from the sorption isotherm and the similar peak position to those of NaH_2AsO_4 and NaH_2AsO_3 . For that reason, we excluded inner-sphere complexation as a sorption mechanism of As(V) and presumed all As ions sorbed through ionic bonding with other ions as precipitates on the biochar surface.

Based on this observation in the As(V) treatment, it was reasonable to conclude that the biochar caused the reduction of As(V) to As(III) and metallic As(0) at different rates upon changes in pH and PT. Numerous previous studies have confirmed the reduction of As caused by biochar, which is mainly attributed to AFGs (Vithanage et al. 2017). Deprotonated AFGs on biochar yield protons and electrons, and As(V) is reduced to arsenite (As(III)). Direct and additional evidence for As(V) reduction was not planned, but indirect proof was found during pH adjustment (Fig. S6). During pH adjustment for the batch experiment, distinct patterns were found in the Cd^{2+} and As(V) treatments, in which the pH of the As(V) treatments increased with increasing As(V) concentration, while the Cd^{2+} treatments showed no significant difference; this pH increase is indirect evidence of As(V) reduction. The peak area ratio of As(III) 3d_{5/2} to metallic As(O) in B400 was 0.97 and 0.80 at pH 7 and 10, respectively, which indicated that reduction to metallic As(0) was more favorable at pH 10. The peak area ratio of As(V) 3d_{5/2} to As(III) 3d_{5/2} in B700 was 1.60, 0.83 and 1.90 at pH 3.5, 7.0 and 10, respectively, indicating that the

reduction of As(V) to As(III) was more abundant at circumneutral pH. In previous studies, the reduction of As(V) to As(III) was favorable under acidic conditions, but the ratio of As(V)/As(III) decreased at pH 3.5 in this study. The reduction of As(V) was governed by the two factors mentioned above, proton and electron concentration, and both factors are essential for reduction. However, protons are abundant at low pH (3.5), while electrons are a limiting factor, and the opposite pattern was presumed to occur at pH 10; thus, the reduction of As(V) was favorable at circumneutral pH. This result did not agree with the observed increase in the reduction of As(V) to As(0) with increasing pH in B400. These results imply that the reduction of As(III) to As(0) requires fewer protons than the reduction of As(V)/As(III), but there is no concrete evidence to prove such reduction in this study.

The sorption isotherm of As(V) showed a linear correlation with concentration, and the XRD results showed no significant precipitation of As-containing crystal structures. In addition, the XPS results showed that ionic bonding was a major sorption mechanism without inner-sphere complexation or precipitation and the reduction of As(III) and As(0) occurred. Based on these results, it is reasonable to exclude the sorption mechanism of precipitation because no precipitation was observed by either XRD or XPS. Additionally, the possibility of inner-sphere complexation should also be eliminated because no peak difference was observed between salts of As(V) and As(III). However, partitioning into porous structures and ionic bonding to positively charged surfaces remain possible sorption mechanisms. The value of $1/n$ close to 1 indicated that partitioning governs the sorption mechanism, but it could not explain the sorption increases at pH 10, and similar sorption occurred at pH 3.5 and 7.0. This sorption behavior could be explained by the electrical attraction of As(V) and As(III) to AFGs on the biochar surface incorporating multi valent cations, such as Ca^{2+} , Mn^{2+} , Mg^{2+} , Al^{3+} and Fe^{3+} . For that reason, a more

Fig. 5-11 The results of pH adjustment for the sorption isotherm study at pH 3.5. The data indicate the pH before pH adjustments, and the pH was adjusted to pH 3.5. A distinct pattern between Cd^{2+} and As(V) was observed, which was caused by the reduction of As(V) to As(III) and As(0) .



dramatic increase in As(V) sorption was observed in B400 than in B700, which has more BFGs and fewer AFGs. In addition, outer-sphere complexes with BFGs would be possible at low pH. Another possible sorption mechanism would be sorption on the surface of precipitates, such as amorphous CaO, CaCO₃ and crystallized quartz, but their contribution would be negligible because precipitates were only observed at pH 7 and 10. Thus, the sorption of As(V) at pH 7 showed no significant difference from that at pH 3.5, and the reported PZNCs of CaCO₃ and SiO₂ are 8.0 and 2.0, respectively, implying that no available for holding anions at high pH. Therefore, partitioning, outer-sphere complexation, hydrophobic interactions and electrostatic bridging with multivalent cations are possible sorption mechanisms for As(V).

5.3.6. Distinct sorption mechanisms of Cd²⁺ and As(V)

Based on the sorption isotherms, molecular observations by SEM, and chemical measurements by XRD and XPS, four sorption mechanisms of Cd²⁺ were proposed: partitioning into the porous structure, outer-sphere complexation through electrostatic attraction, inner-sphere complexation between the oxygen of AFGs and Cd²⁺ as CdO and CdO₂, and precipitation as crystallized otavite. Partitioning into the porous structure did not contribute to the sorbed fraction because Cd²⁺ remained in the porous structure during the filtration process, but it is difficult to separate partitioning and outer-sphere complexation because no modern analytical technique can reveal the difference. The inner-sphere complexes were presumed to be mononuclear bidentate (CdO) or binuclear bidentate (CdO₂) complexes, and such complexation was observable where deprotonated AFGs were abundant, such as at high pH or on B400. Increasing PT led to a decrease in AFGs, decreasing inner-sphere complexation as CdO or CdO₂. Amorphous structures were also identified on the basis of XRD analysis; thus, we concluded that Cd²⁺ interacted with

deprotonated AFGs through inner-sphere complexes. Precipitation as otavite was the major sorption mechanism of Cd^{2+} at high pH with increasing PT. This conclusion is reasonable because the concentration of carbonate species in the aqueous phase dramatically increased with increasing pH (approximately 1,000 times higher at pH 10 than pH 7), and more otavite precipitated.

Under acidic pH conditions, significant amounts of Cd^{2+} containing minerals were not formed since the positively charged surface of biochar had very few deprotonated AFGs (carboxylic, lactonic and phenolic groups), which corresponded to previous results.(Lee et al. 2020) However, with increasing pH from 3.5 to 7.0, Cd^{2+} sorption increased on B400 and B700, but different sorption mechanisms were involved: inner-sphere complexation in B400 and precipitation as otavite in B700. This process occurred due to the degree of deprotonated AFGs on the biochar; thus, carboxylic groups were available at pH 7.0 for inner-sphere complexation. However, B700 showed a lower abundance of carboxylic groups than did B400; for that reason, precipitation governed Cd^{2+} sorption. The results for pH 7.0 and 10 showed that the contribution of inner-sphere complexes increased in B700 due to deprotonated lactonic and phenolic groups, while B400 showed no otavite in the 1 mM treatment because the sorption sites were more abundant than the sorbate molecules.

On the other hand, the sorption of As(V) on the *Miscanthus* biochar was not as favorable as that of Cd^{2+} , even though a high anion exchange capacity (AEC) for the biochar was previously reported. This result could be explained by two reasons: the reduction of As(V) to As(III) and As(O) by electrons from the biochar surface and the low sorption affinity of As onto BFGs. Han et al. (2020) reported the structural configuration and sorption affinity of oxyanions, and arsenate showed a high sorption affinity on iron (hydr)oxides. However, the BFGs of biochar are not as charged as iron

(hydr)oxides; thus, the difference in charge density and sorption site density would lead to a poor sorption capacity for As(V) (Lawrinenko and Laird 2015). In addition, an increase in PT would yield an increase in AEC in comparison with that in most previous studies, but our results did not correlate with previous studies. For the explanation of such phenomena, the sorption mechanism of As(V) should first be understood. Four sorption mechanisms of As(V) were previously identified: partitioning, outer-sphere complexation, hydrophobic attraction and electrostatic bridging complexation.

Under pH 3.5 and 7.0, no precipitation was observed in the As(V) treatments, and no significant difference in sorption capacity was measured between pH 3.5 and 7.0 for B700. However, a slight decrease in sorption capacity was observed for B400. This result indicates that the majority of As(V) sorption was governed by partitioning at pH 3.5 and 7.0; however, outer-sphere complexation contributed to As(V) sorption. Thus, the sorption capacity of B700 for As(V) did not differ at pH 3.5 and 7.0, which was due to the decrease in outer-sphere complexes of As(V) compensating for the increase in outer-sphere complexes of As(III) because As(III) and As(V) interact with different sorption sites, i.e., hydrophobic and hydrophilic surfaces. Based on the results, B700 showed a greater sorption capacity than B400 at pH 3.5 and 7.0, but the opposite trend was observed at pH 10. The dramatic increase in sorption capacity at pH 10 compared with that at pH 7.0 is attributed to multivalent ions acting as a bridge between the AFGs of the biochar surface and negatively charged As(III) and As(V) oxyanions. B400 has more AFGs and dissolved multivalent ions than B700 (Table S3), and bridging complexes would be more prevalent in B400. In addition, the interaction between As(0) and the hydrophobic surface of the biochar would increase the sorption capacity of As, resulting in a higher sorption capacity in B400 at pH 10.

Based on this observation and interpretation, four sorption mechanisms were involved in Cd^{2+} sorption and As(V) sorption with reduction. Partitioning and outer-sphere complexation were proposed as sorption mechanisms for both Cd^{2+} and As(V) , inner-sphere complexation and precipitation were observed for Cd^{2+} , and hydrophobic attraction and electrostatic bridging complexation were presumed for As containing molecules. The partitioning of Cd^{2+} and As(V) into the porous structure of biochar at all pH conditions governed the sorption mechanism at low pH because Cd^{2+} precipitation and electrostatic bridging complexes of As(III) and As(V) were not favorable. Outer-sphere complexation was presumed since the employed techniques were not able to distinguish between partitioning and outer-sphere complexation. Inner-sphere complexation and precipitation were only observed for Cd^{2+} , and no evidence for covalent bonding of As(V) with the biochar surface was observed in this study under all pH conditions because of the difference in the sorption affinity for As(V) onto BFGs, which have a lower charge density than As(V) . Inner-sphere complexation of Cd^{2+} with deprotonated AFGs was observed to be more favorable than precipitation below pH 8; thus, the increase in deprotonated AFGs with increasing pH increased inner-sphere complexation, which was more predominant in B400. Precipitation has been reported to strongly sequester Cd^{2+} in extreme alkaline pH conditions, and the chemical modeling results showed that precipitation as otavite dramatically increased from pH 8 to 10, indicating that precipitation would occur in slightly alkaline soil environments (data not shown). The Cd^{2+} sorption mechanism was proposed on the basis of concrete evidence, but the proposed As(V) sorption mechanism is only an assumption based on the data from this study and knowledge from previous literature. The reduction of As(V) to As(III) and As(0) would lead to hydrophobic interactions of As(III) and As(0) with the biochar surface and electrostatic bridging complexation. Although the

hydrophobic attraction of H_3AsO_3 and $\text{As}(0)$ and electrostatic bridging complexation could not be observed with the techniques employed in this study, two sorption mechanisms were suggested by excluding some sorption mechanisms, such as inner-sphere complexation and sorption with precipitates. More powerful X-ray-based techniques, such as an extended X-ray absorption fine edge and X-ray absorption near edge structure at the interface, would clarify the sorption mechanisms. However, this study clearly confirmed that the reduction of $\text{As}(\text{V})$ occurred and the majority of As containing molecules were more favorably adsorbed in hydrated states than sorbed states on the biochar surface.

5.4. Conclusions

We hypothesized that pH would determine the sorption behavior of two contrasting inorganic pollutants (cationic cadmium (Cd^{2+}) and oxyanionic arsenate ($\text{As}(\text{V})$)) and the response would differ with changes in inorganic pollutants, charge, and PT. This hypothesis was studied by interpreting the sorption mechanism using SEM, XRD and XPS. The pH-dependent sorption of Cd^{2+} and $\text{As}(\text{V})$ to biochar produced from *Miscanthus* pyrolyzed at two different PTs (400 and 700 °C) was tested; four sorption mechanisms for both Cd^{2+} and $\text{As}(\text{V})$ were observed, which were presumed by interpreting the available data or by excluding other possible mechanisms. Partitioning and outer-sphere complexation were identified for both Cd^{2+} and $\text{As}(\text{V})$; inner-sphere complexation with AFGs and surface precipitation as otavite were the governing sorption mechanisms for Cd^{2+} , while hydrophobic attraction of reduced As molecules and electrostatic bridging complexation with multivalent ions on the AFGs were presumed to be additional sorption mechanisms for $\text{As}(\text{V})$. The sorption capacities of Cd^{2+} and $\text{As}(\text{V})$ were expected to exhibit opposite trends with respect to pH because of the SCD of biochar and the high

AEC. However, both Cd^{2+} and As(V) were retained more at high pH than at low pH, which was explained by the reduction of As(V) and the charge difference between As(V) and the BFGs of biochar. These two processes would stabilize cationic metals and anionic metalloids together. However, the degree of stabilization differed significantly because the sorption capacity for Cd^{2+} was approximately 10 times higher than that for As(V) . Its results indicated that phosphate (P(V)) would have similar behavior on *Miscanthus* biochar because of the electrochemical similarities between As(V) and P(V) . On the other hand, anionic nutrients, such as nitrate and sulfate, which have a relatively low sorption affinity, would be precipitated on the B400 surface or evenly distributed on the B700 surface based on the Cl^- distribution in this study because BFGs are more suitable than AFGs for holding such anions. However, concrete evidence should be provided in further investigations. In this study, we confirmed that the pore structure and AFGs of biochar govern the sorption behavior of Cd^{2+} and As(V) , and both sorption mechanisms were controlled by AFGs through inner-sphere complexation and electrostatic bridging complexation. Although this study only addressed the sorption mechanisms in a simplified system without soil, we believe that our findings will contribute to a comprehensive understanding of the sorption behavior of inorganic pollutants to biochar and could help better explain their fate, behavior and transport in soil and water environments.

References

- Ahmad M, Rajapaksha AU, Lim JE, Zhang M, Bolan N, Mohan D, Vithanage M, Lee SS, Ok YS (2014) Biochar as a sorbent for contaminant management in soil and water: A review. *Chemosphere* 99:19–33. doi: 10.1016/j.chemosphere.2013.10.071
- Ahmed MB, Zhou JL, Ngo HH, Guo W, Johir MAH, Sornalingam K (2017) Single and competitive sorption properties and mechanism of functionalized biochar for removing sulfonamide antibiotics from water. *Chem Eng J* 311:348–358. doi: 10.1016/j.cej.2016.11.106
- Basualto C, Poblete M, Marchese J, Ochoa A, Acosta A, Sapag J, Valenzuela F (2006) Extraction of cadmium from aqueous solutions by emulsion liquid membranes using a stirred transfer cell contactor. *J Braz Chem Soc* 17:1347–1354. doi: 10.1590/S0103-50532006000700023
- Boehm HP (1994) Some aspects of the surface chemistry of carbon blacks and other carbons. *Carbon N Y* 32:759–769. doi: 10.1016/0008-6223(94)90031-0
- Boparai HK, Joseph M, O'Carroll DM (2013) Cadmium (Cd²⁺) removal by nano zerovalent iron: Surface analysis, effects of solution chemistry and surface complexation modeling. *Environ Sci Pollut Res* 20:6210–6221. doi: 10.1007/s11356-013-1651-8
- Briggs D, Seah MP (1990) *Practical Surface Analysis, Auger and X-ray Photoelectron Spectroscopy*. Wiley
- Cantrell KB, Hunt PG, Uchimiya M, Novak JM, Ro KS (2012) Impact of pyrolysis temperature and manure source on physicochemical characteristics of biochar. *Bioresour Technol* 107:419–428. doi: 10.1016/j.biortech.2011.11.084
- Cao X, Harris W (2010) Properties of dairy-manure-derived biochar pertinent to its potential use in remediation. *Bioresour Technol* 101:5222–5228. doi: 10.1016/j.biortech.2010.02.052
- Chen B, Zhou D, Zhu L (2008) Transitional adsorption and partition of nonpolar and polar aromatic contaminants by biochars of pine needles with different pyrolytic temperatures. *Environ Sci Technol* 42:5137–5143. doi: 10.1021/es8002684
- Chun-xi LI, Shu-li F, Yun S, Li-na J, Xu-yang LU, Xiao-li HOU (2007) Effects of arsenic on seed germination and physiological activities of wheat seedlings. *J Environ Sci* 19:725–732
- Downs R, Hall-Wallace M (2003) The American Mineralogist crystal structure database. *Am Mineral* 88:247–250
- El-Kamash AM, Zaki AA, El Geleel MA (2005) Modeling batch kinetics and thermodynamics of zinc and cadmium ions removal from waste solutions using synthetic zeolite A. *J Hazard Mater* 127:211–220. doi: 10.1016/j.jhazmat.2005.07.021
- Han JMKH-MR (2020) Factors modifying the structural configuration of oxyanions and organic acids adsorbed on iron (hydr)oxides in soils. A review. *Environ Chem Lett*. doi: 10.1007/s10311-020-00964-4 REVIEW 2
- Huang P, Ge C, Feng D, Yu H, Luo J, Li J, Strong PJ, Sarmah AK, Bolan NS, Wang H (2018) Effects of metal ions and pH on ofloxacin sorption to cassava residue-derived biochar. *Sci Total Environ* 616–617:1384–1391. doi: 10.1016/j.scitotenv.2017.10.177
- Kim WK, Shim T, Kim YS, Hyun S, Ryu C, Park YK, Jung J (2013a) Characterization of cadmium removal from aqueous solution by biochar produced from a giant Miscanthus at different pyrolytic temperatures. *Bioresour Technol* 138:266–270. doi: 10.1016/j.biortech.2013.03.186

- Kim WK, Shim T, Kim YS, Hyun S, Ryu C, Park YK, Jung J (2013b) Characterization of cadmium removal from aqueous solution by biochar produced from a giant *Miscanthus* at different pyrolytic temperatures. *Bioresour Technol* 138:266–270. doi: 10.1016/j.biortech.2013.03.186
- Kloss S, Zehetner F, Dellantonio A, Hamid R, Ottner F, Liedtke V, Schwanninger M, Gerzabek MH, Soja G (2012) Characterization of Slow Pyrolysis Biochars: Effects of Feedstocks and Pyrolysis Temperature on Biochar Properties. *J Environ Qual* 41:990. doi: 10.2134/jeq2011.0070
- Kong Y, Kang J, Shen J, Chen Z, Fan L (2017) Influence of humic acid on the removal of arsenate and arsenic by ferric chloride: effects of pH, As/Fe ratio, initial As concentration, and co-existing solutes. *Environ Sci Pollut Res* 24:2381–2393. doi: 10.1007/s11356-016-7994-1
- Koshizaki N, Umehara H, Oyama T (1998) XPS characterization and optical properties of Si/SiO₂, Si/Al₂O₃ and Si/MgO co-sputtered films. *Thin Solid Films* 325:130–136. doi: 10.1016/S0040-6090(98)00512-4
- Lawrinenko M, Laird DA (2015) Anion exchange capacity of biochar. *Green Chem* 17:4628–4636. doi: 10.1039/c5gc00828j
- Lee S, Han J, Ro HM (2020) Interactive effect of pH and cation valence in background electrolyte solutions on simazine sorption to *Miscanthus* biochar produced at two different pyrolysis temperatures. *Korean J Chem Eng* 37:456–465. doi: 10.1007/s11814-019-0470-0
- Lee S, Han J, Ro HM (2018) Interpreting the pH-dependent mechanism of simazine sorption to *Miscanthus* biochar produced at different pyrolysis temperatures for its application to soil. *Korean J Chem Eng* 35:1468–1476. doi: 10.1007/s11814-018-0054-4
- Lehmann J (2007) Bio-energy in the black. *Front Ecol Environ* 5:381–387. doi: 10.1890/1540-9295(2007)5[381:BITB]2.0.CO;2
- Leon CA, Radovic LR (1991) Influence of Oxygen Functional Groups on the Performance of Carbon-Supported Catalysts. *Mater Sci* 1007–1014
- Liao P, Yuan S, Zhang W, Tong M, Wang K (2012) Mechanistic aspects of nitrogen-heterocyclic compound adsorption on bamboo charcoal. *J Colloid Interface Sci* 382:74–81. doi: 10.1016/j.jcis.2012.05.052
- Luo L, Xu C, Chen Z, Zhang S (2015) Properties of biomass-derived biochars: Combined effects of operating conditions and biomass types. *Bioresour Technol* 192:83–89. doi: 10.1016/j.biortech.2015.05.054
- Mimmo T, Panzacchi P, Baratieri M, Davies CA, Tonon G (2014) Effect of pyrolysis temperature on miscanthus (*Miscanthus × giganteus*) biochar physical, chemical and functional properties. *Biomass and Bioenergy* 62:149–157. doi: 10.1016/j.biombioe.2014.01.004
- Mourdikoudis S, Pallares RM, Thanh NTK (2018) Characterization techniques for nanoparticles: Comparison and complementarity upon studying nanoparticle properties. *Nanoscale* 10:12871–12934. doi: 10.1039/c8nr02278j
- Nanda S, Mohanty P, Pant KK, Naik S, Kozinski JA, Dalai AK (2013) Characterization of North American Lignocellulosic Biomass and Biochars in Terms of their Candidacy for Alternate Renewable Fuels. *Bioenergy Res* 6:663–677. doi: 10.1007/s12155-012-9281-4
- Peng P, Lang YH, Wang XM (2016) Adsorption behavior and mechanism of pentachlorophenol on reed biochars: PH effect, pyrolysis temperature, hydrochloric acid treatment and isotherms. *Ecol Eng* 90:225–233. doi: 10.1016/j.ecoleng.2016.01.039

- Penke YK, Anantharaman G, Ramkumar J, Kar KK (2017) Aluminum Substituted Cobalt Ferrite (Co–Al–Fe) Nano Adsorbent for Arsenic Adsorption in Aqueous Systems and Detailed Redox Behavior Study with XPS. *ACS Appl Mater Interfaces* 9:11587–11598. doi: 10.1021/acsami.6b16414
- Qian L, Chen B (2013) Dual role of biochars as adsorbents for aluminum: The effects of oxygen-containing organic components and the scattering of silicate particles. *Environ Sci Technol* 47:8759–8768. doi: 10.1021/es401756h
- Qian L, Chen B, Hu D (2013) Effective alleviation of aluminum phytotoxicity by manure-derived biochar. *Environ Sci Technol* 47:2737–2745. doi: 10.1021/es3047872
- Qian L, Zhang W, Yan J, Han L, Chen Y, Ouyang D, Chen M (2017) Nanoscale zero-valent iron supported by biochars produced at different temperatures: Synthesis mechanism and effect on Cr(VI) removal. *Environ Pollut* 223:153–160. doi: 10.1016/j.envpol.2016.12.077
- Qu T, Guo W, Shen L, Xiao J, Zhao K (2011) Experimental study of biomass pyrolysis based on three major components: Hemicellulose, cellulose, and lignin. *Ind Eng Chem Res* 50:10424–10433. doi: 10.1021/ie1025453
- Savintsev AP, Gavasheli YO, Kalazhokov ZK, Kalazhokov KK (2016) X-ray photoelectron spectroscopy studies of the sodium chloride surface after laser exposure. *J Phys Conf Ser* 774:. doi: 10.1088/1742-6596/774/1/012118
- Severini F, Formaro L, Pegoraro M, Posca L (2002) Chemical modification of carbon fiber surfaces. *Carbon N Y* 40:735–741. doi: 10.1016/S0008-6223(01)00180-4
- Shaaban A, Se SM, Dimin MF, Juoi JM, Mohd Husin MH, Mitan NMM (2014) Influence of heating temperature and holding time on biochars derived from rubber wood sawdust via slow pyrolysis. *J Anal Appl Pyrolysis* 107:31–39. doi: 10.1016/j.jaap.2014.01.021
- Shafqat MN, Pierzynski GM (2014) The Freundlich adsorption isotherm constants and prediction of phosphorus bioavailability as affected by different phosphorus sources in two Kansas soils. *Chemosphere* 99:72–80. doi: 10.1016/j.chemosphere.2013.10.009
- Silber A, Levkovitch I, Graber ER (2010) PH-dependent mineral release and surface properties of cornstraw biochar: Agronomic implications. *Environ Sci Technol* 44:9318–9323. doi: 10.1021/es101283d
- Sø HU, Postma D, Jakobsen R, Larsen F (2008) Sorption and desorption of arsenate and arsenite on calcite. *Geochim Cosmochim Acta* 72:5871–5884. doi: 10.1016/j.gca.2008.09.023
- Sosulnikov M, Doklady YT-, 1991 undefined X-ray photoelectron study of calcium, strontium, barium and their oxides. *MEZHDUNARODNAYA Kn* 39 ...
- Szekeres M, Tombácz E (2012) Surface charge characterization of metal oxides by potentiometric acid-base titration, revisited theory and experiment. *Colloids Surfaces A Physicochem Eng Asp* 414:302–313. doi: 10.1016/j.colsurfa.2012.08.027
- Tsaneva VN, Kwapinski W, Teng X, Glowacki BA (2014) Assessment of the structural evolution of carbons from microwave plasma natural gas reforming and biomass pyrolysis using Raman spectroscopy. *Carbon N Y* 80:617–628. doi: 10.1016/j.carbon.2014.09.005
- Uchimiya M, Hiradate S (2014) Pyrolysis temperature-dependent changes in dissolved phosphorus speciation of plant and manure biochars. *J Agric Food Chem* 62:1802–1809. doi: 10.1021/jf4053385

- Uchimiya M, Wartelle LH, Lima IM, Klasson KT (2010) Sorption of deisopropylatrazine on broiler litter biochars. *J Agric Food Chem* 58:12350–12356. doi: 10.1021/jf102152q
- Usman ARA, Abduljabbar A, Vithanage M, Ok YS, Ahmad MMM, Ahmad MMM, Elfaki J, Abdulazeem SS, Al-Wabel MI (2015) Biochar production from date palm waste: Charring temperature induced changes in composition and surface chemistry. *J Anal Appl Pyrolysis* 115:392–400. doi: 10.1016/j.jaap.2015.08.016
- Venegas A, Rigol A, Vidal M (2015) Viability of organic wastes and biochars as amendments for the remediation of heavy metal-contaminated soils. *Chemosphere* 119:190–198. doi: 10.1016/j.chemosphere.2014.06.009
- Vithanage M, Herath I, Joseph S, Bundschuh J, Bolan N, Ok YS, Kirkham MB, Rinklebe J (2017) Interaction of arsenic with biochar in soil and water: A critical review. *Carbon N Y* 113:219–230. doi: 10.1016/j.carbon.2016.11.032
- Wang L (2017) Surface Properties and Chemical Composition of Corncob and Miscanthus Biochars : Effects of Production Temperature Surface Properties and Chemical Composition of Corncob and Miscanthus Biochars : Effects of Production Temperature and Method. doi: 10.1080/10426910802679196
- Wang Q, Lemley AT (2006) Reduced adsorption of ametryn in clay, humic acid, and soil by interaction with ferric ion under fenton treatment conditions. *J Environ Sci Heal - Part B Pestic Food Contam Agric Wastes* 41:223–236. doi: 10.1080/03601230500354766
- Wills NK, Ramanujam VMS, Chang J, Kalariya N, Lewis JR, Weng TX, van Kuijk FJGM (2008) Cadmium accumulation in the human retina: Effects of age, gender, and cellular toxicity. *Exp Eye Res* 86:41–51. doi: 10.1016/j.exer.2007.09.005
- Yang Y, Chun Y, Shang G, Huang M (2004) pH-dependence of pesticide adsorption by wheat-residue-derived black carbon. *Langmuir* 20:6736–6741. doi: 10.1021/la049363t
- Yu H, Wang J, Fang W, Yuan J, Yang Z (2006) Cadmium accumulation in different rice cultivars and screening for pollution-safe cultivars of rice. *Sci Total Environ* 370:302–309. doi: 10.1016/j.scitotenv.2006.06.013
- Zhang F, Wang X, Yin D, Peng B, Tan C, Liu Y, Tan X, Wu S (2015) Efficiency and mechanisms of Cd removal from aqueous solution by biochar derived from water hyacinth (*Eichornia crassipes*). *J Environ Manage* 153:68–73. doi: 10.1016/j.jenvman.2015.01.043
- Zhang G, Zhang Q, Sun K, Liu X, Zheng W, Zhao Y (2011) Sorption of simazine to corn straw biochars prepared at different pyrolytic temperatures. *Environ Pollut* 159:2594–2601. doi: 10.1016/j.envpol.2011.06.012
- Zhao J, Li X, Meng J, Ge W, Li W (2019) Microwave-assisted extraction of potassium from K-feldspar in the presence of NaOH and CaO at low temperature. *Environ Earth Sci* 78:1–8. doi: 10.1007/s12665-019-8264-6
- Zhao L, Cao X, Mašek O, Zimmerman A (2013) Heterogeneity of biochar properties as a function of feedstock sources and production temperatures. *J Hazard Mater* 256–257:1–9. doi: 10.1016/j.jhazmat.2013.04.015
- Zheng W, Guo M, Chow T, Bennett DN, Rajagopalan N (2010) Sorption properties of greenwaste biochar for two triazine pesticides. *J Hazard Mater* 181:121–126. doi: 10.1016/j.jhazmat.2010.04.103

CHAPTER 6. SUMMARY AND CONCLUSIONS

6.1. Summary

Biochar is produced from the pyrolysis of various types of feedstocks, such as wood, leaves, and manure under oxygen limited conditions (Lehmann 2007; Chen et al. 2008; Zhao et al. 2013). During the pyrolysis, feedstocks is transformed to eco-friendly energy as bio-ethanol and carbon-rich byproduct, which is considered as biochar, exhibiting a higher content of recalcitrant carbon compared with raw feedstocks (Lehmann et al. 2006). The production of bio-ethanol through the thermal decomposition of feedstocks reduces the emission of methane gas to the atmosphere to that of the natural decomposition in soils (Woolf et al. 2010; Matovic 2011). Consequently, biochar has received a great attention as a byproduct of renewable energy and involved in the mitigation of climate change through the reducing of greenhouse gas emission, recycling of feedstocks, improvement of the soil and water environment, and remediation of environmental pollution (Woolf et al. 2010; Kookana et al. 2011; Mohan et al. 2014).

As briefly mentioned above, biochar is reported as a major contributor in five fields: 1) production of eco-friendly energy such as bio-ethanol and bio-diesel (Nanda et al. 2013; Yuan and Macquarrie 2015); 2) mitigation of climate change through the sequestration of carbon in the soils and reduction of carbon dioxide (Feng et al. 2012; Wang et al. 2012; Mosa et al. 2018) and methane gas (Czimeczik and Masiello 2007; Windeatt et al. 2014); 3) recycling of agricultural and environmental waste such as wood, leaves, manure, peat, and sediment (Mukome et al. 2013; Ronsse et al. 2013); and 4) stabilization of pollutants and retention of nutrients from leaching (Zhang et al. 2013; Ahmad et al. 2014; Tan et al. 2015; Xie et al. 2015).

The research fields of biochar can be categorized as those involving

production and utilization; production can be separated into variations of feedstocks and pyrolysis conditions, which consist of pyrolysis temperature, residence time, and heat transfer rate. From these studies for the production of biochar, the variation of feedstocks and pyrolysis temperature are significant key factors that determine the physiochemical characteristics of biochar; meanwhile, extensive studies have already been conducted to assess the relationship between the key factors and physiochemical characteristics (Cantrell et al. 2012; Zhao et al. 2013). The utilization of biochar can be classified as carbon sequestration for the mitigation of climate change, recycling of by-products obtained through agricultural activity, improvement of soil fertility, and remediation of pollutants (Cha et al. 2016). Many researchers have extensively focused on the biochar in the field of mitigation of climate change, because climate change represents an urgent challenge (Barrow 2012; Ahmad et al. 2014; Shaaban et al. 2014). The application of biochar in soil environments not only causes carbon sequestration but also yields additional effects, such as energy conservation from the recycling of feedstocks and improvement of soil fertility. Not only the carbon sequestration and nutrient retention but also the remediation of pollutants using biochar have received considerable interest, as biochar serves as an eco-friendly and cost-effective biosorbent (Tang et al. 2013; Inyang et al. 2016).

The heterogeneity of biochar produced from various types of feedstocks and diverse pyrolysis conditions have caused adverse effects or unexpected results; however, it also exhibits enormous positive effects for environmental advancement (Mohan et al. 2014; Inyang and Dickenson 2015; Xiao et al. 2018). It implies that an extensive understanding on the production, fundamental physicochemical characteristics of biochar, and environmental conditions would enable the design of the byproduct and biochar. Thus, the complex relationship between production and utilization of biochar need to be fully understood to utilize biochar effectively as a

biosorbent and carbon sequestration. Lacking fundamental knowledge of their mechanism and behavior would result in unexpected side effects in the environment. Consequently, it is essential to fully understand the fundamental characteristics of biochar for utilization in the real environment. This study was constituted to provide comprehensive insight into the fundamental interactions of biochar produced at different pyrolysis temperatures with organic and inorganic pollutants under various environmental conditions. The literature review has summarized previous studies regarding the variation in the physicochemical characteristics of biochar under surrounding environmental conditions, the sorption of organic and inorganic pollutants to biochar, and the reason why environmental change is crucial for sorption.

To verify the ionizable organic pollutant sorption mechanism, the pH-dependent sorption of the pesticide simazine on *Miscanthus* biochar was characterized at two pyrolysis temperatures (400 and 700 °C; hereafter B400 and B700). The specific surface area (SSA) of the micro- and nano-pores, elemental composition, surface acidity, and infrared spectra were determined. The SSA was greater in B700 than in B400, and the former exhibited greater SSA in the micro-pores and lower SSA in the nano-pores than the latter. During pyrolysis, the single-bond structures of the feedstock were converted to aromatic structures, and further pyrolysis led to ligneous structures. Variations in pore structure and a concave-up Scatchard plot corroborated the presence of two sorption mechanisms: electrostatic attraction (S_{es}) and hydrophobic attraction (S_{hp}). Decreases in maximum sorption in the q_{max-L} curve with increasing pH was due to decreased S_{es} via the deprotonation of carboxylic groups on biochar, whereas those in the q_{max-H} curve with increasing pyrolysis temperature was due to a decreased S_{hp} , resulting from pore structure deformation.

To identify the cation valence effects for simazine sorption, the pH- different

electrolytes, and the sorption mechanism was interpreted. The surface charge density (SCD) decreased more in B400 than in B700 at higher pH, owing to the greater deprotonation of acidic functional groups (AFGs); however, greater decreases were observed in B700 than in B400 from pH 2 to pH 3 as a result of alkali salt deposition. The decrease in K_F with increasing pH showed that the simazine sorption decreased with van der Waals forces because the surface of biochar carried a greater negative SCD, which repulses simazine molecules due to the enhanced deprotonation of AFGs. At a given pH, K_F was lower in CaCl_2 than in NaCl because of the formation of larger metal–biochar complexes, resulting in the enhanced blocking of pores available for simazine sorption.

To understand the sorption of heavy metals and metalloids, cationic cadmium (Cd^{2+}) and anionic arsenate (As(V)) on *Miscanthus* biochar pyrolyzed at two different temperatures (400 and 700 °C) were studied with comprehensive observations by scanning electron microscopy, X-ray diffraction, and photoemission spectroscopy. Consequently, four sorption mechanisms for Cd^{2+} and As(V) were observed and analyzed. Partitioning and outer-sphere complexation were characterized as common sorption mechanisms on B400 and B700, and inner-sphere complexation with AFGs and surface precipitation as otavite were proposed for Cd^{2+} ; meanwhile, the hydrophobic attraction of reduced As molecules and electrostatic bridging complex with multivalent ions on the AFGs were presumed as additional sorption mechanisms for As(V) . Based on previous studies, an opposite trend was expected for the pH-dependent sorption of Cd^{2+} and As(V) ; however, both ions experienced greater retention at high pH conditions than at low pH. In addition, the relatively low sorption capacity for As(V) was not expected, which was explained by the reduction and charge difference between As(V) and the basic functional groups on surface of biochar.

6.2. Conclusions

Remediation of environmental pollutants using biochar has received considerable attention because of the eco-friendliness and cost-effectiveness as a biosorbent; however, unexpected results have been frequently reported in previous biochar studies. This is because that the physicochemical characteristics of biochar have not yet been fully addressed; thus, there is limit to the standardization possible for understanding the physicochemical characteristics. In addition, variation during the production of biochar would cause a significant difference in the physicochemical characteristics of the biochar; thus, it is difficult to establish a standard procedure for the characterization. Despite the great potential of biochar for the remediation of organic and inorganic pollutants, its appropriate use as a biosorbent under various surrounding environmental conditions has not yet been comprehensively implemented. Therefore, it is necessary to understand the interaction of organic and inorganic pollutants to biochar under various environmental conditions for the further utilization of biochar as a biosorbent in the soil and aqueous environment.

6.2.1. Sorption mechanisms

Three sorption mechanisms were identified for the organic molecules as simazine: 1) partitioning into the porous structure without interaction on the surface; 2) strong sorption process due to electrostatic attraction (π - π electron donor-acceptor interactions and H-bonding); and 3) weak sorption process *via* hydrophobic attraction (van der Waals interaction). For the cationic Cd^{2+} , four sorption mechanisms were observed: 1) partitioning into the porous structure; 2) outer-sphere complexation through electrostatic attraction; 3) inner-sphere complexation between the oxygen of the AFGs and Cd^{2+} as CdO and CdO_2 ; and 4) precipitation as a crystallized otavite. The As(V) sorption also exhibits four sorption mechanisms: 1) partitioning into the

porous structure; 2) outer-sphere complexation through electrostatic attraction; 3) hydrophobic attraction of reduced As(V), such as As(III) and As(0); and 4) electrostatic cation bridging complex. The abundance of these sorption mechanisms are dependent on environmental conditions, such as proton concentration, cation valence in electrolyte solution, ion composition and concentration, accumulated mineral and surface functional groups on biochar surface and porous structure.

6.2.2. Proton concentration effects

The proton concentration has been known as the most important factor governing chemical reactions in the environment, and similar results are exhibited for the pollutants; however, the detailed mechanisms were not correlated. For simazine, the sorption increased with pH for both B400 and B700, while B400 showed a more dramatic increase compared with B700. For Cd^{2+} , the sorption increased with pH, and most of the Cd^{2+} was immobilized at pH 10 through precipitation, showing no significant difference between B400 and B700. In the case of As(V), the maximum sorption was observed at the pK_a of As(V) in the previous studies; however, in this study, sorption was dramatically increased with increasing pH, since the electrostatic cation bridging complex was the major reason for the sorption of As(V). This study confirmed that the organic and inorganic pollutants were more stabilized on the biochar surface with increase pH through different sorption mechanisms, and the proton concentration is the most critical factor for governing the fate and behavior of pollutants on the biochar surface.

6.2.3. Cation valence effects

The fitting of experimental data for simazine sorption to the Freundlich isotherm model clearly showed that the K_F decreased with increasing pH and cation

valence (CV) owing to the increased electrostatic repulsion for neutral simazine molecules with increasing pH (predominantly) and greater inhibition of internal pore entrances with increasing CV, respectively. The pH-driven decreases in K_F were greater with Ca^{2+} ions (higher CV) than Na^+ ions, and the CV-driven decreases were greater at higher pH values. However, an invariably lower K_F of biochar in B700 than in B400 under any given combination of pH and CV levels was observed, even though higher K_F was expected for the former from its higher SSA and lower AFGs at the surface. This discrepancy means that increasing CV contributes to a greater extent to decreased K_F than increasing pH. From these relations, we deduced that CV-driven variations in pore space and surface morphology predominate over pH-driven through van der Waals forces in controlling the sorption affinity and capacity of biochar for simazine. The results confirmed our hypothesis by revealing that changing the CV alters the available surface coverage for simazine sorption and the blocking of the entrance to internal pore space; meanwhile, the pH governs the protonation/deprotonation of AFGs, and CV predominates over pH in controlling the behavior of simazine (containing lone-pair electrons) sorption to biochar.

6.2.4. Concentration effects

The concentration of pollutants are the factors affecting the abundance of the sorption mechanism upon environmental fluctuation. The organic pollutant simazine showed no significant concentration effects, and the sorbed amounts were attenuated with increasing initial concentration, signifying that the sorption sites on the biochar surface were saturated. Meanwhile, cationic Cd^{2+} and anionic $\text{As}(\text{V})$ showed no attenuation over the increase in concentration, because the sorption was mainly conducted by the precipitation and electrostatic cation bridging complex at low concentration. The increase in concentration led to an increase in the fraction of

the sorption mechanisms, such as partitioning, precipitation, and hydrophobic interactions, which could change the leachability and bioavailability of pollutants upon the realization of environmental fluctuation. In real environments, the concentration would vary and co-exist with other ions for the limited sorption sites; thus, the concentration effects should be understood for the extrapolation of the sorption mechanisms from the lab-scale studies to reactions in real environments.

6.2.5. Molecular scale structures of biochar

The molecular structures, characterized by infrared spectroscopy for polysaccharide, aliphatic, ester, phenol, and carbohydrate structures disappeared during pyrolysis, whereas those indicating aromatic and carbonyl double bonds appeared in B400 but completely disappeared in B700, leaving only lignin C=C and Si-containing structures. In addition, the molecular structures using X-ray photoemission spectroscopy showed that the increase in pyrolysis temperature dramatically decreased the aliphatic C-C and increased the amount of aromatic and graphitic C=C, accompanied by an increase in aromatic and graphite C-O. However, the concentration of oxygen decreased from 25.3% to 19.2% by elemental composition analysis, but the oxygen containing carbons increased, which could be due to the formation of aromatic and graphitic structures inside the biochar structure; meanwhile, the remaining oxygen mainly resided on the surface. The two infrared and X-ray photoemission spectroscopies confirmed that the single bond between the carbon and oxygen disappeared with increasing pyrolysis temperature, and the double bonds remained and formed aromatic structures. Such a transformation of molecular structures is also correlated with observations from electron microscopy and specific surface area measurements. From the results, the characterization of biochar should be comprehensively conducted to understand the sorption mechanisms of pollutants

before the *in situ* application in real environments, and a standard method should be developed to assess the physicochemical characteristics accurately and credibly.

6.2.6. Porous structure effects

With increasing pyrolysis temperature, a dramatic increase in micro-pores was observed, whereas nano-pores decreased due to the collapse of nano-pore by progressive thermal decomposition, causing a total SSA of *Miscanthus* biochar for B400 and B700 of 197.2 and 293.5 m² g⁻¹. Previous investigations on *Miscanthus* biochar reported that the SSA of micro-pores ranged from 2.4 to 381.5 m² g⁻¹ (Kim et al. 2013a), dramatically increasing in the pyrolysis temperature range between 400 and 600 °C owing to the collapse of the nano-pore by progressive thermal decomposition (Kim et al. 2013b; Luo et al. 2015a). The SSA increase was caused by the progressive volatilization of cellulose, hemicellulose, and lignin with increasing pyrolysis temperature (Qu et al. 2011; Mimmo et al. 2014), as the progressive thermal decomposition of molecular structures causes the formation of channel structures with larger pore size. Consequently, the total SSA increased (Cantrell et al. 2012; Kloss et al. 2012; Zhao et al. 2013), which also indicates the possible increase in the hydrophobic surface area of B700 compared with that of B400 (Shaaban et al. 2014; Peng et al. 2016). The SEM morphology images showed the accumulation of Na⁺ or Ca²⁺ on the biochar surface to a greater extent with increasing pH and CV, and Na⁺ or Ca²⁺ were evenly distributed on B700, while these ions were observed as few micrometer precipitates on B400 due to the different pore size distribution. Thus, the amount of simazine sorbed on biochar was higher in the Na⁺ electrolyte solution than in the Ca²⁺ electrolyte solution, resulting in greater blocking of the entrance.

6.2.7. Surface charge density and functional groups

The SCD of B400 was more positively charged than that of B700, and the change in SCD was more significant with increasing pH in B400 than in B700. This is because oxygen containing AFGs, such as carboxylic, lactonic, and phenolic groups, were more abundant in B400 than in B700; thus, the increase in pH caused the deprotonation of AFGs on biochar at the corresponding pK_a values. Leon and Radovic (1991) indicated that the pK_a values of carboxylic, lactonic, and phenolic groups ranged from 4 to 5, 7 to 8, and 10, respectively. From these different physicochemical characteristics of B400 and B700, the sorption behavior of Cd^{2+} and As(V) would be expected to show distinctly different sorption mechanisms as a function of pH. AFGs are known as carboxylic, lactonic, and phenolic groups, whereas the basic functional groups (BFGs) are reported as pyridinium groups, oxonium groups, and protonated aromatic rings (Lawrinenko and Laird 2015). Both functional groups affect the sorption mechanism of charged molecules, such as heavy metals, metalloids, pesticides, and salts (Ahmad et al. 2014), because the surface charge of biochar is governed by protonation and deprotonation of BFGs and AFGs. Under acidic conditions, the SCD of biochar is positive owing to the combination of the deprotonation of BFGs and protonation of AFGs. An increase in pH above the pK_a value (carboxylic ≈ 4.4 , lactonic ≈ 8.2 , and phenolic ≈ 10) causes the surface of biochar to be more negative through deprotonation (Leon and Radovic 1991; Silber et al. 2010); however, no pK_b value has previously been reported for BFGs.

6.2.8. Environmental implication and further prospect

The solution pH and CV exhibit a different effect on the sorption of simazine, which contains lone-pair electrons on the surface of biochar with variable surface charge density. There are many studies in which biochar is used to amend the soil environment to sequester carbon, improving the soil physical characteristics,

maintaining the nutrients, and decomposing the organic pollutants. Many promising results have been demonstrated; however, the fundamental and crucial mechanisms have not yet been fully revealed. Based on this study, we can take one step forward toward understanding feasible mechanisms between organic pollutants and biochar under various pH conditions, which would be applicable to estimating the transport and degradation phenomena of organic pollutants in the presence of biochar under soil environments.

Changing the CV alters the surface coverage available for simazine sorption through the blocking of the entrance to the internal pore space, whereas pH governs the protonation/deprotonation of AFGs. Thus, CV predominates over pH in controlling the behavior of simazine (containing lone-pair electrons) sorption to biochar (carrying variable SCD). Therefore, we believe that our approach and findings will contribute to a more comprehensive understanding of the sorption mechanisms and behavior of ionizable organic pollutants (variable-charge sorbates) to the surface of biochar (variable-charge sorbent) and help better interpret their environmental occurrence, behavior, transport, and fate under natural soils and nearby water environments.

The partitioning and outer-sphere complexation were characterized for both Cd^{2+} and As(V) as sorption mechanisms, whereas the inner-sphere complex with AFGs and surface precipitation as otavite were the governing sorption mechanisms for Cd^{2+} ; meanwhile, the hydrophobic attraction of reduced As molecules and electrostatic cation bridging complex with multivalent ions on the AFGs were presumed to be additional sorption mechanisms for As(V) . The sorption capacity of Cd^{2+} ranged from the isotherm results of the previous studies; however, the sorption capacity for As(V) was not expected based on the SCD study and previous literature because a higher level of anion exchange capacity was expected than the level of CEC.

From the previous studies, an opposite trend between Cd^{2+} and As(V) was expected for pH-dependent sorption; however, both Cd^{2+} and As(V) had greater retention at high pH than at low pH. In addition, the degree of stabilization was significantly different because the sorption capacity of Cd^{2+} was approximately 10-fold higher than that of As(V) . This was explained by the reduction and charge difference between the As(V) and BFGs of biochar. This results suggested that phosphate (P(V)) would exhibit similar behavior on *Miscanthus* biochar because of the electrochemical similarities between As(V) and P(V) . However, anionic nutrients, such as nitrate and sulfate, which have relatively low sorption affinity, would be precipitated onto the surface of B400 or evenly distributed on the B700 surface based on the distribution of Cl in this study, because BFGs are more suitable for holding such anions.

This study only focused on sorption mechanisms by simplifying the system without the consideration of soil; thus, it is hard to extrapolate the results to real soil environment, because many background ions, organic matter and soil components would interact with the biochar surface. Nevertheless, we confirmed that the pore structure and AFGs of biochar govern the sorption behavior of simazine, Cd^{2+} and As(V) , and those are controlled by AFGs through inner-sphere complexation and electrostatic bridging complexes. Therefore, we believe that our findings will contribute to a comprehensive understanding of the sorption behavior of organic and inorganic pollutants to biochar and could help better explain their environmental fate, behavior, and transport under natural soil and water environments.

ABSTRACT IN KOREAN

바이오차는 다양한 농산업 부산물의 열분해 과정에서 생산된 탄소질 물질로, 뛰어난 오염물질 흡착량 때문에 친환경적인 생물 흡착제로 많은 주목을 받고 있다. 열분해와 환경 조건은 바이오차의 물리화학적 특성과 오염물질의 흡착 거동을 결정하지만, 바이오차와 오염물질 간의 복잡한 상호작용을 포괄적으로 이해하기 위한 연구는 부족한 실정이다. 따라서, 이 연구는 바이오차의 열분해 조건에 따른 물리화학적 특성과 오염물질 흡착에 대하여 문헌 조사를 수행하였고, 오염물질 흡착 기작을 설명하기 위해 열분해 조건, pH, 바탕 전해질의 이온 원자가 변화에 따른 거대 액체 바이오차의 시마진, 카드뮴, 비산염의 흡착 실험을 수행하였다. 그 결과, 바이오차의 시마진 흡착에 electron donor-acceptor와 hydrophobic interaction이 주요하게 작용하였고, 바탕 전해질 용액의 양이온은 바이오차에 공극 막힘 효과를 유발하여 시마진 흡착량 감소 효과는 나트륨에 비하여 칼슘이 더 컸다. 카드뮴과 비산염의 흡착 기작에 partitioning과 outer-sphere complexation이 공통으로 확인되었으며, 카드뮴의 경우 흡착에 inner-sphere complexation과 precipitation이, 비산염의 경우 cation bridging complexation과 hydrophobic interaction 작용하였다. 특히 흡착과정에서 바이오차에 의해 환원된 비산염 화학종이 확인되었다. pH와 열분해 온도에 따른 바이오차의 오염물질 흡착은 일반적인 경향을 보이지 않았다. 시마진 흡착량은 pH가 증가할수록 감소하였으나, 카드뮴과 비산염은 반대였다. 열분해 온도가 높을수록 시마진의 흡착량은 감소하였으나, 카드뮴과 비산염의 흡착은

일정한 결과가 없었다. 이러한 연구 결과들을 바탕으로, 열분해 온도와 환경 조건의 변화가 바이오차와 오염물질과의 독특한 상호작용을 일으켰고, 이는 바이오차와 오염물질 사이에 다양한 흡착 기작이 존재하며 주요 흡착 기작이 환경 조건에 따라 변하여 오염물질의 용출도, 생물 유효도, 독성에 영향을 주었다는 것을 밝혔다. 따라서, 본 연구는 바이오차를 실제 환경에서 생물 흡착제로 사용하기 전에 바이오차의 물리화학적 특성, 오염물질의 특성, 환경 조건 간의 기본적인 상호작용을 이해하는 것은 필수적이라는 것을 제시하였다.

중심어: 바이오차, 열분해 온도, 흡착 기작, pH-의존, 전해질 원자가 효과, 시마진, 카드뮴, 비산염

학번: 2013-21180

(This page intentionally left blank)

LIST OF PUBLICATIONS

Published articles

- Lee, S., Han, J., Ro, H., 2020. Interactive effect of pH and cation valence in background electrolyte solutions on simazine sorption to *Miscanthus* biochar produced at two different pyrolysis temperatures 37, 456-465. <https://doi.org/10.1007/s11814-019-0470-0> (SCIE, IF=2.476)
- Lee, S., Han, J., Ro, H., 2018. Interpreting the pH-dependent mechanism of simazine sorption to *Miscanthus* biochar produced at different pyrolysis temperatures for its application to soil 35, 1–9. doi:10.1007/s11814-018-0054-4 (SCIE, IF=2.476)
- Park, J., Lee, M., **Lee, S.**, Kim, J., Lee, T., Ro, H., Kim, S., Jeon 2015. Effect of mixed liquid fertilization on growth responses of red peppers and soil chemical properties 48, 225-232. <https://doi.org/10.7745/KJSSF.2015.48.3.225> (KCI, IF=0.56)
- Park, J., Lee, M., **Lee, S.**, Kim, J., Lee, T., Ro, H., Kim, S., Jeon, S., Seo, S., Kim, Kill., Lee, Geon, Jeong, B., 2015. Effect of mixed liquid fertilization on growth responses of red peppers and soil chemical properties 33, 268-275. <https://doi.org/10.7235/hort.2015.14140> (SCIE, IF=1.531)
- Ro, H., Choi, J., **Lee, S.**, Lee, T., Kim, J., Park, J., Choi, J., Lee, M 2015 Annual increase in carbon and nitrogen stocks of trees and soils in a ‘Niitaka’ pear orchard following standard fertilization recommendations 33, 591-597. <https://doi.org/10.7235/hort.2015.14191> (SCIE, IF=1.531)

(This page intentionally left blank)